Selective Activation of Alkynes through Cumulene Intermediates

Rachel Rosemary Steen

PhD Thesis

Chemistry

University of York

September 2021

Abstract

This thesis is focused on attempts to stabilise ruthenium-supported cumulenes ($Ru=C=\{C\}_n=CR_2$) which are putative intermediates in the activation of alkynes. The use of different aromatic spacer groups in the cumulene and different co-ligands at Ru is explored along the reaction chemistry of the resulting compounds.

Reactions of *trans*-$[RuCl(=C=CHC_6H_4\text{-}4\text{-}C\equiv CH)(dppe)_2]^+$ with H^+/H_2O, NBu_4X (X = Cl, Br, I) or *N*-methylpyrrole results in the formation of *trans*-$[RuCl(=C=CHC_6H_4\text{-}4\text{-}C=OCH_3)(dppe)_2]^+$, and *trans*-$RuCl(C\equiv CHC_6H_4C(X)=CH_2)(dppe)_2$ and *trans*-$[RuCl(=C=CHC_6H_4\text{-}4\text{-}C(C_4H_3N(CH_3))_2CH_3)(dppe)_2]^+$. The Markovnikov addition of these nucleophiles is explained by the initial isomerization of the vinylidene to a cumulene intermediate prior to addition to the more remote quaternary carbon. Utilising the half-sandwich fragment $[Ru(dppe)Cp^*]^+$, acetylide complexes with large terminal groups were synthesised, $Ru(C\equiv CC_6H_4\text{-}4\text{-}C\equiv CR)(dppe)Cp^*$ (R = $(CH_3)_2OH$, C_6H_4-4-OMe, $C_6H_4\text{-}4\text{-}CO_2Me$). These reacted with small electrophiles (H^+, CN^+ and $C_7H_7^+$) at the β carbon to form vinylidene complexes, the large terminal groups are believed to inhibit reactivity of CPh_3^+ at the remote alkyne.

To try to stabilise the putative cumulene intermediate complex, the C_6H_4 spacer group within the organic ligand was changed for $C_{10}H_6$, $C_6H_2(NSN)$ and $C_{14}H_8$. Synthesis of $Ru(C\equiv CAr\text{-}C\equiv CSiMe_3)(dppe)Cp^*$ (Ar = $C_{10}H_6$, $C_6H_2(NSN)$) was achieved through selective lithiation of diethynyl(trimethylsilyl)aryl and addition to $[Ru(dppe)Cp^*]^+$. These reacted with smaller electrophiles (H^+, CN^+ and $C_7H_7^+$) at the β carbon to form vinylidenes. The bulky trityl CPh_3^+ reacted at the remote end of the carbon-rich ligand to give the putative cumulene complexes $[Ru(=C=C=Ar=C=C(H)CPh_3)(dppe)Cp^*]$, followed by internal cyclization to form an indene group, $[Ru(=C=C(H)\text{-}Ar\text{-}indene\text{-}3\text{-}(Ph)_2)(dppe)Cp^*]^+$. The reactions of all electrophiles, with $Ru(C\equiv CH\text{-}C_{12}H_8\text{-}10\text{-}\ C\equiv CSiMe_3)\ (dppe)Cp^*$ gave multiple products including $\{Ru(dppe)Cp^*\}_2(C\equiv CC_{14}H_8\text{-}10\text{-}C(=CCPh_3))_2$, from CPh_3^+ addition and subsequent dimerization.

Electrochemical measurements indicate that complexes $Ru(C\equiv C\text{-}Ar\text{-}C\equiv C(CH_3)_2OH)(dppe)Cp^*$ (Ar = C_6H_4, $C_{10}H_6$, $C_6H_2(NSN)$) and $\{Ru(dppe)Cp^*\}_2(\mu\text{-}C\equiv CC_6H_2(NSN)\text{-}4\text{-}C\equiv C)$ exhibited a reversible single electron oxidation. The resulting cations exhibit a high degree of alkynyl character and bands due to MLCT absorptions in all cases.

Contents

Table of Figures

Table of Schemes

Table of Tables

Table of Photos

Table of Equations

Acknowledgements

After 4 years, 2 universities, 2 continents and one pandemic this project has finally come to an end. I have been blessed to have had the support and encouragement from so many people from this side of the world and the other.

First and foremost, I would like to thank my supervisors Dr Jason Lynam (York) and Prof. Paul Low (UWA) for their wonderful support throughout the years, whether that be in person or at the end of a zoom call. Doing online supervision before it was cool! I am very fortunate to have had such amazing supervisors even though we were only in the same room together once. And also, many thanks to Michael Hall for his insights throughout this project which definitely made it run smoother. I acknowledge that research was carried out on Noongar land, and that Noongar people remain the spiritual and cultural custodians of their land, and continue to practise their values, languages, beliefs and knowledge.

I would also like to thank Lewis Hall, Nina Leeb, Chris Goult and Mauricio Murillo for the laughs and sometimes chaos of first year, along with Joe, Niko, Emily and Adam. And also, to the rest of the lunch crew, especially Ben Coulson, for the, probably too long, lunch breaks and many pub trips that made my first year so much fun.

To the amazing Masnun Naher, Parvin Safari, Mohammad Ghazvini and Dan Harrison for helping me get settled in both Perth and UWA, and Marcus Korb, Varshini Kumar, Elena Gorenskaia, Claire Foster, Dan Mazzucato, Lakshya Daukiya and Justin Freeman for being their wonderful selves and making my time in Australia so amazing. Thank you for the adventures, even when I dragged you to York, WA just for the name. So glad we got to see some Quokkas! I am definitely coming on an adventure to see you all once the world opens up again.

And finally for the support and encouragement through lockdown 2 and 3 (or was it 1 for me…) and for allowing me to annoy you with questions about my thesis my thanks to Johnny Eastwood, Christian Hoffman, Theo Tanner, Aidan Carr and Naomi Elstone. Really couldn't have gotten over this final hurdle without you.

Many thanks for to Gareth Nealson, Heather Fish, Michael Clark, Karl Heaton, Stephen Moggah, Adrian Whitwood and David Pugh for your invaluable help with instruments and in teaching labs. And to the universities for funding my studies. Also, many thanks to the other groups in the chemistry departments, especially those of John Slattey, Ian Fairlamb and

George Kolstontonas. I am coming away from this journey with friends all over the world, 12 countries to be precise and I could not be more pleased.

To my amazing housemates Will, Ali, Saleh and Sanez, Kate and especially to Jay Freeman and Ziggy for being there throughout 2020 and offering your continued love and patience through the trials and tribulations that year contained.

Last but certainly not least all the thanks to my wonderful family, especially Mum, Dad and Charlotte, who put up with me being away from home for two whole years, including one when I was not allowed to visit, though some incredibly difficult times. I would like to express my love and gratitude to my Dad for just being amazing and encouraging me follow my ambitions, words cannot describe my admiration for you, I am incredibly blessed to have you as my parents.

Rachel Steen

In Memory of W A Westgate PhD, Grandad

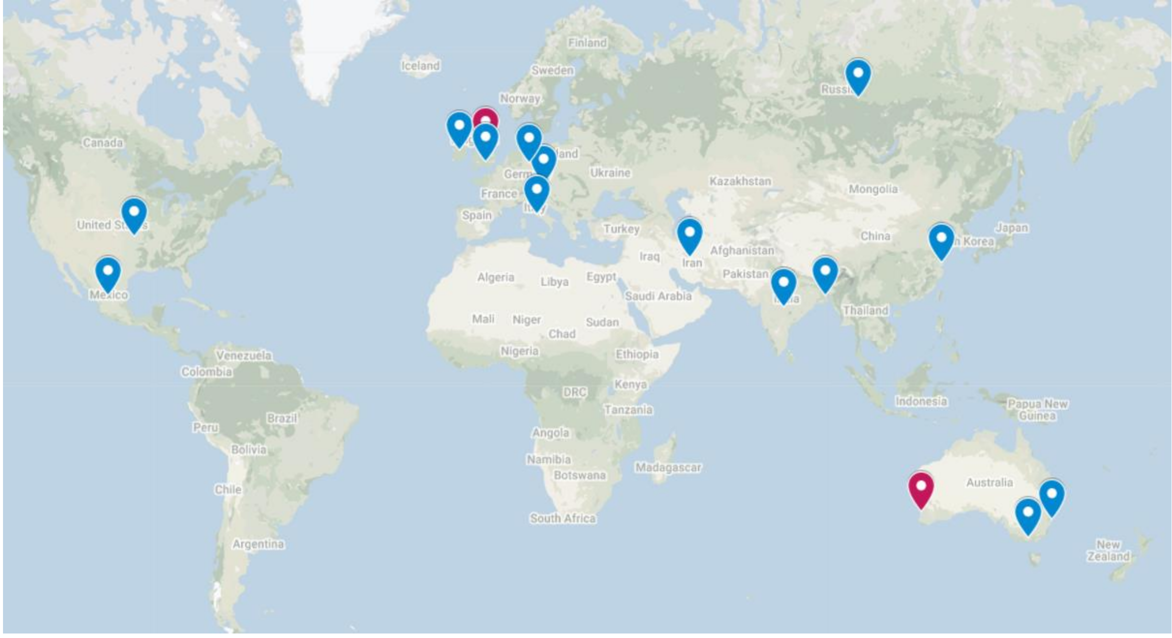

Declaration

I declare that this thesis is a presentation of original work and I am the sole author. This work has not previously been presented for an award at this, or any other, University. All sources are acknowledged as references.

All work is my own except for the following:

- Some ESI-MS experiments were carried out by Karl Heaton.
- X-ray diffraction data was collected, solved and refined by Adrian C Whitwood, Stephen Moggah and Marcus Korb.
- UV-vis-NIR SEC measurements were run by Masnun Naser.

Chapter 1 Introduction

Carbon is one of the most important and well-known elements in the Periodic Table, its tetravalent nature means it can form a wide variety of chemical bonds. Overall 14 different classes of carbon allotropes have been identified to date:[1,2] diamond, graphite, graphene,[3] fullerenes,[4] nanotubes,[5,6] carbon onions (nested hyperfullerenes of carbon[7]), amorphous carbons (both mainly sp^2, mainly sp^3 and synthetically derived types[1]), carbon foams, carbon filters, C_8 (a body-centred cubic crystal of carbon[8]), lonsdaleite[9] (sometimes called hexagonal diamond and therefore it is debated whether it is a discrete allotrope[10]) and, importantly for this work, polyynes which are also known as carbynes. Some of these are shown in Figure 1.1.

Since the discovery of graphene, the 2D allotrope of carbon, in 2004[11] a multitude of applications for it have been found and it has become an important industrial compound,[3] so important that the discovery was awarded a Nobel prize in 2010.[12] As polyynes can be seen as the 1D equivalent to graphene, although with different sp-hybridisation, the interest in its properties and possible applications has increased in recent years.

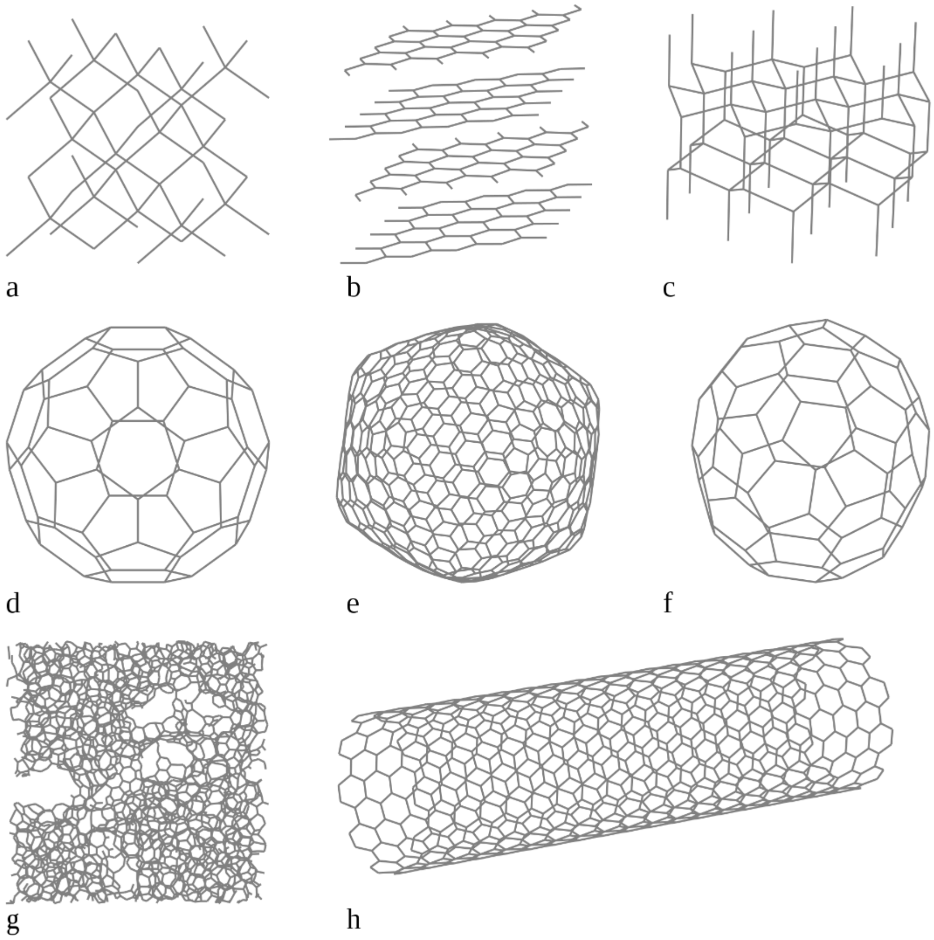

Figure 1.1: Eight allotropes of carbon: a) diamond, b) graphite, c) lonsdaleite, d) C_{60} buckminsterfullerene, e) C_{540}, Fullerite f) C_{70}, g) amorphous carbon, h) zig-zag single-walled carbon nanotube[13]

1.1. Ruthenium

Ruthenium is a rare transition metal element that is obtained as a by-product of mining for other metals, with only 0.001 ppm ruthenium found in the Earth's crust. It is used in alloys in water-resistant electronics and chip resistors.[14] The demand for ruthenium has been steadily increasing from 19.7 tonnes in 2012 to 31 tonnes in 2016, in 2016 7.7 tonnes of ruthenium were for use in the chemical industry, 13.8 tonnes were used in electrical applications, 4.6 tonnes for electrochemical use and 4.8 tonnes for other industries.[15] Despite the numerous biological uses of iron, ruthenium appears to have no biological role and is generally non-toxic. Ruthenium complexes can exist in any oxidation state from -2 (e.g. $Ru(CO)_4^{2-}$) to +8, although complexes most commonly have either a +2, +3 or +4 oxidation state.[16]

Ruthenium complexes are said to be platinum group compounds and are part of the wider group of transition metal complexes. These are formed of one or more transition metal atoms and a variety of ligands with many industrial uses. As there are many transition metals and many possible ligands there is a wide range of chemical processes that rely on the presence of these compounds. Transition metal complexes can also be used as catalysts, speeding up and facilitating numerous reactions, notably the formation of new carbon-carbon and carbon-heteroatom bonds which is difficult to achieve through traditional organic chemistry. They therefore play an important role in the synthesis and formation of various pharmaceutical and agrochemical products,[17] or even as pharmaceutical products themselves.[18] Ruthenium compounds have many advantages as compounds for medical applications: their ability to easily exchange ligands, the high number of oxidation states that can be accessed, and its ability to mimic iron in some biological molecules without being toxic.[19]

Inorganic complexes have been utilised as catalysts in many different reactions and consequently ruthenium is widely used in this capacity. The ruthenium complex $[Ru(bpy)_3]Cl_2$ bpy = 2-2’-Bipyridine (**1.1**) is one of the catalysts that is very widely employed in the field of photo-redox catalysis alongside tris-(2,2’-phenylpyridine)iridium, compound **1.2** $Ir(ppy)_3$, (**Figure 1.2**). This field utilises the ability of visible light to populate a $[Ru(bpy)_3]^{2+}$ excited state which can then be employed as a single electron oxidant or reductant.[20] This gives it a wide range of applications from organocatalysis to greener pathways to access free radical intermediates.[20] Supported ruthenium metal particles are also efficient in the hydrogenation of carbonyls to alcohols in a rapid and selective manner, although the mechanism for this is still unknown.[21] Ruthenium carbene complexes are another example of the use of ruthenium in catalysis (**Section 1.2.1**).[22,23]

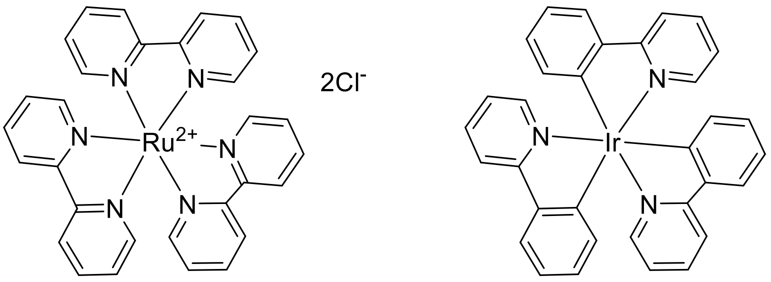

1.1 **1.2**

Figure 1.2: [Ru(bpy)$_3$]Cl$_2$ and Ir(ppy)$_3$ used for photo-redox catalysis

1.2. Alkynes and polyynes

Alkynes are unsaturated molecules with at least one carbon triple bond and are generally more reactive than alkenes because of this. Due to the unsaturated nature of alkynes, they are often used as precursors for various reactions, generally involving the addition of another compound across the triple bond.

A simple rule for determining how the addition of complexes across an unsaturated bond will occur is the Markovnikov rule. The Markovnikov rule was first mentioned by Vladamir Markovnikov in 1870. He stated that during the reaction of an unsymmetrical alkene and hydrohalic acid 'the halogen adds on to the carbon atom containing the fewer hydrogen atoms, that is the carbon that is more under the influence of other carbons' (**Scheme 1.1**).[24,25] The reason that this occurs is that the intermediate in these types of reaction are carbocations. Carbocations are notoriously reactive, as carbon prefers to have four bonds rather than three, meaning that they must be stabilised in some way. Therefore, the carbon which has the most non-hydrogen substituents have the most stabilised carbocation allowing the initial addition of the slightly negatively charged part of the reactant (in this case X) to bond. This rule works in general although there are also many examples of anti-Markovnikov additions.[26–30] Anti-Markovnikov reactions tend to have a different reaction pathway, often utilising sterically bulky groups in order to prevent addition or directing catalysts.

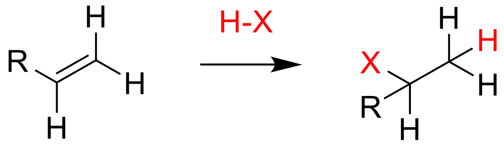

Scheme 1.1: Markovnikov addition of hydrohalic acid across an unsymmetrical alkene

Polyynes are organic extended alkyne chains with sp carbon atoms with alternating single and triple bonds and fall under the carbyne carbon allotrope umbrella. Some natural products contain polyynes moieties, most commonly they are diynes although one with four alkyne units (**Figure 1.3**) has been isolated from *Minquartia guianensis*, part of a family of tropical flowering plants called *Olacaceae*.[31]

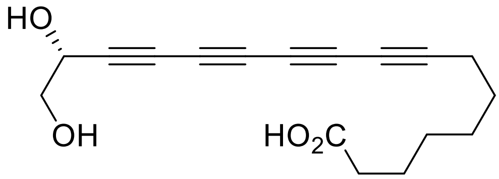

1.3

Figure 1.3: Structure of tetrayne natural product from *Minquartia guianensis*

The longest reported synthetic polyyne chain was made by chain extensions, through which the number of alkyne groups is increased through additions of terminal polyynes to differentially end-capped polyynes. This addition resulted in polyynes with up to 22 acetylene units (44 carbons) and stabilised by two, extremely sterically bulky, tris(3,5-di-t-butylphenyl)methyl moiety terminal groups (**Figure 1.4**).[32]

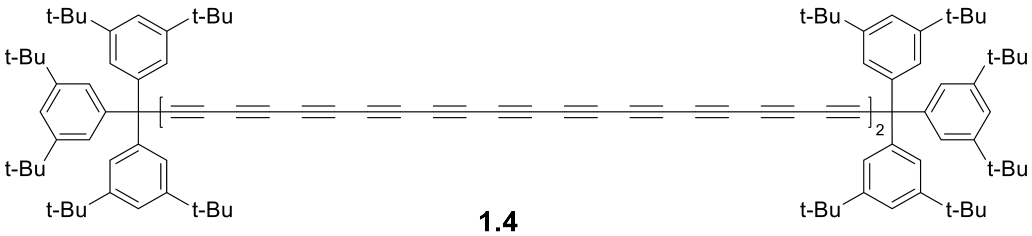

1.4

Figure 1.4: Longest reported synthetic polyyne, 22 acetylene units (44 carbons)

Acetylides are metal bound alkynes or polyynes with the general formula of either M–C≡CH or M–C≡CM, where M is a metal, normally a transition metal. The acetylide ligand can be thought of as isoelectric with the cyanide ion meaning acetylides may be viewed not as organometallic compounds but as coordination compounds due to their bonding properties. They are good σ- and π- donors but poor π- acceptors.[33]

There are many different methods for the synthesis of metal acetylides, many of which rely on metal halides or other unsaturated organometallic compounds.[33] When two terminal metals are used acetylides have been synthesised with up to 12 carbon atoms in a chain, six alkyne units (**Figure 1.5**), this was synthesised through a cross coupling of two identical $RuCl(C{\equiv}CC{\equiv}CC{\equiv}CC{\equiv}CH)(dppe)_2$ fragments, with the use of copper (II) acetate and DBU.[34]

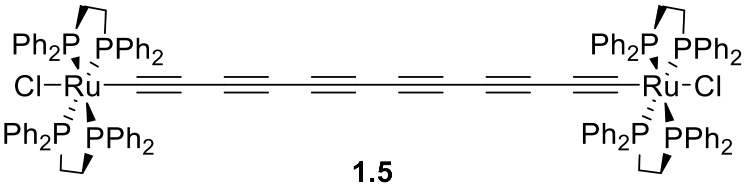

1.5

Figure 1.5: Longest metal capped acetylide chain, 6 acetylene units (12 carbons)[34]

Acetylides and polyynes can form tautomers through the formal 1,2-shift of the alkyne hydrogen, these compounds are known as cumulenes.[35] The simplest example, shown in Figure 1.6, is the alkyne/vinylidene tautomerisation. This isomerisation usually happens spontaneously when in solution although the acetylide form of the molecule is normally the lower energy state and therefore almost exclusively observed.

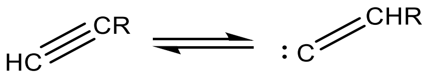

Figure 1.6: Alkyne/vinylidene tautomerisation

1.2.1 Carbenes

Carbenes are neutral molecules that include a divalent carbon atom which has only six valence electrons (**Figure 1.7**). Due to the inherent instability of six valent electrons, carbenes are reactive and can act as both nucleophiles and electrophiles, this is generally dictated by the properties of the substituents. Since the proposal of the existence of carbenes in 1855[36] they have evolved from being a scientific curiosity to an important topic in coordination chemistry within the last 50 years.[37]

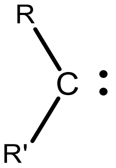

Figure 1.7: General Carbene Structure

There are three possible theoretical ground states for uncoordinated carbenes the triplet state (proposed to be present in Schrock-type carbenes), the singlet state (in Fischer carbenes) and the less well-known linear triplet state (**Figure 1.8**), which are used to model the different reactivities observed for carbenes. Which electronic configuration a molecule takes is influenced by the steric, inductive and mesomeric effects of its substituents.[37]

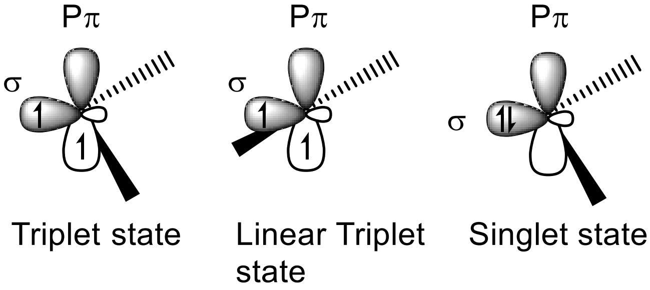

Figure 1.8: Carbene electronic configurations

Initial characterisation of carbenes coordinated to metals was carried out by Fischer[38] (with the compound $W(CO)_5(COCH_3)(CH_3)$ which was identified as having a 'methoxymethylcarbene' bound structure due to the lack of C=O stretch in the IR spectra) and Schrock[39] (with the compound $Ta[CH_2C(CH_3)_3]_3[CHC(CH_3)_3]$ with a structure determined through deuterium labelling studies). Fischer was awarded a Nobel Prize in 1973 partially for this work. Grubbs' catalyst (**Figure 1.9**), which is used to catalyse olefin metathesis, was prepared by Grubbs *et al* in 1992[40] and its applications earned a Nobel Prize in chemistry 'for the development of the metathesis method in organic synthesis'[12] along with Schrock[41] and Chauvin.[42]

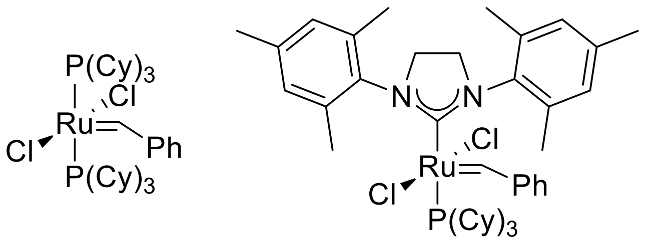

1.6 **1.7**

Figure 1.9: First generation, 1.6, and example second generation, 1.7 *N*-heterocyclic carbene, Grubbs catalyst

The second generation of Grubbs catalysts uses an *N*-heterocyclic carbene (NHC) in place of a phosphine ligand. NHCs are more stable and effective than phosphine ligands as they are both sterically larger than some phosphine ligands and are stabilised by strong σ bond donor properties[43] and back donation from the lone pairs of the nitrogen or other heteroatom to the vacant p-orbital on the carbene, represented by structural resonances (**Figure 1.10**).[44–46]

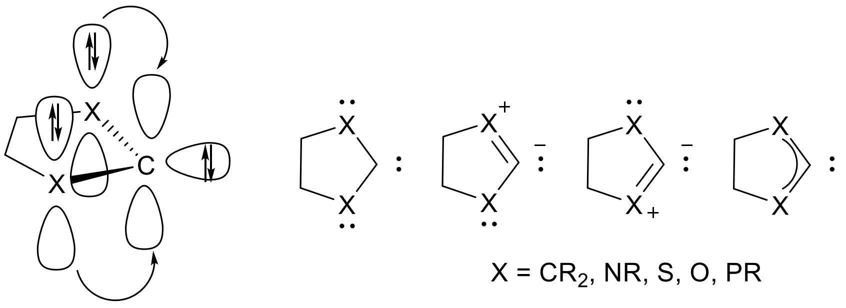

Figure 1.10: General structure of heterocyclic carbenes, with resonance structures

Heterocyclic carbenes (most often *N*-heterocyclic carbene) are a newer class of carbenes (**Figure 1.10**) that are easier to prepare than linear carbenes and can often be isolated making them ideal for catalysts.[46] The first heterocyclic carbene to be reported was a nitrogen-phosphorus compound in 1988[47] followed shortly by an N-heterocyclic compound in 1991[48] which was stable enough to be crystallised (**Figure 1.11**). Synthesis of *N*-heterocyclic carbenes is generally performed in one of three ways: the deprotonation of azolium salts, reductive sulfonation or thermally induced α elimination (**Scheme 1.2**).[49] The most common *N*-heterocyclic carbene scaffold is imidazole-2-ylidene.

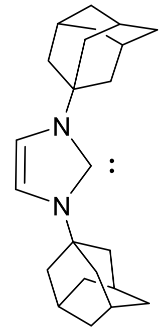

1.8

Figure 1.11: First isolable N-heterocyclic carbene complex, 1.8

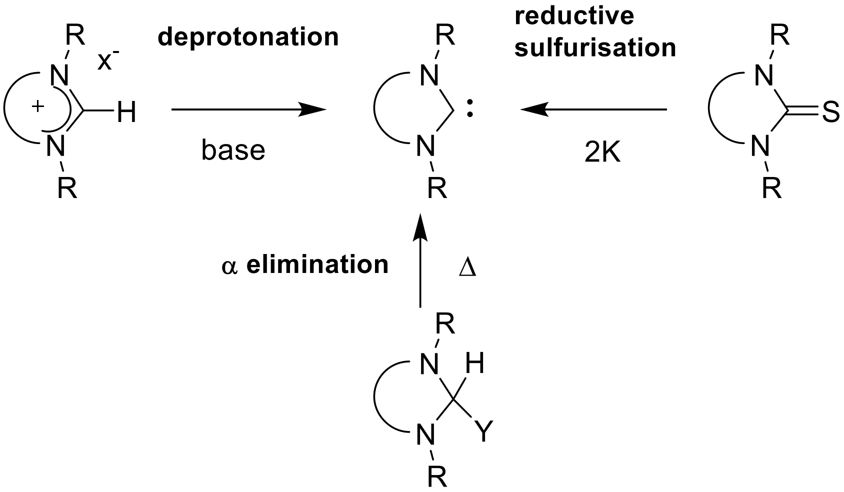

Scheme 1.2: Three general routes of synthesis for N-heterocyclic carbenes

This type of carbene can be coordinated via the carbene carbon to transition metal or p-block elements or used as organocatalysts.[50] Grubbs catalysts have become the ubiquitous example of the use of carbene complexes in catalysis.

1.2.2 Vinylidenes

The formation of vinylidenes, the shortest class of cumulene complex, utilises the tautomer effect of alkynes in their formation. Metal fragments are known to greatly stabilise organic vinylidenes and many different metals have been utilised in this way. Free, organic vinylidenes are extremely reactive, due to it formally having only six valence electrons on the terminal carbon and a vacant orbital (**Figure 1.6**).[51] This lone pair is then very unstable meaning the equilibrium is in favour of the alkyne form of the molecule, having a very short lifetime of 10^{-10} seconds.[52] Experimental and theoretical analysis of this transformation from vinylidene to acetylide is exothermic by between 184 and 197 kJ mol^{-1}.[51,52]

Stabilisation of vinylidenes can be achieved with different metal fragments.[53] The first metal-vinylidene complex was described by Mills and Redhouse (**Figure 1.12**) in 1966[54] synthesised from the irradiation of $Fe(CO)_5$ in a solution of diphenylketene. The second vinylidene complex (**Scheme 1.3**), and the first terminal vinylidene, was reported in 1972[55] and was discovered through the unexpected migration of a chloride from an olefinic carbon to the metal atom and was such a new class of compounds that the authors described it was a ‘dicyanomethylenecarbene’.

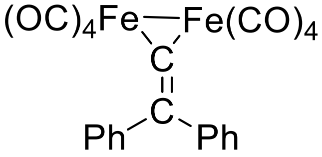

1.9

Figure 1.12: First vinylidene complex reported in the literature, 1.9[54]

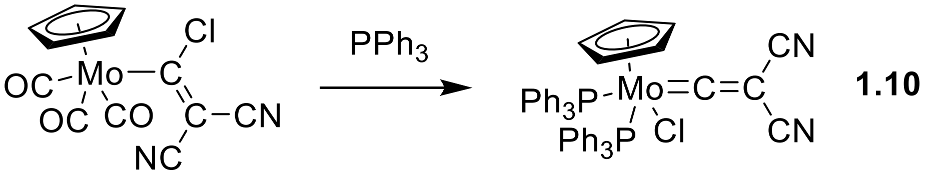

Scheme 1.3: Synthesis of the second vinylidene complex, 1.10, described as dicyanomethylenecarbene[55]

There are three general mechanistic pathways to the synthesis of metal vinylidene complexes from terminal alkynes (**Scheme 1.4**) through: **A**), a 1,2-hydrogen atom migration through the intermediate in pathway A, **B**), a formally oxidative addition across the triple bond giving an alkynyl hydride intermediate followed by a hydride migration, or **C**), a metal alkenyl ligand intermediate from the insertion of an alkyne into the metal hydride bond.[56]

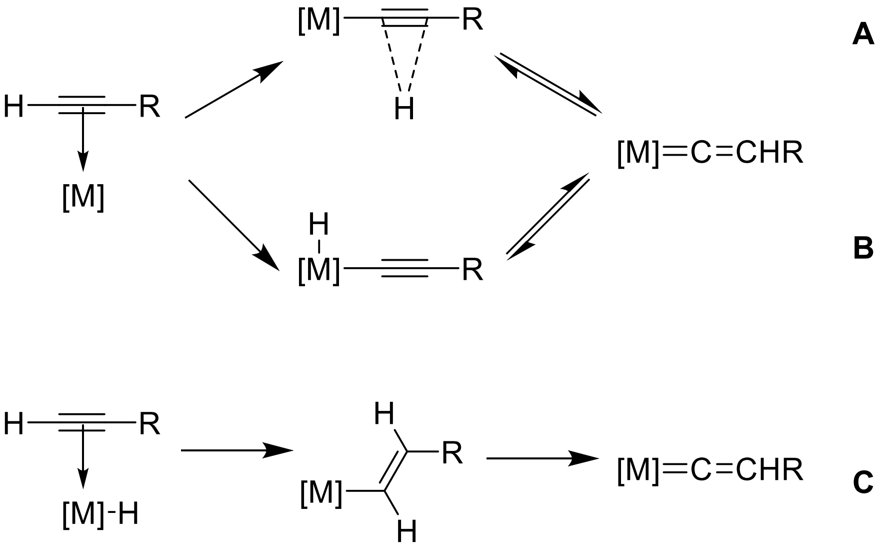

Scheme 1.4: Formation of vinylidenes from terminal alkynes

The isolation of metal vinylidenes has allowed the uses of these complexes to be explored, these include uses in catalysis especially in the electrophilic activation and the dimerization of alkynes.[57] Several extensive reviews have been written on the subject of metal vinylidenes.[52,57–59]

Although Markovnikov additions to vinylidenes are possible, anti-Markovnikov reactions are more common, and were first observed in 1986, which involved the creation of a new C–C bond with many different ruthenium complexes ($RuCl_2(CH_3CN)$(*p*-cymene), $[RuCl(CH_3CN)_2$(*p*-cymene)$][BF_4]$, $RuCl_2(PMe_3)$(*p*-cymene), $RuCl_2(py)_2$(norbornadiene), $RuCl_2(PMe)_3(C_6Me_6)$ and $Ru_3(CO)_{12}$) acting as catalysts, this reaction also involves a vinylidene intermediate species (**Scheme 1.5**).[60]

p-cymene = 4-isopropyltoluene, py = pyridine, norbornadiene = bicyclo[2.2.1]hepta-2,5-diene.

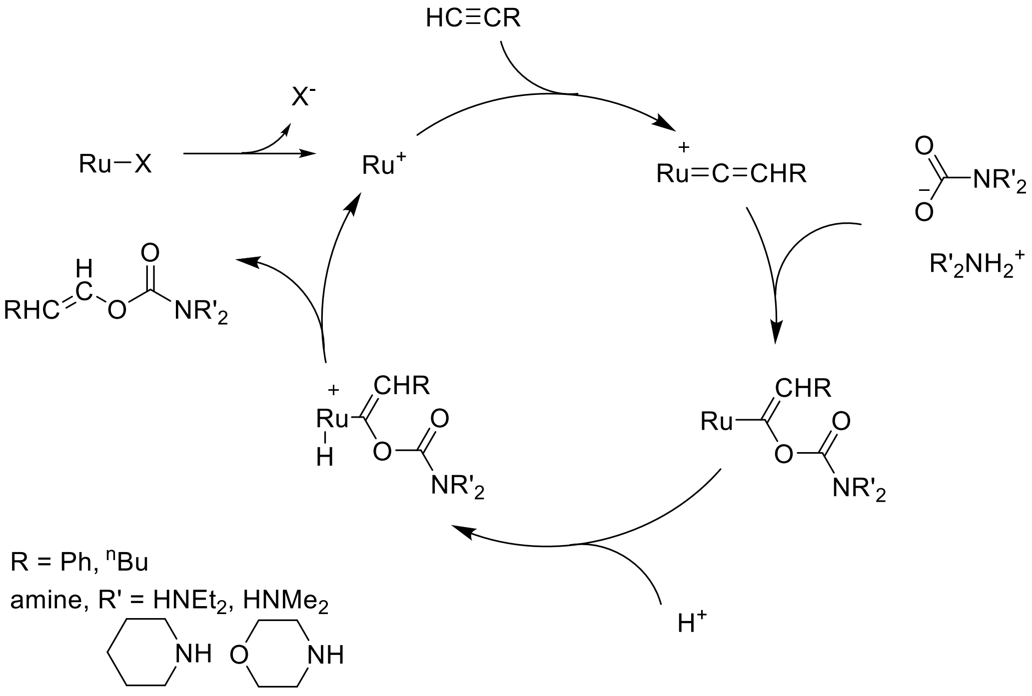

Scheme 1.5: Catalytic cycle for the anti-Markovnikov addition of carboxylic acid

1.3. Cumulenes

Cumulenes are defined as a chain of sp-hybridised carbon atoms, terminated by a sp^2-hybridised carbon atom and often a metal-ligand fragment,[51] and can be thought of as extended carbenes. Free carbenes which have the general formula, $:C(=C)_n=CH_2$, were identified prior to the discovery of metal-bound species and are thought to be a constituent of interstellar gas where hydrogen is scarce.[61,62] Cumulenes with a long enough chain can be thought of as another allotrope of carbon, although 1-D carbon allotrope known as carbyne includes the polyyne configuration in its definition.[63,64]

The very first cumulene complex was synthesised in 1921 by German chemist K. Brand (**Figure 1.13**),[65] with them finally being named by Kuhn and Wallenfels in 1938.[66]

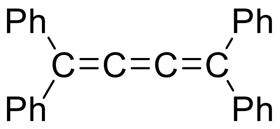

1.11

Figure 1.13: First cumulene structure

Metallocumulenes, with the general structure $L_xM=(C)_nR_2$, were initially seen as an intermediate in the reaction of $RuCl(PMe_3)_2Cl$ and $HC≡CC≡CCPh_2OH$, which was then though to degrade after the rapid in-situ addition of MeOH to the metal-bound (or alpha) carbon by Dixneuf in 1990[67,68] (**Figure 1.14, compound 1.12**) and a few years later by Selegue[69] (**Figure 1.14, compound 1.13**) whose work was then expanded on by Bruce.[70]

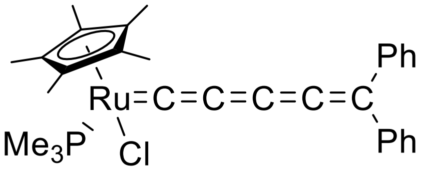

1.12

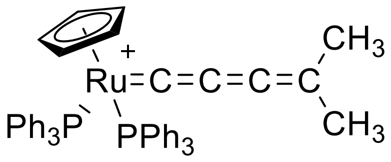

1.13

Figure 1.14: Cumulene structures from Dixneuf[67,68] and Selegue[69]

The cumulated carbon chain has a linear or near-linear geometry, with the largest deviation being found in some manganese compounds[71] and when steric crowding becomes a factor e.g. rotaxane stabilised cumulenes.[72] This crystal structure (**Figure 1.15**) from Franz *et al.*[72] is of the polyyne complex that was then reduced to the cumulene, which was not able to be crystallised. Evidence from the polyyne crystal structure and computational analysis points to a cumulene with bond angles of less than 180 °, and like that of the polyyne between 170 ° and 174 ° due to the steric hindrance of the surrounding atoms.

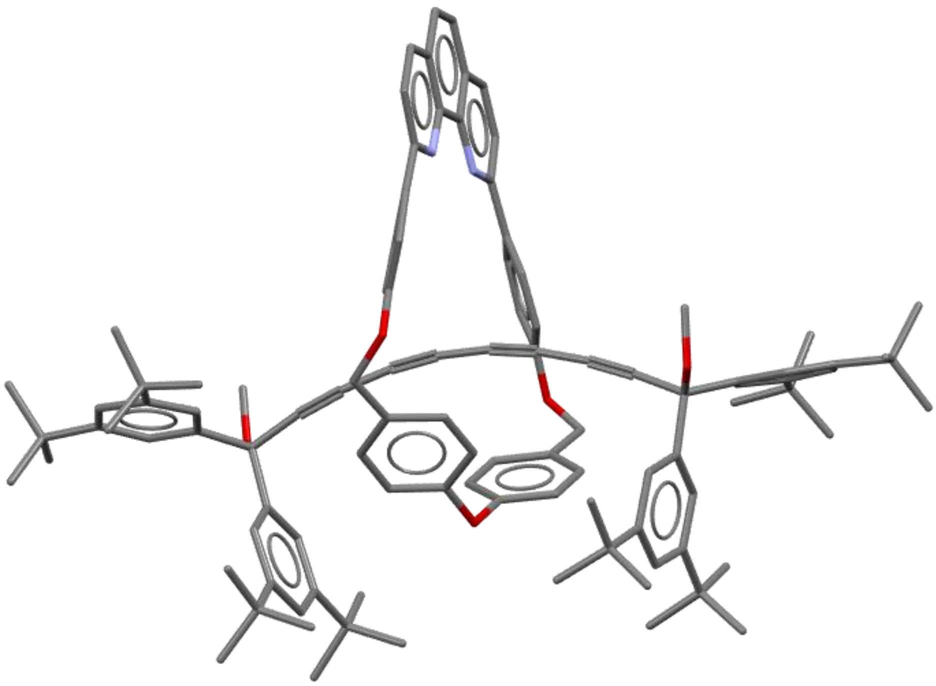

Figure 1.15: Crystal structure of a four polyyne chain stabilised by a rotaxanes, from Franz *et al.* 2015[72]

Naturally occurring cumulenes are significantly rarer than natural polyynes. They mainly consist of two carbon, vinylidene like, carbon chains.[73] There have only been four natural products with three carbon, trienylidene, chains discovered to date (**Figure 1.16**). All four were isolated in the 1960s by Bohlmann and Zdero from the roots of plants and are unstable making purification and assignment difficult.[73]

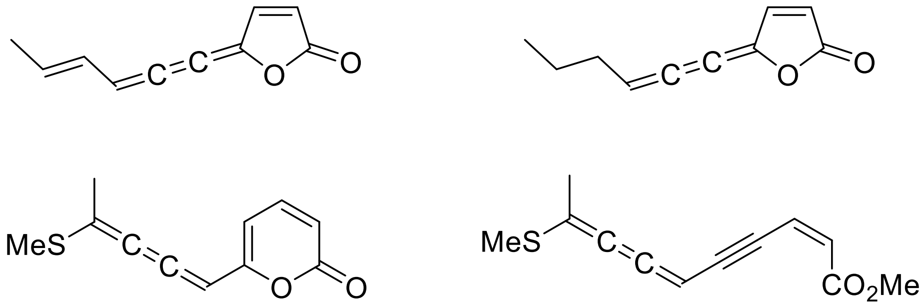

Figure 1.16: Naturally occurring cumulenic compounds[73]

1.3.1 Synthesis

Synthesis of new metallocumulenes requires long synthetic routes which are typically carried out in one of three ways.

- introducing a coordinating precursor to the metal fragment followed by a rearrangement
- constructed in the coordination sphere
- through modification of existing cumulenes.[51]

As the chain length of a cumulene increases their isolation and purification becomes more challenging due to an increase in reactivity, as illustrated by the decreasing number of isolated vinylidenes compared to pentatrienylidenes.

While the increase in chain length does not theoretically make the molecule less thermodynamically stable it does make it more reactive due to the availability of the carbons with a lack of steric hinderance, and therefore more difficult to isolate.[74] For metallocumulenes chain lengths with up to 7 double bonds have been characterised,[51] however, in free cumulenes lengths of up to 9 have been seen, although never isolated, and involve stabilisation from aromatic terminal groups,[75] or by rotaxanes (**Figure 1.15**).[72] As metal-ligand fragments provide high steric hindrance as well as a strong influence on the electronics of a system, many cumulenes are bi-metallic with metal based stabilisation at both ends of the chain. Other interesting synthetic routes involve the assembly of cumulenes within the core of carbon nanotubes by carbon arc-discharge vaporization.[76] As well as stabilisation by assembled carbon films[77,78] and rotaxanes.[72,79]

Several reports focus on the synthesis of odd numbered cumulenes over the even lengths, indicating that these may be easier to synthesise or more stable, even in the interstellar media it is believed that there is a higher abundance of longer cumulenes of odd chain length (or even number of carbons).[80] Despite the similarity in structure to polyynes (**Figure 1.17**), cumulenes are more difficult to synthesise but they appear to have different behaviour to polyynes which makes them more interesting to study.[81]

$$RC{\equiv}C{-}C{\equiv}C{-}C{\equiv}CR$$

polyyne

$$R_2C{=}C{=}C{=}C{=}C{=}CR_2$$

cumulene

Figure 1.17: Comparison of polyynes and cumulene general structures

The initial methods for synthesis for metallocumulenes were devised by Dixneuf and co-workers. Many synthetic schemes involve the reaction of propargyl alcohol derivatives with either a metal species (**Scheme 1.6**)[68,82] or by oxidative homocoupling.[75]

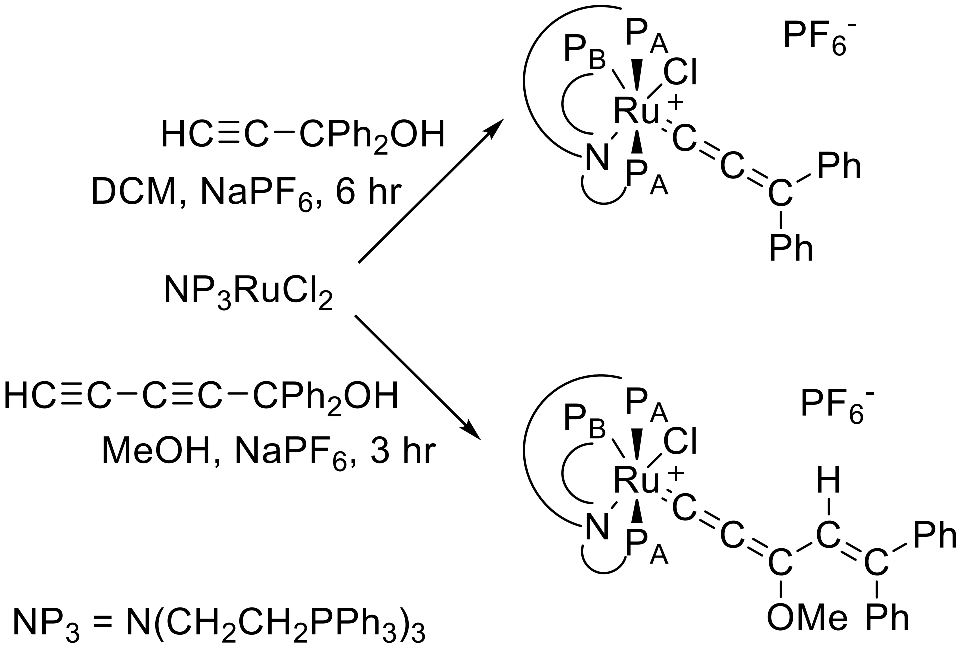

1.14

1.15

Scheme 1.6: Reaction of differing length propargyl alcohols and NP_3RuCl_2 from Wolinska *et al.*[68]

More complicated propargyl alcohol compounds can be used in similar reactions and can therefore give more complicated ligands. Complexes that have been synthesised this way while using aromatic groups as spacer groups can be seen below (**Scheme 1.7**).[83]

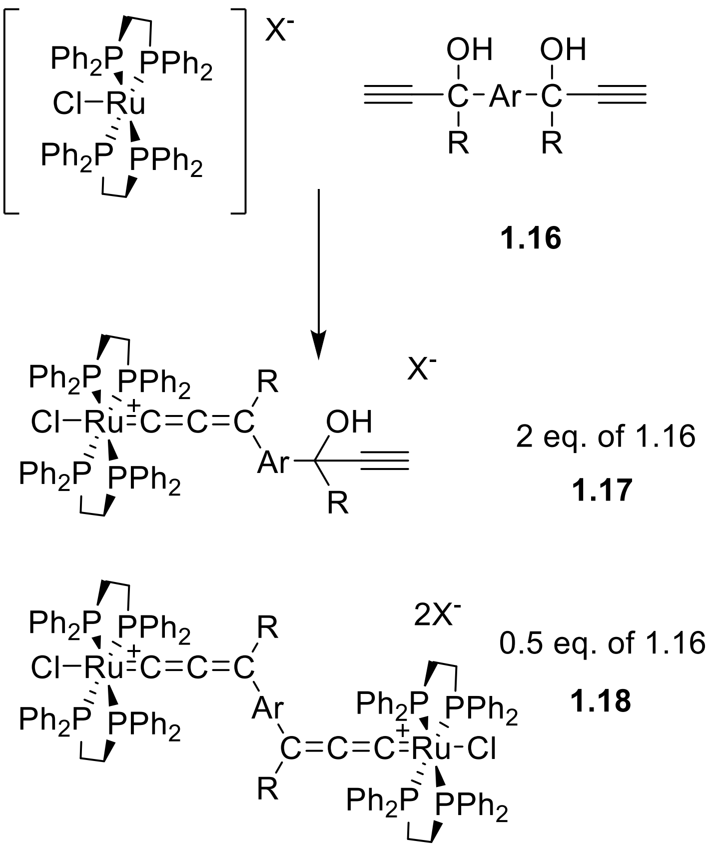

1.16

1.17

1.18

$X = PF_6^-, OTf^-$
R = R. Ph
Ar= 1,4-benzene. 1,4-thiophene, 1,3-benzene, dithiophene, trithiophene

Scheme 1.7: Reaction of $RuCl(dppe)_2^+$ with propargyl alcohol from Rigaut *et al.*[83]

1.3.1.1 Butatrienylidenes

Several early studies on the synthesis of butatrienylidene complexes, from compounds with two connected alkyne groups, showed strong spectroscopic evidence for their formation but could not isolate them.[70,84–86] One of these complexes synthesised by Bruce *et al.* was not observed spectroscopically but reacted immediately with trace water to form a methyl ketone complex (**Scheme 1.8**).[70]

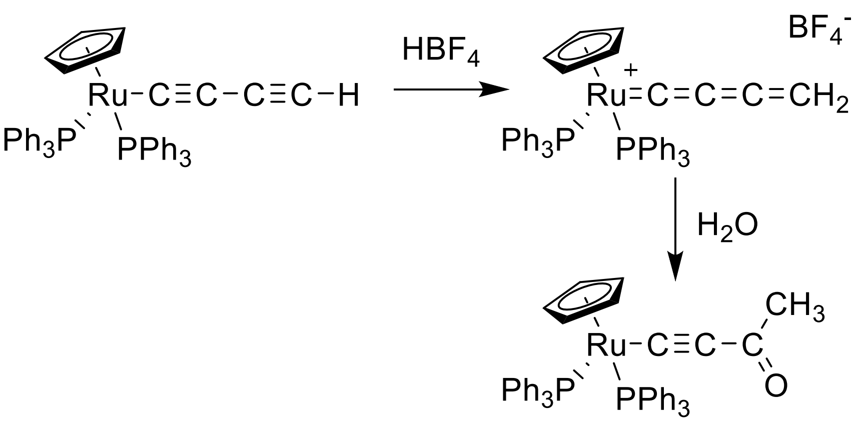

Scheme 1.8: Proposed mechanism for the generation of compound 1.19 $[Cp(PPh_3)_2Ru{=}(C)_4H_2]^+$ by protonation of a butadiynyl complex with tetrafluoroboric acid and the instant reaction with water forming 1.20.[70]

The first isolable butatrienylidene compound was a bimetallic iron species isolated in 1999 by Lapinte (**Scheme 1.9**)[87] by the addition of an electrophile to a neutral butadiynyl complex. As of 2008, 230 different vinylidene complexes had been characterised by X-ray diffraction, however, for butatrienylidene complexes there have only been three.[51]

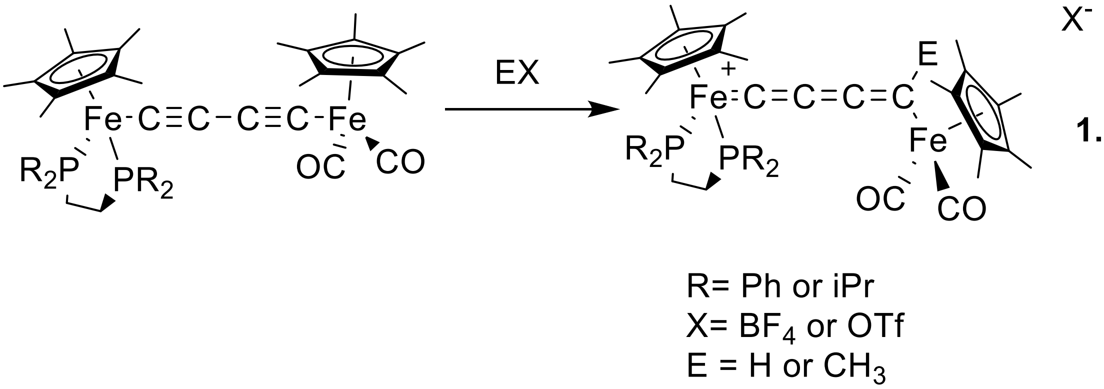

Scheme 1.9: Synthesis of first binuclear butatrienylidene, 1.21[87]

The most successful route to butatrienylidene complexes, such as **1.22**, found to date is *via* 1,4 rearrangement reactions (**Scheme 1.10**).[85,86,88–91] Activated alkynes were utilised as a ligand on two identical iridium metal complexes, which then dimerised to form the first isolated butatrienylidene.[92] The photolysis of manganese compounds with alkynyl(triphenylstannyl)vinylidene ligands has also yielded a butatrienylidene complex.[93]

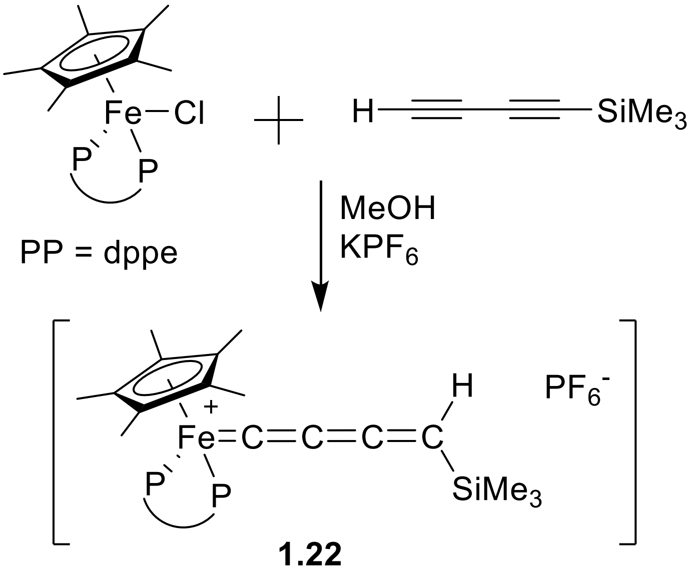

1.22

Scheme 1.10: 1,4 rearrangement of bis-alkyne to butatrienylidene[86]

1.3.1.2 Pentatetraenyidenes

Pentatetraenylidene complexes have been synthesised using suitable C_5 precursors such as penta-1,3-diynyl derivatives. The first ruthenium pentatetraenylidene was proposed as an intermediate in two papers from the Dixneuf group in 1990.[67,94] Followed, in 1994, by the synthesis and isolation of the first pentatrienylidene, $[Cl(dppe)_2Ru{=}(C)_5Ph_2]PF_6$, from a stepwise synthesis using $[RuCl_2(dppe)_2]$ and a TMS-protected precursor followed by the reaction of the acetylide with a bulky trityl cation (**Scheme 1.11**).[82]

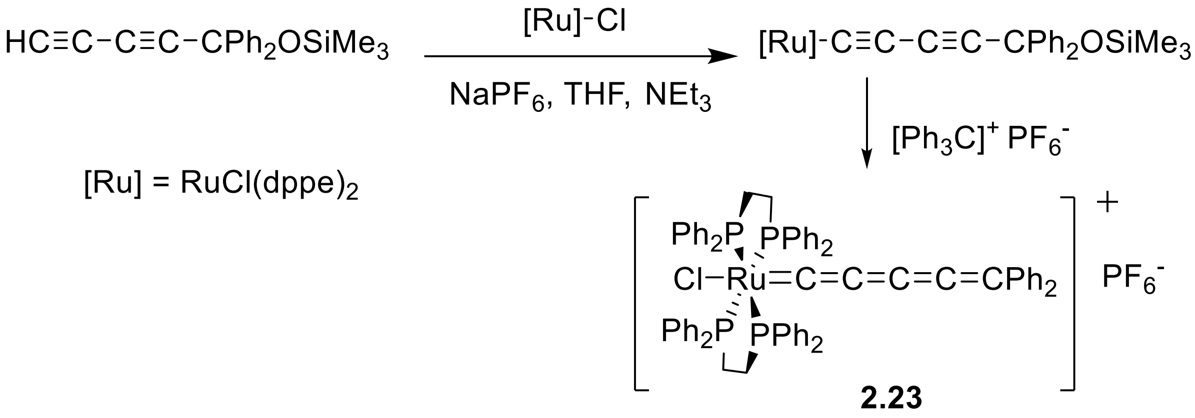

2.23

Scheme 1.11: Synthesis of $[Cl(dppe)_2Ru{=}(C)_5Ph_2]PF_6$ from Touchard *et al*.[82]

1.3.1.3 Higher cumulenes

For many years heptahexaenylidene was thought to only be a reaction intermediate along with hexapentaenylidene,[95] however, a one multi-step synthesis by Dede *et al*. has been successful, and so far is the only isolable one to date (**Scheme 1.12**).[96] Even though hexapentaenylidenes are one carbon shorter than heptahexaenylidenes they have proven to be much more synthetically challenging, as previously stated the synthesis of even numbered cumulenes is more difficult than the odd.

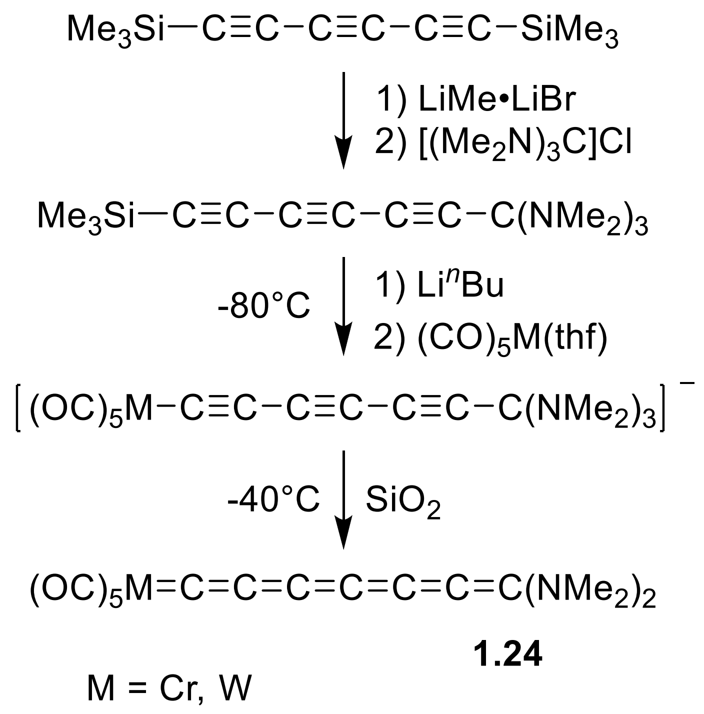

Scheme 1.12: Synthesis of heptahexaenylidene, 1.24, by Dede, Drexler and Fischer, 2007[96]

Theoretical studies on heptahexaenylidene[73] and multiple isomers of H_2C_9 have been carried out.[106] Some organic higher cumulenes (H_2C_7 ,H_2C_8 ,H_2C_9 and D_2C_{10}) have been detected using Fourier transform microwave spectroscopy in lab studies when a gas is passed through an electric field at high velocity and pressures and some physical properties observed.[99]

1.3.1.4 Multi-metallic cumulenes

Some interesting bis(allenylidene)diruthenium cumulene species, $[Ru_2(\mu\text{-}Cl)_3(=C=C=CAr_2)_2(PPh_3)_4]^+PF_6^-$ (**Figure 1.18**), were synthesised in 1996 by Dixneuf[100] with the reaction of two equivalents propargyl alcohols with $RuCl_2(PPh_3)_2$.

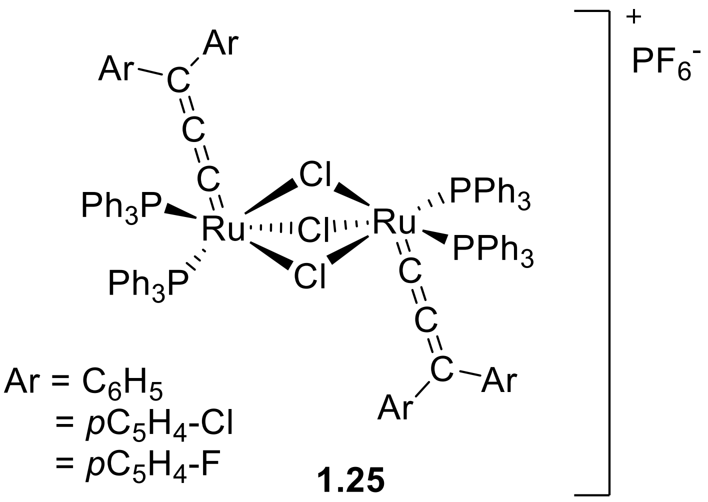

Ar = C_6H_5
= pC_5H_4-Cl
= pC_5H_4-F

1.25

Figure 1.18: 3µ-Cl ruthenium cumulene species, 1.25

Through small changes in the method, single activation is proceeded via a bimetallic species and then the cleavage straight to cumulene complexes.

1.3.2 Structure and Bonding

The bonding and electronic structure of cumulene molecules is influenced by many different factors, which have been thoroughly explored through density functional theory (DFT) calculations. These include:

- The length of the chain, which was independent of the dissociation energies suggesting that there is no limit, thermodynamically, to the possible cumulene chain length.[101]
- The terminal substituents, π-donor substituents increase the lowest unoccupied molecular orbital (LUMO) energy (which is much more pronounced for odd-chain metallocumulenes and leads to a decrease of their reactivity toward nucleophilic attack) while π-acceptors decrease it (which should stabilise higher even-chain metallocumulenes).[102]
- The charge on the metal fragment.[103]
- And the metal-ligand fragment composition i.e. if the other ligands on the metal are generally electron withdrawing or electron donating and their steric bulk.[98]

For all cumulenes the LUMO is mostly localized on the odd numbered carbon atoms, whereas the highest occupied molecular orbital (HOMO) is localized on the even carbon atoms, determining their electrophilic or nucleophilic character. The bonding mode is dominated by σ electron donation from the C_nH_2 lone pair on the first carbon to an empty d_σ metal orbital with contribution from the metal d_π to the lowest energy empty π* orbital on the cumulene.[104] Cumulene compounds have a closed shell ground state with a lone pair on the first carbon, similar to carbene compounds. The conjugated π system has orbitals that are either in plane or perpendicular to the metal plane. If the HOMO or LUMO are in plane is dependent on the length of the chain. For even numbered chain the HOMO is perpendicular and the LUMO in the plane, which is reversed for odd length chains (**Figure 1.19**).[101,103] (The synthetic difficulties to prepare metallocumulenes with carbon chains longer than three carbon atoms are mainly due to the high reactivity of these species as they react as soon as they are formed.)

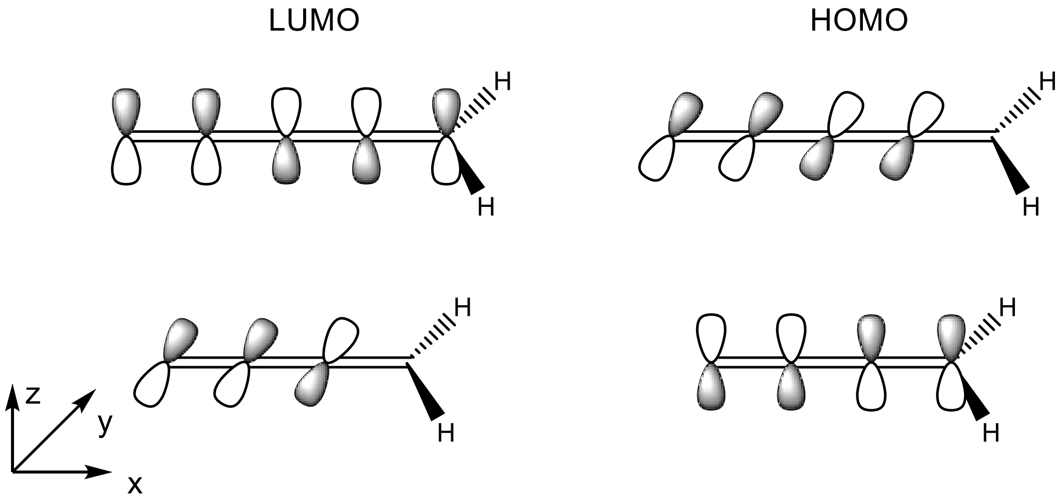

Figure 1.19: Molecular orbitals of odd and even chain cumulenes, C_5H_2 and C_4H_2

It is this difference in the orientation that causes the difference in the relative ease in the synthesis of odd numbered cumulenes compared to even as the main π accepting properties of the cumulene, which helps with stabilisation of the compound, are dependent on the position of the LUMO. The increase of reactivity with longer cumulenes correlates with a general decrease in the HOMO-LUMO gap, even with the odd/even alteration (**Table 1.1**).[104,105]

Table 1.1: Change in HOMO-LUMO gap with increasing chain length for $[(CO)_5Cr(=C)_nH_2]$ complexes, n = 3–9[105]

Chain Length	3	4	5	6	7	8
Orbital energy (eV)	1.10	1.50	0.80	1.10	0.60	0.80

Recent theoretical calculations have shown that organic cumulenes can sometimes form helical orbitals (**Figure 1.20**). For those with an odd chain length the terminal groups have to be perpendicular to each other, and for even length chains the addition of *trans* groups. Generally helical orbitals only occur when there is a loss of symmetry in the system.[106]

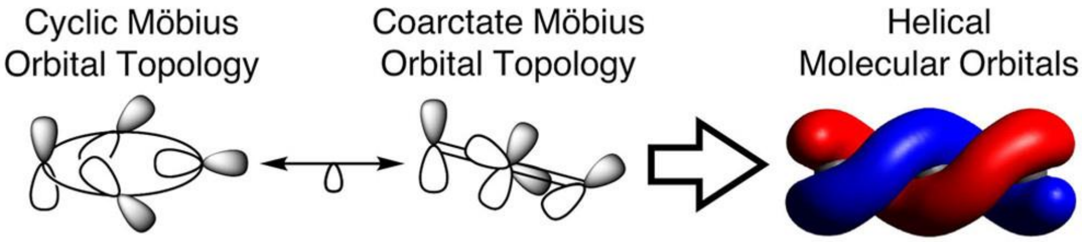

Figure 1.20: Basic rationalisation of the formation of helical orbitals. From Garner *et al.* 2018[106] **Reprinted from ACS central science, CC-BY-NC-ND licence**

Different stabilisation strategies involving the terminal substituents are needed dependent on the chain length because of the orientation of the orbitals. Various metals have been used in the stabilisation of cumulenes, commonly ruthenium,[51,82] but they have also been made using or iron[107] (or ferrocene),[108,109] manganese,[71] chromium,[95,96,110,111] tungsten,[95,110,111] molybdenum,[112] rhodium,[113] iridium,[92,114,115] rhenium,[116,117] osmium,[118] and even a *pseudo*-cumulene with neodymium (**Figure 1.21**).[119]

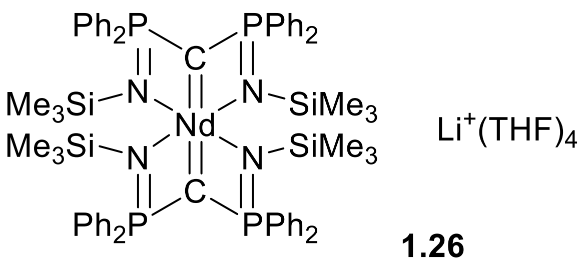

1.26

Figure 1.21: Neodymium pseudo-cumulene, 1.26

The structure and reactivity of cumulenes are closely linked. There is an overall trend in both the crystal structures obtained and theoretical calculations[120,121] that the double bond ligated to the metal is shorter than the average metal-carbon double bond, the next one in the chain is longer (**Figure 1.22**).[102]

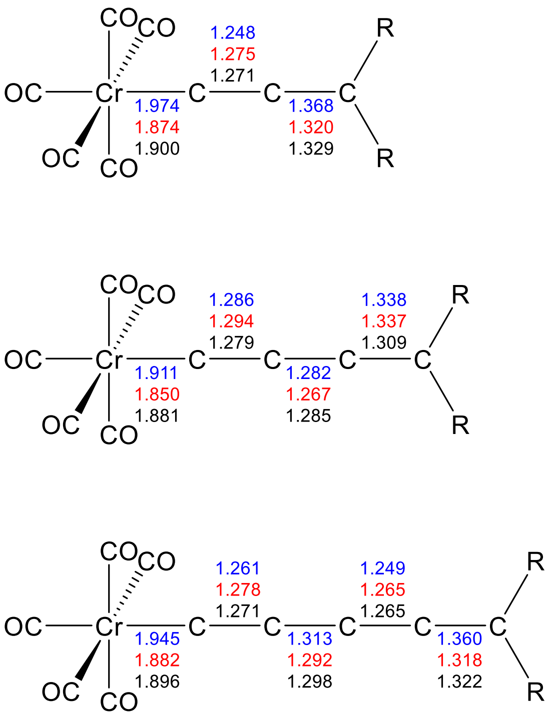

Figure 1.22: DFT-optimised bond lengths (Å) in [(CO)$_5$Cr(=C)$_n$R$_2$] complexes, n =3-5 and R = H (black), NH$_2$ (blue), or NO$_2$ (red).[102]

The trend in the relative lengths of the carbon-carbon bonds extends along the entire cumulene chain. This trend then influences the reactivity of the alternate carbons in the cumulene backbone so that electrophilic attack is more likely to occur at the even numbered carbons whereas nucleophilic attack is more likely at the odd numbered carbons.[51] Therefore cumulenes are molecules that can act as both electrophiles and nucleophiles which is uncommon making cumulenes an interesting class of molecules to study as they could play an important role on the synthesis more complex molecules. Vinylidene and allenylidene organometallic complexes, two of the shorter cumulenes, are known play a key role in many catalytic cycles[57,51] and it is believed that higher cumulenes could also serve the same purpose or serve as the building blocks for new polymers.[122]

1.3.3 Reactivity

Due to the high reactivity of cumulenes there is a high potential for reactions with many classes of compounds which could result in interesting new molecules. Most known reactions are for allenes (organic vinylidene compounds).[123] Theoretically cumulenes can react in the same ways that alkene complexes do, e.g. addition reactions[123], diels-alder reactions[124] and click reactions[125] as well as reactions catalysed by rhodium, palladium, copper, silver and gold. [123]

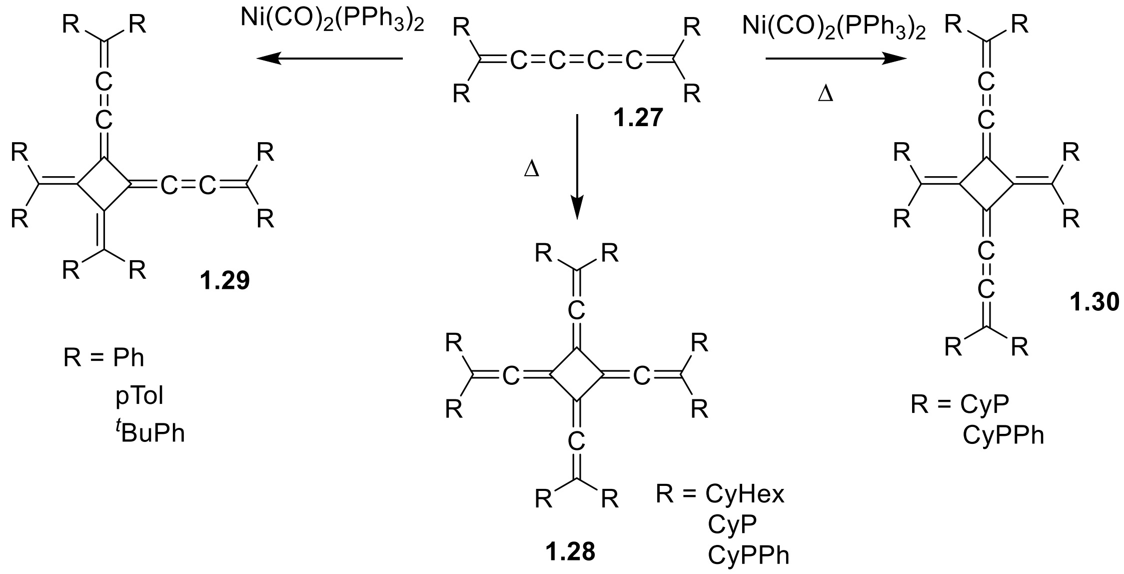

Scheme 1.13: Nickel catalysed dimerization of [5]cumulenes [126]

Longer cumulenes, such as **1.27**, have been shown to react in a 2+2 cycloaddition fashion, with a variety of alkenes[81] as well as with other cumulenes, or as dimerization reactions (**Scheme 1.13**).[126] In this paper it was shown that the conditions in which the cumulene is dimerized influences the carbon position in which the dimerization takes place. When heat is applied to the six-carbon cumulene a symmetrical 2+2 cycloaddition takes place, forming compound **1.28** that is symmetrical around the new four membered ring. However, when the nickel catalyst, $Ni(CO)_2(PPh_3)_2$, is used the major product is dependent on whether heat is applied to the reaction, **1.29**, or not, **1.30**. Both products are asymmetrical with the one at room temperature forming a '*cis*' product in either THF, DMF or benzene. Whereas, at reflux the '*trans*' product is formed in benzene.

Cyclodimerization reactions can also occur at the terminal carbons, forming large 12 membered rings with an alkyne bonding structure.[127]

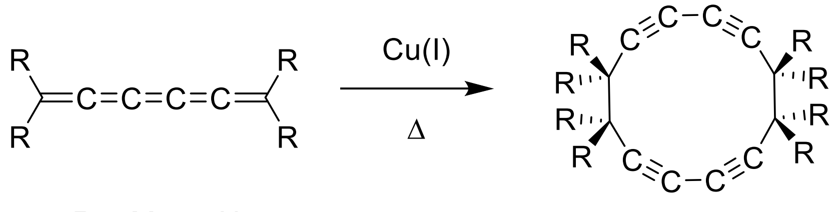

1.31

Scheme 1.14: Cyclodimerization of [5]cumulenes forming 1.31[127]

Cumulenes can also be involved in reactions with radical compounds, such as the addition of hydroxyl radicals.[123]

1.4. Cyclic carbon structures

Cumulenes hold specific interest in relation to materials chemistry where they have produced an array of interesting nano-scale structures including C-18 rings (**Figure 1.23**)[128–130] and macrocycles.[131]

The first synthesis and purification of a ring formed by 18 carbon atoms, with no other elements, was carried out in 1984[132] although it was an obscure, understudied compound for many years. In recent years it has been the subject of many academic papers, with 43 papers containing the phrase 'cyclo[18]carbon' since the beginning of 2020.[133] Before this time there were only 12 articles containing this word, and a few before that referenced 'cyclo[18]carbon' type structures without using this exact phrase. Most of the interest has been the debate surrounding which of the two theoretical allotropes of this molecule (**Figure 1.23**) is in the ground state. In either form this molecule is said to have 'double' aromaticity due to delocalisation of electrons in both planes of p-electrons (in plane and perpendicular to the ring).[134,135]

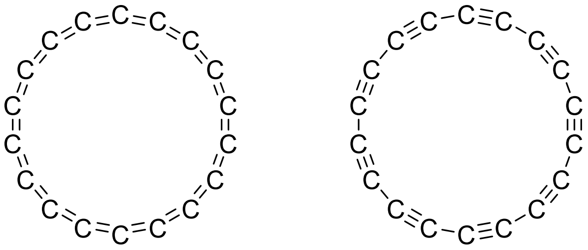

Figure 1.23: Isomers of the C-18 ring

It was determined through high-resolution atomic force microscopy that the most stable of the C-18 ring isomers is the alkyne form rather than the cumulenic form, as alternating bond lengths were observed.[130]

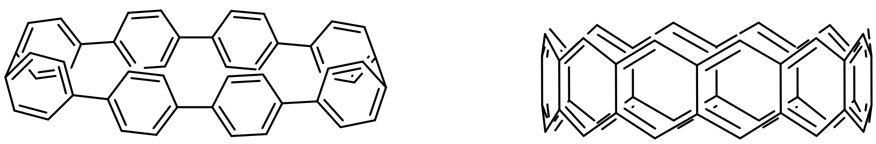

Figure 1.24: General structure of carbon nanohoops and nanobelts

Carbon-18 rings can also be thought of as a single slice from carbon nanotubes which are more common. Although not purely made of carbon both nanohoops[136–138] and nanobelts (**Figure 1.24**)[139] are also describes as slices of carbon nanotubes. Nanohoops are a relatively new class of compounds defined as an arrangement of aromatic sections that are curved out of planarity by the molecules cyclic structure. They were first synthesised in 2008,[136] despite being of scientific interest for many years.

1.5. Practical applications of cumulenes

There are multiple areas, generally in the field of molecular electronics and nanotechnology (particularly as molecular wires[140,141]) which makes cumulenes an interesting field of study with many potential applications as molecular electronic components or synthetic intermediates. Currently the longest chain cumulenes with real-world applications are vinylidenes which are used as catalysts in organic synthesis.[142]

These compounds are of particular interest in the field of molecular electronics, due to the theoretical calculations, which show the presence of helical orbitals.[106] Generally, when an electrical current is passed through a molecule the measured conductance decreases when the chain length is increased as there is a certain amount of inherent resistance in a molecule as the electrons must jump between molecular orbitals, as with polyyne compounds. However, with cumulenes this is the opposite, as chain length increases the conductance can increase slightly. The current theoretical understanding for this is that the π orbitals on each of the carbon atoms are rotated slightly, meaning that they form a continuous helical orbital along the length of the molecule. A helical orbital means that the electrons do not have to jump orbitals and therefore no energy is lost making the potential wire more efficient (**Figure 1.20**).[106]

It has also been shown theoretically that these helical orbitals contribute to an unusual increase in electronic transmission with molecular length (**Figure 1.25**).[121] When looking to turn small molecules into wires a loss of transmission is to be expected (and is seen in traditional metal wires), however, the reverse in the case of cumulenes make them interesting in this capacity. However, cumulenes are inherently unstable so isolating the longer cumulenes required for wires will be difficult.

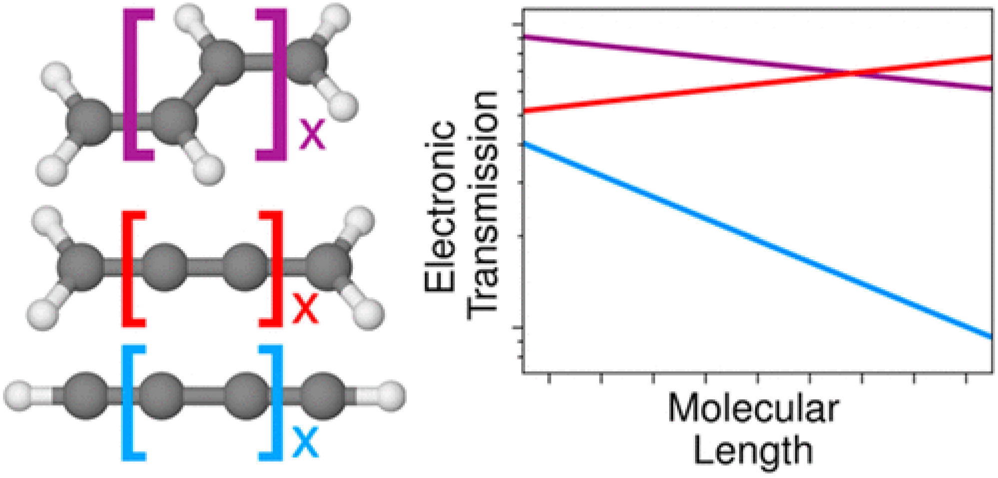

Figure 1.25: Electronic transmission vs molecular length for [n]alkenes (purple), [n]cumulenes (red) and [n]alkynes (blue). From Garner *et al.*[121] Reprinted with permission from *J. Phys. Chem. C* 2018, 122, 47, 26777–26789. Copyright 2018 American Chemical Society.

Other than molecular wires, another area of possible electronic interest for cumulenes is in transistors.[143] Tetraphenylbutatriene (**Figure 1.26**) was chosen as a model cumulene molecular semiconductor due to its thermal stability derived from the large terminal groups. It was discovered that it was possible to fabricate inherently well-behaved p-type field-effect transistors from pure tetraphenylbutatriene.

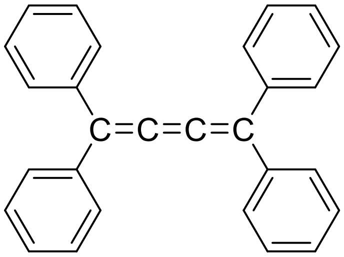

1.32

Figure 1.26: Structure of tetraphenylbutatriene, 1.32

The synthesis of and characterization of amorphous sp-sp^2 carbon films (20 % sp carbon contribution) was carried out with the dominant sp species being cumulenes, this was assembled at very low temperatures (150 K) and at high vacuum (~10^{-9}

mbar).[78] The cumulenes were stable up to roughly 250 K but rearranged into polyynes by 325 K. It was determined by Raman spectroscopy and current measurements that the presence of cumulenes in this system had an effect on the bulk electronic properties of the carbon system by decreasing the density of the sample.

1.6. Evidence for quinoidal cumulenes

As the synthesis and stabilisation of higher cumulenes, with a chain length of more than five carbons is difficult it was hypothesised that introducing an aromatic group into the chain may help with stabilisation of the longer cumulenes. Previous work in the Lynam and Low groups, performed by PhD student Samantha Eaves, has shown that an aryl-spaced cumulene is likely to be the intermediate in the reaction of metal-vinylidene *trans*-[Ru(=C=CH–C_6H_2-2,5-R_2-4-C≡CH)Cl$(dppm)_2$]$^+$ (R = H, R=Me) and [N^{n}Bu$_4$]Cl. The vinylidene was synthesised from *cis*-RuCl$_2$(dppm)$_2$ and 1,4-diethynyl benzene in the presence of TlBF$_4$ (**Scheme 1.15**).[144]

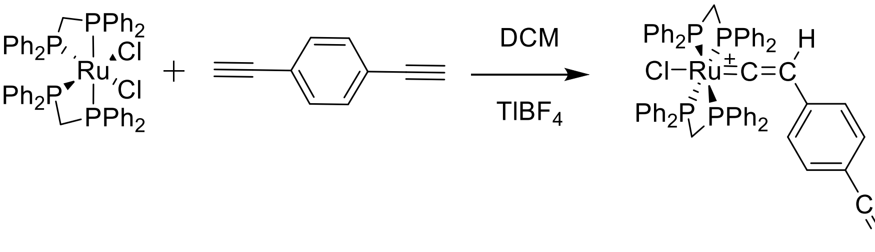

Scheme 1.15: Synthesis of vinylidene 1.33 from *cis*-RuCl$_2$(dppm)$_2$ and 1,4-diethynyl benzene

The subsequent reaction with [N^{n}Bu$_4$]Cl showed the addition of nucleophilic chloride to the anti-Markovnikov carbon to give *trans*-[Ru(C≡CC_6H_4-4-CCl=CH_2)Cl$(dppm)_2$], **1.32**. DFT calculations probing the mechanism of the addition of chloride across the alkyne showed that the most energetically favourable mechanism was *via* a cumulene intermediate (**Scheme 1.16**). The quinoidal cumulene could not be observed and it was calculated to be at a high energy reactive intermediate.

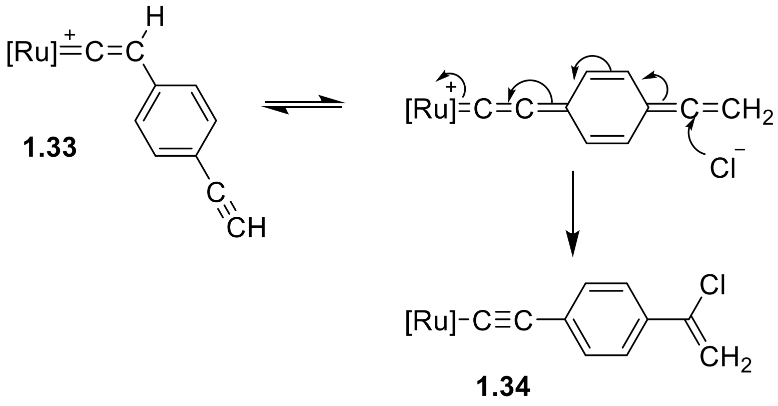

Scheme 1.16: Proposed mechanism for activation of the terminal alkyne by HCl

It has also been suggested that alternative aromatic spacers can be used to stabilise cumulene chains.[145] In this case a thiophene spacer was used on an iron metal centre, a series of up to two thiophene rings separated by alkynes was created through a variety of synthetic pathways (**Scheme 1.17**).

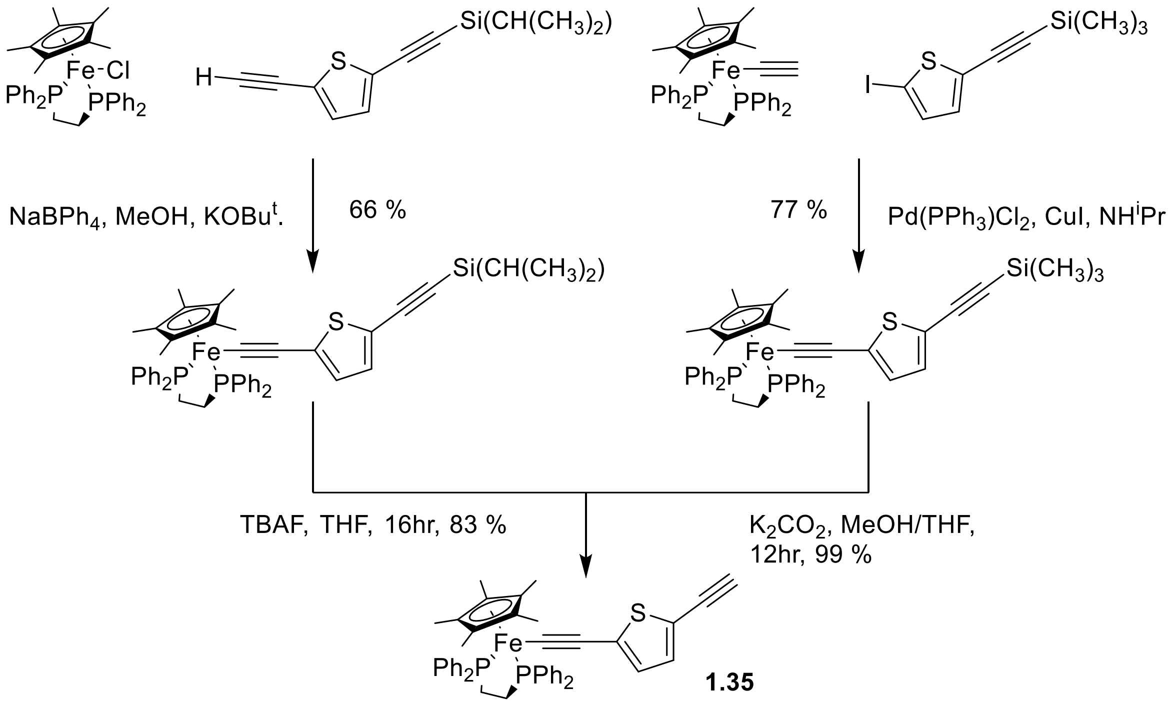

Scheme 1.17: Synthesis of thiophene spaced acetylide complex

According to cyclic voltammetry experiments the oxidised form of this molecule (**Scheme 1.17**) should have been stable, although chemical oxidation with $[Cp_2Fe][PF_6]$ resulted in a mixture of products which included both a diamagnetic complex, and a paramagnetic compound. Evidence from mass spectrometry indicated that the addition of one proton to the parent acetylide had occurred with the formation of the cumulene complex shown in **Figure 1.27**.

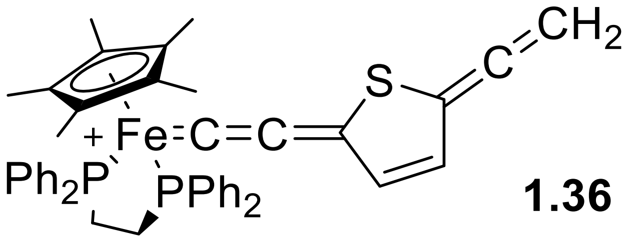

1.36

Figure 1.27: Proposed structure of thiophene spaced cumulene, 1.36

1.7. Aims and Objectives

The aim of this project was to prepare metal cumulene complexes and exploit their reactivity in carbon-carbon and carbon-hetero atom bond forming reactions. As seen in the literature aromatic spacer groups can be utilised in order to stabilise longer chain cumulenes. Due to the large volume of literature utilising ruthenium as a stabilising group for cumulenes, the focus of this project was using ruthenium metal fragments. The general structure for these compounds is seen in **Figure 1.28**, involving at least one metal-containing fragment, an aromatic spacer group and a terminal group, which may either be an organic fragment or a second metal fragment. Both ruthenium bis-dppe and ruthenium half sandwich complexes were used and compared.

M=C=C=Ar=C=C=T

M = metal fragment
Ar = aromatic spacer group
T = terminal group

Figure 1.28: General structure of cumulenes stabilised by a metal fragment and an aromatic spacer group

As there is literature precedence for the stabilisation of cumulenes with use of the 1,4-diethynylbenzene spacer group this is where this work started, followed but the use of other spacer groups e.g. 9,10-diethynyanthracene, 1,4-diethynynaphthalene, and 4,7-diethynybenzo[1,2,5]thiadiazole, which theoretically should form a cumulene intermediate easier as there is less aromatic stabilisation energy to overcome when the cumulene is formed (**Figure 1.29**). The last is also known to form polymeric complexes with a stable low-energy band gap.[146] It was believed that by utilising these effects the chain length of isolable cumulene complexes could be increased.

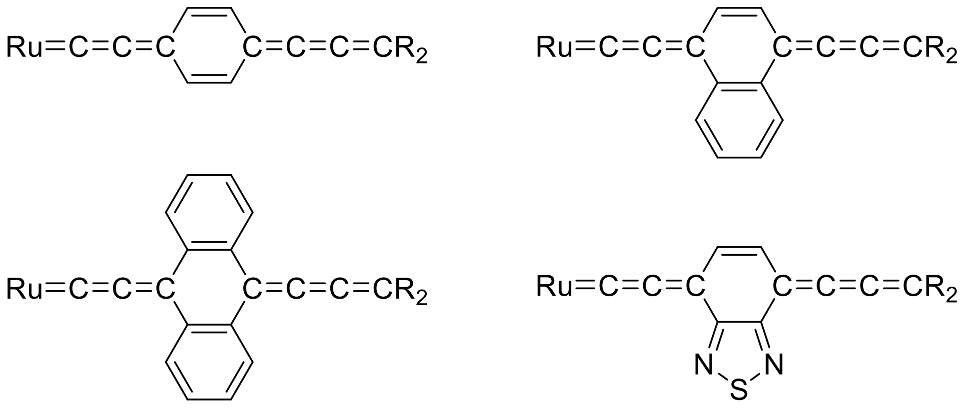

Figure 1.29: Target cumulated compounds with different aromatic spacer groups

Stability of cumulenes can also be increased through sterically bulky terminal groups, therefore multiple terminal groups were utilised in an attempt to stabilise the cumulenic intermediates. Once cumulenic chains, or their precursors were produced, it was then important to probe their reactivity and electrochemical properties to determine if they are good candidates for catalytic uses or in molecular electronics.

Chapter 2 Benzene-spaced cumulenes

1.1 Bis-(dppe) Compounds

Building upon the work done by Eaves *et al.*[144] (**Section 1.6**) the synthesis and reactivity of the vinylidene *trans*-$[RuCl(=C=CH–C_6H_4\text{-}4\text{-}C≡CH)(dppm)_2]^+$ and the analogous acetylide *trans*-$RuCl(C≡CH–C_6H_4\text{-}4\text{-}C≡CR)(dppm)_2$ (R = H, $(CH_3)_2OH$, C_6H_4-4-OMe or C_6H_4-4-CO_2Me) towards nucleophiles were investigated here. As the Eaves' method for preparation of the vinylidene precursor involved the use of thallium tetrafluoroborate, which is an excellent halide abstractor but very toxic, a different synthetic method was desirable. The spectator ligands were therefore changed from 1,1-*bis*(diphenylphosphino)methane (dppm) to 1,1-*bis*(diphenylphosphino)ethane (dppe) in order to access the stable five-coordinate species $[RuCl(dppe)_2]^+$ as a precursor which in turn can be obtained from *trans*-$RuCl_2(dppe)_2$ without using thallium salts, but instead using silver[147] or sodium.[148]

The five-coordinate $[RuCl(dppe)_2][OTf]$ reagent was synthesised from $RuCl_3.nH_2O$ in three steps following the literature procedure[147] with an overall yield of 82 % (**Scheme 2.1**).

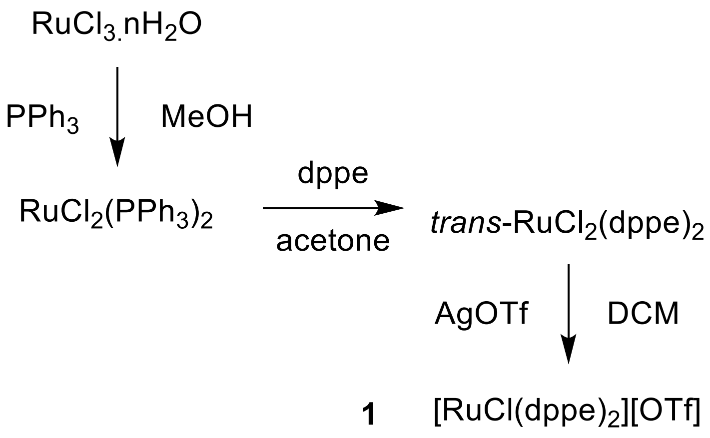

Scheme 2.1: Synthesis of $[RuCl(dppe)_2][OTf]$, 1, from $RuCl_3.nH_2O$

2.1 *trans*-[RuCl(=C=CHC$_6$H$_4$-4-C≡CH)(dppe)$_2$][OTf]

The reaction of [RuCl(dppe)$_2$][OTf], **1**, with 1,4-diethynylbenzene under an inert nitrogen atmosphere resulted in the formation of two different products, *trans*-[RuCl(=C=CHC$_6$H$_4$-4-C≡CH)(dppe)$_2$][OTf], **2**[OTf], and a bimetallic vinylidene species, *trans*-[(RuCl(dppe)$_2$)$_2$(=C=CHC$_6$H$_4$-4-CH=C=)]$_2$[OTf] (**3**[2OTf]), shown in **Figure 2.1**. Stoichiometric reactions of [RuCl(dppe)$_2$][OTf] with 1,4-diethynylbenzene achieved almost full conversion to **2**[OTf] after 30 minutes (**Scheme 2.2**), however after 20 hours there appears to be an increase in the amount of **3**[2OTf], as shown by ^{1}H and ^{31}P{^{1}H} NMR.

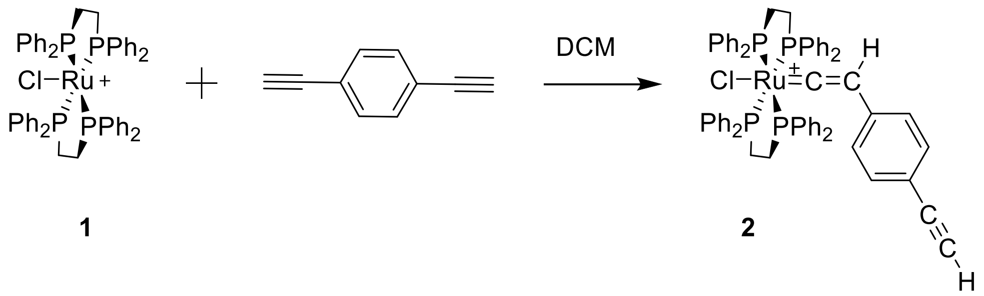

Scheme 2.2: Reaction of [RuCl(dppe)$_2$][OTf], 1, with 1,4-diethynylbenzene to form [RuCl(=C=CHC$_6$H$_4$-4-C≡CH)(dppe)$_2$][OTf], 2[OTf]

The reaction of **2**[OTf] with 2 equivalents of diethynyl benzene gave the vinylidene within 30 min. However, a stoichiometric reaction or reactions carried out over longer time periods resulted in formation of a bimetallic ancillary product. On a 250 mg scale it was then possible to produce and purify **2**[OTf] with a yield of 80 %.

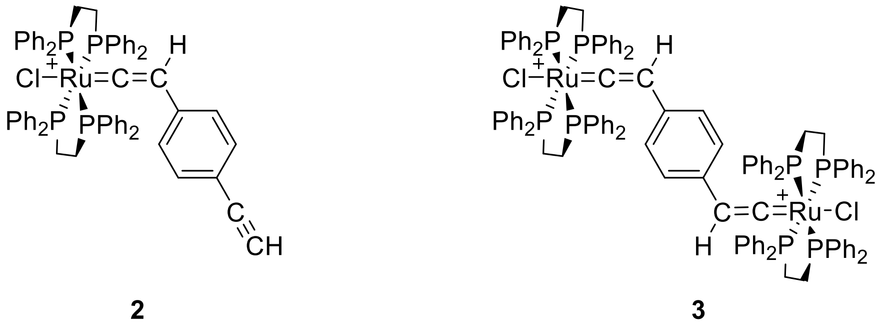

Figure 2.1: *trans*-[RuCl(=C=CHC$_6$H$_4$-4-C≡CH)(dppe)$_2$][OTf], 2[OTf], and a bimetallic species, 3[2OTf]

The ^{1}H NMR spectrum of **2**[OTf] displayed four peaks of interest: a singlet resonance at 3.08 ppm from the terminal alkyne proton, a quintet at 3.39 ppm (J_{HP} = 2.7 Hz) which is indicative of the vinylidene proton coupled to the four phosphorus nuclei bonded to ruthenium, and two doublet peaks at 5.60 and 6.83 ppm (J_{HH} = 8.3 Hz) for the protons of the 1,4-disubstituted phenyl ring. The aliphatic ^{1}H resonances for the aliphatic protons of the dppe ligand were observed as two multiplets at 2.78 and 2.97 ppm whilst the aromatic resonances were found between 7.06 and 7.37 ppm. A single phosphorus resonance was observed at 38.2 ppm indicating that the chloride and vinylidene ligands are mutually *trans* around the metal centre. The ^{13}C{^{1}H} NMR spectrum showed a small, distinctively low field resonance at 355.4 ppm which is characteristic of a vinylidene α-carbon,[149] and the β-carbon resonance at 109.6 ppm. This NMR analysis was supported by an accurate mass ESI-MS spectrum, which exhibited an ion envelope at *m/z* of 1023.2179 with an appropriate ion-pattern for **2**$^+$ with the chloride ligand lost, $[C_{62}H_{54}P_4Ru]^+$. The dissociation of the chloride ligand from the parent ion is a common feature of such compounds.[150]

In contrast to **2**[OTf] as **3**$[OTf]_2$ is a centrosymmetrical molecule only one doublet resonance, at 5.68 ppm (J_{HH} = 8.36 Hz), was observed for the spacer group as the molecule consistent with all the protons are in the same environment. Only a small shift in the ^{31}P{^{1}H} NMR spectrum from **2**[OTf] was seen from 38.2 to 38.9 ppm as the phosphorus environments are similar. This is known and was synthesised by Dixneuf[151] from $[RuCl(dppe)_2]PF_6$ and 1,4-di(1-hydroxyprop-2-yn-1-yl)benzene. The structure of the bimetallic complex was confirmed by X-ray diffraction, grown by slow diffusion from CD_2Cl_2 (**Figure 2.2**).

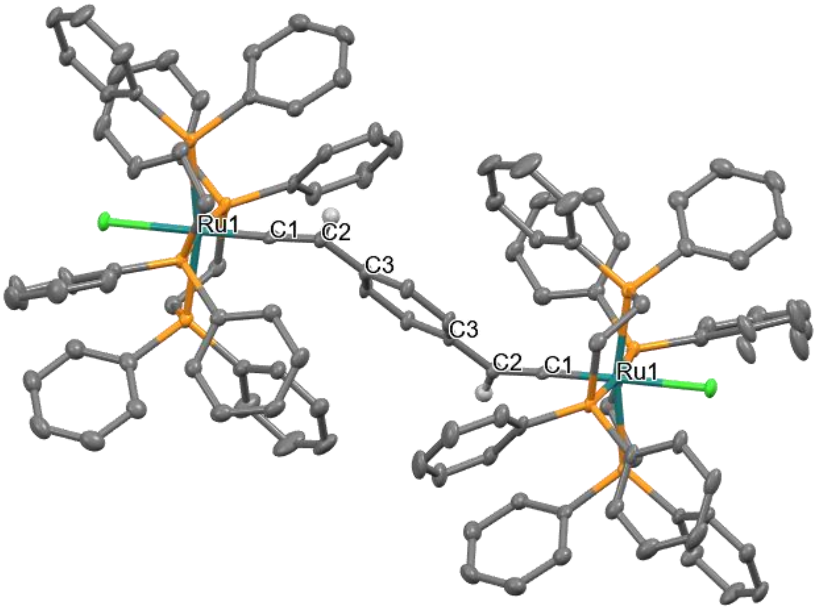

Figure 2.2: Molecular structure of compound 3, *trans*-[(RuCl(dppe)$_2$)$_2$(=C=CHC$_6$H$_4$-4-CH=C=)][OTf]$_2$ as determined by single crystal X-ray diffraction. Thermal ellipsoids are shown at the 50% level, DCM molecules, OTf anions and most hydrogen atoms omitted for clarity. Grey = C, White = H, Dark green = Ru, Bright green = Cl, Orange = P

When comparing the crystal structure of **3**[OTf]$_2$ to the crystal structure seen for the half-sandwich mono(vinylidene) complex Ru((=C=C(H)-C$_6$H$_4$-C≡CH)(dppe)Cp*, **4**, (**Figure 2.3**) similar atom placements were observed for the comparable parts of the structures. The bond between the ruthenium and the α carbon is 1.848(4) Å in compound **3** whereas it is 1.86(2) Å in compound **4**, the bond to the metal is normally elongated due to the large atomic size of ruthenium. The distance between the α and β carbons is then significantly shorter than the bond to the metal at only 1.296(5) Å which is almost identical to this bond length in compound **4** at 1.30(2) Å. Between the β and γ carbon the atomic distance is increased again up to 1.470(5) Å for compound **3** (which is again close to the length of 1.48(2) Å for compound **4**) as this bond is a single bond rather than a double. The aromatic carbon distances are in the expected region between 1.390(5) and 1.396(5) Å (these are between 1.38 (2) and 1.45 (2) Å for compound **4**). The bond angles from Ru-C(1)-C(2) was observed at 176.9(3)° which is almost linear in nature as expected for cumulenic structures, for comparison this bond angle for compound **4** (**Figure 2.3**) is not quite as linear with a bond angle of 171(1)°. The other bond angle of interest is the C(1)-C(2)-C(3) angle which is 128.1(3)°, compared to 130(1)°, this angle indicates two groups are bonded to the β carbon, those being the aromatic spacer group and a proton.

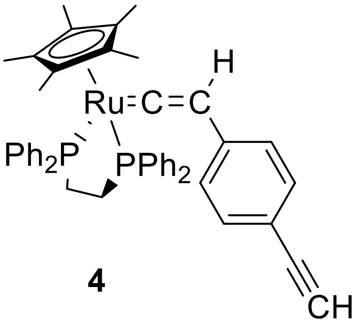

4

Figure 2.3: The model vinylidene cation, 4, [Ru(=C=C(H)-C_6H_4-C≡CH)(dppe)Cp*]$^+$; the crystal structure of the BF_4 salt having been determined by Hall *et al.*[152]

The formation of **2**[OTf] *via* this simple addition reaction, as seen in Eaves *et al.*[144] indicates that the *bis*-dppe complex is likely to have similar reactivity to the *bis*-dppm compound and mean that thallium can be replaced with silver as a halide abstractor.

2.1.1 Reactions *trans*-[RuCl(=C=CHC_6H_4-4-C≡CH)$(dppe)_2$][OTf] with nucleophiles

2.1.1.1 Reaction of [2]OTf with water

During the synthesis of *trans*-[RuCl(=C=CH–C_6H_4-4-C≡CH)$(dppe)_2$][OTf], **2**, evidence was obtained for a compound which appeared to be the result of water addition to the seventh carbon in the chain in a Markovnikov fashion in relation to the terminal alkyne (**Figure 2.4**) followed by a rearrangement, which is consistent with the understanding that cumulenes can form *in situ* from this ligand (**Scheme 2.3**). Evidence for the formation of **5**[OTf] was provided by mass spectrometry with a peak at 1041.2313 *m/z* corresponding to the product with the loss of HCl. Slight changes in the NMR spectra confirmed a change from **2**[OTf], especially the ^{1}H NMR singlet peak at 2.52 ppm which was lower than the terminal alkyne proton in **2**[OTf] and had an integration of 3H in comparison to the spacer group protons. This is consistent with the presence of an acyl group. The resonances for the aromatic spacer group are at 6.57 and 7.68 ppm (J_{HH} = 8.4 Hz). Only a slight shift was seen in the ^{31}P NMR at 37.8 ppm from 28.2 ppm for **2**[OTf]. The two dppe ligands have very similar resonances in the ^{1}H and ^{13}C{^{1}H} NMR spectra regardless of the ligand of interest. For this compound, the aliphatic ^{1}H resonances can be observed as a multiplet at 2.70 ppm, and the aromatic resonances as triplets at 6.93, 7.06, 7.18 and 7.25 ppm with the same J_{HH} value at 7.6 Hz and doublets at 7.30 (J = 6.6 Hz) and 7.43 ppm (J = 6.9 Hz). In the ^{13}C{^{1}H} NMR spectrum the *para* carbons can be seen at 127.4 and 127.6 ppm, the *meta* carbons at 129.2 and 129.6 ppm, the *ortho* carbons at 134.2 and 135.0 ppm and finally the *ipso* carbons at 130.2 and 136.5 ppm.

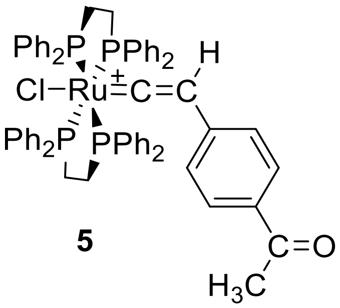

5

Figure 2.4: Structure of *trans*-[RuCl(=C=CHC$_6$H$_4$-4-C=OCH$_3$)(dppe)$_2$][OTf], 5[OTf]

To try and understand the mechanism through which **5**[OTf] was formed, 1 µL (3.3 eq.) of water was added to 20 mg of isolated **2**[OTf] in dry DCM-d_2. The subsequent reaction was monitored by ^{1}H NMR spectroscopy and a clear additional peak in the spectrum at 1.5 ppm for water was observed: the rest of the spectrum remained unchanged. Using undried DCM-d_2, which had a water content of between 33.7 and 47.3 ppm, to run an NMR spectrum also showed no change. This indicates that once [**2**]$^+$ is formed, no direct reaction with water occurs, and means that **5**[OTf] is formed through an alternative pathway.

When a stoichiometric amount of HBF$_4$.OEt$_2$ was used the same colour change to a darker red occurred during the reaction. After 1 hour the NMR spectra of the reaction mixture showed a variety of products, possibly up to 4 different spacer group doublets were observed. However, after 3 days the spectra showed the hydrated species, **5**[OTf] as the major product, this indicates that this is the thermodynamic product of the reaction and that **2**[OTf] will react with any residual water in the system when acid is present. The mass spectrometry data showed a peak at 1077.20 m/z, also consistent with [**5**]$^+$.

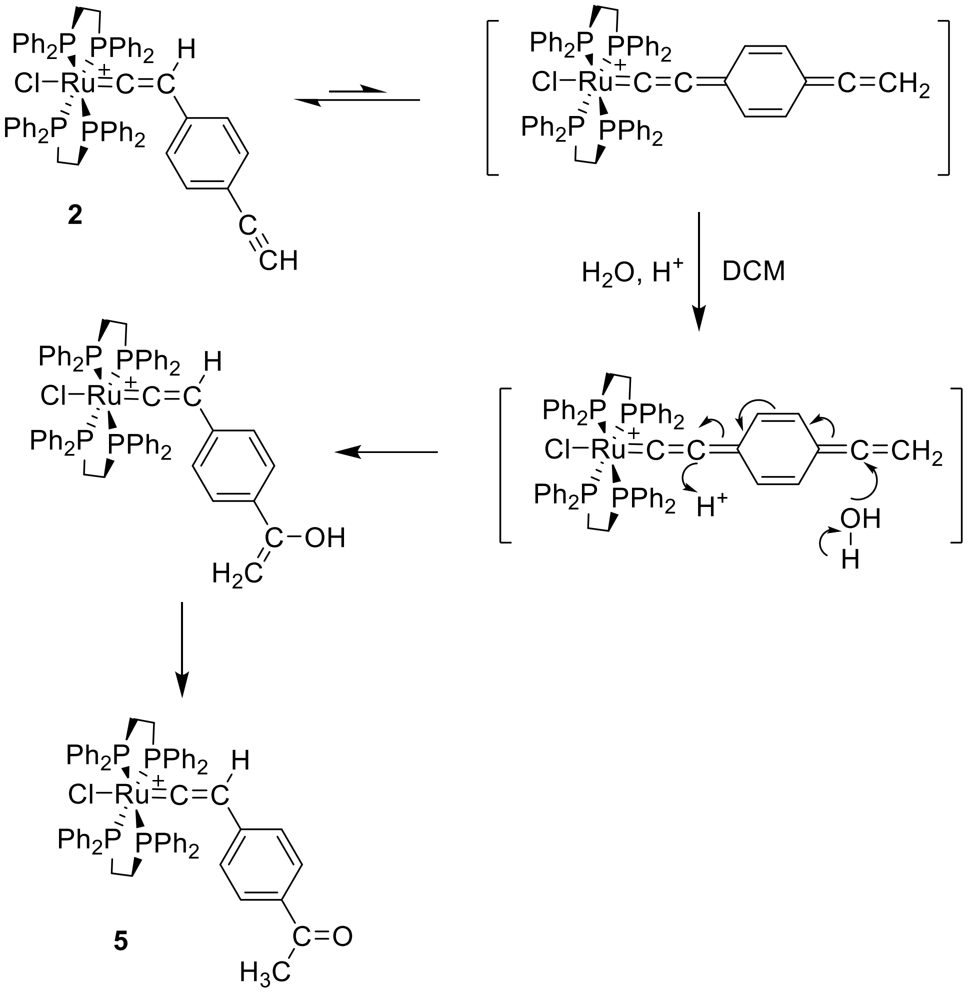

Scheme 2.3: Addition of water to the terminal alkyne, [2]$^+$, through a cumulene intermediate to form compound [5]$^+$

To further investigate the hypothesis that the water addition is being assisted by the presence of acid, **2**[OTf] was dissolved in wet chloroform-*d* which is known to accumulate a small amount of HCl over time;[153] the sample of the solvent used had a pH of approximately 5 as shown by universal indicator paper. After one hour the presence of **5**[OTf] was detected by ^{1}H NMR spectroscopy through growth of a doublet resonance at 5.70 ppm (J_{HH} = 8.2 Hz) for two of the protons of the aryl spacer group (the other doublet was overlapped with the dppe resonances) and three aliphatic hydrogen resonances at 2.41 ppm which corresponds to the CH_3 group in [**5**]$^+$, 2.94 ppm arising from the backbone of the dppe ligand in either compound and 3.16 ppm from the terminal alkyne proton of unreacted [**2**]$^+$. These data indicated that the additional acid present in the $CDCl_3$ solution was important in promoting the conversion of [**2**]$^+$ to [**5**]$^+$, which is consistent with the previously published work.[144] This study indicates that a proton transfer step is required to form cumulene [**6**]$^+$ (**Figure 2.5**), and acts as a further evidence for its role in the chemistry of these species. Although it should be possible to form a small amount of compound **6** in the absence of acid, the addition helps in the formation of **6**.

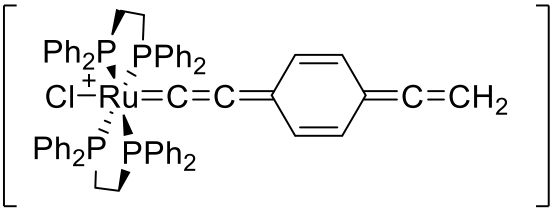

Figure 2.5: Proposed cumulene intermediate, 6

An authentic sample of complex **5**[OTf] may also be prepared by a reaction of the [RuCl(dppe)$_2$][OTf] with 4-ethynylacetophenone (**Scheme 2.4**). The reaction of stoichiometric amounts [RuCl(dppe)$_2$][OTf] with 4-ethynylacetophenone gave **5**[OTf] as a red powder in 79 % yield after stirring in either dry DCM or dry MeOH under nitrogen for 1 hour. The product was purified through the removal of the solvent under vacuum and washing with diethylether and hexanes. The characterisation data were the identical to when **5**[OTf] was produced through the addition of water to **2**[OTf].

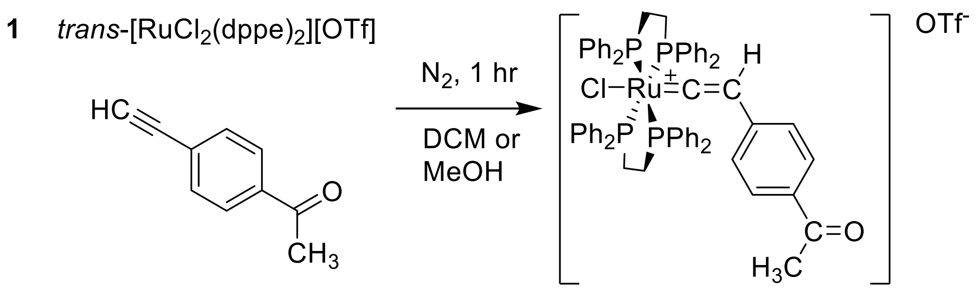

5

Scheme 2.4: Alternative synthesis of 5[OTf] from 4-ethynylacetophenone

Crystals of complex **5**[OTf] suitable for X-ray diffraction were obtained from DCM solution (**Figure 2.6**). The bond angles derived from the crystal structure are as expected for a half-sandwich acetylide complex. The Ru-C(1)-C(2) angle was 175.9(2)° which is close to the idealised 180°, as is common with vinylidenes and cumulenes,[51] the slight bend can be attributed to a mix of the steric effects from the vinyl proton as well as the dppe ligands. The bond lengths around the carbonyl group are very similar to those of the organic acetophenone,[154] 1.488(3) Å for C(6)-C(9) (vs. 1.494(2) for acetophenone), 1.509(4) Å for C(9)-C(10) (vs. 1.499(2) for acetophenone) and 1.211(3) Å for C(9)-O(1) (vs. 1.216(2) for acetophenone), this similarity to the free acetophenone is expected as this fragment of the ligand is far from the metal centre and therefore acts like an organic compound. The bond length for Ru=C(1), 1.836(2) Å, is longer than for the C(1)=C(2) bond, 1.313(3) Å. These are within the expected range for these kinds of bonds with literature values for Ru=C(1) between 1.780(8) and 1.862(7), and between 1.24(1) and 1.352(0) Å for C(1)=C(2).[155]

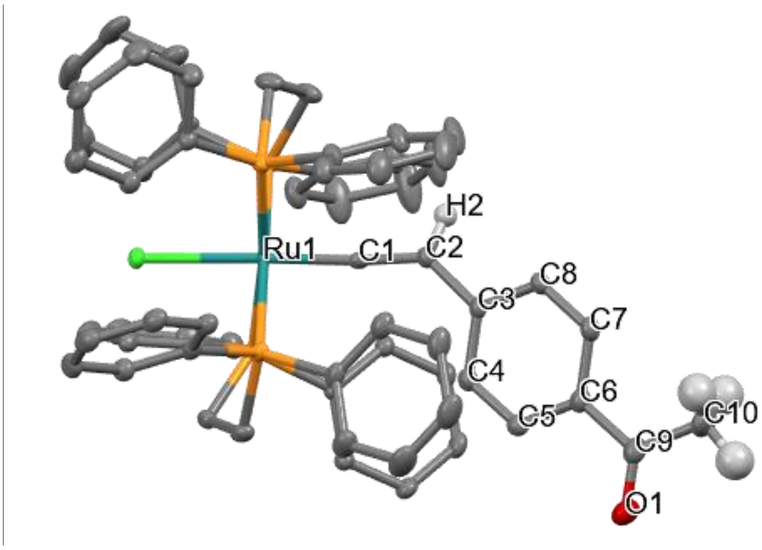

Figure 2.6: Molecular structure of compound 5, *trans*-[RuCl(=C=CHC$_6$H$_4$-4-C=OCH$_3$)(dppe)$_2$][OTf] as determined by single crystal X-ray diffraction. Thermal ellipsoids are shown at the 50 % level, DCM molecules, OTf anion and hydrogen atoms omitted for clarity. Grey = C, White = H, Dark green = Ru, Bright green = Cl, Orange = P, Red = O.

A control reaction of phenyl acetylene, the organic analogue of **2**$^+$, with HBF$_4$.OEt$_2$ showed no reactivity. This proves that the ruthenium is required for the reaction to proceed, likely because it stabilises the proposed cumulene intermediate.

Addition of the very strong acid, triflic acid (pKa = -14) to **2**[OTf] caused an immediate colour change to black. When monitored overnight (for 18 hours) by NMR spectroscopy the number of products observed increased from two (compounds [**2**]$^+$ and [**5**]$^+$) to five, as determined by the number of spacer group resonance pairs. These additional spacer group protons appeared at 5.75 and 5.49 ppm, 5,70 and 5.45 ppm and 5.47 and 5.25 ppm (**Figure 2.7**). However, no new ^{31}P{^{1}H} NMR resonances were observed, but the major product changed from the resonance at 37.66 ppm to 37.32 ppm. This is likely the change from [**2**]$^+$ being the major product to [**5**]$^+$ as the acid leads to further reaction with water.

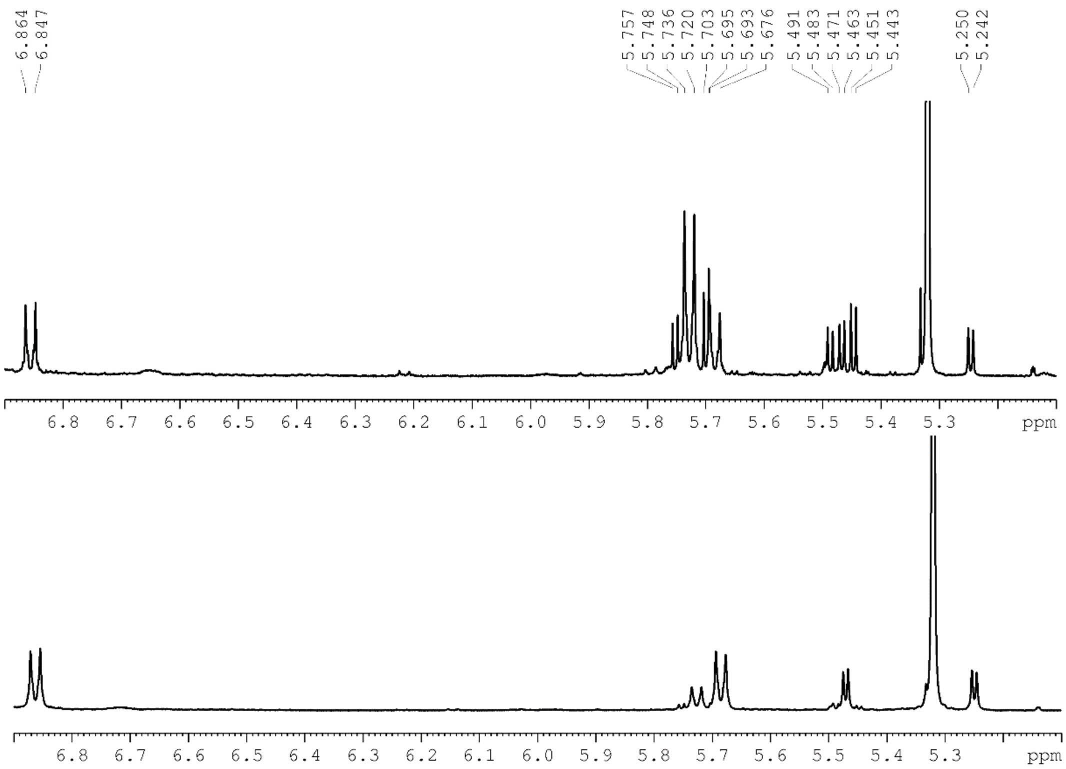

Figure 2.7: NMR data, between 5.1 and 6.9 ppm, showing the progression of the reaction between compound 2, *trans*-[RuCl(=C=CH–C_6H_4-4-C≡CH)(dppe)$_2$][OTf], and triflic acid. Bottom spectrum = after 10 mins, top spectrum = after 18 hours.

2.1.1.2 Addition of *N*-methyl pyrrole to 1[OTf]

As the addition of water to **2**[OTf] occurs at the electrophilic carbon in the cumulene chain it may be possible to observe the addition of other nucleophiles at the same position on the chain.[88] *N*-methylpyrrole (**Figure 2.8**) was chosen as it is a nucleophile but it is also not basic which will ensure that simple deprotonation of the vinylidene ligand in **2**[OTf] will not occur.

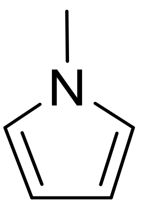

Figure 2.8: Structure of *N*-methylpyrrole

The addition of two or more equivalents of N-methylpyrrole to **2**[OTf] in dry DCM did not lead to any resonance in the ^{1}H NMR spectrum that could not be assigned to the starting materials. The subsequent addition of 1 equivalent of $HBF_4.OEt_2$ led to an immediate colour change of the solution from red to black and eventually to a dark blue over two days. When using double the amount of $HBF_4.OEt_2$ with the same reaction conditions gave a blue solution immediately.

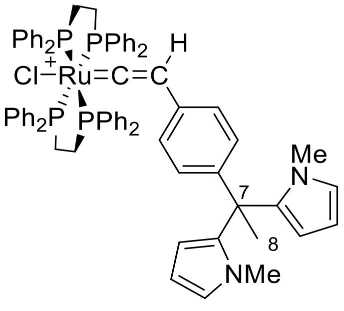

7

Figure 2.9: ***trans*-[RuCl(=C=CHC$_6$H$_4$-4-C(C$_4$H$_3$NCH$_3$)$_2$CH$_3$)(dppe)$_2$][OTf or BF$_4$], [7]$^+$**

Analysis of the resulting *in situ* spectroscopic data proved that a new vinylidene species was formed, in which two *N*-methylpyrrole molecules were added to the seventh carbon of the organic ligand, across the terminal alkyne (**Figure 2.9**). Three different aliphatic proton environments were observed in the ^{1}H NMR analysis: at 3.05 ppm, a singlet with an integration of three, attributed to a CH_3 group as the terminal carbon, at 3.30 ppm the vinylidene proton with quintet splitting and finally 3.59 ppm with an integration of 6 and a similar shift to the methyl group of the free *N*-methylpyrrole (3.63 ppm). There were significant changes in the positions of the aromatic *N*-methylpyrrole protons during the addition to **2**[OTf], from a symmetrical molecule with two triplet resonances at 6.06 and 6.59 ppm (J_{HH} = 2.1 Hz), to an unsymmetric molecule with three apparent triplet resonances at 5.80, 6.19 and 6.53 ppm, this shift could be attributed to a reduction of shielding due to the loss of one proton. The $^{13}C\{^1H\}$ NMR spectrum also showed a distinctive resonance for the metal-bound vinylidene carbon at 335.1 ppm and peaks at 35.2 ppm (the terminal CH_3 carbon) and the adjacent quaternary carbon with a resonance of 137.6 ppm.

A singlet resonance in the $^{31}P\{^{1}H\}$ NMR spectrum attributed to [**7**]$^{+}$ was observed at 40.4 ppm as well as a smaller resonance at 37.7 ppm which is attributed to **5**[OTf]. This tells us that the product, purified by washing with hexane and ether, is not completely pure, however, the conditions of the reaction are such (requiring the addition of an acid catalyst) that the formation of compound **5**[OTf] can be seen as an unavoidable by-product. However, when using tribromoacetic acid, which exists as a powder, in place of $HBF_4.OEt_2$ a reduced amount of [**5**]$^{+}$ was observed. This is likely because this acid can be more effectively dried than $HBF_4.OEt_2$. This was true even upon heating for 45 minutes. This indicates that although compound [**5**]$^{+}$ can be formed in situ, from [**2**]$^{+}$, acid and water, it is reversible and can be used as a starting material for other products. A peak in the mass spectrum at 1221.31 *m/z*, corresponds to the addition of two *N*-methylpyrrole units and subsequent loss of Cl and a proton, which is common with this metal fragment.

This addition to an odd number carbon is constant with the theory that the intermediate in a cumulene, as odd numbered carbons are slightly electrophilic in character. Although the exact carbon on the *N*-methylpyrrole ring which reacted with compound [**2**]$^{+}$ could not be determined, even with the use of 2D NMR, there is precedent for electrophilic addition at the carbon *ortho* to the nitrogen through literature[88,156] of similar *N*-methylpyrrole addition compounds, as well as an understanding of the stabilisation of intermediates through resonances.

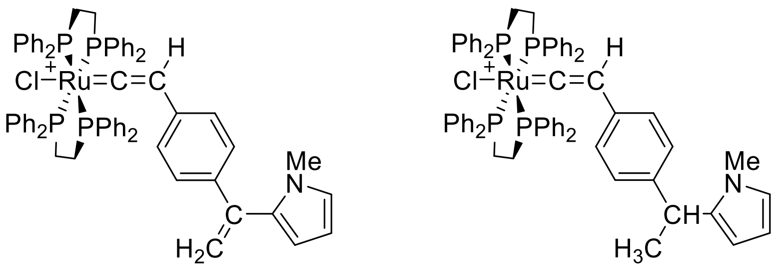

8a **8b**

Figure 2.10: Two possible structures for the addition of a single *N*-methylpyrrole molecule, 8a and 8b

The two theoretical addition products arising from addition of single *N*-methylpyrrole (**Figure 2.10**) can be discounted as present due to the presence of a CH_3 group, both from integrals in relation to the spacer group protons and the data from the multiplicity edited HSQC spectra which showed this resonance to be either a CH or CH_3 group which rules out complex **8a**. In addition, compound **8b** is excluded due to the lack of a CH proton, which would have been expected to be present on the 7th carbon.

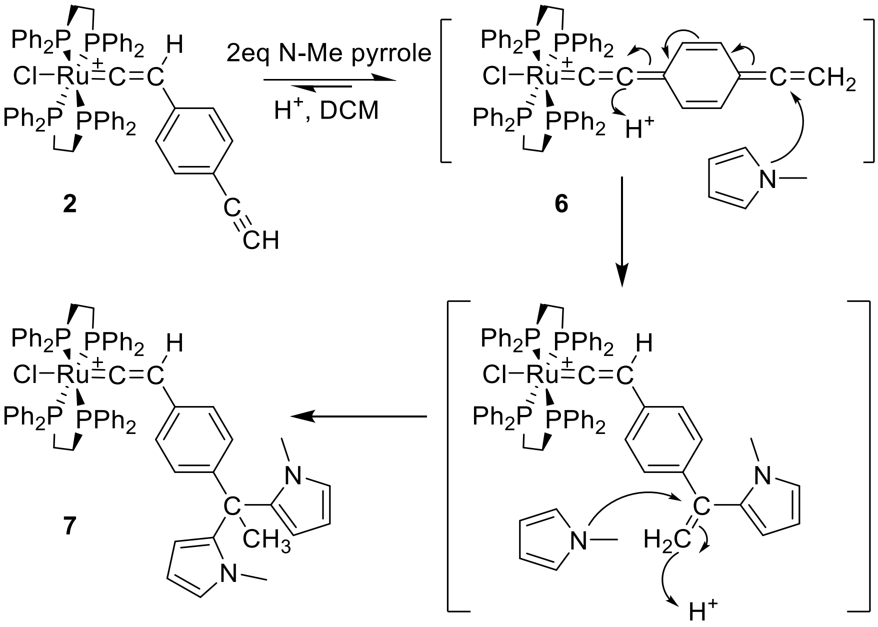

Scheme 2.5: Proposed mechanism for the addition of 2 N-methylpyrrole molecules to compound 2, *trans*-[RuCl(=C=CH–C_6H_4-4-C≡CH)(dppe)$_2$][OTf]

The proposed mechanism for the sequential addition of two *N*-methylpyrrole molecules to [**2**]OTf uses two different pathways for the first and second addition (**Scheme 2.5**). The addition of the initial molecule of *N*-methylpyrrole is likely to occur via a cumulene intermediate state, which is consistent with other reactions of [**2**]OTf with nucleophiles. However, the addition of the second molecule of *N*-methylpyrrole must occur via a different mechanism because if the compound was to return to the cumulene intermediate it would, by definition, lose the first molecule of *N*-methylpyrrole. It is very unlikely that it occurs via simultaneous addition of both molecules to the cumulene. Therefore, the most likely mechanism for the addition of the second molecule of *N*-methylpyrrole is through conventional nucleophile addition to the alkene.

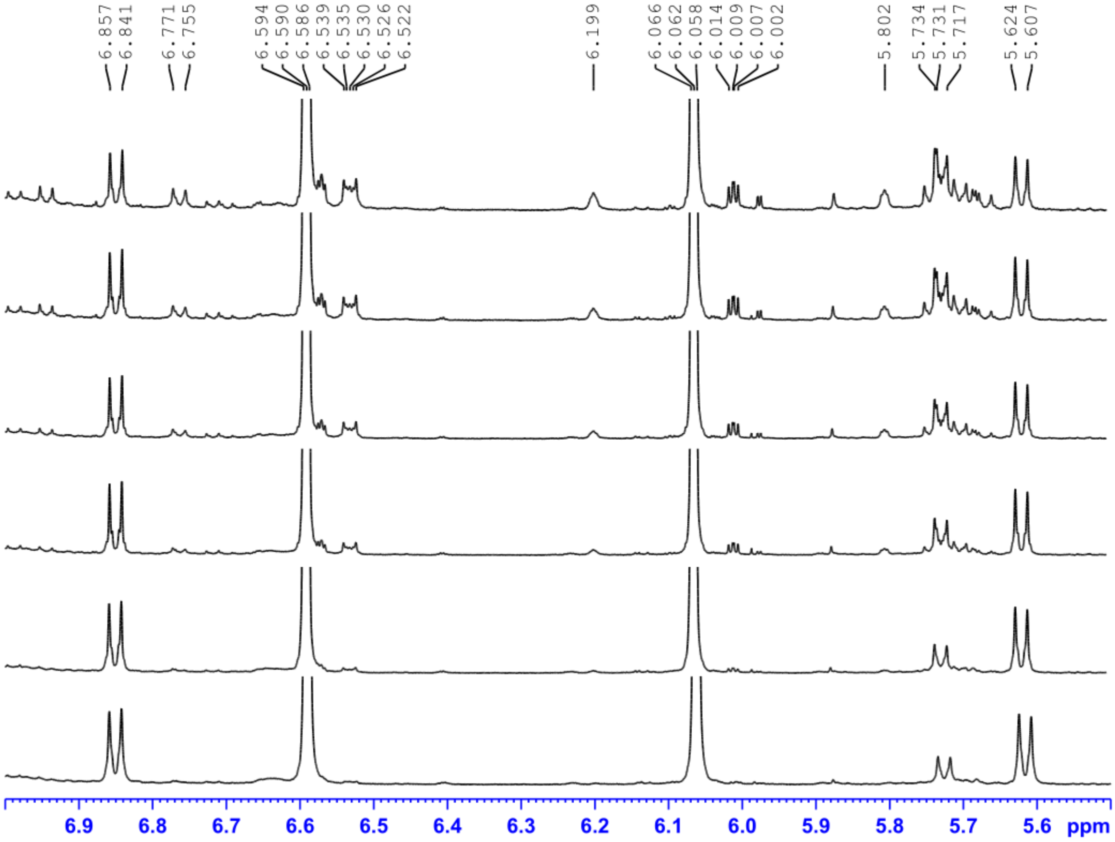

Figure 2.11: ^{1}H NMR data, between 5.5 and 7.0 ppm, showing the progression of the reaction between *N*-methylpyrrole and compound 2, *trans*-[RuCl(=C=CH–C_6H_4-4-C≡CH)(dppe)$_2$][OTf], with the bottom spectrum recorded 10 minutes after the addition of tribromoacetic acid, up to 24 hours reaction time for the top spectrum

These two figures (**Figure 2.11 and Figure 2.12**) show the NMR data for the progression of the reaction of 2 equivalents of N-methylpyrrole and *trans*-[RuCl(=C=CH–C_6H_4-4-C≡CH)(dppe)$_2$][OTf] (**2**[OTf]) over a 24 hour period, using tribromoacetic acid as a catalyst. There are two important regions to look at in these spectra, both involving the changes to the N-methylpyrrole. The two aromatic protons on free *N*-methylpyrrole can be seen in all the spectra as two triplet resonances at 6.06 and 6.59 ppm, and as the reaction progresses three new triplet resonances (these data do not show the triplets particularly well, but they were better resolved in other samples, **Figure 2.14**) are at 5.80, 6.19 and 6.53 ppm. As the *N*-methylpyrrole reacts it loses its symmetry resulting in the change from two aromatic environments to three. The CH_3 protons for *N*-methylpyrrole are in the aliphatic region and move from 3.63 ppm in the free molecule to 3.59 ppm once it has reacted.

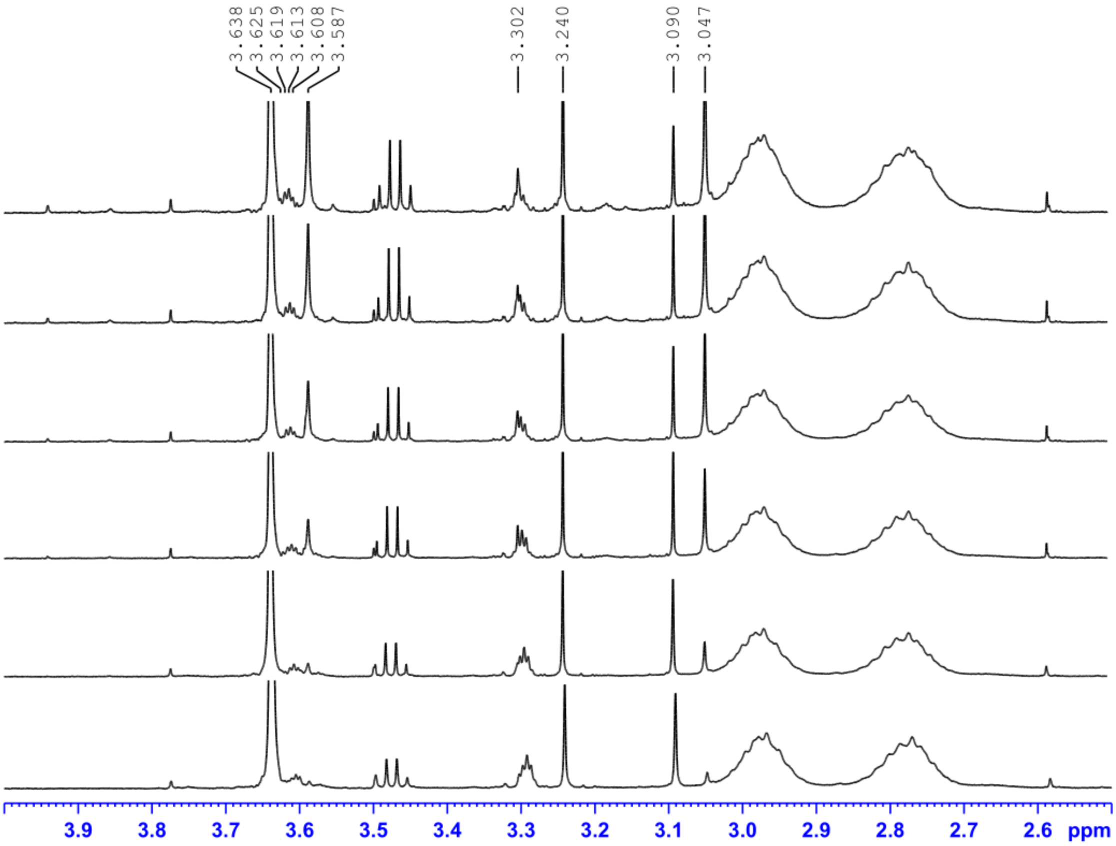

Figure 2.12: ^{1}H NMR data, between 2.5 and 4.0 ppm, showing the progression of the reaction of N-methylpyrrole and compound 2, *trans*-[RuCl(=C=CH-C_6H_4-4-C≡CHI(dppe)$_2$][OTf], with the bottom spectrum being 10 minutes after the addition of tribromoacetic acid, up to 24 hours reaction time for the top spectrum

The vinylidene proton in both the starting material and the product appears at around 3.0 ppm, this can be seen in the spectra as the shape of that peak appears to change and shift to a slightly higher ppm. Another peak of interest that is seen to increase during this reaction is that at 3.05 ppm, this is not related to either the product, the starting material nor the water addition product, [**5**]$^+$, that is often seen (its CH_3 resonance coming at 2.52 ppm), also this resonance appears to grow in at the same rate that the peak at 3.09 ppm decreases. These two resonances were not assigned; however, they were not present when HBF_4 was used as a catalyst instead of tribromoacetic acid so they can probably be attributed to the acid, a by-product or an impurity.

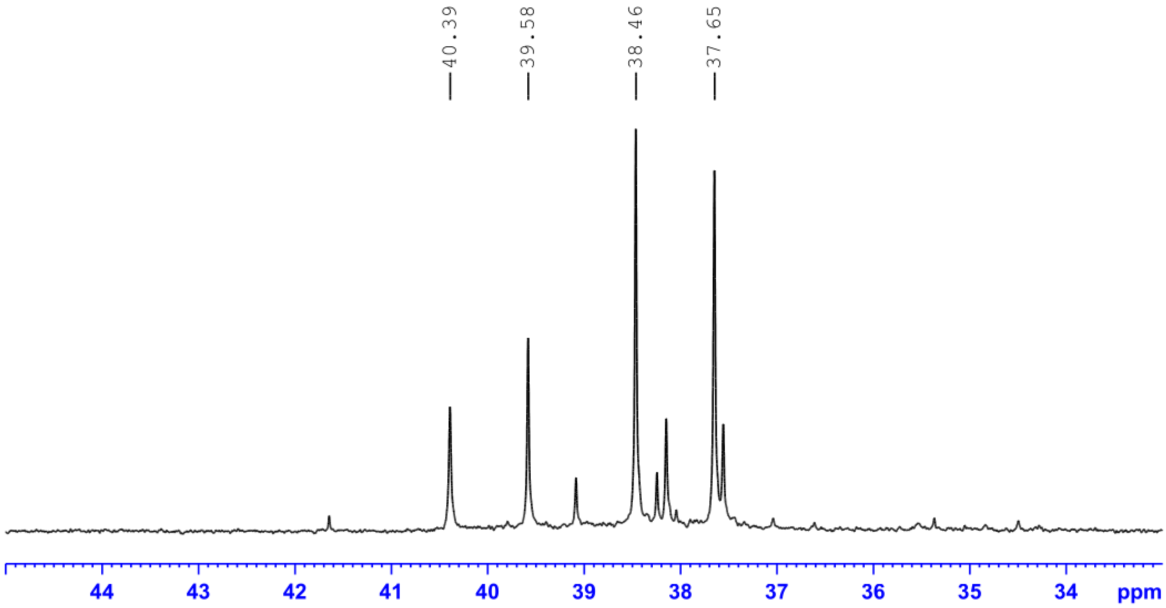

Figure 2.13: $^{31}P\{^1H\}$ NMR spectrum from the reaction of N-methylpyrrole and compound 2, *trans*-[RuCl(=C=CH–C_6H_4-4-C≡CH)(dppe)$_2$][OTf] with tribromoacetic acid, unpurified

There are likely to be other products of this reaction, as there are multiple unassigned but minor peaks in the ^{31}P NMR spectrum (**Figure 2.13**), one, 37.65 ppm, is for **5**[OTf], although some of this may have been present as an impurity in the starting material **2**[OTf] and another could possibly be attributed to the mono-substituted species.

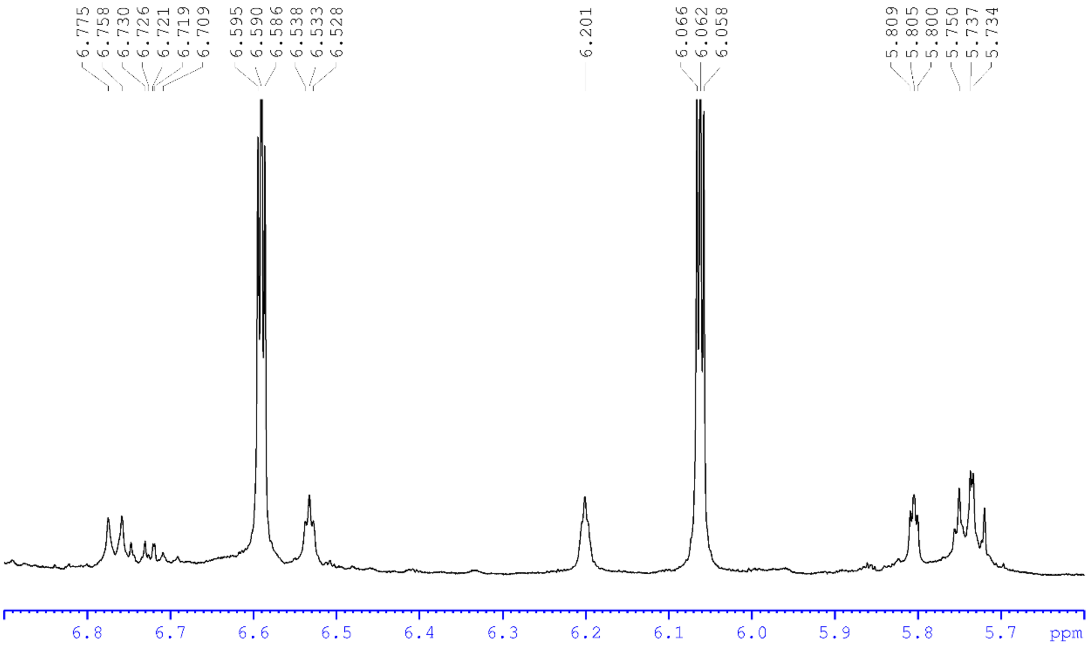

Figure 2.14: ^{1}H NMR data, between 5.6 and 6.9 ppm, showing the product for the addition of *N*-methylpyrrole to compound 2, *trans*-[RuCl(=C=CH–C_6H_4-4-C≡CH)(dppe)$_2$][OTf] with $HBF_4.OEt_2$

When the same reaction conditions, two equivalents of N-methylpyrrole and $HBF_4.OEt_2$ in DCM, were reacted with **5**[OTf] as the starting material (**Figure 2.4**) (instead of **2**[OTf]) the same product, [**7**]$^+$, was formed. This indicated that, in solution, [**5**]$^+$ undergoes reversible loss of water to form [**2**]$^+$, allowing the N-methylpyrrole to react (**Scheme 2.6**). As the addition of the second *N*-methylpyrrole does not occur *via* a cumulene species this makes the product more energetically favourable and the reversal to the cumulene less likely to occur spontaneously.

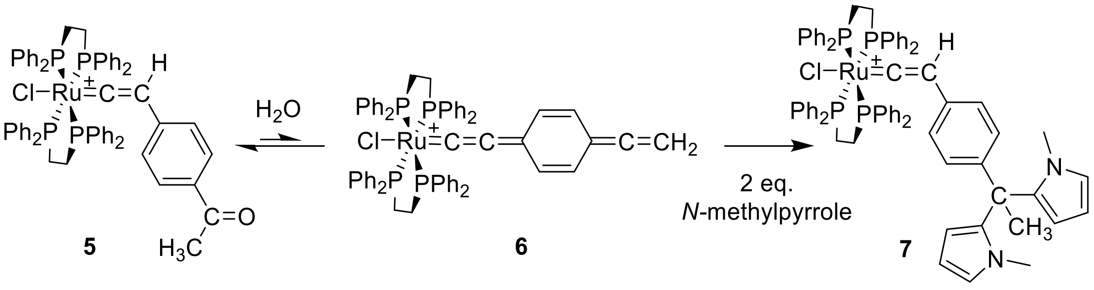

Scheme 2.6: Conversion of water addition product, 5, to N-methylpyrrole addition product, 7, via the cumulene intermediate

The attempted deprotonation of the N-methylpyrrole addition product, [**7**]$^+$ using NEt_3 yielded the acetylide equivalent of [**5**]$^+$, *trans*-$RuCl(C{\equiv}CHC_6H_4\text{-}4\text{-}C(=O)CH_3)(dppe)_2$, **9** (**Figure 2.15**), instead of the expected acetylide analogue, *trans*-$RuCl(C{\equiv}CHC_6H_4\text{-}4\text{-}C(C_4H_3NCH_3)_2CH_3)(dppe)_2$, **10**.

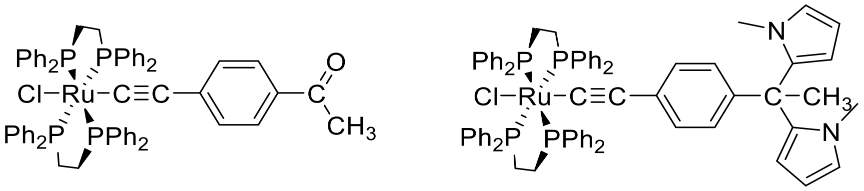

9 **10**

Figure 2.15: Structure of *trans*-$RuCl(C{\equiv}CHC_6H_4\text{-}4\text{-}C{=}OCH_3)(dppe)_2$, 9, and *trans*-$RuCl(C{\equiv}CHC_6H_4\text{-}4\text{-}C(C_4H_3NCH_3)_2CH_3)(dppe)_2$, 10

The only characterisation that indicated the desired *N*-methylpyrrole acetylide, **10**, was formed is a small peak in the mass spectroscopy data at 1185.30 *m/z*. However, the major *m/z* was at 1041.2251 which can be attributed to compound **9**, (Calculated 1041.2241).

However, in the NMR data only the resonances for **9** were observed. One singular resonance was observed in the $^{31}P\{^1H\}$ NMR at 48.38 ppm, which is consistent with other acetylide complexes with this metal fragment. The ^1H NMR showed no resonances for *N*-methylpyrrole, and the terminal CH_3 group resonance was observed at 2.52 ppm. The aromatic benzene spacer group protons were observed as doublets at 6.57 and 7.68 (J_{HH} = 8.38 Hz) ppm. For the dppe protons the *ortho* protons occur at 7.30 and 7.43 ppm (J_{HH} = 6.92 Hz), the *meta* protons at 6.93 and 7.06 ppm (J_{HH} = 7.58 Hz) and the *para* protons at 7.18 and 7.25 ppm (J_{HH} = 7.58 Hz). In the $^{13}C\{^1H\}$ NMR the terminal CH_3 carbon resonance was observed at 26.55 ppm, followed by the carbonyl carbon at 197.28 ppm. The α carbon possibly appears at 120.16 ppm and the β carbon is identified by HMBC correlation as the resonance at 115.14 ppm. The protonated carbons on the aromatic spacer group appear at 128.17 and 130.18 ppm, with the other quaternary aromatic carbons at 131.71 and 135.73

ppm. The dppe carbons can also be fully assigned in this case with the aliphatic ethane carbons at 30.83 ppm, the *ortho* carbons at 134.31 and 134.96 ppm, the *meta* carbon at 129.22 and 129.48 ppm and the *para* at 127.43 and 127.61 ppm. The *ipso* carbons by contrast could not be directly assigned through 2D NMR experiments, however, are likely to be some of the small carbon resonances between 131.50 and 133.24 ppm.

In contrast to the formation of compound **9**, the deprotonation of vinylidene products tends to remove the proton from the beta carbon, forming a triple bond between the alpha and beta carbons.[152] The fact that this does not occur for compound **7** indicates that the pyrrole molecules are not very strongly bonded to the seventh carbon and can easily be removed under basic conditions and then the excess of water in NEt_3 would ensure that **9** is the favoured product. This is possibly due to the steric influences of three aromatic groups bound to the same carbon.

Several control experiments were set up to ensure that no other reaction was taking place over this time period. No reaction was observed between *N*-methylpyrrole and **2**[OTf] in the absence of $HBF_4.OEt_2$ meaning that the acid must play a role in the reaction. However, there was also no reaction between $HBF_4.OEt_2$ and *N*-methylpyrrole which indicates that the acid is reacting with **2**[OTf] as expected. When light was excluded from these reactions, no difference in reactivity was observed meaning that these reactions are not sensitive to or catalysed by light.

2.1.1.3 Addition of halides to *trans*-[RuCl(=C=CHC$_6$H$_4$-4-C≡CH)(dppe)$_2$][OTf]

In the literature[144] it was determined that the addition of tetrabutylammonium chloride to *trans*-[RuCl(=C=CH–C_6H_2-2,5-R_2-4-C≡CH)(dppm)$_2$]$^+$ (R = H, Me) resulted in the formation of *trans*-[RuCl(C≡C–C_6H_2-2,5-R_2-4-CCl=CH_2)(dppm)$_2$]. The net results is addition of chloride to the seventh carbon in the chain, most probably *via* a cumulenic intermediate. Therefore, it was expected that the same reactivity would occur with [**2**]$^+$ and a variety of tetrabutylammonium halide salts (Cl, Br and I).

When 1.1 equivalents of NBu_4Cl were added to a solution of **2**[OTf] in DCM an immediate colour change from brown to red occurred, followed by a change to yellow upon deprotonation using basic alumina. The resulting NMR spectrum from the reaction showed the clean addition of chloride to the seventh carbon in the chain (**Figure 2.16**) consistent with the results of Eaves *et al.* with the analogous dppm complexes described above.[144] Characteristic of this addition, the ^{1}H NMR spectrum includes CH_2 doublet resonances at 5.42 and 5.72 ppm ($^2J_{HH}$ = 1.8 Hz) and the spacer group resonances at 6.57 and 7.38 ppm (J_{HH} = 8.4 Hz). The ^{31}P NMR spectrum had a higher frequency resonance than [**2**]$^+$ at 48.6 ppm, however this is consistent with literature that acetylide complexes tend to have phosphorus resonances 10 ppm to lower field than the corresponding vinylidene-containing species.[157,158] An *m/z* of 1059.1920 was observed and could be attributed to [M-Cl]$^+$ complex (calculated for 1059.1908 *m/z*).

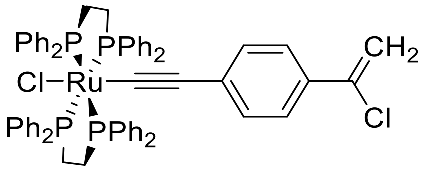

11a

Figure 2.16: $RuCl(C{\equiv}CHC_6H_4CCl{=}CH_2)(dppe)_2$, 11a

When using tetrabutylammonium halides (Br and I), the ^{1}H NMR spectra provided evidence for the expected addition of bromide to the seventh carbon in the cumulene chain. For bromide addition (**11b**) the CH_2 doublet resonances were found at 5.67 and 6.07 ppm ($^2J_{HH}$ = 2.2 Hz), or for iodide (**11c**) at 6.00 and 6.44 ppm ($^2J_{HH}$ = 1.8 Hz). However, the crude reaction solutions from these heavier halide additions gave rise more complex NMR spectra, indicating the formation of other products. The ^{1}H NMR analysis showed similar CH_2 resonances to the chloride complex at around 5.42 and 5.72 ppm and the mass spectrum exhibited a peak at *m/z* of

1059.1920 which relates to $[C_{62}H_{54}ClP_4Ru]^+$. The mass spectrometry data for bromide addition product also showed a mass of 1151.1270 for $[C_{62}H_{54}BrClP_4Ru]^+$ for ^{79}Br and the iodide addition product at 1187.1118 for $[C_{62}H_{54}IClP_4Ru]^+$. The $^{31}P\{^1H\}$ NMR spectrum also showed and identical peak for **11a** obtained through the addition of $[NEt_4]Cl$ to [**2**]$^+$ at 48.63 ppm as well as additional signals at 46.75 ppm for bromine addition (**11b**) and 43.92 ppm for iodine (**11c**). However as seen with other mass spectra from $RuCl(dppe)_2$ complexes the ruthenium-coordinated halide ligand is lost therefore the spectra are not diagnostic for position of the bromide in the four possible products from the addition of Bu_4NBr to [**2**]$^+$ (**Figure 2.17**). A small amount of compound [**5**]$^+$ was also observed, possibly due to the hygroscopic nature of the tetrabutylammonium salts introducing water into the reaction.

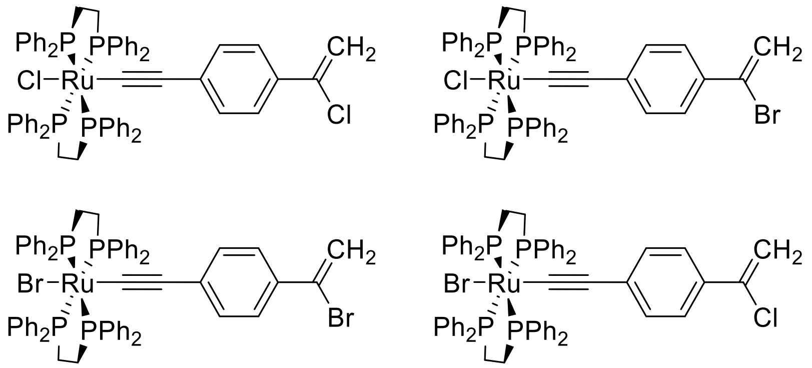

Figure 2.17: Possible products from the addition of Bu_4NBr to [2]$^+$

These data demonstrate that it may be possible for the chloride which was initially attached to the ruthenium atom in [**2**]$^+$ to dissociate and therefore halide ligand exchange may take place on the metal. The then free chloride to act as a nucleophile at the seventh carbon position of the organic ligand (**Scheme 2.7**). It is unknown whether the halide exchange happens at the vinylidene or the cumulene isomers, or at the final acetylide stage. Although the carbene type nature of vinylidenes and cumulenes means the increased *trans* effect makes the loss of halide unlikely at this stage, the halide exchange has been observed in the absence of base which is required to form the final acetylide.

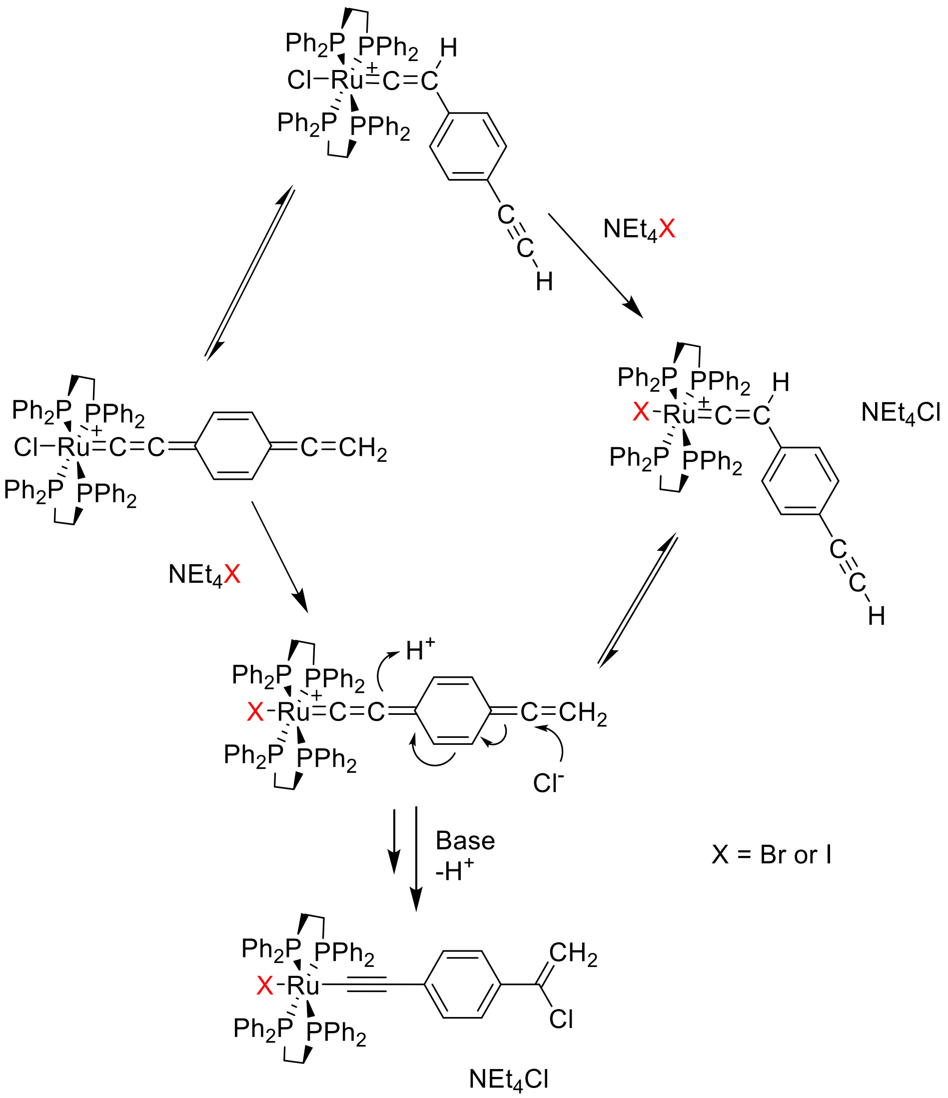

Scheme 2.7: Two of the possible routes for the halide scrambling of chloride with bromide or iodide

2.1.1.4 Additional compound formed during the reaction of compound 2 and halides

In the proton NMR spectrum for the chloride addition compound (**Figure 2.16**) some small extra doublet peaks at 5.72 and 5.42 ppm (**Figure 2.18**) were observed and the compound responsible for these could not be removed with typical purification methods. This indicates that there is a second species present with similar properties to the desired product.

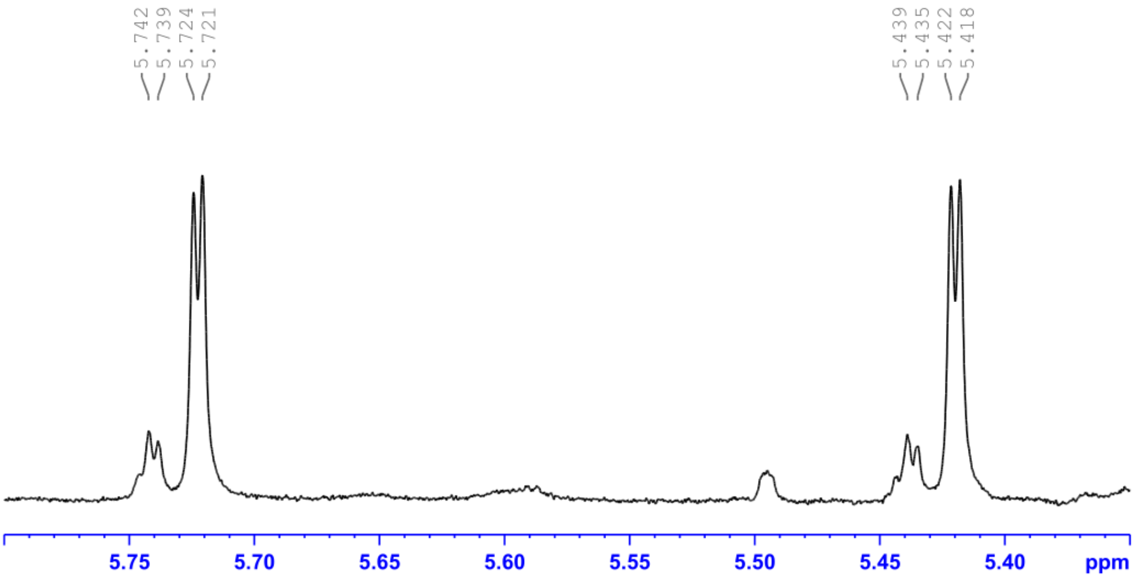

Figure 2.18: ^{1}H NMR of compound 11 showing additional resonances at 5.72 and 5.42 ppm

It was hypothesised that the second compound could have been due to double addition of 1,4-diethynylbenzene to **2**[OTf] to form compound **12**. From the halide addition experiments it was concluded that the Ru-chloride bond is weak enough to break, leading to the loss of the chloride, and therefore leave a space in the coordination sphere, which could be filled by a second alkyne. This would result in the formation of compound **12** (**Figure 2.19**). If a compound like this existed, then it would be difficult to differentiate from the bulk as the NMR signals would be overlapping.[159]

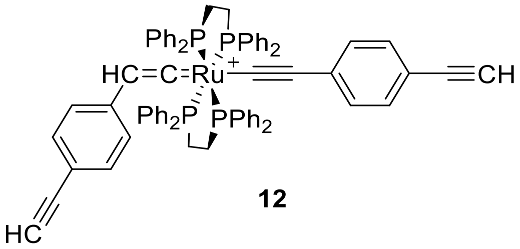

12

Figure 2.19: Structure of double alkyne addition to Ru(dppe)Cl, compound 12

However, experimentally this second alkyne addition did not occur under the conditions used to make compound **2**. Even when forcing conditions were used, 3 equivalents of diethynylbenzene to [Ru(dppe)$_2$Cl][OTf] , no evidence of double alkyne addition was observed by NMR after 1 hour of stirring. Within this standard reaction time the expected colour change from red to green occurred. As acetylide complexes tend to allow chloride to be more labile an excess of base (DBU) was added and stirred for a further 22 hours. If the second alkyne was ligated a yellow powder would be expected to form, however, the reaction mixture only turned orange, and double addition was not observed by ^{1}H NMR.

A second more likely explanation is that the presence of a free chloride ion can act as a proton shuttle and promote the removal of the vinylidene proton from compound **2**, which forms the cumulene. The highly reactive cumulene could then react with the mildly basic triflate ion. As triflate does not contain any proton nuclei which could be seen in the ^{1}H NMR spectra this could not be directly identified through this method, however the shift in the two CH$_2$ NMR resonances would be small but observable, as seen in this case. Although triflate is present in the starting material it does not react with the metal vinylidene under normal conditions. This is probably because triflate is only mildly basic and needs the addition of the tetrabutylammonium halide, which can remove the vinylidene proton and form the cumulene. Cumulene compounds are extremely reactive so can then react with triflate, despite it usually being inactive. However, the triflate compound was not observed in the mass spectroscopy either with or without a direct chloride or triflate ligand.

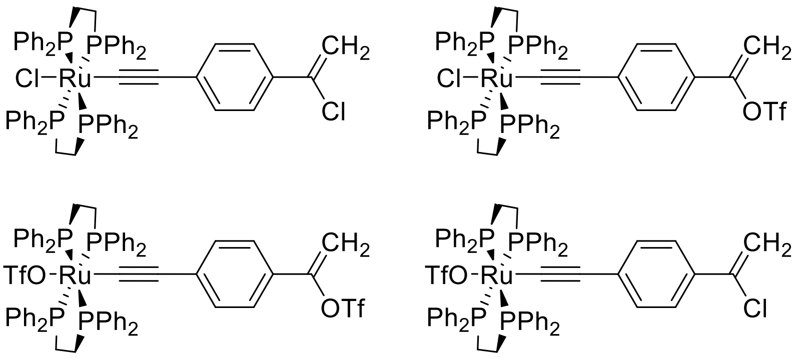

Figure 2.20: Additional four compounds that may be being formed from the addition of Bu_4NCl to 1[OTf]

As with the addition of Bu_4NX (X = Br or I) to **2**[OTf] there is the possibility for up to four different compounds that could be formed, which can be seen in Figure 2.20 for the reaction with Bu_4NCl. This, therefore, means that the number of possible products formed during the addition of bromide or iodide is nine.

2.1.2 Reactions of *trans*-$RuCl(C{\equiv}CHC_6H_4\text{-}4\text{-}C{\equiv}CH)(dppe)_2$ with electrophiles

Cumulene compounds are not just susceptible to attack from nucleophiles, the alternative nucleophilic and electrophilic character of the carbons in the chain mean that cumulenes can also react with electrophiles. However, in this work so far, all the reactions have focused on the addition of nucleophiles to the odd numbered carbons within the quinoidal cumulene chain. Therefore, if the cumulenic intermediate is being formed in these reactions then the reaction with electrophiles should take place at the even numbered carbons. With the addition of the aromatic benzene spacer group then there are only two positions open to electrophile attack: the second, beta, carbon and the eighth, terminal, carbon (**Figure 2.18**). It is possible that the larger steric bulk of two dppe ligands may inhibit the tendency for small electrophiles to react at the beta carbon and could push the reactivity to the terminal carbon and form a cumulene species that may be stable. An addition at the beta carbon would form a substituted vinylidene species.

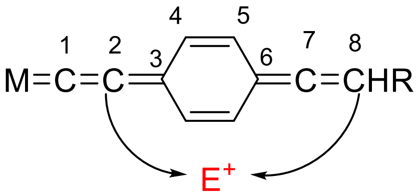

Figure 2.21: Two possible positions for electrophile addition to a quinoidal cumulene

The acetylide RuCl(C≡CC$_6$H$_4$-4-C≡CH)(dppe)$_2$, **13**, was prepared from the reaction of [RuCl(dppe)$_2$][OTf] with an excess of 1,4-diethynylbenzene in methanol, addition of base (NEt$_3$) after 1.5 hours resulted in the deprotonation of the green vinylidene complex **2** into the acetylide, which precipitated from solution as a yellow powder in a 90 % yield. This can also be achieved from the deprotonation, using base, of purified **2**[OTf]

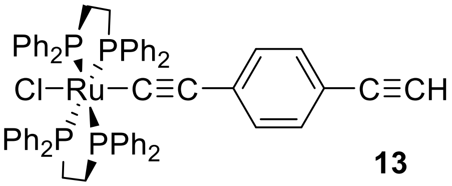

13

Figure 2.22: Structure of RuCl(C≡CHC$_6$H$_4$-4-C≡CH)(dppe)$_2$, 13

As expected for a vinylidene to acetylide transformation the major resonance in the ^{31}P{^{1}H} NMR spectrum was shifted from 38.24 ppm to 49.21 ppm, this change of *ca.* 10 ppm is consistent with all proton vinylidene and acetylide transformations.[157,158] In the ^{1}H NMR spectrum the two doublet resonances for the spacer group were identified at 6.51 and 7.22 ppm (*J* = 8.14 Hz) and the terminal alkyne proton is at 3.10 ppm as this is the only aliphatic peak that has an integration close to 1H and is within the expected range. The IR spectrum showed a single stretch in the C≡C region at 2058 cm^{-1}. The high-resolution MS gave a peak at 1023.2134 *m/z* with the ruthenium splitting pattern which corresponds to the mass of **13** with the loss of the chloride ligand.

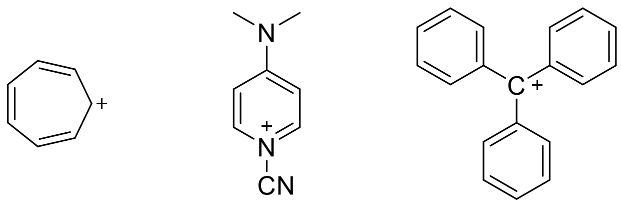

$[C_7H_7]BF_4$ $[CAP]BF_4$ $[CPh_3]BF_4$

Figure 2.23: Electrophiles and electrophile donors used in these reactions

The reactivity of tropylium tetrafluoroborate ($[C_7H_7]BF_4$), 1-cyano-4-dimethylaminopyridinium tetrafluoroborate ($[CAP]BF_4$) and trityl tetrafluoroborate ($[CPh_3]BF_4$) (**Figure 2.23**) towards **13** was explored. These electrophiles were chosen as they each have a different steric size and therefore will show how sterics can affect the reactivity. The reactivity of cumulenic compounds predicts that the electrophiles will be attacked from either the second carbon, forming vinylidene species, or the terminal eighth carbon as these are the only two nucleophilic carbons that are not aromatic. These predicted structures are shown in **Scheme 2.8**, as identified by Hall *et al.*[152]

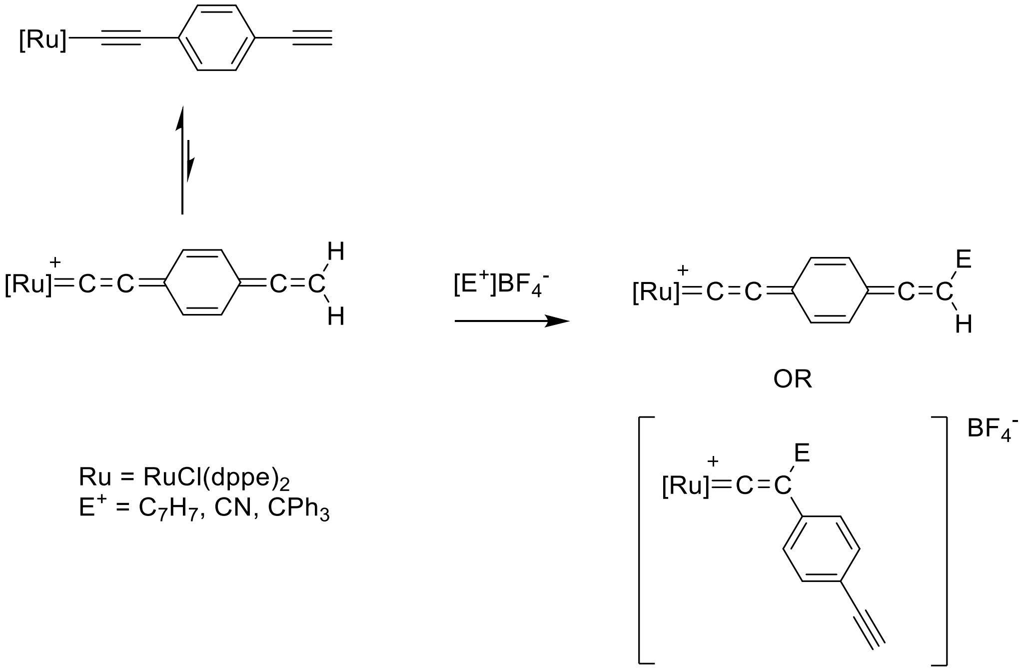

Scheme 2.8: Predicted structures from the reaction of $\mathrm{RuCl(C{\equiv}CHC_6H_4\text{-}4\text{-}C{\equiv}CH)(dppe)_2}$ with electrophiles

Despite the addition of these electrophiles causing a colour change from yellow to red or orange, neither the vinylidene (addition to the beta carbon) nor addition to the terminal carbon took place cleanly in any of the reactions. These reactions were carried out stoichiometrically in DCM at room temperature for either 4 hours or overnight.

The single product from the attempted addition of $C_7H_7^+$ to the acetylide **13** appears to be a carbonyl degradation compound **14** (**Figure 2.24**). This is supported by a peak in the mass spectrum at *m/z* of 961.1410 which corresponds to the mass of this compound, predicted to be 961.1382. The $^{31}P\{^1H\}$ NMR spectrum also only exhibited a single resonance at 41.63 ppm, which despite not being in the literature has also turned up in other phosphorus NMR spectra with this metal fragment (including the addition of CN^+ to **13**). The ^1H NMR spectrum only exhibited aromatic peaks related to the dppe ligands and the expected set of doublets for the benzene spacer group are not found.

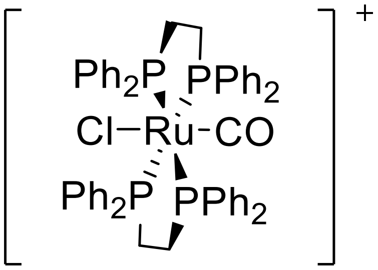

Figure 2.24: Carbonyl degradation product, 14

In contrast, the addition of [CAP][BF_4] to **7** gave a much more complicated series of products. The $^{31}P\{^1H\}$ NMR spectrum showed 10 different resonances between 38 ppm and 50 ppm. The mass spectrum also showed many peaks of which a few could be identified. These included the [**2**]$^+$ cation at 1091.2171 is the closest to the desired product with the mass being of compound **15**, this is proof that the addition of CN^+ did occur and therefore that the cumulene intermediate is likely to have been formed, although if the addition occurred at the second or eighth carbon is unknown.

Another peak at 1213.2998 corresponds to **15** with the addition of 4-Dimethylaminopyridine (DMAP), the by-product from the loss of CN from CAP. Despite there being no bimetallic complex present in the starting material for this reaction several dications were also identified, and their splitting patterns correspond to bimetallic complexes however their exact composition has yet to be identified.

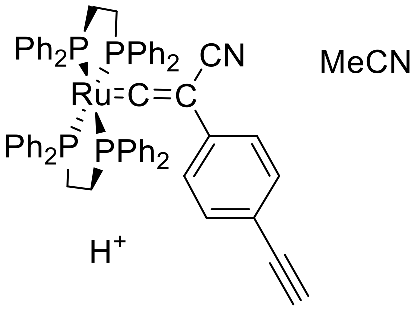

Figure 2.25: Major 1+ cation seen by mass spec, 15

There was no evidence of the addition of $[C_7H_7]BF_4$ or $[CPh_3]BF_4$ to compound **14** at either the beta carbon position or the terminal carbon. The addition of $[CPh_3]BF_4$ was expected to occur at the terminal carbon as there is no steric hindrance in this part of the molecule.

2.2 Summary

The additions of nucleophiles to compound [**2**]$^+$ all occur at the seventh carbon in the chain of the organic ligand, this reinforces the theory that these additions occur *via* a quinoidal cumulene intermediate. For cumulated carbon chains it is the odd numbered carbons that are electrophilic meaning they will readily react with nucleophiles and the even are nucleophilic and react with electrophiles. This cumulene intermediate with terminal protons is not sterically protected in any way so is expected to be very reactive.

Therefore, it is unsurprising that in the other reactions of [**2**]$^+$ always showed evidence of the formation of the water addition product [**5**]$^+$, this was present in various quantities in relation to how dry the solvents and reagents were in the reactions. However, this shows that the cumulene intermediate is formed in the solution and is highly reactive.

The addition of electrophiles to **13** was not successful, possibly due to steric hindrance of the beta carbon from the two dppe ligands close by which can be mitigated by changing the metal fragment from $[RuCl(dppe)_2]^+$ to a half-sandwich fragment e.g. $[Ru(PPh_3)_2Cp]^+$ or $[Ru(dppe)Cp^*]^+$. This steric hinderance however cannot account for the lack of addition to the terminal carbons.

1.2 Half-Sandwich Compounds

The initial work on half-sandwich quinoidal cumulenes was carried out by Michael Hall[160] which can be seen in **Scheme 2.9**. In this work, both ruthenium and iron diethynylbenzene acetylide complexes were used as an entry into cumulene intermediates rather than vinylidenes. The acetylide is used rather than the vinylidene because it reduces the reactivity of the electrophile with the vinylidene proton. Four electrophiles of increasing size were used in this work; acid ($HBF_4{\cdot}OEt_2$), a cyano group ([CAP]$[BF_4]$), tropylium ($[C_7H_7][BF_4]$), and trityl ($[CPh_3][BF_4]$), which have been used in previous work.[152] These reactions were performed in DCM at room temperature and the workup involved a precipitation from ice-cold diethylether.

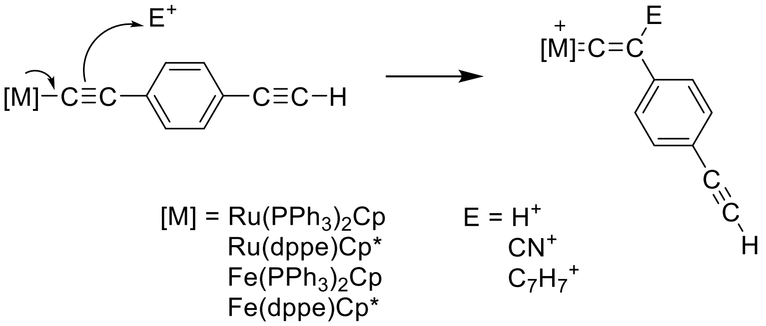

Scheme 2.9: Addition of small electrophiles to half-sandwich diethynylbenzene acetylide complexes[152]

The reduction in the steric bulk around the metal group with the half sandwich groups when compared to the Ru(dppe)$_2$ group meant that the reactions with the smaller electrophiles (H^+, CN^+ and $C_7H_7^+$) occurred with the second carbon in the chain, forming vinylidene type products (**Scheme 2.9**). Although these reactions could have used either the cumulene intermediate or a direct electrophile addition at the beta carbon.

However, the electrophile with the largest steric bulk (CPh_3) had a different reaction profile. This was unable to react at the beta carbon and addition to the terminal carbon occurred. It was anticipated that this would have resulted in the formation of a cumulene compound. However, this species was not isolated, an immediate reaction with the residual water in the system resulted in the formation of [M{C≡C-1,4-C_6H_4-C(=O)CH_2CPh_3}(LL)Cp’] (**Scheme 2.10**).

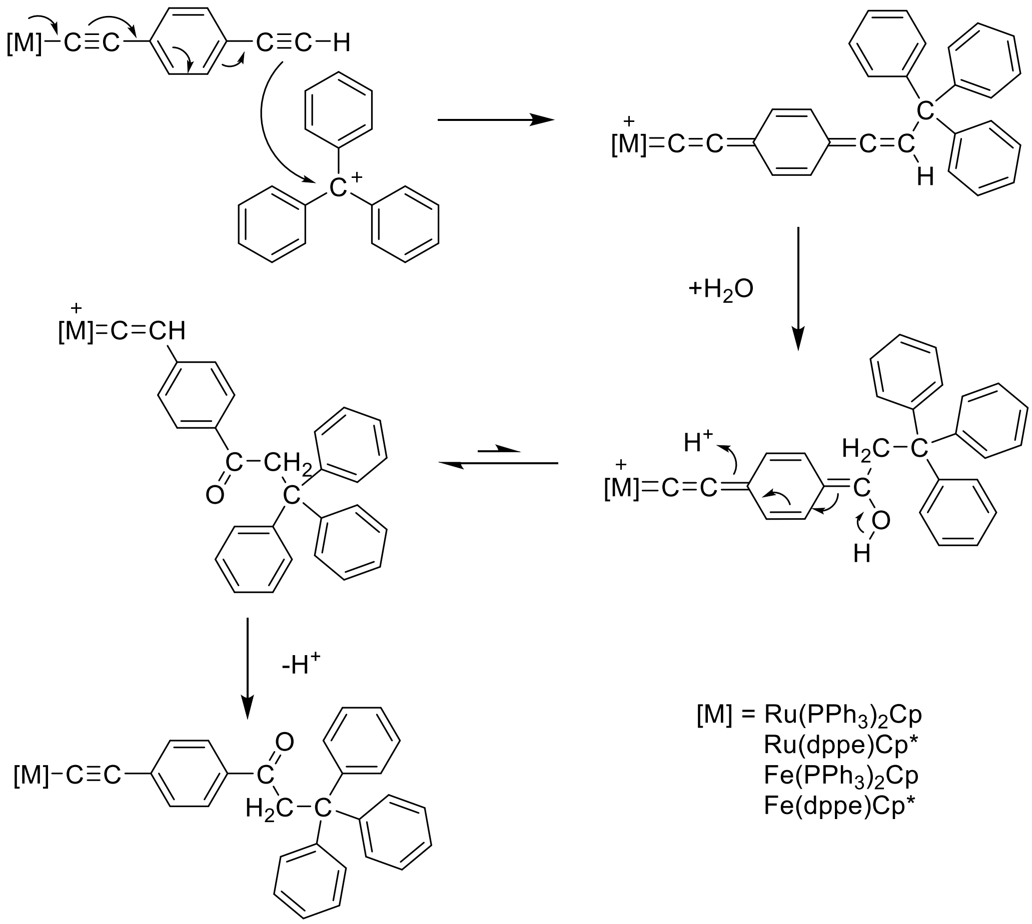

[M] = $Ru(PPh_3)_2Cp$
$Ru(dppe)Cp^*$
$Fe(PPh_3)_2Cp$
$Fe(dppe)Cp^*$

Scheme 2.10: Suggested cumulenic intermediate mechanism for formation of observed terminal alkynyl addition products during the reaction of acetylide terminal alkynes with electrophilic trityl cation and subsequent in situ reaction with nucleophilic water.[152]

Interestingly there was very little difference in reactivity between the ruthenium and iron half sandwich complexes despite the higher steric crowding of the ligands around iron.[152]

2.3 $C(CH_3)_2OH$ terminal group

The addition of water to the odd numbered, electrophilic, carbon in the cumulenic intermediate means that the cumulene intermediate can not be isolated or even observed spectroscopically. It was therefore proposed that by incorporating a sterically larger terminal group into the organic ligand the addition of water, or other small nucleophiles, to the cumulenic intermediate would be inhibited. One easily assessable terminal group is $C(CH_3)_2OH$, which is often used as a polar protecting group for alkynes.[161] The desired terminal substituent stabilised cumulene compound **16** is shown in **Scheme 2.11**. For this and subsequent reactions, the metal fragment was changed from [RuCl(dppe)$_2$] to [Ru(dppe)Cp*] for three reasons. Firstly, having a half sandwich complex eliminated the possibility of double alkyne addition, (**Section 2.1.1.4**), secondly, there is no possibility of halide exchange reactions occurring (**Section 2.1.1.3**) and thirdly the alkyne complexes can be synthesised using fewer steps.

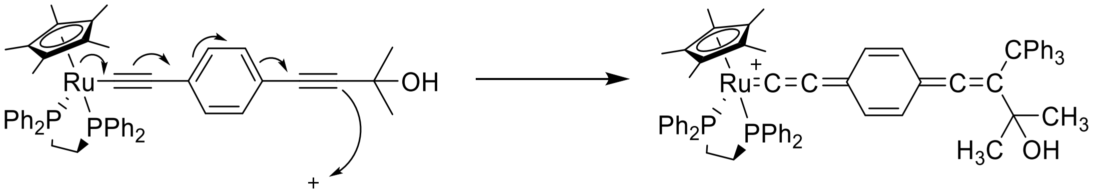

16

Scheme 2.11: Formation of the desired terminal substituent stabilised quinoidal cumulene

The protected benzene compound, **17** (**Scheme 2.12**), was made by Mohammad Hosseni Ghazvini (UWA). Synthesis of compound **18**, Ru(C≡CC$_6$H$_4$-4-C≡C(CH$_3$)$_2$OH)(dppe)Cp* was carried out using potassium fluoride to remove the TMS protecting group from 4-[(trimethylsilyl)ethynyl]-1-(3-hydroxyl-3-methylbutynyl)benzene, compound **17** (**Scheme 2.12**) and triethylamine to ensure the formation of the acetylide which precipitated from methanol solution as a bright yellow powder with a good yield of 60 %. The use of potassium fluoride to facilitate the removal of a TMS protecting group and the addition to a metal chloride was first described by Lomprey and Selegue in 1993[69] however despite it being used by other groups[162] the exact mechanism of action is unknown. It is thought to act as both a source of fluoride which is used to remove TMS protecting group resulting in the formation of a terminal acetylene[162] and as a base to remove the proton from the vinylidene, though the addition of additional base can speed up the reaction, which is originally formed giving the product as an acetylide.

A single resonance was observed in the $^{31}P\{^{1}H\}$ NMR spectrum at 80.70 ppm, which is consistent for acetylides on this metal fragment.[152] The two CH_3 groups of the terminal group exhibited a single proton resonance at 1.59 ppm with an integration of 6 confirming that these two groups are in the same environment. The benzene spacer group protons occurred at 6.64 and 7.07 ppm (J_{HH} = 8.3 Hz) which is similar to the other benzene spacer group resonances. Although the OH proton was not observed in the ^{1}H NMR spectrum, evidence that it was present is provided the infrared with a band at 3490 cm^{-1}. The $^{13}C\{^{1}H\}$ MNR showed the resonance for the α carbon at 131.55 ppm, followed by the β at 110.74 ppm, and the aromatic γ at 115.87 ppm. The carbon resonances for the protecting group are seen at 31.76 and 65.89 ppm, and the alkyne group carbons at 83.43 and 93.25 ppm. The four aromatic carbons which have protons are seen as two resonances at 130.07 and 131.03 ppm. As this compound is new electrochemical and spectroelectrochemical analyses were performed (**Chapter 4, Sections 4.1, 4.3 and 4.5**).

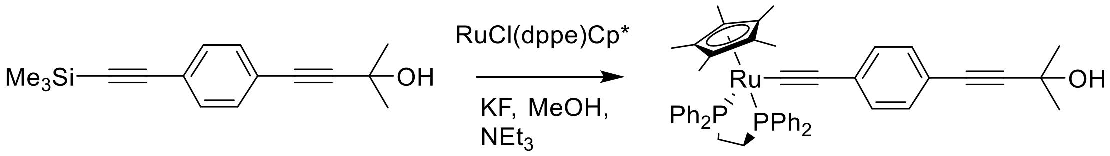

17 **18**

Scheme 2.12: Synthesis of $Ru(C\equiv CC_6H_4\text{-}4\text{-}C\equiv C(CH_3)_2OH)(dppe)Cp^*$, 18

Previous work by Dixneuf[68,82] suggest that the loss of water from a propargylic alcohol group can lead to the formation of cumulene species, so it is possible that a cumulene could be produced from the propargylic alcohol protected alkyne by the 1,3 elimination of H-OH (**Scheme 2.13**), although no evidence for this reactivity was seen during the electrophile addition reactions or with the addition of base.

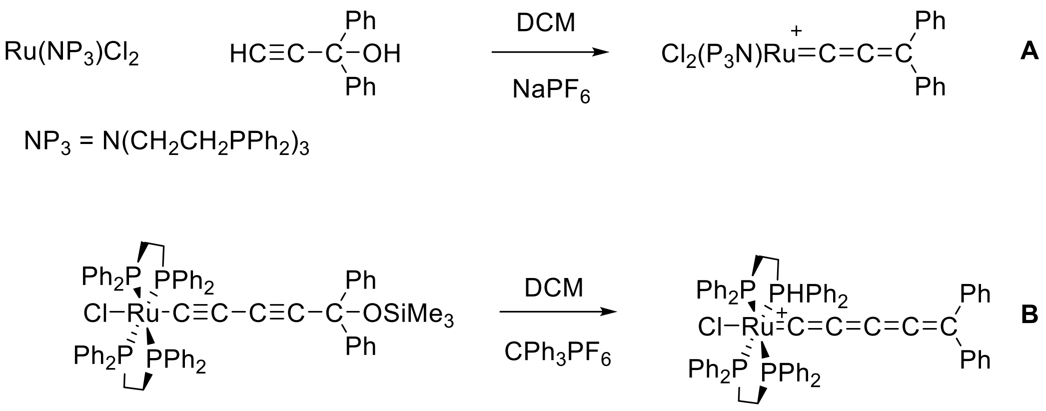

Scheme 2.13: Synthesis of cumulenes from propargylic alcohols, A) Dixneuf, 1991[68], B) Dixneuf, 1994[82]

A different method of removing the alcohol was reported by Masaji Oda *et al.*[163] in which a two-step process results in a cumulenic structure, this utilises the addition and then removal of iodine. In this work they primarily used small, symmetrical substituted 3-hexyn-2,5-diols. It is therefore theoretically possible to apply this procedure to the acetylides used in this work, shown in Scheme 2.14.

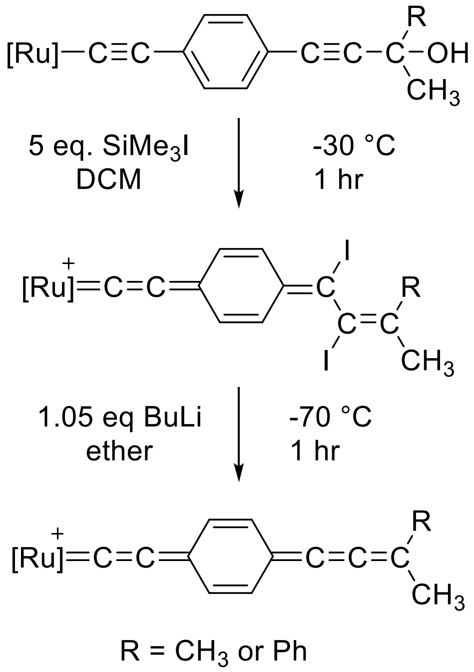

Scheme 2.14: Possible method of cumulene synthesis from the removal of OH- from the propargylic alcohol protected alkyne, using a modified procedure from Masaji Oda *et al.*[163]

Despite the rich literature using propargylic alcohol compounds to directly access cumulenes, in this work the group is utilised as a sterically bulky group to attempt to block reactivity at the seventh carbon. Deprotection of the terminal alkyne, to give the terminal alkyne complex, was carried out at either 3 hours at reflux in methanol or at room temperature overnight and was catalysed by KOH or KO^{t}Bu. This method for reaching the terminal alkyne compound only involves one additional step in the synthesis from a dihalo-benzene (**Scheme 2.15**). However, it does stop the formation of bimetallic complexes e.g. [**3**]$^+$ meaning that one equivalent of ligand can be used opposed to 4 equivalents used in the literature[152] and the product of water addition e.g. [**5**]$^+$ which could be beneficial in certain circumstances.

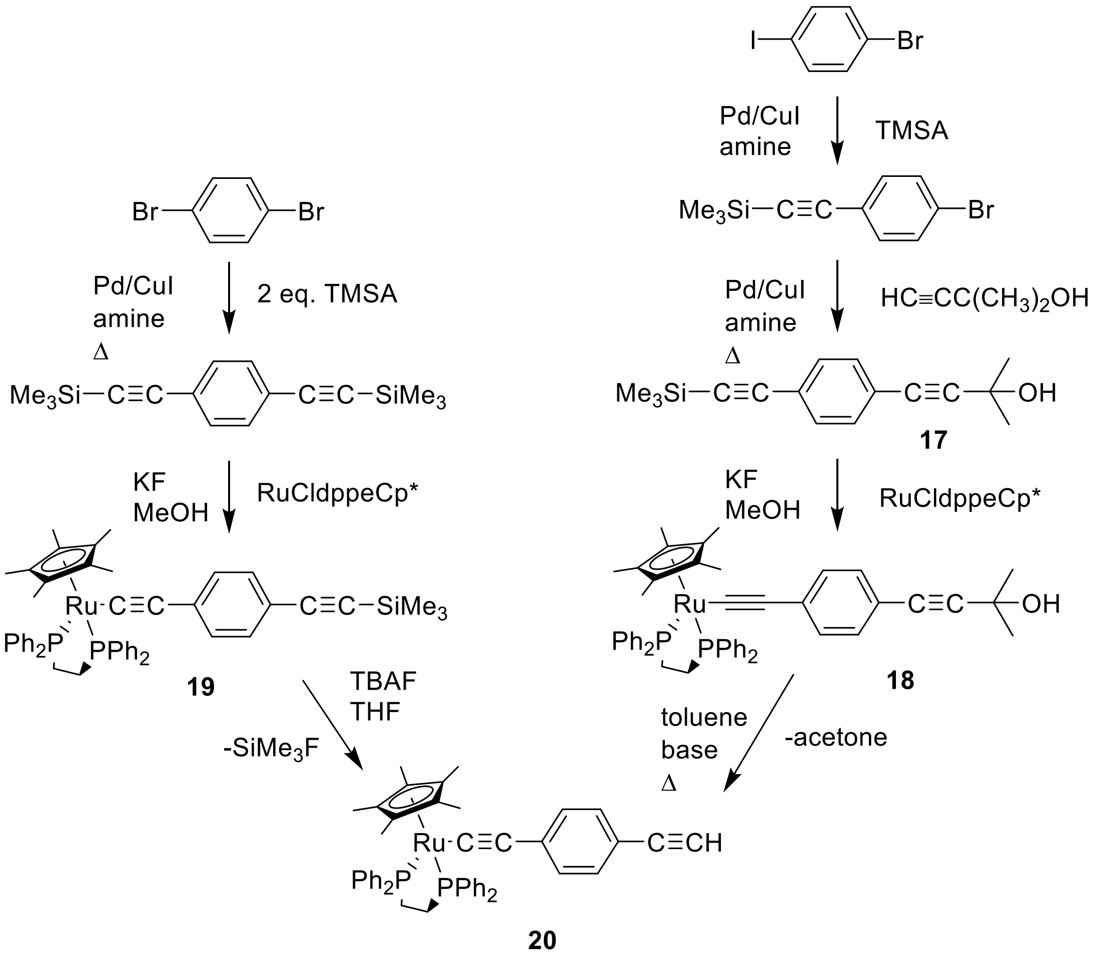

Scheme 2.15: Formation of Ru(C≡CC$_6$H$_4$-4-C≡CH)(dppe)Cp*, 20, *via* a symmetrical alkyne[152] and the unsymmetrical alkyne, 17

2.3.1 Reaction of $Ru(C\equiv CC_6H_4\text{-}4\text{-}C\equiv C(CH_3)_2OH)(dppe)Cp^*$ with acid

The addition of electrophiles to compound **18** was carried out in dry DCM at room temperature with stirring for up to 4 hours. The smaller electrophiles, H^+, CN^+ and $C_7H_7^+$ were added to the compound at the beta position as described in the literature.[152]

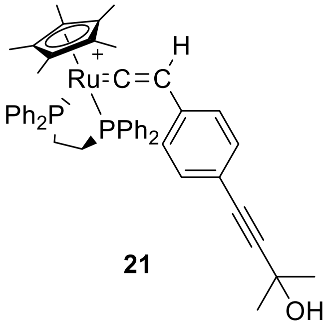

21

Figure 2.26: Structures of the addition of H^+ to 18.

Analysis of compound **21** (**Figure 2.26**) from the addition of acid ($HBF_4{\cdot}OEt_2$) gave the key ^1H NMR resonances at 6.02 and 6.89 ppm (J_{HH} = 8.3 Hz) for the spacer group protons and 1.65 ppm for the terminal CH_3 groups. The dppe $^{13}C\{^1H\}$ NMR peaks appear at 28.04 ppm, and the aromatic peaks at 129.10, 129.47, 131.91, 132.09, 133.09 and 133.2 ppm, and the Cp* at 10.41 ppm for the methyl groups and 103.76 ppm for the aromatic carbons. Most of the quaternary carbons and the alpha carbon were not observed in the carbon NMR when run for 4 hours. However, some $^{13}C\{^1H\}$ NMR resonances were characterised through 2D NMR experiments. These were 31.68 and 63.49 ppm for the $(CH_3)_2OH$ terminal group with 99.72 ppm for the adjoining alkyne carbon. The β carbon appeared at 105.08 ppm and the spacer group protons at 125.60 and 131.75 ppm.

2.3.2 Reaction of $Ru(C{\equiv}CC_6H_4\text{-}4\text{-}C{\equiv}C(CH_3)_2OH)(dppe)Cp^*$ with CN^+

A stoichiometric amount of [CAP][BF_4] was required to form compound **22** (**Figure 2.27**) from compound **18**. This is because when CN^+ is lost from [CAP] it results in the formation of 4-dimethylaminopyridine (DMAP) which has similar solubility characteristics to the desired compound making it difficult to separate out of the reaction mixture, so a minimal use of the reagent is desirable.

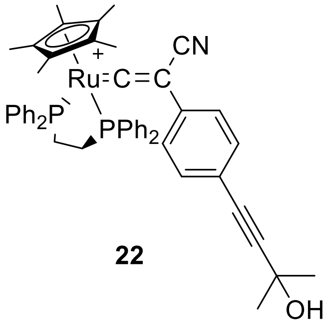

22

Figure 2.27: Structures of the addition of CN^+ to 18.

The ^1H NMR peaks of interest were the terminal CH_3 groups at 1.61 ppm and the spacer group protons at 6.41 and 6.95 ppm which were almost the same as the starting material. For this molecule, the ^{13}C NMR was more informative with the addition of the CN resonance at 108.25 ppm and the alpha carbon at 343.58 ppm indicating that a CN-vinylidene has been formed. This is supported by the resonance in the $^{31}P\{^1H\}$ NMR spectrum of a vinylidene at 70.49 ppm, a characteristic band for a C≡N vibration was observed in the IR spectrum at 2197 cm^{-1}, a peak of the C=C stretch of the vinylidene was observed at 1643 cm^{-1}. The mass spectrum exhibited a peak for the correct calculated mass-to-charge ratio of 844.2451 *m/z*.

2.3.3 Reaction of $Ru(C{\equiv}CC_6H_4\text{-}4\text{-}C{\equiv}C(CH_3)_2OH)(dppe)Cp^*$ with $C_7H_7^+$

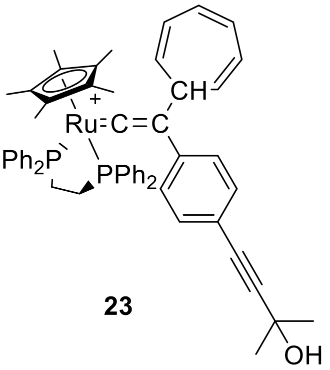

23

Figure 2.28: Structures of the addition of $C_7H_7^+$ to 18.

The reaction of compound **18** with tropylium resulted in the selective formation of compound **23** (**Figure 2.28**) which was confirmed by a peak with a mass-to-charge ratio of 909.3024 *m/z* as was calculated for M^+. The appearance of key resonances in the ^1H NMR spectrum at 6.76 and 6.95 ppm (J_{HH} = 8.1 Hz) for the spacer group protons and 1.63 ppm (6H) for the terminal CH_3 groups which are similar to the starting material. The peaks for the C_7H_7 group were seen at 4.98 (dd, J_{HH} = 5.4 Hz, J_{HH} = 9.1 Hz), 5.96 (d, J_{HH} = 9.1 Hz), 6.28 (t, J_{HH} = 2.9 Hz) and a singlet at 1.60 ppm, this final aliphatic proton with an integration of one can be assigned to the proton attached to the carbon in the ring directly bound to the beta carbon of the organic ligand and proves that the tropylium ion has lost its aromaticity. The alpha carbon resonance that would be expected to reside higher than 300 ppm but was not observed. The $^{31}P\{^1H\}$ NMR spectrum displayed a single resonance at 74.45 ppm, which is in the expected region for this vinylidene and the corresponding vinylidene stretch is seen in the IR spectrum at 1649 cm^{-1} (M=C=C) along with one C≡C at 1962 cm^{-1}.

2.3.4 Reaction of $Ru(C{\equiv}CC_6H_4\text{-}4\text{-}C{\equiv}C(CH_3)_2OH)(dppe)Cp^*$ with CPh_3^+

In contrast to the reactions observed with H^+, CAP and $C_7H_7^+$, the larger electrophile CPh_3^+ did not appear to react directly with **18** (only **21**, the product arising from protonation was observed). Despite efforts to synthesise $[CPh_3][BF_4]$ it proved impossible to obtain as a neutral powder. Synthesis of $[CPh_3][BF_4]$ is usually carried out with an excess of acid ($HBF_4.OEt_2$) in order to ensure complete conversion of triphenylmethanol to the triphenylmethyl cation[164] (**Scheme 2.16**) and an ether wash to remove the remaining acid. In order to try and reduce the amount of acid present a stoichiometric amount of $HBF_4.OEt_2$ was used, however even after the standard work up the compound was acidic. It was then washed three times with hexane, which left the final wash neutral, however when the product was dissolved in DCM it was still acidic. Finally, a slow diffusion crystallisation of the trityl cation from DCM and hexane also left the compound acidic. Therefore, it must be assumed that the acid co-crystallises with trityl.

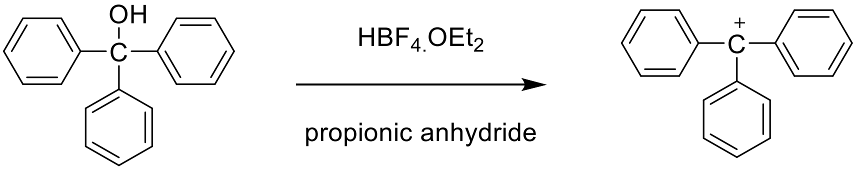

Scheme 2.16: Synthesis of $[CPh_3][BF_4]$

No evidence was obtained for the addition of any of the electrophiles to the terminal atoms of the organic ligand. Based on Hall's experiments (**Section 2.1.2**) it would have been expected that such an addition would result in a short-lived cumulene that would have been rapidly hydrolysed to give a complex such as **24** (**Figure 2.29**). However, no evidence for such a species was obtained, supporting the proposal that in these cases, addition occurs exclusively at the beta-carbon atom.

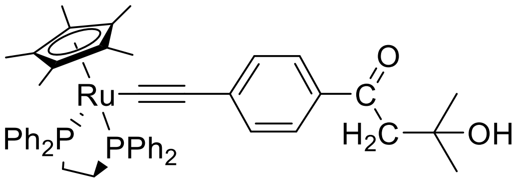

24

Figure 2.29: Possible product from water addition to 18

2.4 Tolan terminal groups, RuCl(-C≡C–C_6H_4-4-C≡C-C_6H_4-4-R)(dppe)Cp* (R = OMe, CO_2Me)

A tolan group is a group which consists of an unsaturated hydrocarbon with the general formula $C_6H_5C{\equiv}CC_6H_5$. The tolans used in this work are substituted with a ruthenium acetylide on one end and either OMe or CO_2Me on the other, compounds **25** and **26** (**Scheme 2.17**). The attempted reaction with the electrophiles, H^+, CN^+, $C_7H_7^+$ and CPh_3, were also carried out in the same way as in **Section 2.3** with these aromatic groups as the terminal substituent. Two different ethynyl tolan groups were used: the electron donating group OMe and the electron withdrawing group CO_2Me. Because tolans are aromatic they are less sterically bulky than the $C(CH_3)_2OH$ substituent meaning that they might encourage electrophile addition at the 8th carbon position while still blocking water addition at the seventh.

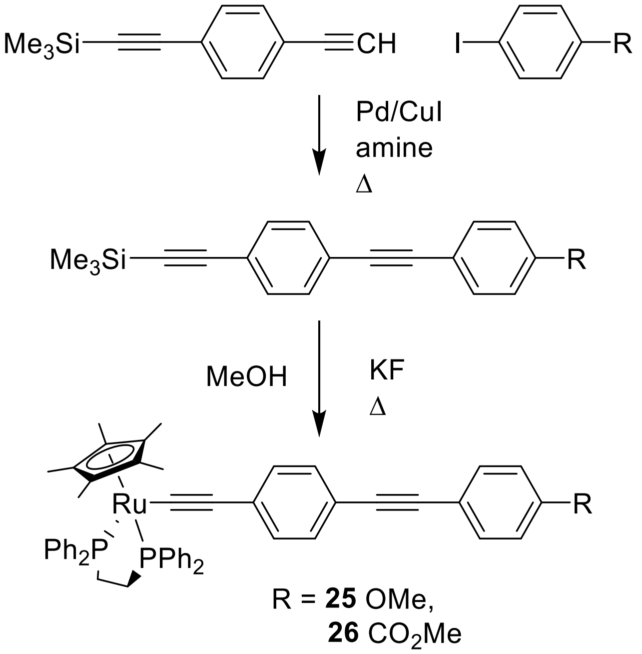

Scheme 2.17: Synthetic route to tolan acetylide complexes, 25 and 26

The tolan acetylides were synthesised through Sonogashira cross coupling reactions of 4-(trimethylsilylethynyl)phenylacetylene and 4-iodoanisole or methyl-4-iodobenzene, which was achieved in high yields (86 % and 84 % respectively). The organic compounds were then added to ruthenium chloride fragemnts using KF as a catalyst in methanol (88 % for **25** and 85 % for **26**), following the procedure by Bruce *et al.*[162]

The recorded NMR data for these complexes matched the literature[165] values (which were made through a different synthetic route, starting with Ru(C≡CC$_6$H$_4$C≡CH)(PPh$_3$)Cp and iodobenzene) with resonances in the ^{31}P{^{1}H} NMR spectra at 80.70 ppm (OMe) and 80.66 ppm (CO$_2$Me). For compound **25**, the spacer group doublets were observed at 6.69 and 7.17 ppm (*J* = 8.3 Hz) and the terminal benzene at 6.85 and 7.42 ppm (*J* = 8.8 Hz) with the three OMe protons at 3.82 ppm in the ^{1}H NMR spectrum. For compound **26**, the spacer group doublets appeared at 6.70 and 7.19 ppm (*J* = 8.3 Hz) and the terminal benzene doublets at 7.53 and 7.98 ppm (*J* = 8.5 Hz) with the CO$_2$Me singlet at 3.92 ppm.

In the previous work[165] the initial synthesis of the metal fragment occurred via a vinylidene intermediate. In this paper it was reported that this route provided better yields than using the 'KF' method described above (**Scheme 2.17**). It was speculated that the low yields could have been due to other isomeric vinylidene side products. In this work the yields of the RuCl(dppe)Cp* fragment were consistently high, but those for RuCl(PPh$_3$)$_2$Cp were lower and therefore not carried forward for further reactions.

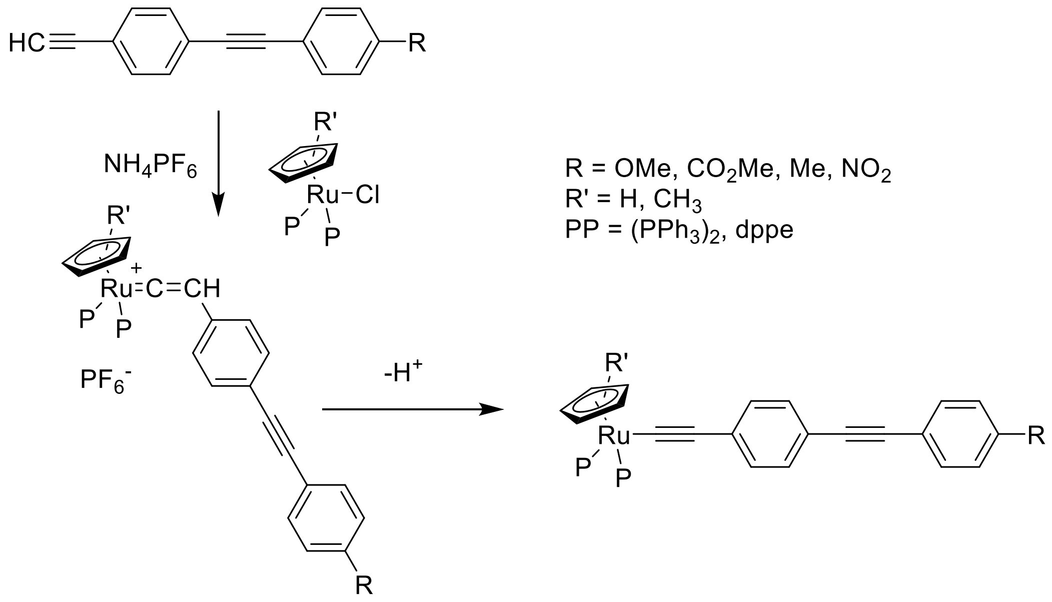

Scheme 2.18: Synthesis of ethynyl tolan compounds seen in Khairul *et al.*[165]

A second route to synthesise the tolan acetylides was also tested based on the work of Khairul *et al.*[165] It was anticipated that the Sonogashira reaction of the Ru(=C=CHC$_6$H$_4$-4-Br)(dppe)Cp* and 4-ethynylanisole or 4-ethynylbenzoic acid methyl ester (**Scheme 2.17**) when using PdCl$_2$(PPh$_3$)$_2$ as the palladium catalyst could provide direct access to **25** and **26** respectively. Sonogashira reactions, and other C-C bond forming reactions, involving compounds containing a variety metals have been well documented in the literature and were reviewed by Ren in 2008.[166] This synthetic route is of interest because it eliminates the possibility for bimetallic compounds to form as when using symmetrical alkynes, as well as the possibility for the formation of more complex molecules.

However, only partial conversion to the desired product was observed through analysis of ^{1}H NMR showed a mixture of resonances for the starting materials and the desired product even after a long reaction time (44 hours). When Pd$_2$(dba)$_3$ (dba = dibenzylideneacetone) with JohnPhos, (2-Biphenyl)di-tert-butylphosphine, was used as alternative catalyst the reaction went to completion and the desired product was identified in the crude NMR spectra. However attempted purification using prep-TLC caused product degradation and column chromatography was difficult with the starting materials and product having very similar Rf values in many solvent systems. This meant that co-elution occurred making this method impractical to prepare pure samples of **25** and **26**.

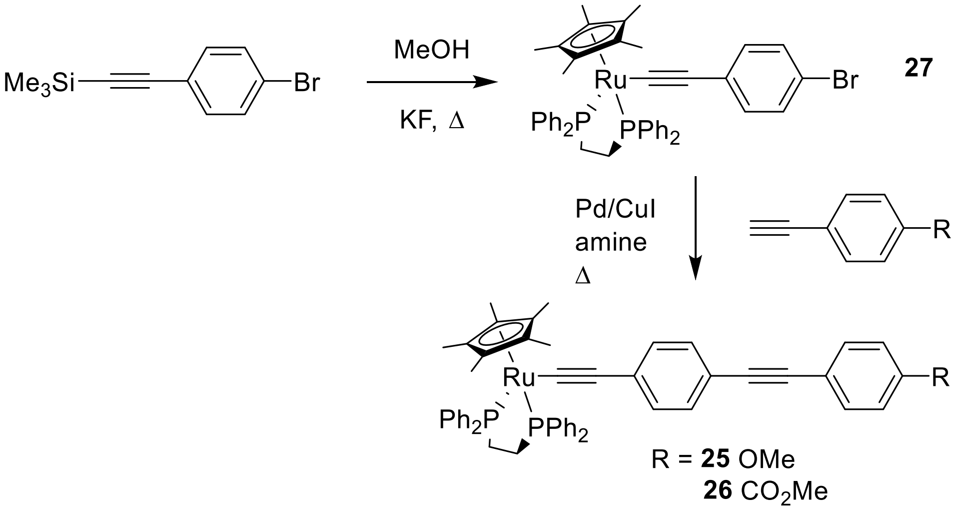

Scheme 2.19: Attempted second synthetic route to tolan acetylide complexes 25 and 26, through a metal complex Sonogashira reaction

The intermediate compound **27** was synthesised as a bright yellow powder which was stable in air, through the 'KF' catalyst method (**Scheme 2.19**), and the organic ligand precursor was made from the Sonogashira reaction of 1-bromo-4-iodobenzene and trimethylsilylacetylene (TMSA). Compound **27** was identified through NMR spectroscopy by the characteristic benzene proton doublets at 6.57 and 7.10 ppm (J = 8.5 Hz), the acetylide alpha carbon at 115.64 ppm and a resonance in the $^{31}P\{^{1}H\}$ spectrum at 80.78 ppm. The IR spectrum showed a single acetylide C≡C stretch at 2065 cm^{-1} and the mass spectrum showed an *m/z* at 814.1038 for ^{79}Br, which is very close to the expected mass-to-charge ratio, with a clear bromine isotope pattern as well as the ruthenium isotope pattern.

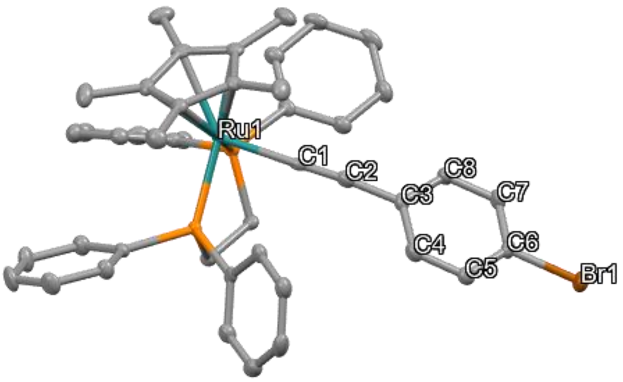

Figure 2.30: Molecular structure of compound 27, Ru(C≡CHC$_6$H$_4$-4-Br)(dppe)Cp* as determined by single crystal X-ray diffraction. Thermal ellipsoids are shown at the 50 % level, DCM molecules, and hydrogen atoms omitted for clarity. Grey = C, Dark green = Ru, Orange = P, Brown = Br

A clear light-yellow block-shaped crystal of **27** was grown by slow diffusion from DCM into hexanes (**Figure 2.30**). The ligand has an almost linear structure with an Ru-C(1)-C(2) angle of 178.8(2)°, a C(1)-C(2)-C(3) angle of 174.8(7)° and a C(3)-C(6)-Br angle of 178.8(0)° which are all close to 180°. In comparison the similar acetylide complex Ru(C≡C-C$_6$H$_4$-COCH$_3$)(dppe)Cp* **28**, seen in Figure 2.31,[152] has similar bond angles with the Ru(1)-(C1)-C(2) angle being 174.7(3)° and the C(1)-C(2)-C(3) angle 171.9(3)°. The bond distances are similar to the expected distances with Ru-C(1) being 2.025(3) Å (vs 2.005(3) Å for compound **28**), followed by the shorter triple bond C(1)-C(2) of 1.191(5) Å (1.224(4) Å for compound **28**) and then the single bond C(2)-C(3) of 1.446(5) Å (1.425(4) Å for compound **28**). The C(6)-Br distance is 1.904(3) Å, which is consistent with the average aromatic carbon-Br bond length of 1.899 Å.[167]

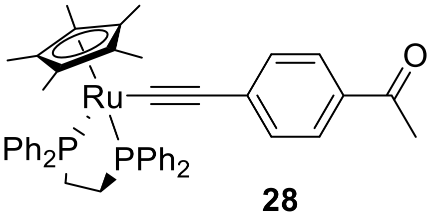

28

Figure 2.31: Structure of compound 28, Ru(C≡C-C_6H_4-$COCH_3$)(dppe)Cp* from which a crystal structure was recovered by Hall *et al*.[152]

The Sonogashira reaction of 4-ethynylbenzoic acid methyl ester with the metal containing species, **27**, was carried out under a variety of conditions, using both $PdCl_2(PPh_3)_2$ and $Pd_2(dba)_3$/JohnPhos, both with CuI and amine. The reaction with $Pd_2(dba)_3$ catalyst was the most successful as the desired product was observed in the crude reaction mixture, ^1H and ^{31}P NMR spectra was matched to the product made by the original method, however upon attempted work up by either TLC or column chromatography degradation occurred.

2.4.1 Reactivity of RuCl(-C≡C–C_6H_4-4-C≡C-C_6H_4-4-R)(dppe)Cp* (R = OMe, CO_2Me) with electrophiles

Both tolan derivatives **25** and **26** exhibited the same reactivity towards electrophiles despite the different electronics of the R groups. The reaction of the tolan acetylides with acid ($HBF_4{\cdot}OEt_2$), tropylium ([C_7H_7][BF_4]) and a cyano group ([CAP][BF_4]) in DCM (**Scheme 2.20**) was carried out at room temperature and purified through precipitation from DCM into ice-cold ether.

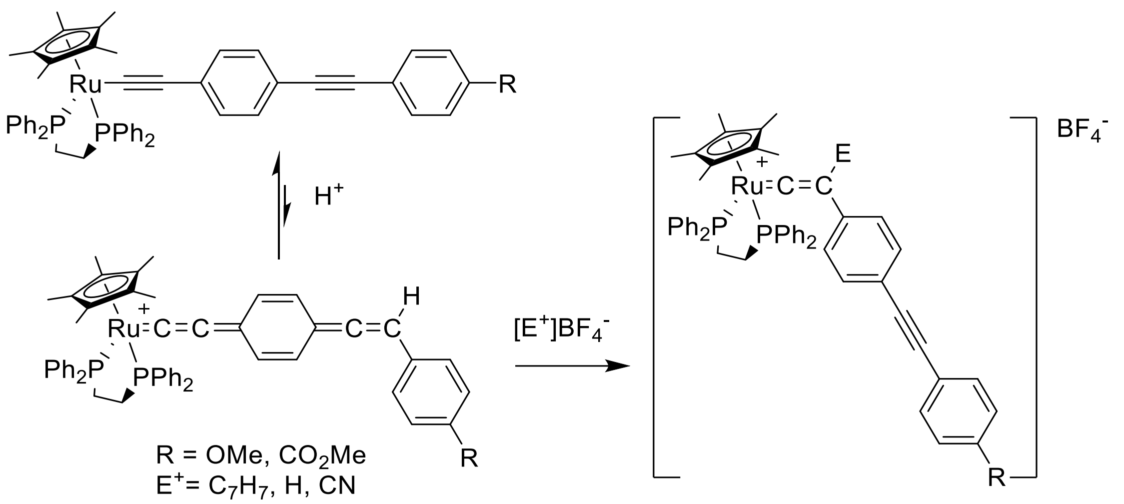

Scheme 2.20: Addition of small electrophiles to tolan acetylide complexes, and assumed mechanism based on previous work

2.4.1.1 Reactions with acid

The addition of the acid $HBF_4{\cdot}OEt_2$ gave the protio-vinylidene, as would be expected from this the smallest of electrophiles (**Figure 2.32**). For compound **29** this was shown through the single vinylidene type resonance in the $^{31}P\{^1H\}$ NMR spectrum at 71.97 ppm and the apparent triplet proton resonance at 4.39 ppm for the vinyl proton. Two sets of doublets were observed for the two benzene groups at 6.04 and 6.96 ppm (J_{HH} = 8.30 Hz) for the spacer group and 6.88 and 7.42 ppm (d, J_{HH} = 8.87 Hz) for the terminal benzene, the OMe resonance was at 3.83 ppm. The characteristically high vinylidene alpha carbon was also observed in the $^{13}C\{^1H]$ NMR spectrum for this molecule at 353.83 ppm along with the M=C=C stretch at 1630 cm^{-1} in the IR spectrum. A peak at *m/z* 867.2287 was recorded in the mass spectrum which is close to the calculated mass of 867.2453.

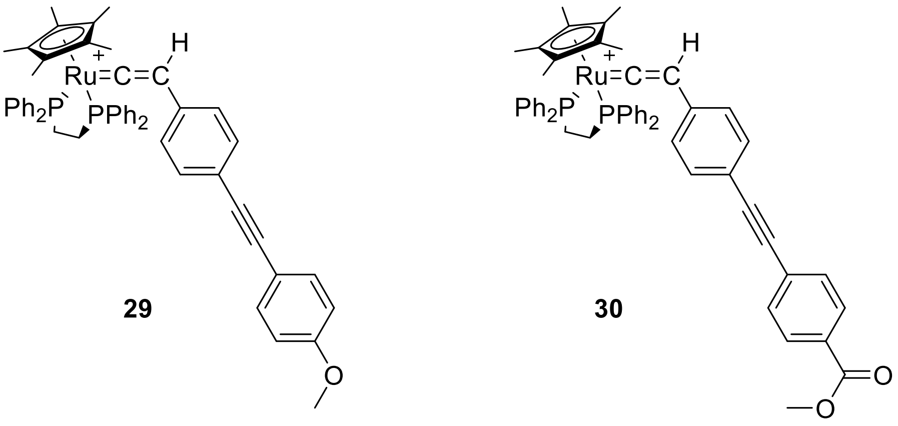

29

30

Figure 2.32: H$^+$ addition to compounds 25 and 26

For the corresponding CO_2Me tolan, **30** (**Figure 2.32**), very similar NMR data were observed, with the resonance in the $^{31}P\{^1H\}$ spectrum occurring at 71.80 ppm and the apparent triplet ^1H NMR resonance at 4.39 ppm. The aromatic protons also occur at similar spacer group doublet resonances of 6.07 and 6.98 ppm (J_{HH} = 8.3 Hz) and terminal benzene doublets at 7.54 and 8.01 ppm (J_{HH} = 8.4 Hz). The CO_2Me resonance at 3.93 ppm was very similar to that of the starting material, **26**, at 3.91 ppm, this similarity can be attributed to the fact that the changes at the β carbon have very little effect on the shielding of the atoms at this end of the molecule. The α carbon was observed at 343.58 ppm, the M=C=C stretch at 1623 cm^{-1} and a mass-to-charge ratio of 895.2219 *m/z* which is close to the expected value of 895.2402 *m/z*. A very small mass peak was observed at 913.2295 which can be related to the water addition product compound **30** (**Figure 2.33**), however as this is not observed by any other spectroscopic method then it can be assumed that it is a very small by-product of the reaction or is a result of exposure to water during the acquisition of the ESI-MS.

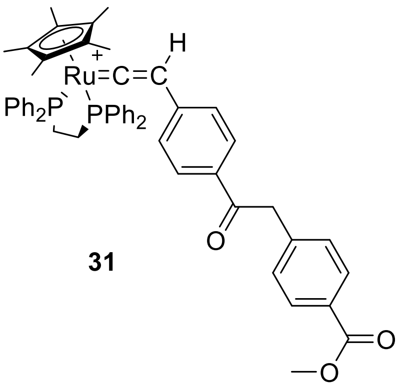

31

Figure 2.33: Possible product from water addition to 30

2.4.1.2 Reactions with CN$^+$

The addition of CN from [CAP]BF_4 also occurred at the beta carbon forming a cyano-vinylidene, **32** (**Figure 2.34**). The NMR $^{31}P\{^1H\}$ NMR spectrum gave a single resonance at 70.70 ppm as expected for a vinylidene, in the $^{13}C\{^1H\}$ NMR spectrum the α carbon was identified at 343.76 ppm and the M=C=C stretch at 1650 cm^{-1} in the IR spectrum. The CN group was identified through $^{13}C\{^1H\}$ NMR at 122.87 ppm and the C≡N stretch at 2198 cm^{-1}. The spacer group protons doublets were seen at 6.04 and 6.96 ppm (J_{HH} = 8.44 Hz), the terminal benzene doublets at 6.88 and 7.42 ppm (J_{HH} = 8.90 Hz) and the OMe group as a singlet at 3.83 ppm. The observed mass-to-charge ratio of 892.2150 *m/z* was very similar to the expected mass of 892.2406 *m/z*.

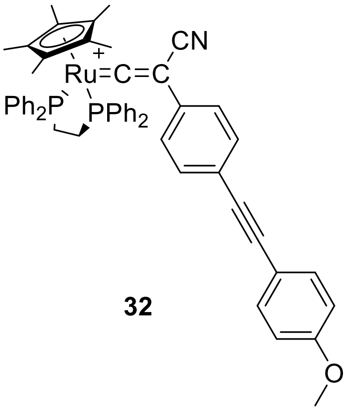

32

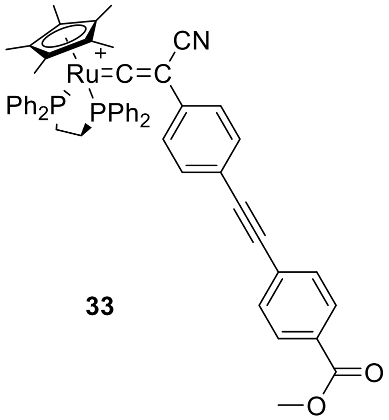

33

Figure 2.34: CN$^+$ addition to compounds 25 and 26

For the analogous CO_2Me tolan, compound **33** (**Figure 2.34**) the vinylidene resonance in the $^{31}P\{^1H\}$ spectrum occurred at 70.55 ppm, in the $^{13}C\{^1H\}$ NMR spectrum the α carbon was identified as an apparent triplet at 343.20 ppm and the M=C=C stretch at 1649 cm^{-1}. The proton NMR spectrum showed the spacer group doublets at 6.47 and 7.07 ppm (J_{HH} = 8.40 Hz), the terminal benzene at 7.57 and 8.02 ppm (d, J_{HH} = 8.50 Hz) and the three CO_2Me group protons at 3.92 ppm. The existence of the CN group was confirmed through the CN carbon resonance at 122.07 ppm, the C≡N resonance at 2199 cm^{-1} and the ion having a mass of 920.2140 *m/z* (calculated to be 920.2355).

2.4.1.3 Reactions with $C_7H_7^+$

The third electrophile used was C_7H_7, which also reacted with the tolan compounds at the beta position. The reaction with compound **25** resulted in the formation of compound **34** (**Figure 2.35**). The resonance in the $^{31}P\{^1H\}$ spectrum was in the expected region for a Ru(dppe)Cp* vinylidene at 74.48 ppm, the M=C=C stretch was at 1648 cm^{-1} and the proton NMR gave the two sets of doublets at 6.78 and 7.03 ppm (d, J_{HH} = 8.35 Hz) for the spacer and 6.89 and 7.47 ppm (d, J_{HH} = 8.89 Hz) for the terminal benzene, with a singlet for OMe at 3.85 ppm. The ^1H NMR spectrum also showed four resonances for the C_7H_7 group: the proton attached to the carbon adjacent to the beta carbon had a triplet splitting pattern and was aliphatic in nature at 1.64 ppm (J_{HH} = 5.34 Hz). The other resonances occurred in the aromatic region despite not being aromatic and are, in order, 5.02 ppm (dd, J_{HH} = 5.37 Hz, J_{HH} = 9.19 Hz), 5.98 ppm (d, J_{HH} = 9.19 Hz), and 6.29 ppm (t, J_{HH} = 2.96 Hz), even though the *J* coupling values do not match for the triplet at 2.96 ppm it is well defined by the coupling in the COSY NMR spectra. It proved impossible to observe the alpha carbon resonance in the $^{13}C\{^1H\}$ NMR spectrum on a reasonable experiment length. The mass spectra did not show the expected mass for **34** but showed an *m/z* of 867.2480 which can be related to compound **29** arising from formal protonation, however the other characterisation techniques prove that the expected complex has been made and the C_7H_7 is likely lost during ionisation in the mass spec.

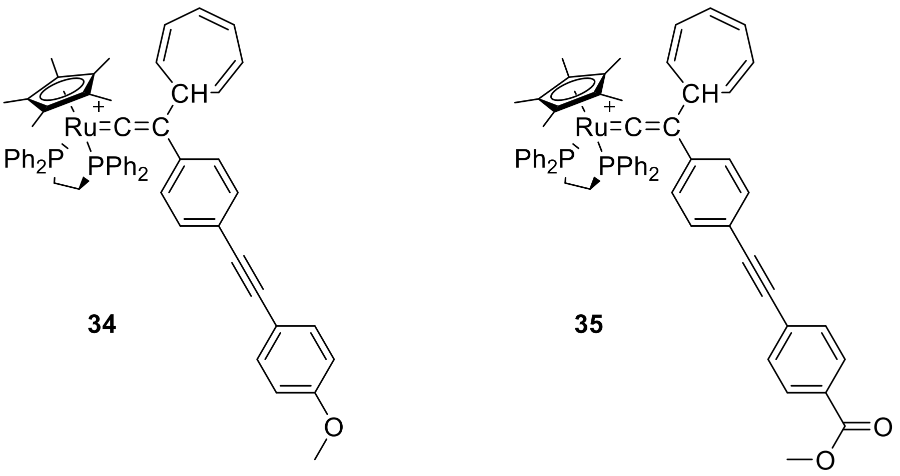

34

35

Figure 2.35: $C_7H_7^+$ addition to compounds 25 and 26

Further evidence that compound **34** was successfully synthesised comes from the single crystal analysis of a crystal grown by slow diffusion from DCM into hexanes (**Figure 2.36**). The crystal showed an interesting structure with the vinyl-C_7H_7 fragment taking on a curved shape indicating that the aromaticity has been lost. Consistent with this, the bond lengths around the tropylium follow the single bond and double bond lengths. The C(3)-C(4) and C(3)-C(9) bond lengths are 1.514(5) Å and 1.515(5) Å, followed by C(4)-C(5) and C(9)-C(8) bond lengths are 1.308(5) Å and 1.312(5) Å, then C(5)-C(6) and C(8)-C(7) bond lengths are 1.449(6) Å and 1.450(5) Å and finally the C(6)-C(7) bond length is 1.345(6) Å. The Ru-C(1) double bond is 1.852(3) Å, followed by the C(1)-C(2) bond of 1.305(4) Å. This proves that this is no longer aromatic as the general bond lengths around the benzene rings are between 1.376(5) Å and 1.408(5) Å. The bond between the beta carbon and the tropylium ion is a single bond of 1.543 Å. Ru-C(1)-C(2) angle is 171.5(9)°, the C(1)-C(2)-C(3) angle is 122.2(2)°. The angles around the C_7H_7 are all between 113.3(2)° and 125.8(7)°.

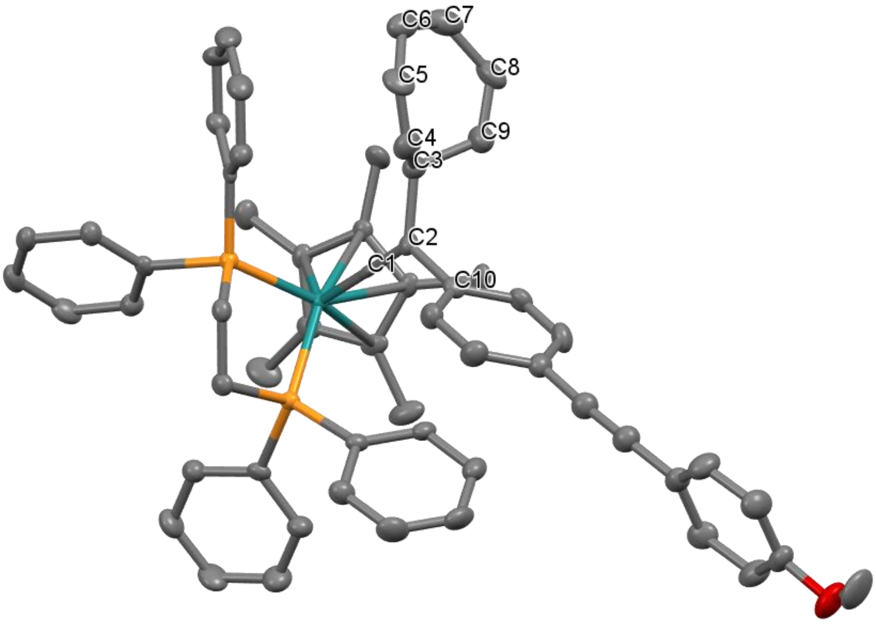

Figure 2.36: Molecular structure of 34, [Ru(=C=C(C_7H_7)C_6H_4CCC_6H_4OMe)(dppe)Cp*]BF_4 from addition of [C_7H_7]BF_4 to Ru(CCC_6H_4CCC_6H_4OMe)(dppe)Cp*as determined by single crystal X-ray diffraction. Thermal ellipsoids are shown at the 50% level, DCM molecules, BF_4 anions and hydrogen atoms omitted for clarity. Grey = C, Dark green = Ru, orange = P, Red = O

Compound **35** (**Figure 2.35**) was formed from RuCl(-C≡C–C_6H_4-4-C≡C-C_6H_4-4-CO_2Me)(dppe)Cp* and [C_7H_7][BF_4] and the analysis showed all of the expected features for a vinylidene including a phosphorus NMR at 74.41 ppm and the M=C=C IR stretch at 1653 cm^{-1}. As with compound **34** there was no mass peak for the parent ion but a mass of 895.2221 which can be attributed to the loss of C_7H_7 and subsequent addition of H, which likely occurs during the acquisition of the mass spectrum. The proton NMR spectrum showed the expected benzene doublets at 6.82 and 7.07 ppm (J_{HH} = 8.42 Hz) for the spacer and 7.59 and 8.03 ppm (J_{HH} = 8.67 Hz) for the other, with the CO_2Me singlet occurring at 3.85 ppm. For the C_7H_7 ring the resonances were observed at 1.64 ppm (t, J_{HH} = 5.67 Hz), 5.02 ppm (dd, J_{HH} = 5.42 Hz, J_{HH} = 9.13 Hz), 5.98 ppm (d, J_{HH} = 9.13 Hz) and 6.24 ppm (t, J_{HH} = 2.92 Hz).

The reactions followed the same reactivity profile as seen with compound **18** and previous work in the group.[152] These electrophiles are sterically small enough so that they can react at the beta carbon of the ligand and form the substituted vinylidene complexes. The reactivity could be explained by either a cumulene intermediate, with the eighth carbon being sterically hindered by the second aromatic group or straight electrophile addition to the beta carbon, or a combination of both.

2.4.2 Addition of acid to [Ru(=C=C(C_7H_7)C_6H_4CCC_6H_4-OMe)(dppe)Cp*]BF_4

The addition of one drop of HBF_4.OEt_2 to compound **34** (**Figure 2.35**) in DCM gave an immediate colour change from pale orange to purple, and a purple solid was recovered. The proton NMR spectrum of the purple powder revealed it to identical to compound **29** when HBF_4·OEt_2 was added directly to the parent tolan acetylide. Therefore, the acid must be displacing the C_7H_7 at the vinylidene position (**Scheme 2.21**). These data indicate that the addition of $C_7H_7^+$ is reversible and it is proposed that **34** is in equilibrium with its cumulene form (**Scheme 2.21**). On addition of HBF_4.OEt_2 the cumulene may then react with the $C_7H_7^+$ (to reform **34**) or H^+ to give **29**. Due to the increased stability of the protio-vinylidene and availability of H^+ means that only **29** is observed.

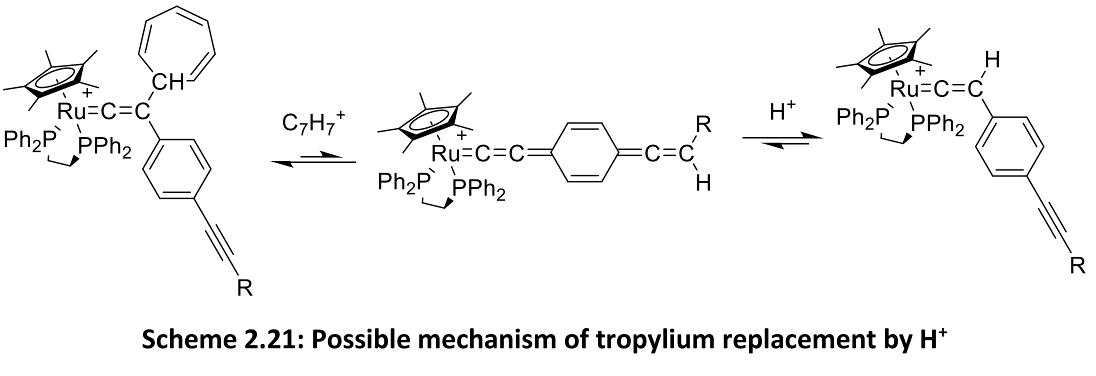

Scheme 2.21: Possible mechanism of tropylium replacement by H^+

2.4.3 Trityl additions to Ru(C≡CC$_6$H$_4$-4-C≡CC$_6$H$_4$-4-CO$_2$Me)(dppe)Cp*

The final electrophile that was reacted with compound **26** was CPh$_3$, which is the most sterically demanding electrophile used. Multiple reactions of the CO$_2$Me tolan, complex **26**, with CPh$_3$ were carried out stoichiometrically in DCM from 15 mins to 4 hours to overnight.

These reactions gave a single, very clean product with identical NMR and mass spectrometry data to the reaction with HBF$_4$·OEt$_2$, compound **30**. It was assumed that there was a small amount of acid present from the synthesis of CPh$_3$ (which could not be removed post synthesis), therefore a reaction with the addition of NEt$_3$ in situ was also run. However as with previous reactions run with a base in-situ no reactivity was observed. Initial darkening of the solution upon CPh$_3$ addition can be attributed to the formation of the protio-vinylidene before it was deprotonated again by the base turning the solution bright yellow again. It can be assumed that there is steric hindrance to the addition of CPh$_3$ at carbon number eight (as seen with the terminal alkyne) due to the bulk of the tolan group. Possibly a slightly less bulky group, i.e. an alkyl chain, could allow for CPh$_3$ addition at the eighth carbon.

1.3 Conclusion

The addition of the nucleophiles used to *trans*-[RuCl(=C=CHC$_6$H$_4$-4-C≡CH)(dppe)$_2$][OTf] works well, giving a series of compounds with substitutions at the seventh carbon. The addition of multiple nucleophiles with the same substitution pattern gives further evidence that a cumulene intermediate is being formed and directing the nucleophile addition at the seventh carbon in the chain (**Scheme 2.22**). During the addition of some nucleophiles a further rearrangement or addition reaction also takes place.

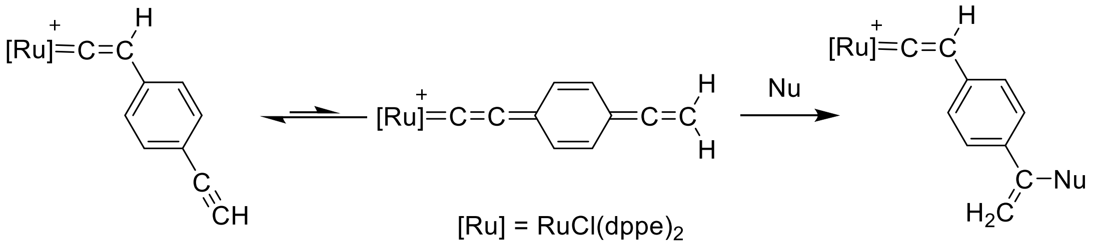

Scheme 2.22: Addition of nucleophiles to ruthenium vinylidenes through a cumulene intermediate

However, for the corresponding acetylide complex the addition of electrophiles does not occur. The beta addition site is blocked by steric hindrance from the large dppe ligands, but this does not cause the reactivity to move to the terminal 8th carbon.

In contrast to the bis-dppe ruthenium complex the addition of small electrophiles (H^+, CN^+, $C_7H_7^+$) to both ruthenium and iron half sandwich complexes at the beta carbon is successful.[152] This is expanded to similar ruthenium half sandwich complexes which have large terminal groups (**Sections 2.3 and 2.4**) in the place of the terminal proton (**Scheme 2.23**).

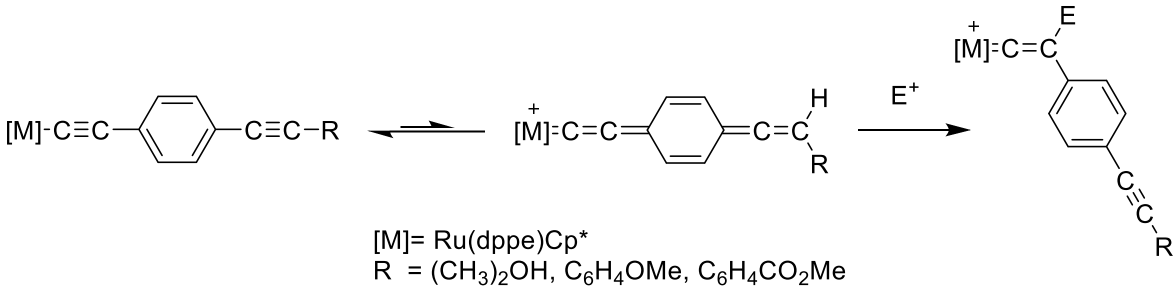

Scheme 2.23: Addition of small electrophiles to substituted terminal alkynes through a cumulene intermediate

The addition of CPh_3 has only been observed for the unsubstituted diethynyl benzene at the terminal carbon position. For the substituted alkynes the addition of CPh_3 was not observed, instead the residual acid from the synthesis of $[CPh_3][BF_4]$ meant that the protio-vinylidene was formed.

Chapter 3 Alternative spacer groups

Although there is a growing body of evidence from reactions with nucleophiles and electrophiles, which is described in Chapter 2, pointing to the fact that a quinoidal cumulene intermediate is present in these the reactions of ruthenium alkynyl complexes with pendant alkyne groups, (**Scheme 3.1**) the cumulenes have yet to be isolated or even observed spectroscopically. The inability to observe the cumulene intermediates could be due to the relatively high aromatic stabilisation energy (ASE), per ring, of benzene which is lost when these intermediates are formed. This means that there is a driver for the aromatic system to reform either through equilibrium with the starting material or reactivity with other compounds in the system.

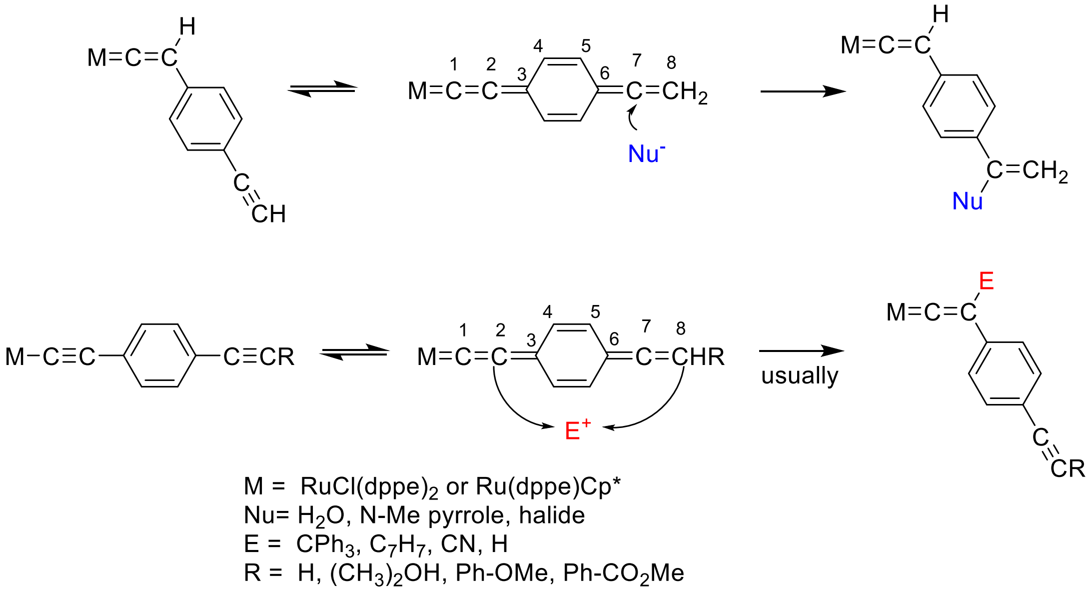

M = $RuCl(dppe)_2$ or Ru(dppe)Cp*
Nu= H_2O, N-Me pyrrole, halide
E = CPh_3, C_7H_7, CN, H
R = H, $(CH_3)_2OH$, Ph-OMe, Ph-CO_2Me

Scheme 3.1: Reactions via a cumulene intermediate, summarised from Chapter 2.

It was therefore proposed that the use of fused aromatic compounds could be used in a similar way to benzene but as they have lower aromatic stabilisation energy per ring, they may be easier to stabilise, because there a is lower penalty for cumulene formation. For this work, three alternative spacer groups were used: naphthalene, 2,1,3-benzothiadiazole (BDT) and anthracene (**Figure 3.1**).

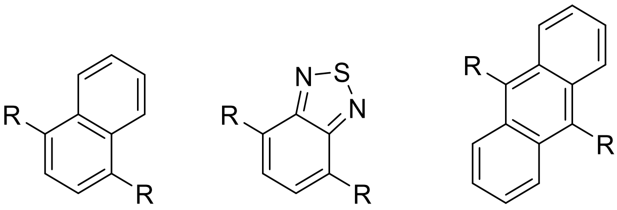

Figure 3.1: Structures of naphthalene, 2,1,3-benzothiadiazole (BDT) and anthracene.

Anthracene has the lowest ASE of the carbon-only compounds at 115.6 kJ mol^{-1} per ring (347 kJ mol^{-1} overall) followed by naphthalene 127.5 kJ mol^{-1} (255 kJ mol^{-1}) (**Figure 3.2**). The same can also be applied to heteroaromatic systems with thiophene also having an ASE of 121 kJ mol^{-1}, which is lower than for benzene (151 kJ mol^{-1})[168]. Other heteroaromatic compounds have an even lower aromatic stabilisation energy than thiophene, however, other chemical considerations make them less suitable for use as a cumulene stabilising spacer group. The ASE for BDT is currently unknown; however, it is often used as a component of polymers with very low stable band-gaps.

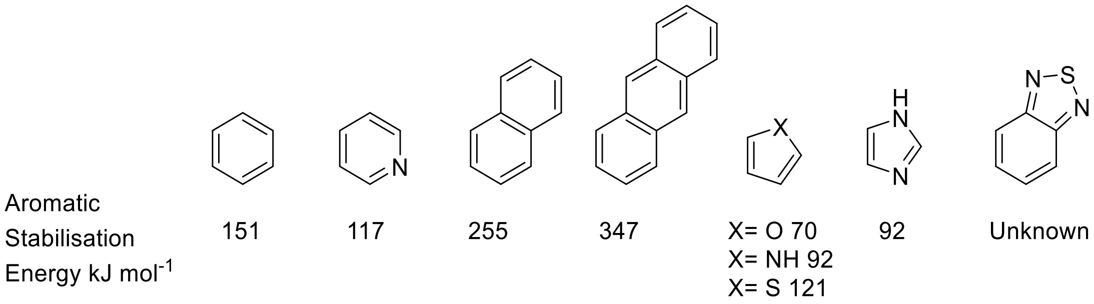

Figure 3.2: Aromatic stabilisation energy (ASE) of various aromatic compounds[168]

3.1 Naphthalene-spaced cumulenes

The first alternative spacer group chosen to study was naphthalene. This was because it has a lower ASE per ring than benzene but the increase in steric size is not as large as anthracene. This makes the naphthalene spacer group more similar to the benzene spacer group but the cumulene intermediate may be stabilised with respect to the vinylidene form. Three methodologies were considered in the design of the synthetic route to compound **36** (**Figure 3.3**). These are based on using a symmetrically TMS-protected dialkyne (**Scheme 3.3**),[169] an unsymmetrically protected dialkyne (**Scheme 3.4**) and through single lithiation of the TMS-protected dialkyne **(Scheme 3.7)**.[34,170] Each of these approaches presents different advantages, and were explored in turn.

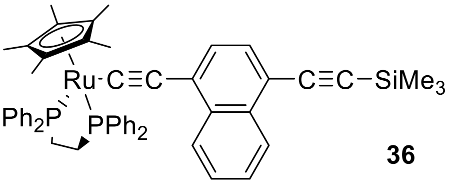

36

Figure 3.3: Structure of desired mono-metallic naphthalene, 36

3.2 Synthesis of 1,4-bis(trimethylsilyl)ethynyl naphthalene

The synthesis of bimetallic diethynyl naphthalene complexes has been described by the group previously,[169] from the reaction of RuCl(dppe)Cp* and 1,4-bis(trimethylsilyl)ethynyl naphthalene in a 2:1 ratio, utilising potassium fluoride as a catalyst. It was hoped that by increasing the number of equivalents of ligand in comparison to the metal to four equivalents that the formation of the bimetallic species could be supressed, especially as this approach had been successful for the diethynylbenzene complexes (**Chapter 2, Section 2.2 and 2.3**). However even when a large excess of TMS-diethynyl naphthalene, 2.3 equivalents, was used in the 'KF'-catalysed addition reaction in methanol over a 5-hour period, less than half of the resulting precipitate was the desired mono-metallic complex **36a**, with the rest comprising of the bimetallic species, **37** (**Scheme 3.2**).

This was demonstrated by the presence of two $^{31}P\{^{1}H\}$ NMR resonances at 80.91 ppm (bimetallic) and 81.22 ppm (monometallic) and by examination of integration of the resonances in the ^{1}H NMR spectrum by comparing the amounts of spacer group protons to that of the ligands. If the resonance at 1.60 ppm where the Cp* ligand generally appears is set to 15H then the naphthalene group doublet at 6.65 ppm (J_{HH} = 7.56 Hz) only has an integration of 0.57H instead of the expected 1H meaning that some of the Cp* integral must be due to the bimetallic complex. The presence of the characteristic TMS resonance at 0.07 ppm, with an integration of 2.4H instead of 9H, indicates that a small amount of the desired monometallic product was present in the sample.

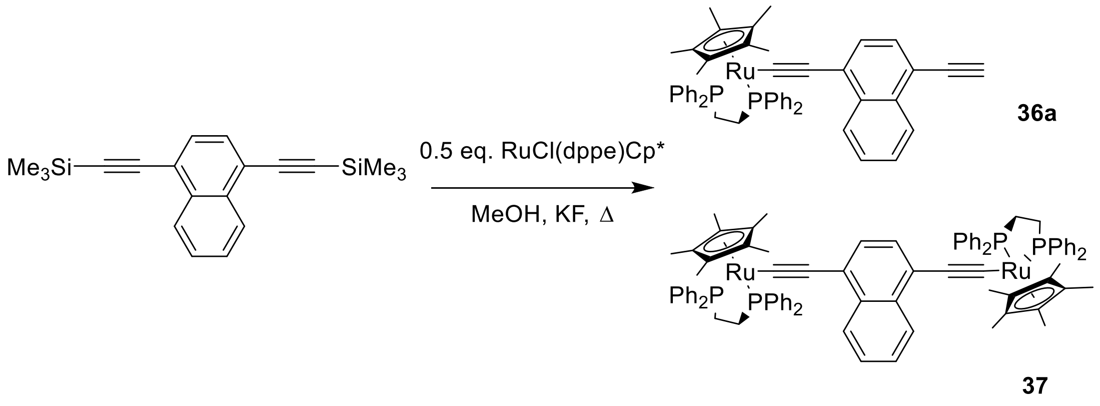

Scheme 3.2: Addition of RuCl(dppe)Cp* to TMS-protected 1,4-diethynylnaphthalene to produce both mono- and bi-metallic species

Separation of the mono-metallic compound, **36a**, from the bimetallic compound, **37**, was not possible by preparative TLC methods as there was obvious degradation on the silica. The major products being the same for both the fractions collected by preparative TLC, which had $^{31}P\{^{1}H\}$ NMR resonances at 29.12 ppm (a phosphorus oxide) and 50.25 ppm for **37**. Performing the 'KF' reaction for 16 hours and washing the brown solid with diethylether did give a pure product- which as shown by the ^{1}H NMR spectra to be the bimetallic product, compound **37**, even when 2.3 equivalents of 1,4-bis(trimethylsilyl)ethynyl naphthalene were used. This, along with the short reaction times required to make the bimetallic compound in the literature[169] (90 mins), indicates that under these conditions the formation of **37** is favoured.

As this procedure preferentially formed the bimetallic species, **37**, rather than the desired monometallic compound, **36a**, it was determined that an alternative synthetic methodology was required. It is known from the experiments to make $Ru(C\equiv CC_6H_4\text{-}4\text{-}C\equiv CC_6H_4\text{-}4\text{-}OMe)(dppe)Cp^*$, **25**, that Sonogashira reactions on the metal bound acetylide-bromide species (**Chapter 2, Section 2.4**) is possible however difficulties in the purification of these compounds are likely to be the same for the naphthalene analogues, therefore this synthetic route was not explored.

3.3 Synthesis of $Ru(C{\equiv}CC_{10}H_6\text{-}4\text{-}C{\equiv}C(CH_3)_2OH)(dppe)Cp^*$

Another possible synthetic route to prepare complex **36** was targeted which used an orthogonally protected organic fragment whose protecting groups could be removed under different conditions and therefore only allow the addition of one metal fragment to the functionalised alkyne. The protecting groups chosen for this were trimethylsilyl (TMS) and the acetone protecting group, $(CH_3)_2OH$ (**Scheme 3.3**).

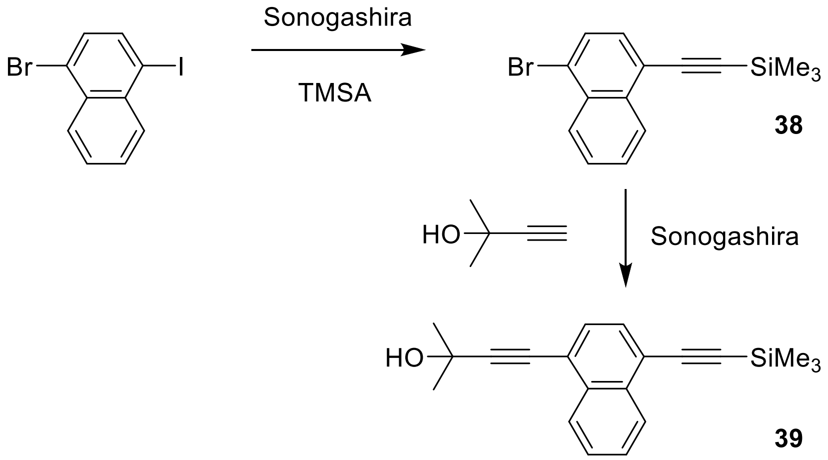

Scheme 3.3: Synthetic route to the unsymmetrically protected diethynyl naphthalene product, 39

A Sonogashira coupling between trimethylsilylacetylene (TMSA) and iodide, from 1-bromo,-4-iodonaphthalene was carried out at room temperature following literature methods[171] and gave **38** as a yellow or orange oil. Although **38** has been prepared by other groups[172] the addition of a second alkyne has not been carried out previously. The Sonogashira coupling of 2-methyl-3-butyn-2-ol at the bromide position of **38** was carried out at reflux due to the lower reactivity of Br when compared to I. The final product, **39**, was isolated as a pale-yellow oil with an overall yield of 56 %. The ^1H NMR spectrum of **39** showed a nine-proton resonance at 0.33 ppm for the TMS protecting group and another six-proton resonance at 1.74 ppm for methyl groups of the $(CH_3)_2OH$ moiety. The aromatic naphthalene resonances occurred at 7.60 ppm for four protons on the non-alkyne substituted ring and the final two at 8.27 ppm and 8.34 ppm. The corresponding $^{13}C\{^1H\}$ NMR spectrum exhibited resonances at 0.15 ppm for TMS and 31.70 and 66.01 for $(CH_3)_2OH$. The four alkyne resonances were also observed at 80.19, 100.87, 101.36 and 102.85 ppm, along with aromatic carbons between 121 and 133 ppm.

This unsymmetric alkyne, **39**, was then reacted with RuCl(dppe)Cp* using the 'KF' catalyst method described previously (**Chapter 2, Section 2.3**). This yielded the compound Ru(4-ethynyl-1-(3-hydroxyl-3-methylbutyl)naphthalene)dppeCp*, **40**, as a microcrystalline orange or yellow powder with a yield of 89 % (**Scheme 3.4**).

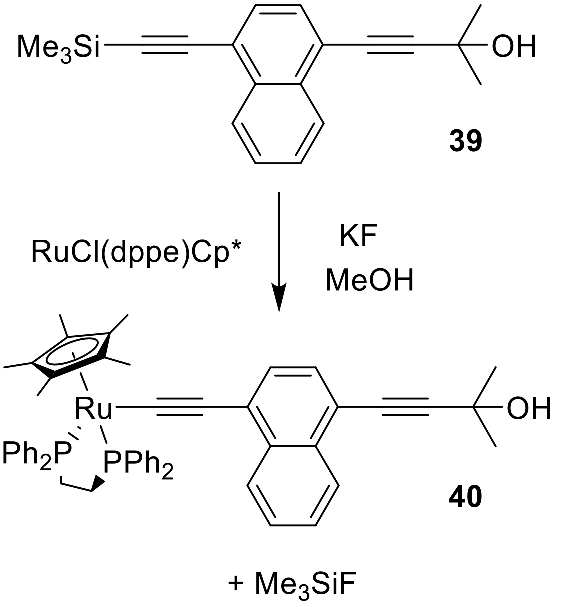

Scheme 3.4: Synthesis of Ru(4-ethynyl-1-(3-hydroxyl-3-methylbutynyl)naphthalene) (dppe)Cp*, compound 40

Compound **40** was identified through ^1H NMR spectroscopy with the resonances for the naphthalene spacer group appearing as a doublet at 6.66 ppm (J_{HH} = 7.6 Hz) with a corresponding multiplet at 7.33 ppm, these two resonances are analogous to those observed in the benzene spacer group for compound **18** (**Chapter 2, Section 2.3**). The protons for the non-alkyne containing ring occur as multiplets at 7.02 and 7.38 ppm and doublets at 7.71 (d, J_{HH} = 8.3 Hz) and 8.11 ppm (d, J_{HH} = 8.3 Hz). A resonance for the methyl groups of the protecting group were observed as a six-proton resonance at 1.71 ppm. The other ligands had characteristic resonances including a singlet resonance at 1.62 ppm (15H) for the Cp* group, the aliphatic dppe multiplets at 2.14 and 2.75 ppm, and aromatic dppe resonances at 7.04, 7.21- 7.37 and 7.76 ppm (t, J_{HH} = 8.4 Hz). The $^{31}P\{^1H\}$ NMR resonance at 80.94 ppm is indicative of an alkyne compound with this Ru(dppe)Cp* metal fragment.[152] Although the OH proton was not observed in the ^1H NMR spectrum other characterisation techniques prove that this functional group has not been lost. In the $^{13}C\{^1H\}$ NMR spectrum the alpha carbon resonance occurred as a multiplet at 130.08 ppm followed by the beta carbon at 109.84 ppm, the other alkyne resonances were observed at 81.75 and 97.88 ppm. The carbons from the (CMe_2OH) protecting group also occurred at similar resonances to the organic compound **39**, at 31.94 and 66.13 ppm. The six CH naphthalene resonances occurred at 124.91, 125.56, 125.99, 127.17, 128.40 and 128.95 ppm and the four quaternary ones at 113.39, 130.46, 133.49 and 133.97 ppm. The Cp* carbons occur at 10.27 (for the CH_3) and 93.04 ppm, and dppe has $^{13}C\{^1H\}$ NMR resonances at 29.54, 127.60, 129.12, 133.31 and 133.79 ppm. The ESI(+)-MS showed a compound with a ruthenium isotope pattern at 869.2791 *m/z* (for ^{102}Ru) which can be attributed to the mass of the expected compound with the addition of a proton (869.2610 *m/z*). The IR spectrum showed a single acetylide C≡C stretch at 2047 cm^{-1} and an OH stretch at 3284 cm^{-1}. The electrochemical analysis of **40** is reported in **Chapter 4, Sections 4.1.2.2, 4.3.2.2 and 4.5.2.2**.

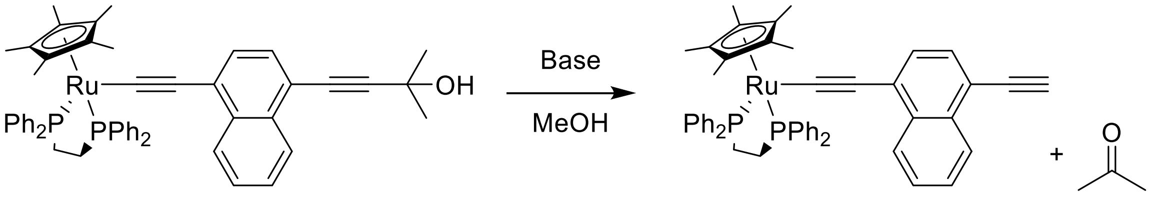

Scheme 3.5: Desired acetone deprotection reaction

As it was possible to remove the $(CH_3)_2OH$ group from the benzene analogue of this compound (**Chapter 2, Section 2.3**) it was expected that it would be possible when the naphthalene spacer was used (**Scheme 3.5**). However, despite heating the complexes with either KOH and KO^{t}Bu, and running the reaction for either 3 hours at reflux in methanol or at room temperature overnight no reaction was observed and pure compound **40** was recovered. It was therefore concluded that this deprotection was not possible and an alternative route was sought.

3.4 Lithiation of 1,4-diethynyl(trimethylsilyl)naphthalene

Lithiated TMS-acetylides have been used to prepare ruthenium complexes containing both long alkyne chains[34] or add ones with a benzene spacer group (**Scheme 3.6**).[170] It was therefore believed that this method could also be used to synthesise compound **36**.

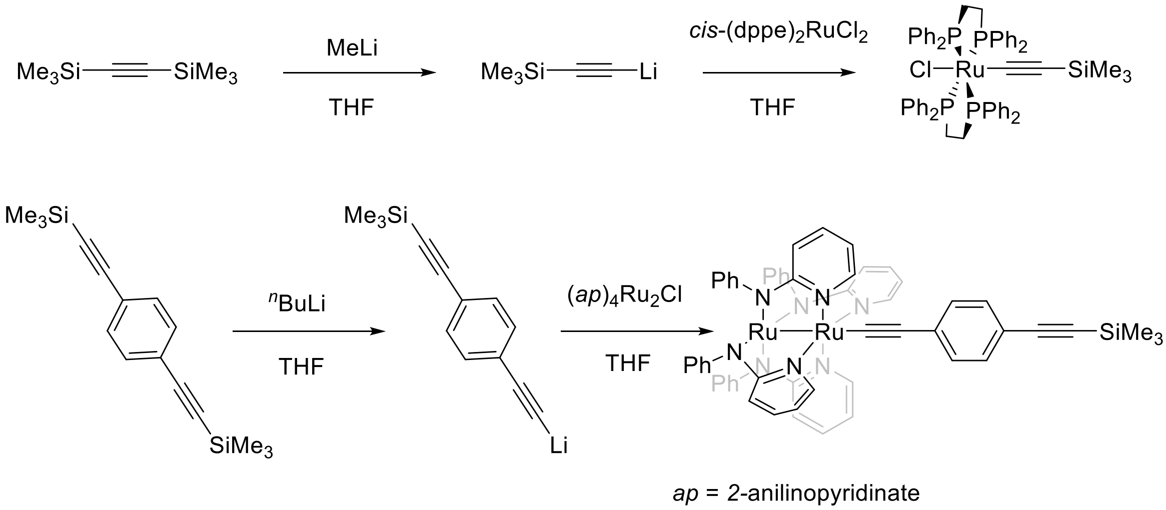

Scheme 3.6: Synthesis of alkynes using *in-situ* lithiation of TMS-protected alkynes by Dixneuf *et al*.[34] and Hurst and Ren[170]

The literature scheme used by Dixneuf *et al.*[34] used *cis*-$RuCl_2(dppe)_2$ as the metal fragment, because of this the initial lithiation reactions were carried out with this ligand set. The methods used previously[34,170] were modified to make pure compound **42** (**Scheme 3.7**). This procedure involved the addition of one equivalent of methyl lithium to 1,4-diethynyl(trimethylsilyl)naphthalene at -78 °C which lithiated one of the protecting groups making 1-ethynyl(trimethylsilyl),4-ethynyl(lithium) naphthalene, **41**. This was accompanied by a colour change from orange to blue/grey. Lithiated compound **41** was then reacted with *cis*-$RuCl_2(dppe)_2$, to give the desired product as an orange solid and lithium chloride by-product (**Scheme 3.7**). The compound was purified using a short alumina column, using hexane to elute the impurity followed by diethylether to remove the product. This second band was then dissolved in DCM and precipitated from pentane, which turned the product from dark brown to orange.

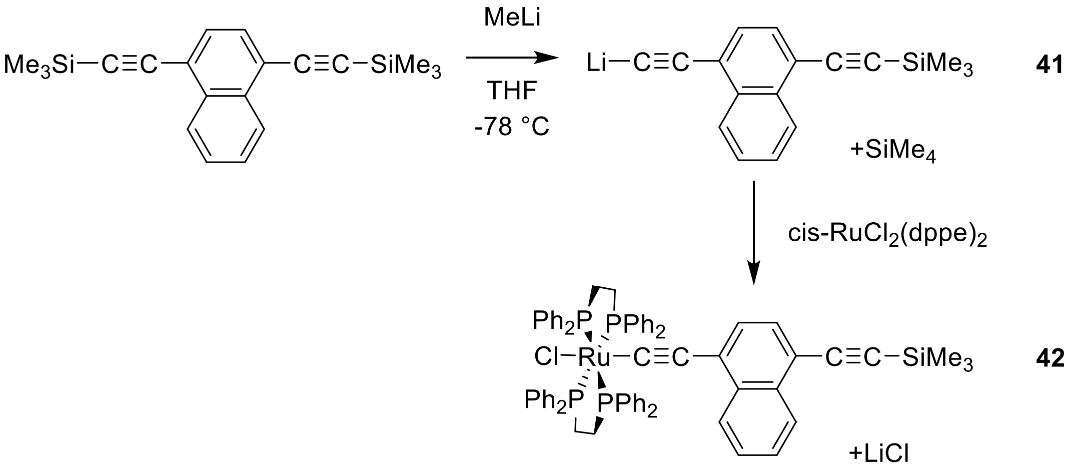

Scheme 3.7: Single pot lithiation of 1,4-[di(trimethylsilyl)ethynyl]-naphthalene and addition of *cis*-RuCl$_2$(dppe)$_2$ forming compound 42.

The ^{31}P{^{1}H} NMR spectrum of **42** exhibited a singlet resonance 48.05 ppm. The retention of one TMS group was identified through a resonance in the ^{1}H NMR spectrum at 0.35 ppm which integrated to 9 protons and a related peak in the ^{13}C{^{1}H} NMR spectrum at 2.40 ppm. The naphthalene proton resonances were observed as doublets or multiplets at 6.61 (d, J_{HH} = 7.6 Hz), 6.90, 7.36, 7.38, 7.42 (d, J_{HH} = 7.6 Hz) and 8.17 ppm (d, J_{HH} = 8.4 Hz). The aliphatic dppe multiplet resonances were observed at 2.76 and 2.86 ppm and the aromatic groups at 6.87, 7.00, 7.10 and 7.20 ppm. A ^{1}H NMR resonance at 6.90 ppm that was completely obscured by the dppe triplet at 6.78 ppm, was identified through 2-D NMR experiments (COSY, HSQC and HMBC correlations). A direct correlation to the naphthalene multiplet at 7.36 ppm as well as the ^{13}C{^{1}H} resonance at 125.28 ppm indicated that it was a proton from the naphthalene ring. The other naphthalene ^{13}C{^{1}H} resonances occurred at 127.75 and 130.89 ppm for the two protonated carbons in the aromatic backbone, and at 129.77, 126.36, 125.82, 125.28, 128.28 and 129.27 ppm in order around the attached benzene. The alpha carbon appeared as a multiplet at 138.72 ppm followed by the beta at 115.15 ppm. The other alkyne resonances occurred at 98.94 and 104.86 ppm, and the final quaternary carbons which join the alkyne to the aromatic group at 114.16 and 133.90 ppm. The ESI(+)-MS showed a compound with a ruthenium splitting pattern at 1145.2680 *m/z* which can be attributed to the mass of the expected compound with the loss of the chloride ligand during processing (calculated 1145.2687 *m/z*).

The electrophile addition reactions were not carried out with this compound as it is known from **Chapter 2, Section 2.1.2** that the addition of electrophiles to *trans*-Ru(C≡CHC$_6$H$_4$-4-C≡CH)Cl(dppe)$_2$ could not be achieved in a selective manner. The larger steric bulk of naphthalene presumably makes these reactions less likely to occur.

Once it was known that the lithiation method worked for the synthesis of copound **42** then a similar method was used with the RuCl(dppe)Cp* fragment. The use of RuCl(dppe)Cp* rather than RuCl$_2$(dppe)$_2$ means that an extra synthetic step is required. The chloride ligand is less labile in this species than RuCl$_2$(dppe)$_2$ which means that a silver salt (in this case AgBF$_4$) is required to remove the chloride from the half sandwich compound with the formation of silver chloride (**Scheme 3.8**). The lithiation of 1,4-diethynyl(trimethylsilyl)naphthalene was carried out in the same manner as before and the lithiated alkyne was added to a mixture of RuCl(dppe)Cp* and AgBF$_4$ in THF at room temperature The previous literature[70] method removes the silver chloride by filtration before the addition of a ligand, however the retention of the silver precipitate did not appear to inhibit the product formation or yield.

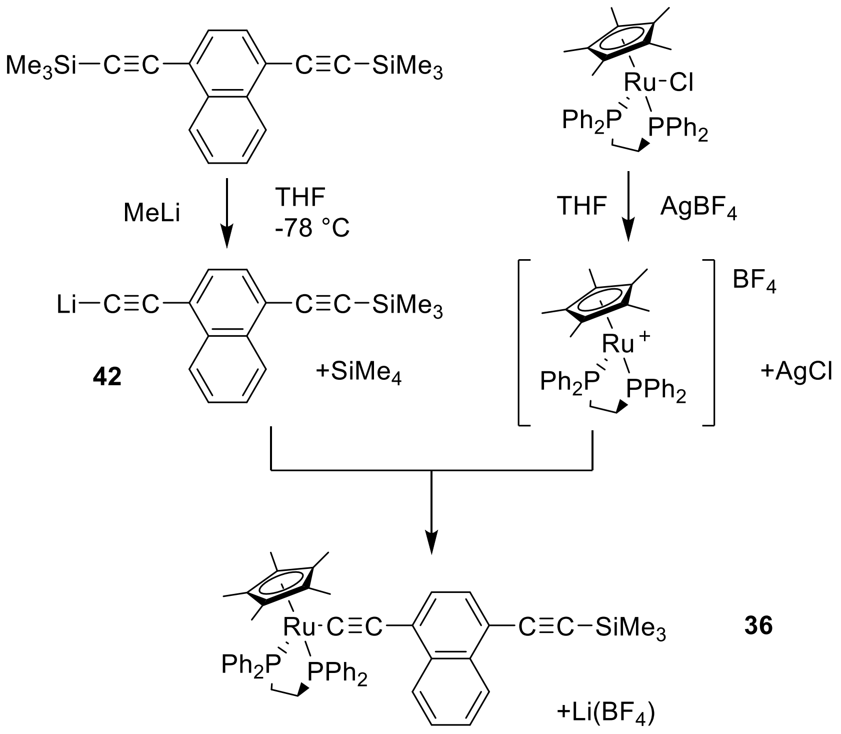

Scheme 3.8: Synthesis of compound 36 in a three step, two pot synthesis from 1,4-diethynyl(trimethylsilyl)naphthalene

Compound **36** was recovered as a dark orange microcrystalline powder. A yield of 34% was achieved, although this contained a relatively large amount of RuCl(dppe)Cp* as seen through a resonance in the $^{31}P\{^{1}H\}$ NMR spectrum at 75.19 ppm which is the literature value for this compound.[173] The $^{31}P\{^{1}H\}$ NMR spectrum for compound **36** was observed at 80.85 ppm. Compound **36** was also identified by ^{1}H NMR spectroscopy with the naphthalene protons were seen as multiplets at 7.05 and 7.69 ppm for the substituted aromatic group, followed by the other four as doublets or apparent doublets in order around the ring from 6.64 (J_{HH} = 7.4 Hz) to 7.32 (J_{HH} = 7.4 Hz) to 7.36 to 8.11 (J_{HH} = 8.3 Hz). The TMS protons were observed at 0.30 ppm, and the carbon seen in the $^{13}C\{^{1}H\}$ NMR spectrum at 1.30 ppm. The alkyne adjoining the TMS appeared at 93.30 and 108.91 ppm and attaching to the naphthalene at the quaternary carbon at 135.24 ppm. At the other end of the ligand the alpha carbon was observed as a multiplet at 137.46 ppm, the beta carbon at 110.24 ppm and the attaching naphthalene carbon at 113.76 ppm. The carbons joining to the proton resonances at 7.05 and 7.69 ppm were 125.23 and 128.50 ppm respectively. The carbon resonances on the other naphthalene ring appear at, starting with the quaternary carbon closest to the metal centre and finishing at the other quaternary carbon, 133.83, 127.38, 128.30, 126.39, 125.86 and 133.42 ppm. The final piece of evidence that compound **36** was synthesised is the ESI(+)-MS in which a peak with an *m/z* of 883.2646 was seen which corresponds closely to $[C_{53}H_{55}P_2RuSi]^+$.

As the presence of unreacted RuCl(dppe)Cp* was observed by $^{31}P\{^1H\}$ NMR spectroscopy it was speculated that the activation of the metal compound with $AgBF_4$ was not complete. However, the use of a larger excess of newly purchased silver salts did not change the ratio of product to RuCl(dppe)Cp* observed after work up.

3.4.1 Reactivity of Ru(C≡CC$_{10}$H$_6$-4-C≡CSiMe$_3$)(dppe)Cp* with electrophiles

The addition of the four electrophiles (H^+, CN^+, $C_7H_7^+$ and CPh_3^+) used in **Chapter 2 Section 2.12** was carried out for compound **36**, Ru(C≡CC$_{10}$H$_8$-4-C≡CSiMe$_3$)(dppe)Cp*. These were run at a small scale, in deuterated-DCM, using a sample of compound **36** in an attempt to understand the reactivity of the complex, despite the 40 % RuCl(dppe)Cp* impurity.

Addition of $HBF_4.OEt_2$ to compound **36** caused an immediate colour change from orange to yellow, a change of colour is indicative of an acetylide to vinylidene transformation. Due to the use of $HBF_4.OEt_2$ as the source of H^+ the ^1H NMR spectrum showed resonances from components of that source including diethylether and water.

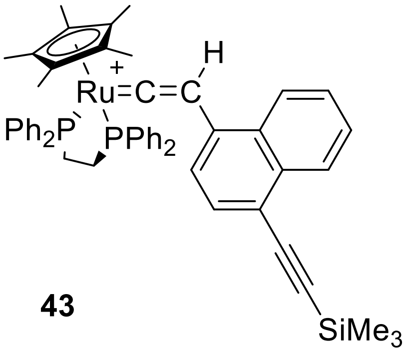

43

Figure 3.4: Structure of Ru(=C=C(H)$C_{10}H_6$-4-C≡CSiMe$_3$)(dppe)Cp*, compound 43

The formation of compound **43** (**Figure 3.4**) was confirmed through ^{1}H, ^{13}C{^{1}H} and ^{31}P{^{1}H} NMR analysis. In keeping with the colour change, a shift in the main ^{31}P{^{1}H} NMR resonance from 80.85 ppm for compound **36** to 72.33 ppm occurred. It was possible to identify the Cp* protons in the ^{1}H NMR spectrum at 1.71 ppm, and the dppe at 2.21 and 3.02 ppm with their aromatic protons as apparent triplets at 7.12, 7.40, 7.49 and 7.57 ppm. The naphthalene protons were observed as doublets at 6.19 and 7.02 (J_{HH} = 7.6 Hz) for the substituted benzene group and the pendant benzene at 6.34 (J_{HH} = 7.7 Hz), 7.20 (app. d), 7.55 (app. d, H^{13}) and 8.26 (J_{HH} = 8.9 Hz) ppm in order from the proton close to ruthenium. Importantly the beta, vinylidene proton was observed as at triplet with a J_{HP} value of 1.7 Hz at 1.61 ppm. The presence of the TMS protecting group was confirmed through ^{1}H NMR spectrum with a resonance at 0.33 ppm and ^{13}C{^{1}H} NMR spectrum at 0.12 ppm. The alkyne connected to the TMS fragment had carbon resonances at 100.33 and 107.1 ppm, with the joining quaternary naphthalene carbon at 124.50 ppm. The high field alpha carbon was observed through HMBC measurements at 348.8 ppm, followed by the beta carbon at 111.53 ppm and the quaternary naphthalene carbon at 120.94 ppm. For the substituted naphthalene the carbons connected to protons had resonances at 126.37 and 131.18 ppm, and for the other ring at 133.19 ppm for the quaternary carbon closer to ruthenium, followed by 126.75, 125.00, 134.12, 127.10 and 131.88 ppm to the final quaternary carbon. The Cp* carbons resonances appeared in the ^{13}C{^{1}H} NMR spectrum at 10.46 and 104.15 ppm and the ethane dppe resonances at 27.82

and 30.02 ppm. For the aromatic dppe carbons nine singlet resonances were observed between 128.89 and 133.29 ppm.

Analysis by ESI(+)-MS did not show any peaks with the expected *m/z* for compound **43**, however, a large peak for Ru(dppe)Cp* was observed. It is therefore likely that the vinylidene ligand was lost during ionisation.

The reaction of **36** with $[C_7H_7][BF_4]$ was then explored. An immediate orange to yellow colour change that occurred upon the addition of $[C_7H_7]^+$ to compound **36** was the same as for the synthesis of **43** which indicated the formation of a vinylidene-containing complex (**Figure 3.5**). This was confirmed through $^{31}P\{^1H\}$ NMR with a resonance at 71.67 ppm.

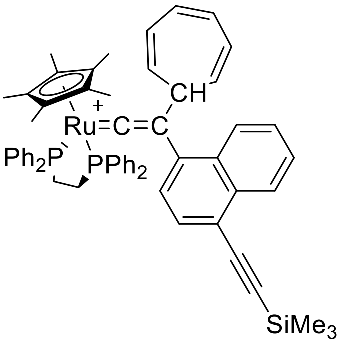

Figure 3.5: Structure of $Ru(=C=C(C_7H_7)C_{10}H_6\text{-}4\text{-}C\equiv CSiMe_3)(dppe)Cp^*$, compound 44

The product from this reaction, **44**, was assigned on the basis of its NMR spectra and mass spectra. Evidence for the formation of compound **44** arises from its ^1H NMR spectrum with resonances for the protons on the C_7H_7 ring at 1.78, 6.25 (app. dd), 6.37 (t, J_{HH} = 3.0 Hz) and 6.70 ppm (t, J_{HH} = 3.0 Hz). The naphthalene resonances appeared at 6.16 and 6.97 ppm (d, J_{HH} = 7.5 Hz) for the substituted aromatic ring, and the other protons as apparent doublets at 7.05, 7.25, 7.50 and 7.97 ppm (d, J_{HH} = 7.0 Hz). The presence of the TMS group was confirmed by a resonance at 0.38 ppm. The ^1H resonance for Cp* was observed at 1.72 ppm, and the aliphatic dppe protons at 2.39 and 2.79 ppm, followed by the aromatic protons as multiplets at 7.15, 7.30, 7.35, 7.44 (t, J_{HH} = 7.0 Hz) and 7.65 ppm.

In the $^{13}C\{^1H\}$ NMR spectrum of **44** the Cp* resonances were present at 10.69 and 104.11 ppm. The dppe carbons were also observed at 30.08 ppm for the aliphatic carbons and between 127.84 and 133.37 ppm for the aromatic ones. The TMS carbons occurred at 0.20 ppm, which were adjacent to the alkyne carbons at 103.20 and 100.37 ppm. The high field alpha carbon was possibly seen through HMBC correlation to the Cp* ligand at 339.8 ppm. The beta carbon was at 125.28 ppm, with the connected quaternary naphthalene carbon at 124.40 ppm. For naphthalene the proton adjacent carbons appeared at 125.89 and 132.27 ppm and 130.00, 134.77, 128.90 and 127.08 ppm. The final quaternary carbon could not be identified. In the C_7H_7 ring the carbons occurred at 35.23 ppm for the non-aromatic carbon, followed by, in order, 126.00, 131.20 and 131.89 ppm.

The addition of the large CPh_3^+ cation to **36** occurred in a different manner to the smaller electrophiles. The large steric bulk of this electrophile means that there was no space for attack at the beta position, meaning that the addition could only occur at the remote position of the ligand. The reaction of **60** with $[CPh_3][BF_4]$ was carried out in DCM-*d* and an immediate colour change from orange to green/brown occurred, indicating that a reaction had taken place.

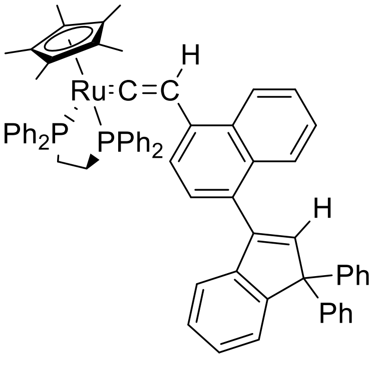

Figure 3.6: Structure of compound 45, $[Ru(=C=C(H)C_{10}H_6\text{-indene-3-}(Ph)_2)(dppe)Cp^*]BF_4$

The structure of the major product, **45**, was determined to be that of Figure 3.6 through ^1H, $^{13}C\{^1H\}$, $^{31}P\{^1H\}$ and 2D NMR experiments. The main $^{31}P\{^1H\}$ NMR resonance at 72.36 ppm indicates that a vinylidene product has been formed. This was confirmed through the presence of a proton in the beta position (5.03 ppm) as an apparent triplet from splitting to the two phosphorus nuclei. The other proton of significance is the indene proton which was observed as a singlet at 5.56 ppm. The naphthalene proton resonances were seen as doublet or multiplets at 6.17 and 6.98 ppm (d, J_{HH} = 7.5 Hz) and 7.91, 6.41, 7.28 and 6.96 ppm. It was difficult to identify all the protons from the indene benzene or the phenyl groups, but two that were from the phenyl were identified as a doublet at 7.12 ppm (J_{HH} = 7.2 Hz) and an apparent triplet at 7.29 ppm. The other aromatic resonances were at 7.21 (t, J_{HH} = 7.4 Hz), 7.34, 7.40 (app. t) and 7.52 ppm and could belong to the indene, phenyl or dppe protons. The aliphatic dppe resonances were at 2.49 and 3.15 ppm and Cp* at 1.76 ppm.

In the $^{13}C\{^1H\}$ NMR spectrum it was possible to identify the vinylidene alpha carbon at 352.0 ppm through HMBC correlations. The beta carbon resonance was observed at 107.65 ppm, with the joining naphthalene quaternary carbon at 118.83 ppm. The naphthalene carbons were observed at 126.68 and 132.26 ppm for the substituted benzene carbons, and 135.14, 129.52, 128.53, 126.68, 129.17 and 135.52 ppm for the pendant benzene of naphthalene starting at the quaternary carbon closest to ruthenium. The final naphthalene quaternary carbon was at 129.34 ppm and was joined to the indene carbon at 129.72 ppm. The hydrogen-substituted indene carbon was at a lower chemical shift of 57.21 ppm and the one with two phenyls at 144.37 ppm. Again, it was difficult to assign the aromatic indene carbons from the phenyl and dppe carbon resonances, 8 resonances were observed between 128.26 and 134.37 ppm. The aliphatic dppe carbons however were identified at 29.65 ppm, along with Cp* at 10.36 and 104.12 ppm.

This intra-cyclization to form an indene group is different to the reactivity observed for the benzene spaced analogue (**Chapter 2, Scheme 2.5**),[152] in which water addition was observed after the addition of CPh_3^+. The possible mechanism for the intramolecular cyclization is shown in Scheme 3.9. This could occur through two routes after the addition of CPh_3^+ depending on whether a cumulene intermediate is formed or not. The presence of free H^+ ions is due to the residual acid from the synthesis of $[CPh_3][BF_4]$.

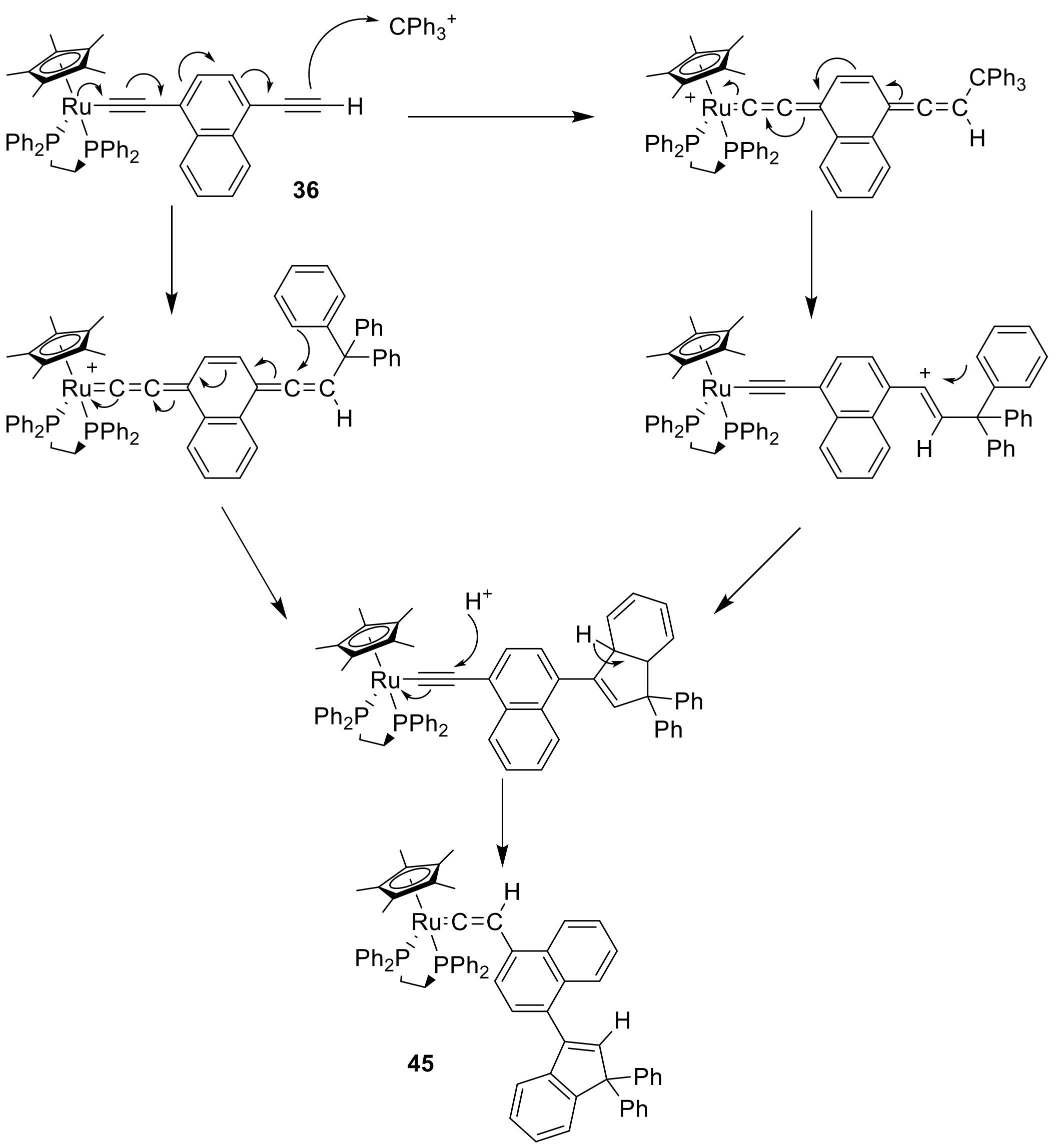

Scheme 3.9: Possible synthetic route for the synthesis of 45 from [CPh3][BF4] and Ru(C≡C-C10H6-4-C≡CSiMe3)(dppe)Cp*

In contrast to the benzene spacer group compounds (**Chapter 2**) addition of CN^+ to the beta carbon of compound **36** did not appear to occur. This was shown by the absence of the colour change which normally accompanies an acetylide to vinylidene transformation and the persistence of the acetylide $^{31}P\{^1H\}$ NMR resonance at 80.88 ppm. However, during analysis by mass spectroscopy, a compound with the *m/z* of 908.2529 was observed, this can be attributed to a compound with the formula $[C_{54}H_{54}NP_2RuSi]^+$ (calculated *m/z* 908.2539) which may be formed from CN addition to compound **36**. It is possible this is seen in the mass spectroscopy as this uses MeCN as a solvent rather than DCM, in which [CAP][BF_4] is much more soluble, allowing for reaction during processing. Or only a small amount of the product is formed, meaning it is not observed by NMR, but the compound is readily ionised leading to a larger than anticipated peak.

3.5 Benzothiadiazole-spaced cumulenes

The ligand 4,7-di(trimethylsilylethynyl)-2,1,3-benzothiadiazole was synthesised as it was anticipated that the benzothiadiazole (BTD) group would be very electron withdrawing. This is based on literature work which indicates that benzothiadiazole can be used as part of polymeric complexes with low lying LUMOs and small band gaps[146] (**Figure 3.7**) and as part of proposed photosensitizers for dye- sensitized solar cells.[174]

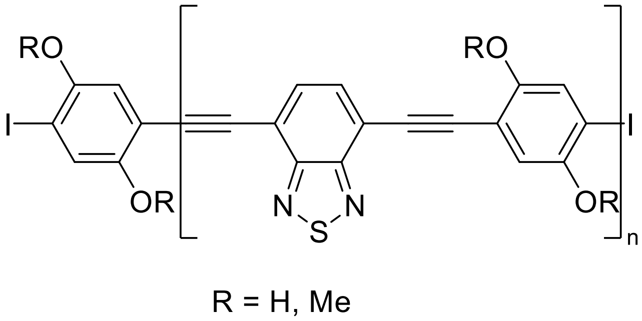

Figure 3.7: Structure of low-band gap polymer compound using a diethynyl-benzothiadiazole moiety.[146]

In conjugated polymers which include the BTD moiety have very low stable band-gaps have been observed multiple times, the first paper from 2001 gave a band-gap of 6.32 eV with both the HOMO and LUMO being low lying, from semiempirical calculations[146] and a second gave values between 2.1 and 1.7 eV, as estimated from UV measurements[175]. A fluorescent polymer with both diethynyl-BTD and bipyridyl moieties has been synthesised that is quenched in the presence of copper ions.[176] There is only one example in the literature of 2,1,3-benzodiathiazole being used in organometallic compounds with either a single divinylarylene or two vinylarylene with an alkene or alkyne linker (**Figure 3.8**).[177] However even though the compounds look similar the attachment to the metal complex, $RuClCO(P^iPr_3)_2$ as seen in **Figure 3.8** is with an acetylene rather than an alkyne or vinylidene.

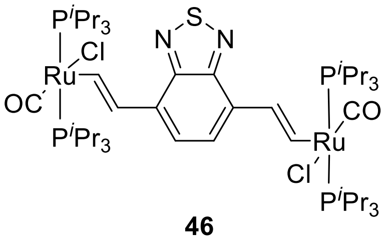

46

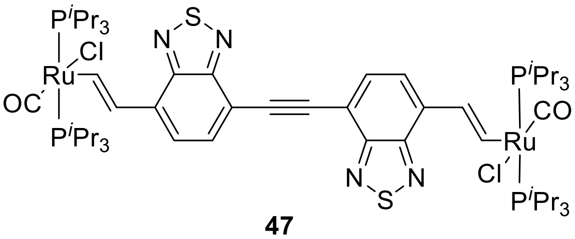

47

Figure 3.8: Structure of [{Ru(CO)Cl(P^iPr_3)$_2$}$_2$(μ-4,7-CH=CH−BTD−CH=CH)], 46, and Bis[7-{Ru(CO)Cl(P^iPr_3)$_2$(CH≡CH)}-4,4′-BTD]-1,2-acetylene, 47 (BTD = benzothiadiazole), from the only paper including organometallic complexes incorporating the benzothiadiazole moiety.[177]

3.6 Synthesis of 4,5-[di(trimethylsilyl)ethynyl]-2,1,3-benzothiadiazole

The synthesis of 4,7-di(trimethylsilylethynyl)-BDT was carried out under standard Sonogashira conditions from 4,7-dibromo-BDT (**Scheme 3.10**) although this diyne compound was believed to be air-sensitive,[176] it could still be isolated if a non-air sensitive work up procedure (column chromatography on silica) were used and exhibited and relatively long term storage, of up to 2 months, at 0 °C under air. The compound was isolated as a yellow/orange powder in 88% yield.

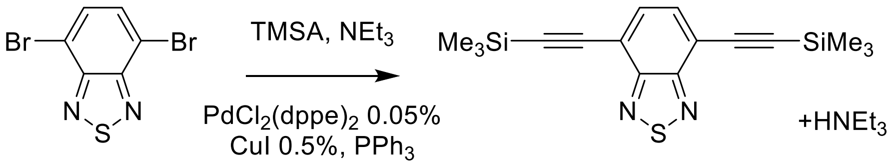

Scheme 3.10: Synthesis of 4,7-di(trimethylsilylethynyl)-2,1,3-benzodiathiazole

The metalation of diethynyl-BDT to Ru(dppe)Cp* was carried out under standard 'KF' addition conditions. The resulting bright blue, slightly air sensitive compound (work up can be done in air but should be stored at reduced temperature) was recovered in low yields. Characterisation of the blue product shows complete formation of the bimetallic complex, **48**, regardless of the ratio of ligand-to-metal used in the reaction (**Scheme 3.11**). A large amount of the mass balance appears to have been lost in the initial workup as **48** is partially methanol-soluble, as well as soluble in hexane and diethylether which is unusual for acetylide complexes of this type as they usually precipitate from methanol during their synthesis.[162] Interestingly the colour of the complex is slightly different in each of these solvents with hexane being more purple than blue (see **Chapter 4, Section 4.7 for a discussion of the electronic spectra**). As with the naphthalene case (**Section 3.1**), it is not possible to produce the unprotected monometallic complex through this synthetic route.

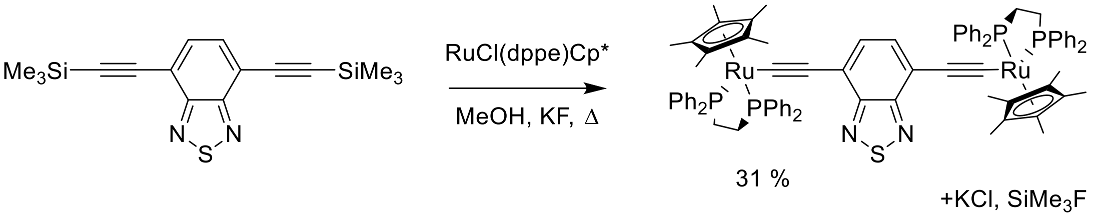

48

Scheme 3.11: Formation of the bimetallic (Ru(dppe)Cp*)$_2$4,7-diethynyl-2,1,3-benzodiathiazole, 48

Analysis of this bimetallic complex, **48**, by ^{1}H and ^{13}C{^{1}H} NMR spectroscopy, showed that although it appears to have symmetry and the two ruthenium atoms should be identical, multiple resonances were observed for protons of the Cp* and spacer group protons, this may represent that two metal fragments are held in different orientations leading to the difference in environments. The fact that **48** is a bimetallic complex, despite the unsymmetrical structure implied by the NMR analysis, is demonstrated by the ESI(+)-MS of the complex in which a peak at *m/z* of 1452.3467 was observed which can be attributed to a compound with the formula $[C_{82}H_{80}N_2P_4P_4Ru_2S]^+$ (which has a calculated mass of 1452.3080). Associated peaks for a dication were observed at *m/z* at around 727. A single ^{31}P{^{1}H} NMR resonance was seen at 80.64 ppm in the expected range for an acetylide with this metal fragment.[152]

In the ^1H NMR spectrum of **48**, the spacer group protons appear as doublets at 6.76 and 7.46 ppm, with a J_{HH} value of 7.7 Hz. As shown by a HSQC experiment these are connected to carbon atoms with resonances of 127.90 and 132.80 ppm, respectively. The presence of the Cp* ligands was confirmed through singlet resonances in the ^1H NMR spectrum at 1.60 ppm with a shoulder at 1.62 ppm. Together these have an integration of 30 protons which is the expected number for two Cp* ligands. The aliphatic dppe multiplets occurred at 2.17 and 2.95 ppm, and the aromatic ones mainly as apparent triplets at 7.01, 7.20 (t, J_{HH} = 7.9 Hz), 7.28, 7.34, 7.58 and 7.79 (m) ppm. This shift from mainly triplets seen with other dppe complexes to apparent triplets is further evidence for a unsymmetric dimeric complex. The Cp* carbons were identified in the $^{13}C\{^1H\}$ NMR spectrum at 10.05 and 10.22 ppm for the CH_3 carbon and 93.50 and 93.67 ppm for the quaternary ones and multiple ethane carbons from dppe at 29.51, 29.70 and 29.88 ppm. The two α carbons were observed as multiplets at 132.54 and 132.81 ppm followed by the β alkyne carbons had resonances at 99.65 and 104.98 ppm. Only one resonance was observed for the *para* quaternary aromatic carbons at 124.23 ppm. The resonances for the final spacer group carbon atoms occurred at 153.53 and 156.38 ppm which are deshielded by the connecting nitrogen nuclei.

Although only one stretch for the C≡C group was observed in the IR spectrum at 2040 cm^{-1} (**Figure 3.9**) the slightly asymmetrical shape of the peak indicated that maybe a second stretch is also present at just below 2040 cm^{-1} which would be consistent with the rest of the data.

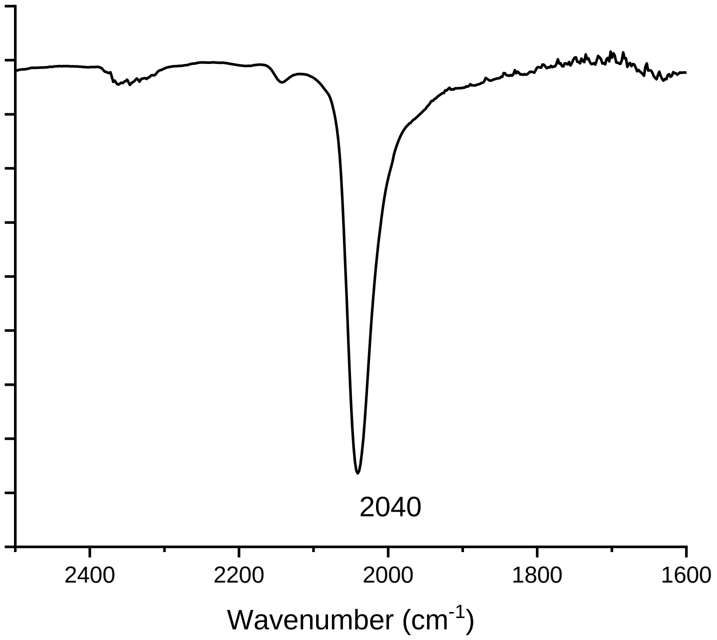

Figure 3.9: Nujol mull IR data for 48, with an unsymmetrical alkyne stretch indicating the presence of a second stretch with similar transmittance.

Although the bimetallic benzothiadiazole complex was not the desired product of this reaction it is a compound that has not been described previously. Therefore, electrochemical and spectroelectrochemical analysis was carried out on this complex (See **Chapter 4, Sections 4.1.2.4, 4.3.2.4 and 4.5.2.4**). This complex was mostly stable when stored in the freezer under air for 1 month as only minor alterations were observed in the ^{1}H NMR spectrum and the $^{31}P\{^{1}H\}$ spectrum showed the growth of the resonance at 71.57 ppm which can be attributed to either the related vinylidene complex, due to the 10 ppm shift in resonance, or RuO(dppe)Cp*.

3.7 Synthesis of $Ru(C\equiv CC_6H_2(NSN)\text{-}4\text{-}C\equiv C(CH_3)_2OH)(dppe)Cp^*$

It was decided that the same orthogonally protected strategy used in the synthesis of the related naphthalene complex should be used (as in **Section 3.2**) as the slightly different properties of this spacer group could make this route viable. This was synthesised following a slightly different route to the naphthalene complex. In this case, the acetone protecting group was added before the TMS (**Scheme 3.12**) as reported in the literature.[177] As 4-bromo-7-iodobenzo[c]-1,2,5-thiadiazole is not commercially available, the synthesis had be carried out using 4,7-dibromobenzo[c]-1,2,5-thiadiazole as the starting material.

To reduce the amount of double alkyne substitution occurring at 4,7-dibromo-BDT two slight modifications were made to the procedure used with naphthalene: a larger excess of 4,7-dibromo-BDT was used, 3.4 equivalents rather than the 3 equivalents used in the literature. The reaction was also performed for 50 minutes at room temperature instead of 16 hours starting at 0 °C and warming to room temperature. This increased the yield of compound **49** from this reaction from 26 % in the literature to nearly 77 %. Some di-substitution did occur although this product was removed during purification. A small amount of 4,7-dibromo-BDT was still present after the first step of the reaction, despite having been purified using column chromatography, rather than running as second column it was decided to use this in the next step of the reaction as it is significantly easier to separate 4,7-di(trimethylsilylethynyl)-BDT from compound **50**. The addition of TMSA was performed using standard Sonogashira conditions in accordance with the literature,[177] with an overall yield of 52 % as a yellow/orange powder for compound **50**.

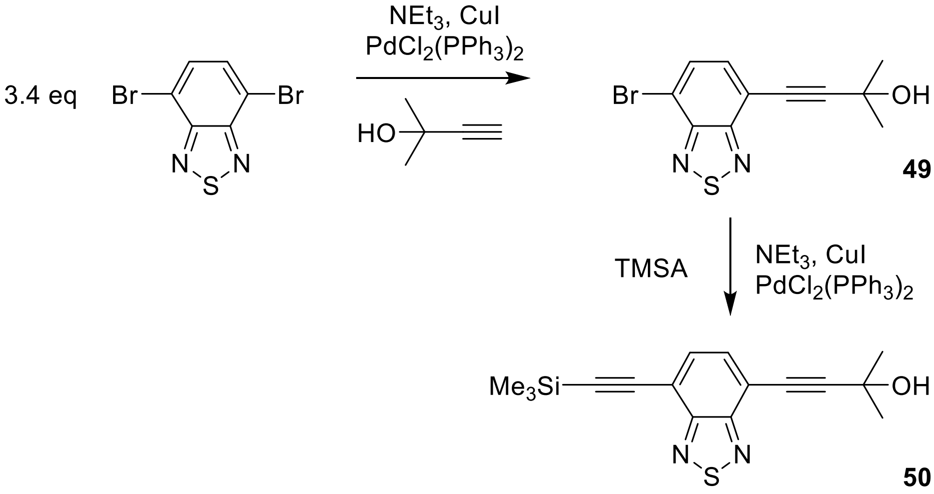

Scheme 3.12: Synthetic route to the unsymmetrically protected diethynyl-BDT product, compound 50.

The synthesis of this unsymmetrically protected alkyne, **50**, was confirmed through multiple analytical techniques with the ^{1}H and ^{13}C{^{1}H} NMR spectra matching the literature values.[177] IR analysis was not present in the literature, however a spectrum recorded in a nujol mull exhibited two different alkyne C≡C IR stretches at 2148 and 2158 cm^{-1} and an OH stretch at 3468 cm^{-1}. The ^{1}H NMR resonances occurred at 0.33 ppm for the TMS protecting group and 1.69 ppm for the (C**H₃**)₂OH group, although the OH proton, which was expected to appear at 2.37 ppm was not observed. The two aromatic protons appeared as doublets at 7.64 and 7.70 ppm with a J_{HH} value of 7.35 Hz. The associated ^{13}C{^{1}H} NMR resonances occurred at 0.01 ppm for TMS and for (**C**H₃)₂OH at 31.46 ppm. The next carbon in the chain, **C**(CH₃)₂OH, appeared at 65.95 ppm. The four alkyne resonances were seen at 78.11, 100.05, 102.17 and 103.62 ppm: 78.11 ppm is lower than expected for alkyne carbon nuclei however this assignment is derived from the HMBC spectrum. The two *para* quaternary carbons had resonances at 117.09 and 117.19 ppm, the two with protons at 132.58 and 133.30 ppm and only one resonance for the two deshielded carbons close to nitrogen nuclei at 154.36 ppm. However, the extremely close match of the NMR spectra and the OH stretch in the IR spectrum confirmed that compound **50** was successfully synthesised.

This unsymmetrical alkyne **50** was then reacted with RuCl(dppe)Cp* following the 'KF' catalyst method to form compound **51** (**Figure 3.10**) as a dark blue microcrystalline powder. Unlike the benzene and naphthalene analogues this compound is partially soluble in methanol meaning that a small volume of solvent was used, 10 mL for 300 mg of RuCl(dppe)Cp*, 45 millimolar, and cooling the reaction mixture to 0 °C before filtration. This increased the yield to 75 % from the initial yield of 33 %.

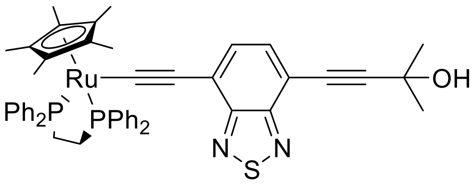

Figure 3.10: Structure of compound 51 with an acetone protecting group.

The IR spectrum of the metal complex **51** exhibited two alkyne stretches at 1964 and 2035 cm^{-1} which were lower than that of the free alkyne: an OH stretch at 3374 cm^{-1} was also observed. The ESI-MS of the **51** exhibited a peak at *m/z* of 877.2115 which can be attributed to the molecular ion of **51**$^{+}$ with the addition of H^{+} (Calculated 877.2079). A single resonance was observed in the $^{31}P\{^{1}H\}$ NMR spectrum at 80.69 ppm, in a region typical of a ruthenium acetylide complexes of this was type.[173] The ^{1}H NMR spectrum showed evidence for the $C(CH_3)_2OH$ group at 1.69 ppm for the CH_3 groups and 2.41 ppm for OH nuclei. The aromatic spacer group protons appeared as doublets at 6.87 and 7.40 ppm with a J_{HH} value of 7.5 Hz. The $^{13}C\{^{1}H\}$ NMR spectrum exhibited resonances for the protecting group at 31.75 and 66.04 ppm, like the organic compound **50**. The α carbon was seen as a multiplet at 138.5 ppm and the other three alkyne carbons at 107.91, 79.77 and 98.35 ppm. The quaternary aromatic carbons appeared at 112.24 and 125.15 ppm and the two adjacent to the nitrogen nuclei at 155.26 and 156.37 ppm. The final two C-H carbon atoms exhibited at 127.16 and 134.25 ppm. The resonances for the Cp* and dppe ligands occurred in the expected range.[173]

As with the naphthalene analogue, **40**, the attempted deprotection using a base and high temperatures to liberate acetone from **50** was not successful. The conditions used were: 1) stirring with K^{t}OBu in methanol at room temperature for 3 hours and 2) heating to reflux with K^{t}OBu in methanol for 3 hours, in each of these cases a precipitate was observed but was found to be unreacted starting material, **50**. Considering that the removal of acetone from the naphthalene analogue could not be achieved either it was reasoned that it might be the same for this complex.

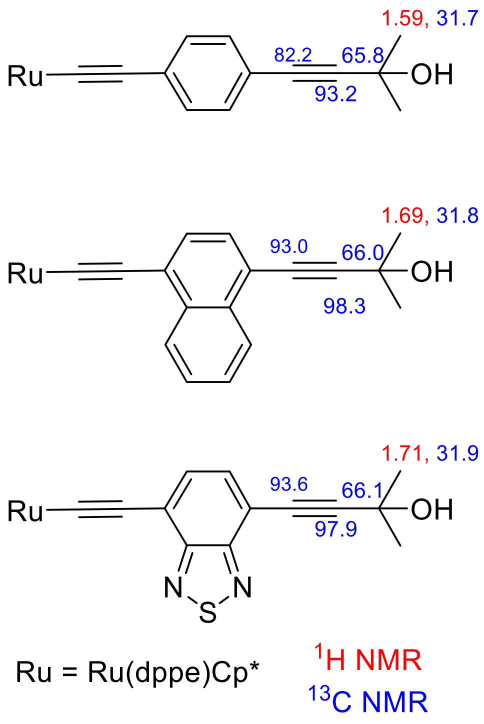

Figure 3.11: NMR resonances of the three spacer groups with the acetone protected alkyne

An analysis of the ^{1}H and ^{13}C{^{1}H} NMR spectroscopic data around the acetone protecting group (**Figure 3.11**) shows that the resonances for the naphthalene and BTD spacer groups are very similar however there is a small but significant difference with the benzene spacer group. This is especially evident at the alkyne carbons with a change from ~98 ppm down to 93.2 ppm, and from ~93 ppm down to 82.2 ppm. This difference will change the reactivity of the alkyne and therefore is likely to be contributing to the difference in reactivity of the protecting group.

Also, similarly to the naphthalene analogue of this compound no electrophile additions were attempted but electrochemical analysis was performed (**Chapter 4 Sections 4.1.1.3, 4.3.1.3 and 4.5.1.3**).

3.8 Lithiation of 4,7-[di(trimethylsilyl)ethynyl]-2,1,3-benzothiadiazole

An alternative approach to prepare the desired mono-substituted alkyne complexes with a BTD spacer was investigated. Given the success of the lithiation route and the naphthalene spacer reported in **Section 3.4**, this was attempted in the BTD case.

Methyl lithium was used to selectively replace one TMS group from 4,5-[di(trimethylsilyl)ethynyl]-2,1,3-benzothiadiazole (**Scheme 3.13**), before addition to the desired metal fragment. The metal fragment $RuCl_2(dppe)_2$ was again used as a test for this reaction due a higher degree of similarity to the literature procedure and the metal fragment being readily available.

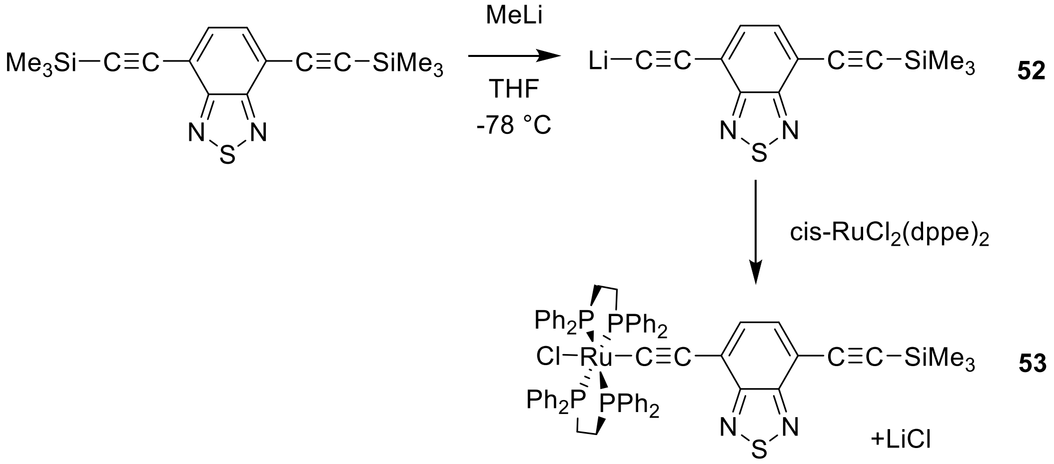

Scheme 3.13: Single pot lithiation of 4,7-[di(trimethylsilyl)ethynyl]-2,1,3-benzothiadiazole and addition of *cis*-$RuCl_2(dppe)_2$ forming compound 53

Compound **53** was recovered as a bright purple powder, as with the other benzothiadiazole spacer group compounds, although only a low yield of 8 % was obtained. The ^1H NMR spectroscopic shifts for this complex were observed at 5.88 and 7.40 ppm for the aromatic protons as doublets with a coupling constant of 7.5 Hz and 0.33 ppm for the TMS protecting group. The aliphatic dppe protons were observed at 2.76 and 3.06 ppm, and the aromatic resonances were observed at 6.68, 7.01, 7.09, 7.12, 7.12, 7.27 and 7.57 ppm as either triplets or multiplets. The TMS group was also observed in the $^{13}C\{^1H\}$ NMR spectrum at 0.30 ppm with the adjacent alkyne carbons at 99.55 and 102.64 ppm. The alpha carbon was seen at 115.61 ppm, followed by the beta at 108.92 ppm. In the benzothiadiazole group the carbons with protons appeared at 129.73 and 134.59 ppm, with the alkyne quaternary carbons at 124.41 and 134.79 ppm. The other carbons next to the nitrogen nuclei are more deshielded at 155.51 and 156.60 ppm. For the dppe ligands the aliphatic carbons were seen at 30.90 ppm, and eight aromatic resonances were seen between 127 and 137 ppm. The $^{31}P\{^1H\}$ NMR resonance at 47.83 ppm came in the expected $RuCl(dppe)_2$ region.[147] The presence of the TMS protecting group was also confirmed through ESI(+)-MS with an *m/z* of 1153.2221 seen for the desired compound with the loss of the chloride ligand (Calculated 1153.2157).

Repeating the procedure with the RuCl(dppe)Cp* metal fragment (**Scheme 3.14**) was also successful, made following the same conditions and work up as with the analogous naphthalene compound **36** (**Section 3.4**). Although a 24 % yield of purple compound was achieved, a noticeable amount of RuCl(dppe)Cp* (seen by a $^{31}P\{^1H\}$ NMR resonance at 75.19 ppm) and the organic benzothiadiazole starting material (seen by a ^1H NMR resonance at 7.70 ppm for the aromatic benzothiadiazole protons).

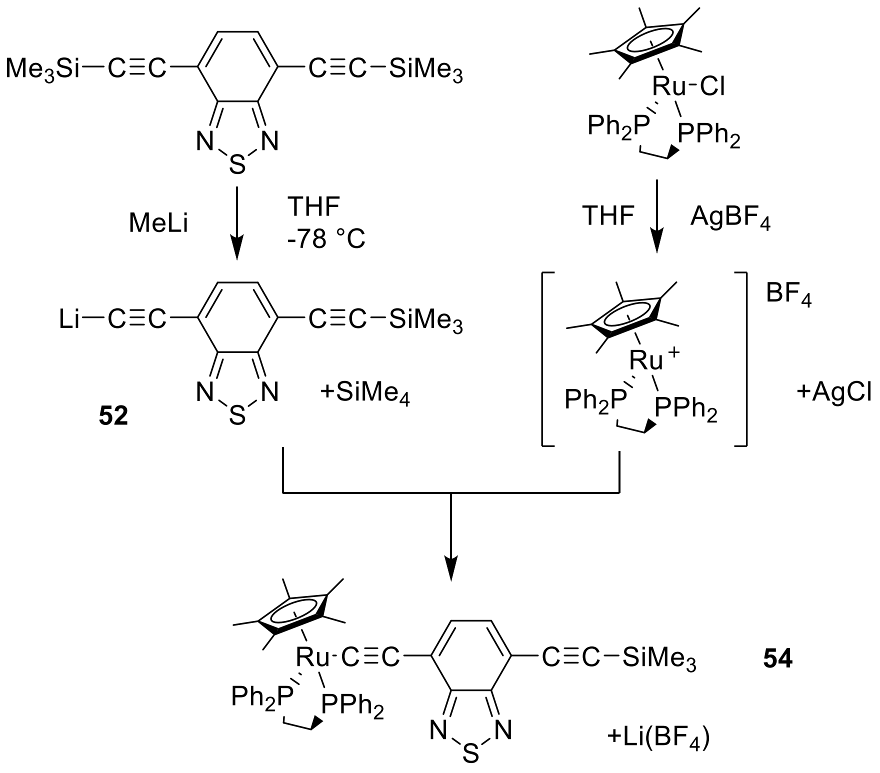

Scheme 3.14: Synthesis of compound 54 in a three step, two pot synthesis from 4,5-[di(trimethylsilyl)ethynyl]-2,1,3-benzothiadiazole

Despite the presence of RuCl(dppe)Cp* (60 %) impurities, it was possible to characterise compound **54** through NMR techniques. The $^{31}P\{^1H\}$ NMR spectrum showed a resonance at 80.56 ppm, in the range for Ru(dppe)Cp* acetylide complexes. In the ^1H NMR spectrum the dppe resonances were observed at 2.11 and 2.60 ppm for the ethane protons and seven resonances between 7.19 and 7.67 ppm as either triplets (J_{HH} = 8.2 Hz), apparent triplets or multiplets. The Cp* protons were observed as a singlet at 1.41 ppm. In the acetylide ligand the aromatic benzothiadiazole proton resonances appeared at doublets at 6.91 and 7.44 ppm (J_{HH} = 7.5 Hz), with the TMS protons at 0.33 ppm. In the $^{13}C\{^1H\}$ NMR spectrum the TMS was also observed with a resonance at 0.25 ppm. The resonances for the joining alkyne the resonances appeared at 100.45 and 103.71 ppm. The beta carbon resonance was observed at 117.54 ppm, but the alpha carbon could not be identified. In the benzothiadiazole group the carbons with protons appeared at 127.56 and 134.99 ppm, with the alkyne quaternary carbons at 113.71 and 125.59 ppm. The other carbons next to the nitrogen nuclei are more deshielded at 154.67 and 155.58

ppm. The ethane dppe $^{13}C\{^1H\}$ NMR resonances appeared at 28.67 and 30.04 ppm, with seven aromatic resonances between 127.76 and 135.66 ppm.

It was also possible to observe two ν(C≡C) stretches in the ATR IR spectrum at 1970 and 2037 cm^{-1} for the organic and metal bound alkynes respectively. The presence of the TMS protecting group was confirmed through ESI(+)-MS as a peak at *m/z* of 891.2093 was observed which correlates to a compound with the structure $[C_{49}H_{51}N_2P_2RuSSi]^+$ which has an expected *m/z* of 891.2055.

3.8.1 Reactivity of $Ru(C{\equiv}CC_{10}H_6(NSN)\text{-}4\text{-}C{\equiv}CSiMe_3)(dppe)Cp^*$ with electrophiles

The addition of the four electrophiles (H^+, CN^+, $C_7H_7^+$ and CPh_3^+) used in **Section 3.11** was carried out for compound **54**, $Ru(C{\equiv}CC_6H_2(NSN)\text{-}4\text{-}C{\equiv}CSiMe_3)(dppe)Cp^*$. These were run at a small scale, in deuterated-DCM, using an impure sample of compound **54** in an attempt to understand the reactivity of the complex.

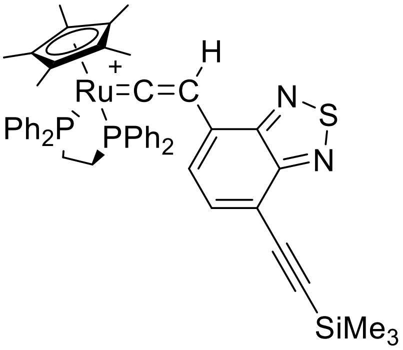

Figure 3.12: Structure of $Ru(=C=C(H)C_6H_2(NSN)\text{-}4\text{-}C{\equiv}CSiMe_3)(dppe)Cp^*$, compound 55

The addition of acid ($HBF_4.OEt_2$) to compound **54** in DCM gave an immediate colour change from purple to orange. This resulted in the formation of the expected vinylidene **55** (**Figure 3.12**) as confirmed by the vinylidene type $^{31}P\{^1H\}$ NMR resonance at 71.92 ppm and an ESI(+)-MS *m/z* of 891.2099 which matches the expected *m/z* for this complex of 891.2055. The vinylidene alpha carbon was seen by

$^{13}C\{^1H\}$ NMR at 351.54 ppm, with the vinylidene proton in the ^1H NMR spectrum as an apparent triplet (from the phosphorus nuclei) 1.72 ppm.

The two protons in the benzothiadiazole spacer were identified as doublets at 5.90 and 7.06 (J_{HH} = 7.4 Hz) in the ^1H NMR spectrum along with the TMS group at 0.32 ppm. The TMS was also seen in the $^{13}C\{^1H\}$ NMR spectrum at 0.12 ppm, which was attached to the alkyne carbon resonances at 104.46 and 100.41 ppm. In the spacer group the protonated carbon resonances appeared at 124.82 and 134.24 ppm, the nitrogen adjacent carbons at 152.91 and 154.75 ppm, and the other quaternary carbons at 117.57 and 123.88 ppm. The beta carbon resonance was at 103.74 ppm.

The presence of the spectator ligands were confirmed by ^1H NMR resonances at 1.65 for Cp*, 2.21 and 3.20 ppm for the aliphatic dppe protons and at 6.82, 7.41, 7.51 and 7.60 ppm for the aromatic dppe. Also, in the $^{13}C\{^1H\}$ NMR spectrum at 15.42 and 104.15 ppm for Cp*, 28.25 and 30.49 ppm for aliphatic dppe and seven resonances between 128.89 and 133.52 pm for the aromatic dppe carbons.

The addition of $[C_7H_7]^+$ to **54** showed the same colour change from purple to orange as with H^+ addition, which indicates a similar reaction has taken place and the formation of a C_7H_7 vinylidene. The structure of **56** (**Figure 3.13**) was confirmed by NMR spectra and ESI(+)-MS.

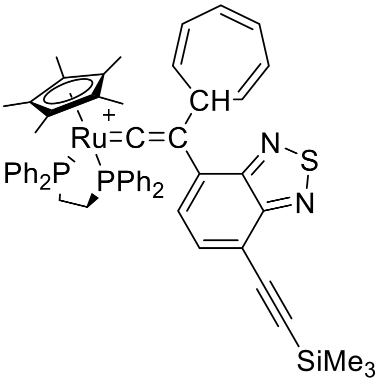

Figure 3.13: Structure of $Ru(=C=C(C_7H_7)C_6H_2(NSN)\text{-}4\text{-}C{\equiv}CSiMe_3)(dppe)Cp^*$, compound 56

The ESI(+)-MS showed a peak with an *m/z* of 981.2525 which was very close to the predicted *m/z* of this compound at 981.2620. The presence of a vinylidene was supported by a $^{31}P\{^1H\}$ NMR resonance at 71.93 ppm, roughly 10 ppm to higher field than the parent acetylide **54** (80.56 ppm).

In the ^1H NMR spectrum it was shown that the TMS protecting group was still present with a resonance at 0.32 ppm. In the benzothiadiazole group the proton resonances appeared as doublets at 5.90 and 7.06 (J_{HH} = 7.4 Hz) ppm. Then the C_7H_7 protons from the singlet at 1.50 ppm around the ring to a doublet of triplets at 6.18 ppm (J_{HH} = 8.9 Hz, J_{HH} = 3.1 Hz) to triplets at 6.34 ppm (J_{HH} = 3.1 Hz) and 6.59 ppm (J_{HH} = 3.1 Hz). For the Cp* protons a resonance was observed at 1.71 ppm and the aliphatic dppe resonances at 2.53 and 3.04 ppm. In the $^{13}C\{^1H\}$ NMR spectrum the dppe carbon resonances were observed at 26.15 and 30.43 ppm for the aliphatic carbons and seven resonances between 127.74 and 133.78 ppm for the aromatic, and the Cp* resonances at 10.50 and 104.17 ppm. The vinylidene beta carbon resonance was seen at 103.72 ppm, but the alpha carbon could not be identified within the spectral range used. The carbon resonances for the C_7H_7 ring were observed at 33.64, 130.61 and 131.24 ppm, but the final carbon in this ring could not be identified. In the benzothiadiazole fragment the resonances for the protonated carbons appeared at 124.89 and 132.49 ppm, the ones next to the nitrogen nuclei at 154.66 and 155.76 ppm and the other quaternary carbons at 117.72 and 123.68 ppm. The TMS carbon resonance was seen at 4.50 ppm, with the adjoining alkyne carbons at 104.49 and 100.44 ppm.

Upon addition of $[CPh_3][BF_4]$ to compound **54** a colour change from purple to brown was observed. This is a slightly different colour change than seen for **55** and **56**, which indicates that a slightly different reaction has taken place. The only peak in the ESI(+)-MS has an *m/z* of 891.2099 which is identified as **55**, as there is residual acid in the sample of $[CPh_3][BF_4]$ it is possible for some of the starting material to be directly protonated before the CPh_3^+ addition. However, the indene type structure (**Figure**

3.14) which likely follows the same mechanism as the formation of compound **45** (**Scheme 3.9**), was identified by ^{1}H and ^{13}C{^{1}H} NMR.

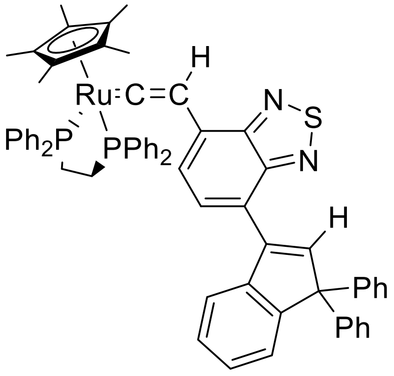

Figure 3.14: Structure of [Ru(=C=C(H)C$_6$H$_2$(NSN)-indene-3-(Ph)$_2$)(dppe)Cp*]BF$_4$, compound 57

The vinylidene group was identified by the ^{31}P{^{1}H} NMR resonance at 71.92 ppm, and the vinylidene proton resonance in the ^{1}H NMR spectrum at 5.30 ppm, this had triplet character from splitting by the two phosphorus nuclei of dppe (J_{HP} = 1.7 Hz). The vinylidene alpha carbon was also identified by HMBC analysis at 352.7 ppm with the beta carbon in the ^{13}C{^{1}H} NMR spectrum at 107.66 ppm.

Other resonances in the ^{1}H NMR spectrum were observed as a singlet at 5.55 for the indene proton, and doublets at 5.90 and 7.07 ppm (J_{HH} = 7.4 Hz) for the benzothiadiazole fraction. The other resonances were at 1.72 ppm for Cp*, 2.50 and 3.16 ppm for the aliphatic dppe protons and from 7.12 to 7.60 for the aromatic dppe protons. In the ^{13}C{^{1}H} NMR spectrum the resonances for the benzothiadiazole fragment appeared at 125.24 and 133.95 ppm for the protonated carbons, 151.48 and 154.67 ppm for the nitrogen adjacent carbons and the quaternary carbons at 117.62 and 123.16 ppm. The indene carbons from the 5-membered ring were observed at 129.40 ppm for the quaternary carbon, 57.20 ppm for the protonated carbon and the one with two phenyls at 144.37 ppm. It was hard to distinguish the other indene, phenyl and dppe aromatic carbons, other than 129.72 ppm for the terminal phenyl groups. There are 13 other resonances between 126.67 and 134.37

ppm. Other resonances were observed for Cp* at 10.36 and 104.48 and the aliphatic dppe carbons at 26.16 and 29.85 ppm.

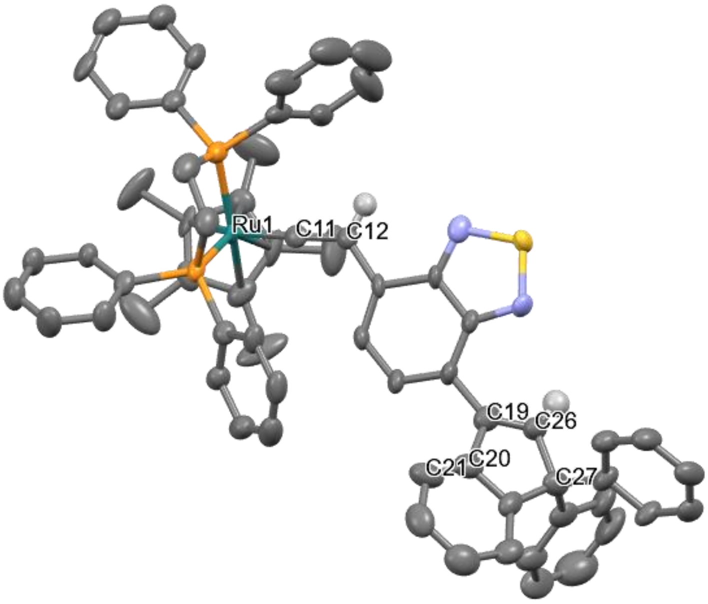

Figure 3.15: Molecular structure of [Ru(=C=C(H)C_6H_2(NSN)-indene-3-$(Ph)_2$)(dppe)Cp*]BF_4 55 from addition of [CPh_3]BF_4 to Ru(C≡C-C_6H_2(NSN)-4-C≡$CSiMe_3$)(dppe)Cp*as determined by single crystal X-ray diffraction. Thermal ellipsoids are shown at the 50% level, DCM molecules, BF_4 anions, most hydrogen atoms and disorder omitted for clarity. Grey = C, White = H, Dark green = Ru, Orange = P, Blue = N, Yellow = S.

Further evidence that compound **55** was successfully synthesised comes from the single crystal analysis of a crystal grown by slow diffusion from DCM-*d* into pentane (**Figure 3.15**). Some twinning was seen in the benzothiadiazole fragment of the molecule, with a slight rocking of is group. The Ru-C(11) double bond had a length of 1.819(12) Å, and C(11)-C(12) length of 1.338(16) Å which is similar to that of compound **34**. The aromatic benzene C-C bond lengths across the whole molecule were between 1.358(19) and 1.44(2) Å which are within the expected range,[154] with one outlier being the C(20)-C(21) bond length of 1.32(2) Å. The C(19)-C(26) indene double bond has a length of 1.275(19) Å, and the single bonds have a length of 1.521(17) Å for C(26)-C(27) and 1.56(2) Å for C(19)-C(20). The C-N bond lengths for one of the twins appear at 1.339(16) Å and 1.375(19) Å, which is similar to the bond length for a benzothiadiazole moiety of Q-BBT in the literature (**Figure 3.16**) at 1.360 Å[178] and the N-S distances are identical at 1.632(12) Å and 1.632(11) Å (with the value in the literature occurring at 1.606 Å).[178] The Ru-C(11)-C(12) angle is 168.7(9)°, which is further from linear than for compound **34** and other vinylidene compounds,[152] indicating that the spacer group is interacting with the dppe ligand, pushing the vinylidene out of its preferred orientation. The C(11)-C(12)-C(13) angle at 126.9(11)° is closer to the expected angle.[152] The angle between N(1)-S-N(2) is 101.4(7)° (*vs* 101.87 Å in the literature).[178]

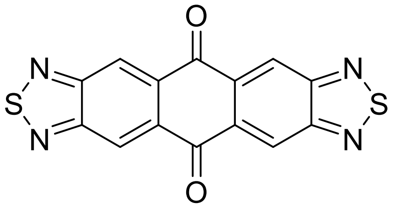

Figure 3.16: Structure of Q-BBT, a benzoquinone-fused bis-benzothiadiazole[178]

As with the attempted addition of CN^+ to the naphthalene analogue, **36**, the reaction did not proceed under the conditions used. As seen by a lack of colour change upon addition of the electrophile and the persistence of the acetylide $^{31}P\{^1H\}$ NMR resonance at 80.56 ppm. The presence of an *m/z* with the expected mass of 916.2037 (calculated *m/z* 916.2008 for $[C_{50}H_{50}N_3P_2RuSSi]^+$) is likely due to reaction in acetonitrile prior to the mass spectroscopy experiment or high ionisation of the small amount of compound that was formed.

3.9 Anthracene-spaced cumulenes

Anthracene has one of the lowest aromatic stabilisation energies per ring, of 115.6 kJ mol^{-1} (**Figure 3.2**) of all the spacers considered. This means that the cumulene intermediate may lie at a relatively low energy when compared to the vinylidene tautomer. The sterically larger spacer group might also affect the synthesis and reactivity of mono-metallic ruthenium complexes.

As previous synthesis of the Ru(dppe)Cp* bimetallic anthracene[169] required a long reaction time (40 hours) a shorter reaction time was predicted to form the desired monometallic, TMS protected species.

Synthesis of 9,10-bis(trimethylsilyl)ethynylanthracene (**Figure 3.17**) was carried out under general Sonogashira coupling conditions,[179] the purification was modified slightly as instead of using column chromatography it was possible to obtain a pure product, **58**, through hexane extraction. Compound **58** was obtained as an orange, red microcrystalline powder in 94 % yield, which fluoresces blue when in solution.

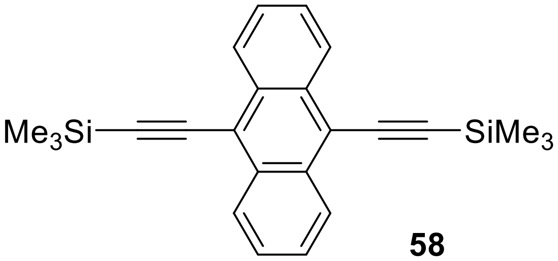

58

Figure 3.17: Structure of 9,10-bis(trimethylsilyl)ethynyl benzene

9,10-bis(trimethylsilyl)ethynylanthracene was reacted with the ruthenium half-sandwich ruthenium complexes, RuCl(dppe)Cp* and $RuCl(PPh_3)_2Cp$, using the KF synthetic route with both giving dark red/purple powders. The same methodology was also used as with TMS-diethynylbenzene although a longer reaction time of 6 hours was required to achieve yields of more than 50 %. The yield of the reaction with the RuCl(dppe)Cp* fragment (> 70 %) was significantly higher than with the $RuCl(PPh_3)_2Cp$ fragment (< 20 %) and was therefore used for further analysis (**Figure 3.18**). These monometallic anthracene compounds, **59** and **60**, have little to no solubility in hot methanol meaning that they precipitate from solution during the reaction inhibiting the formation of the bimetallic complexes. Therefore, in this case the methyl lithium synthetic route that was used for compounds **36** and **54** was not required (**Sections 3.3 and 3.6**).

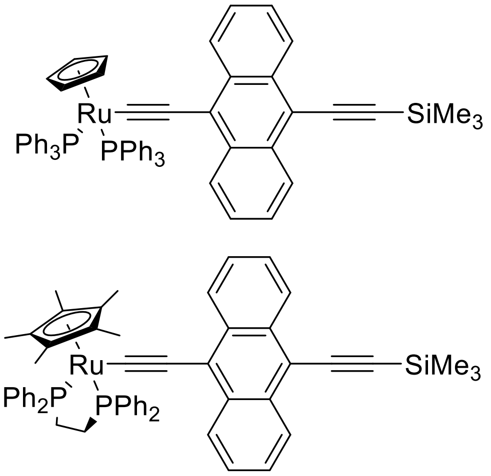

59

60

Figure 3.18: Structure of Ru($C≡CH-C_{12}H_8$-10-$C≡CSiMe_3$)($(PPh_3)_2$)Cp, 59, and Ru($C≡CH-C_{12}H_8$-10-$C≡CSiMe_3$)(dppe)Cp*, 60.

The mass spectrum **59** exhibited a peak at *m/z* 988.2433 by ESI(+)-MS, was very close to the expected *m/z* of 988.2357 (**Figure 3.18**). A single $^{31}P\{^1H\}$ NMR resonance was observed at 49.73 ppm. The TMS group was identified by ^1H NMR resonance at 0.01 ppm, along with the Cp resonance at 4.44 ppm. The anthracene proton resonances were identified by ^1H NMR and COSY at 8.59 and 7.16 ppm and 8.41 and 7.44 ppm. However, as these were difficult to assign completely the $^{13}C\{^1H\}$ NMR spectrum was not run.

The ^1H NMR spectrum of compound **60**, Ru($C≡CH-C_{12}H_8$-10-$C≡CSiMe_3$)(dppe)Cp* (**Figure 3.18**) showed four distinct aromatic doublets that can be assigned to the anthracene proton environments and although it was possible to determine the order of the resonances around the ring, 7.83 (d, J_{HH} = 8.6 Hz) to 6.87 (t, J_{HH} = 7.1 Hz) to 7.35 (app. t) to 8.39 ppm (d, J_{HH} = 8.6 Hz), it was not possible to show which was closest to the ruthenium. The resonance for the $SiMe_3$ group appeared at 0.38 ppm with integration 9 and the Cp* at 1.67 ppm (15 H). In the $^{13}C\{^1H\}$ NMR spectrum, the resonance for the $SiMe_3$ group was seen at 0.63 ppm, and the Cp* at 10.47 ppm for CH_3 and 93.49 ppm for the quaternary carbon atoms. The aromatic carbon resonances could be ordered as with the protons from 128.38 to 133.55 to 129.12 then 123.52, 126.15, 126.41, 133.35 and finally 131.86 ppm. The acetylide resonances appeared at 103.84, 109.20 and 110.91 ppm, with the α carbon at 127.72 ppm. The $^{31}P\{^1H\}$ NMR resonance was at 81.13 ppm at a similar ppm to other Ru(dppe)Cp* acetylide resonances and the two acetylide stretches were observed in the IR spectrum at 2016 and 2119 cm^{-1}. The *m/z* of 932.2755 was very close to the calculated value of 932.2670 *m/z* for the M+H and showed Ru isotope pattern.

The removal of the TMS protecting group from compound **60** to form compound **61** (**Figure 3.19**) was carried out according to the literature procedure[180] (addition of TBAF in methanol) showed only a slight change in colour and the resonances in the $^{31}P\{^1H\}$ NMR spectum stayed the same, however the correct mass of 860.227 m/z was seen by mass spectroscopy and the TMS protected species was absent. The lack of change in the phosphorus NMR is likely because the change from TMS to H only changes the electron density at the phosphorus slightly, especially as this group is so far removed from the phosphorus atoms.

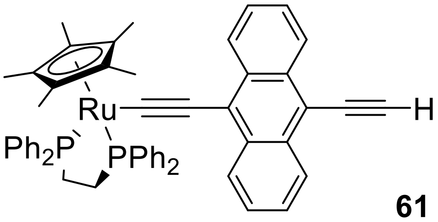

61

Figure 3.19: Structure of Ru(C≡CC$_{14}$H$_8$-10-C≡CH)(dppe)Cp*, compound 61

3.10 Addition of electrophiles to Ru(C≡CH-C$_{12}$H$_8$-10-C≡CSiMe$_3$) (dppe)Cp*

As the synthesis of compound **60** was successful the reaction of electrophiles was carried out in an attempt to stabilise the cumulene intermediate. The large steric bulk of the anthracene spacer group makes the formation of vinylidenes less likely as the bend it would induce in the molecule would force the anthracene into close contact with the other ligands in the coordination sphere of the metal.

The addition of the acid $HBF_4{\cdot}OEt_2$ to purple **60**, Ru(dppe)(C≡CH-$C_{12}H_8$-10-C≡CSiMe_3)Cp*, caused the room temperature solution in DCM to turn dark green immediately. The solvent was removed after 23 hours and the resulting solid washed with hexane. The infra-red spectrum of the residue showed a strong peak at 1906 cm^{-1} which could indicate the presence of metal carbonyl functional group as seen with the benzene-spaced analogue (**Chapter 1, Section 2.2**).

The same reaction between **61** and $HBF_4{\cdot}OEt_2$ also saw the immediate colour change to green and a similar IR spectrum was recorded. However, despite this tantalising evidence of a cumulene and multiple reaction conditions being tried it proved impossible to purify anything component of this reaction.

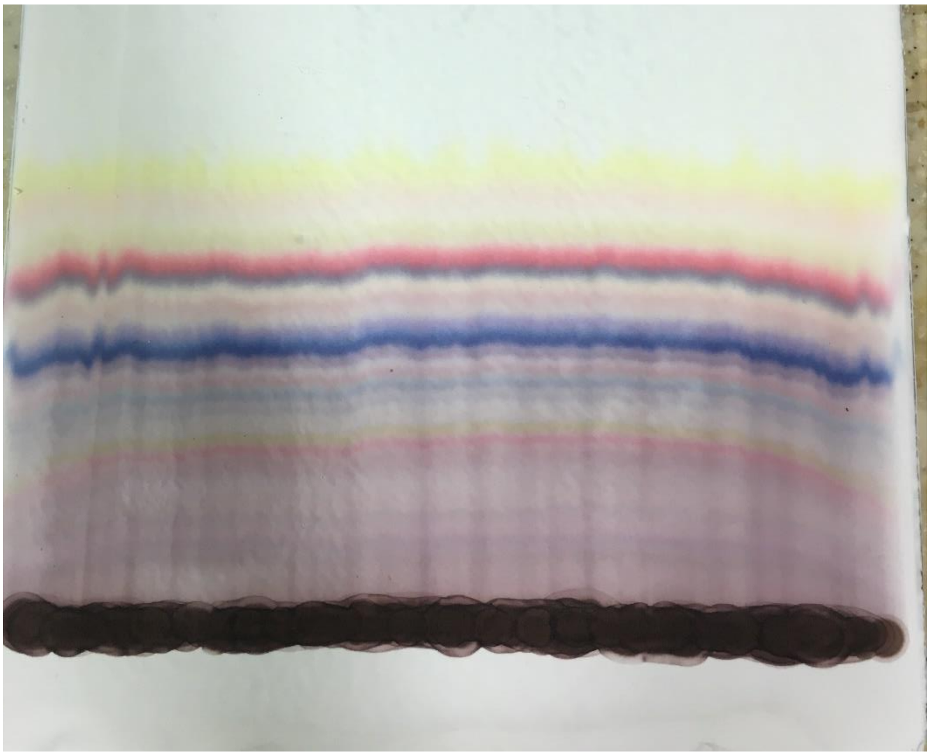

Photo 3.1: Prep-TLC plate from the attempted purification of the reaction of $HBF_4.OEt_2$ with Ru(C≡CH$C_{12}H_8$-10-C≡CSiMe_3)(dppe)Cp*.

The large number of compounds that are formed in the reaction of compound **60** and $HBF_4{\cdot}OEt_2$ can be see when purification using a silica prep-TLC plate with Hexane/DCM 3:2 as multiple different coloured bands can be seen (**Photo 3.1**). Even when taking the major yellow, pink and blue bands multiple $^{31}P\{^{1}H\}$ NMR resonances were observed. It was also determined by 2D TLC (on standard TLC plates) that the compound was not degrading on the plate meaning that these coloured compounds are all a result of the reaction conditions.

As with previous compounds (**18, 25, 26, 36 and 54**) the addition of other electrophiles ($[C_7H_7]^+$ and $[CN]^+$) to Ru(C≡CH-$C_{12}H_8$-10-C≡CSiMe_3)(dppe)Cp*, **60**, was also explored. Initially the addition of $[C_7H_7]^+$ was carried out at room temperature in DCM solution for 16 hours. Initial electrophile addition to **60** resulted in an immediate colour change from dark purple to dark green, however the material precipitated from DCM into cold diethylether exhibited four different $^{31}P\{^{1}H\}$ NMR resonances. Reducing the reaction time to two hours, from 16, changed this to one $^{31}P\{^{1}H\}$ NMR resonance at 71.54 ppm, however the associated ^{1}H NMR spectrum was unclear, with broad resonances around the aromatic and Cp* region, meaning that the structure of the compound was difficult to assign.

The addition of $[CN]^+$ to **60** was also carried out at room temperature in DCM for 4.5 hours and worked up by precipitation in cold diethylether. For this reaction only one $^{31}P\{^{1}H\}$ NMR resonance was observed at 71.55 ppm, a very similar resonance to the $[C_7H_7]^+$ product. This reaction had a clean ^{1}H NMR spectrum, however the main resonances could be attributed to DMAP which is difficult to remove from this type of product due to similar reactivities (**Chapter 2, Section 2.3.2**).

The addition of $[CPh_3][BF_4]$ to **60** was of particular interest due to the interesting additions to the terminal carbon in previous work.[152] In this case the addition of $[CPh_3]^+$ to **60** in DCM or THF solution also showed an initial colour change from purple to green, which could be then reverted back to purple upon addition of a base (NEt_3, DBU or KO^{t}Bu). A colour change is indicative of an acetylide to vinylidene transformation. This reaction mixture again contained multiple products that could not be separated by traditional purification techniques.

Table 3.1: Different conditions used in the attempt to optimise the reaction of 60 with [CPh_3][BF_4]

[CPh_3][BF_4] equivalents	Reaction Time	Temp.	Base used	^{31}P resonances (ppm)	IR (cm^{-1})	Special conditions/ notes
1	15 mins	rt	-	71.5	1902	Washed with Et_2O and hexane
0.1	2.5 hrs	rt	-	-	-	Starting material recovered
1 (PF_6)	2.5 hrs	0 °C	-	74.56	1949	
1	18 hrs	rt	Alumina	71.50	1908	
1	18 hrs	rt	Alumina	-	1910	
1	21 hrs	rt	DBU	81.19	2025, 1949	CRYSTAL
1 (PF_6)	2.5 hrs	rt	DBU	(75.86) 81.68	-	
1 (PF_6)	2.5 hrs	0 °C	DBU[a]	81.19	2021	
1	18 hrs	rt	DBU	81.68	2048, 1943	CRYSTAL
1	3.5 hrs	rt	DBU[b]	-	2015, 1943	Diethylether work-up
1	1.5 hrs	rt	DBU	81.20	-	
2.3	2 hrs	rt	DBU	81.26	-	
2	4 hrs	rt	DBU	-	-	
1	5.5 hrs	rt	DBU	-	-	
2	2.5 hrs	-78 °C	DBU	81.26	-	TLC- degradation
1	3 hrs	rt	KO^tBu[a]	75.42	1948	Green powder- indicates it is still protonated
1	3 hrs	rt	KO^tBu	81.7	2026	
1	3.5 hrs	rt	KO^tBu[a]	-	-	Ru added to CPh_3 and base
1	19 hrs	rt	KO^tBu[a]	-	-	THF
2.3	2 hrs	rt	DBU	-	-	Ru free control

[a] = Base added before ruthenium. [b]= Base added after ruthenium. When not stated base is added in a second step after removal of solvent and dissolution of reaction mixture in MeOH. ^{31}P of final product or intermediate (before addition of base) in brackets.

A small amount of the bimetallic compound **62 (Figure 3.20**) was recovered from the addition of the trityl anion to compound **61** in DCM, followed by deprotonation with DBU in MeOH. As only a small amount of this was purified (< 15 % yield) as a red powder it is believed to be a side product. The rest of the material decomposed upon attempted purification by preparative TLC. Two of the conditions used to try and optimise this synthesis (**Table 3.1**) yielded the same product (as shown by single crystal X-ray diffraction and one structure exhibited more disorder (**Figure 3.21 and Figure 3.22**).

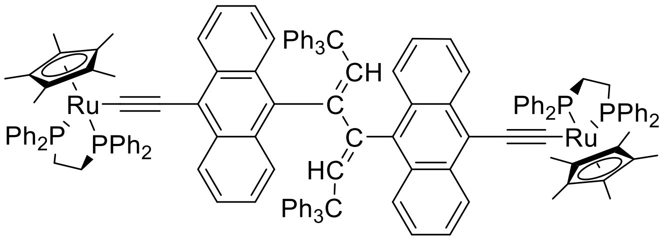

Figure 3.20: Structure of dimerization product from addition of [CPh_3] cation to Ru($C\equiv CHC_{12}H_8$-10-$C\equiv CSiMe_3$)(dppe)Cp*, compound 62

The crystal structure of compound **62** (**Figure 3.21**) shows the bimetallic structure of this compound. The compound is symmetrical, with the same bond lengths being observed around each of the metal atoms. Both of the Ru(1)-C(1) bond lengths are 1.991(8) Å, followed by C(1)-C(2) triple bond length of 1.205(10) Å and the single C(3)-C(4) bond length of 1.428(9) Å. On the other side of the anthracene ring there is a single bond between C(10)-C(11) has a length of 1.482(8) Å and a double bond between C(11)-C(12) with a length of 1.346(9) Å, the C(12)-C(13) single bond of 1.514(9) Å. Finally, the bond lengths between C(13) and the three aromatic groups of CPh_3 have bond lengths of 1.543(9), 1.547(8) and 1.557(9) Å. In the aromatic anthracene ring bond lengths appear between 1.347(10) Å and 1.458(8) Å as expected for aromatic carbons, the two longest bond lengths are between the quaternary carbons. Similarly, the aromatic bond lengths from CPh_3 occur between 1.331(15) Å and 1.405(12) Å.

For the bond angles the Ru-C(1)-C(2) angle is close to linear at 178.4(8)° as expected for an acetylide complex. Also, the C(1)-C(2)-C(3) angle is 179.3(10)°. The C(10)-C(11)-C(12) angle is 125.5(5)°, the C(11)-C(12)-C(13) angle is 134.7(5)°, the C(12)-C(11)-C(12') angle is 119.0(6)° and the C(11)-C(11')-C(10) angle is 115.5(6)°. The angles around the aromatic groups are all between 116.6(6)° and 123.1(7)°.

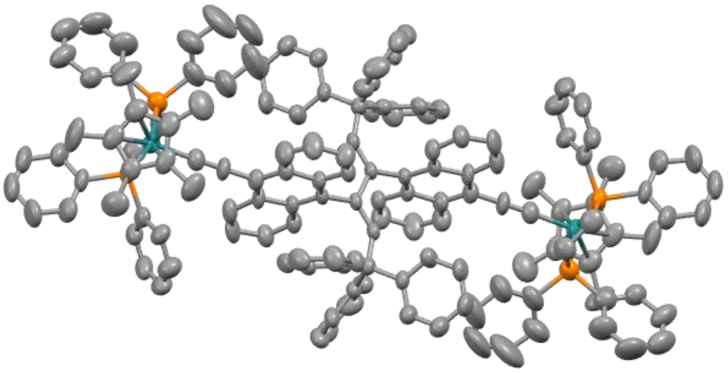

Figure 3.21: Molecular structure of compound 62, from addition of [CPh_3] cation to Ru(C≡$CHC_{12}H_8$-10-C≡$CSiMe_3$)(dppe)Cp* as determined by single crystal X-ray diffraction. Thermal ellipsoids are shown at the 50% level, DCM molecules and hydrogen atoms omitted for clarity. Grey = C, Dark green = Ru, Orange = P

A single crystal suitable for X-ray crystallography was grown from DCM/Hexane (**Figure 3.21**). Analysis of the resulting data demonstrated that complex **62** had been formed which appears to have arisen from the addition of Ph_3C^+ to **61**, followed by a dimerization. These crystals were grown from two different reactions, showing that it was reproducible. The second crystal sample had different packing but had poor diffraction quality, meaning only a rudimentary structure was collected, the positions of the protons could not be distinguished but showed the connectivity of the heavier atoms (**Figure 3.22**).

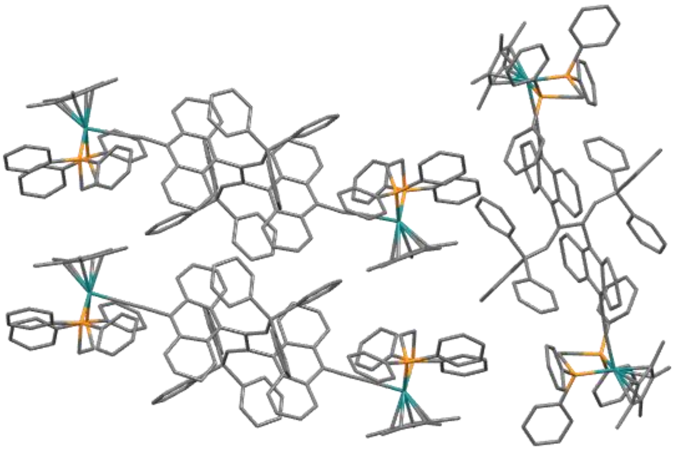

Figure 3.22: Packing of second, more disordered crystal structure of compound 62, see text for an explanation

Compound **62** had an observed *m/z* of 2205.6689 in the ESI(+)-MS which can be attributed to a compound with the formula $[C_{146}H_{125}P_4Ru_2]^+$ with a predicted *m/z* of 2205.6813. The corresponding peak for the dication was observed at 1103.8357 *m/z*, it is common to observed 2+ peaks for bimetallic compounds as it is possible for both metal fragments to be oxidised.[181]

A single $^{31}P\{^1H\}$ NMR resonance was observed in the isolated sample at 81.69 ppm for compound **62**, which has a similar chemical shift to the starting material, **60** (81.13 ppm). According to the ^1H NMR spectrum this compound contains a plane of symmetry as only one resonance was observed for the Cp* (1.71 ppm) and dppe ligands (aliphatic multiplets at 2.21 and 3.00 ppm and aromatic triplets or multiplets at 7.01, 7.12, 7.31, 7.36 and 7.79 ppm). The resonances for the CPh_3 groups were observed as a multiplet at 6.45 ppm. The resonances for the anthracene protons were seen at 7.74, 6.61, 7.21 and 8.17 ppm in this order around the ring. Another resonance in the ^1H spectrum was observed in the aliphatic region of the spectra, a proton on the original terminal carbon at 6.42 ppm was observed as a multiplet due to multiple splitting that can occur from either anthracene, CPh_3 or both.

The $^{13}C\{^1H\}$ NMR spectrum also showed the expected resonances for Cp* and dppe ligands, although some resonances at 129.02, 129.19 and 129.67 could possibly be attributed to the phenyls of the CPh_3 group. The alpha carbon could not be seen due to either low concentration or a longer resonance time, and the same can be said for the quaternary carbons on the anthracene spacer group. The beta carbon was attributed to a resonance at 98.21 ppm and the central carbon of CPh_3 group was seen at 58.79 ppm. The two alkene carbons were observed at 141.34 and 146.04 ppm although they could not be differentiated. The final carbons resonances that could be assigned were the four carbons with protons in the anthracene ring, with the one at 127.11 being assigned to either or both carbons closest to the central benzene and 124.02 and 125.08 ppm for the final two carbons.

This characterisation confirms the structure that was observed by single crystal X-ray diffraction. A possible mechanism for the dimerization is via a radical coupling mechanism, as the structure indicates that the addition of CPh_3 is likely to have occurred initially, followed by the reaction of two identical fragments. The only way this would be possible is through a radical mechanism. This could be similar to the one which was first proposed by Berke[182], who coupled two manganese vinylidene radicals (**Scheme 3.15**). This mechanism is proposed because compound **63** has a similar type of structure, with a single bond between the identical two fragments.

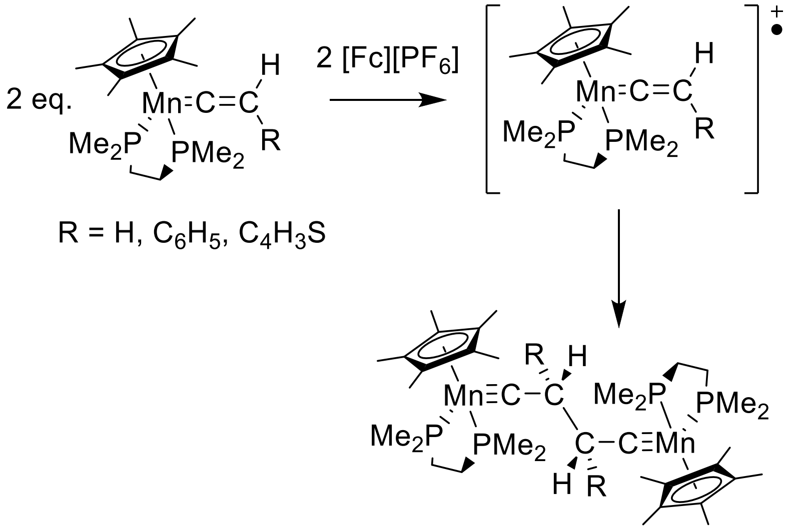

63

Scheme 3.15: Radical coupling mechanism by Berke *et al*.[182]

It is known in the literature that $[CPh_3]^+$ can act as a radical initiator,[183] so therefore it must be carrying out multiple roles in this reaction. This type of coupling is only likely to take place after the cumulene intermediate was formed, and the CPh_3 electrophile has reacted with the terminal carbon.

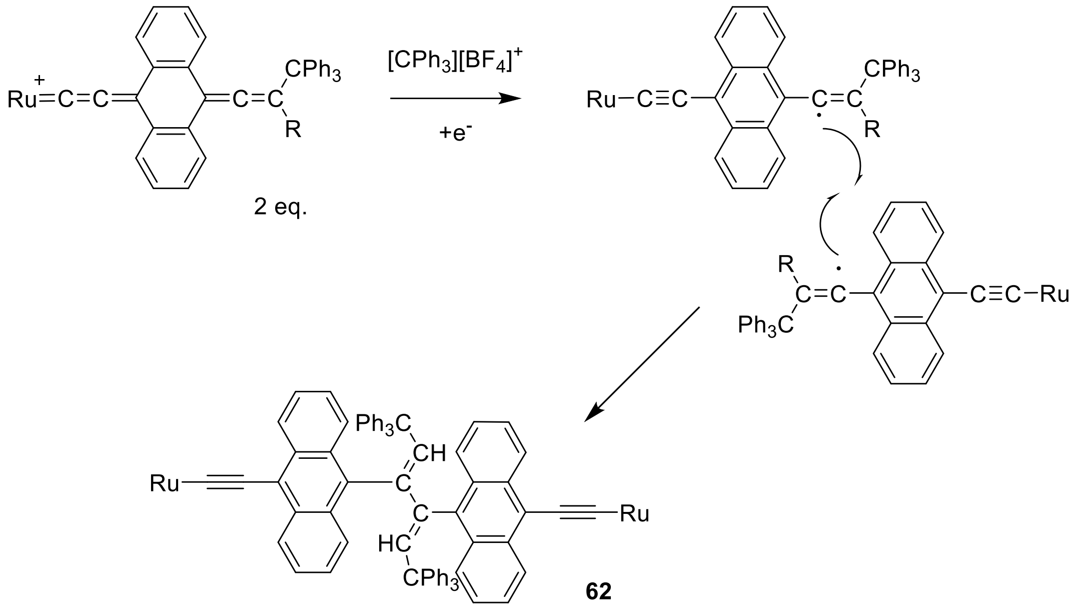

62

Scheme 3.16: Probable radical coupling mechanism for formation of Ru(=C=CC$_{14}$H$_8$-10-=C=C(H)CPh$_3$)(dppe)Cp*, 62

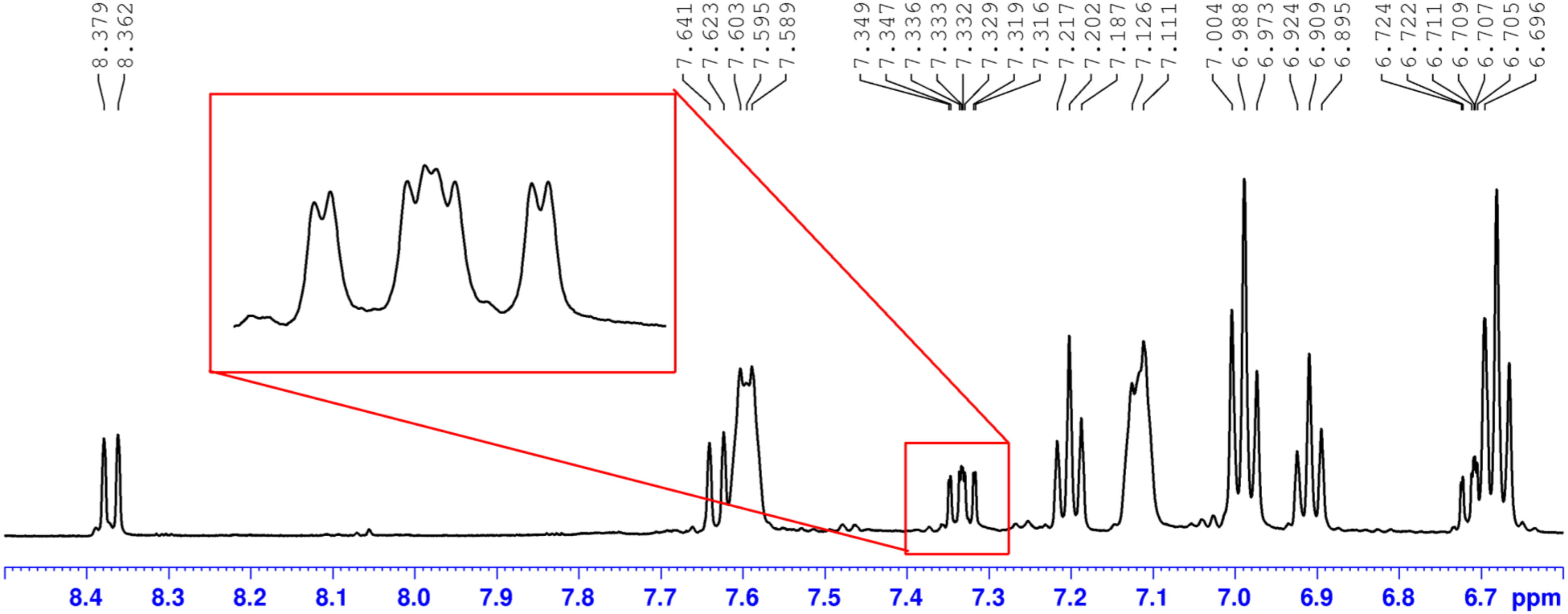

Figure 3.23: Aromatic region of the ^{1}H NMR spectrum for RuCl(C≡CC$_{14}$H$_8$-10-C≡CSiMe$_3$)(dppe)$_2$, compound 65

3.11 Lithiation of 9,10-bis(trimethylsilyl)ethynylanthracene

As with naphthalene and benzothiadiazole spacer groups it was possible to synthesise the bis-dppe ruthenium analogue containing a bridging naphthalene group through the selective lithiation of 9,10-diethynyl(trimethylsilyl)anthracene followed by addition to *cis*-RuCl$_2$(dppe)$_2$ to form compound **65** as a bright red solid (**Scheme 3.17**).

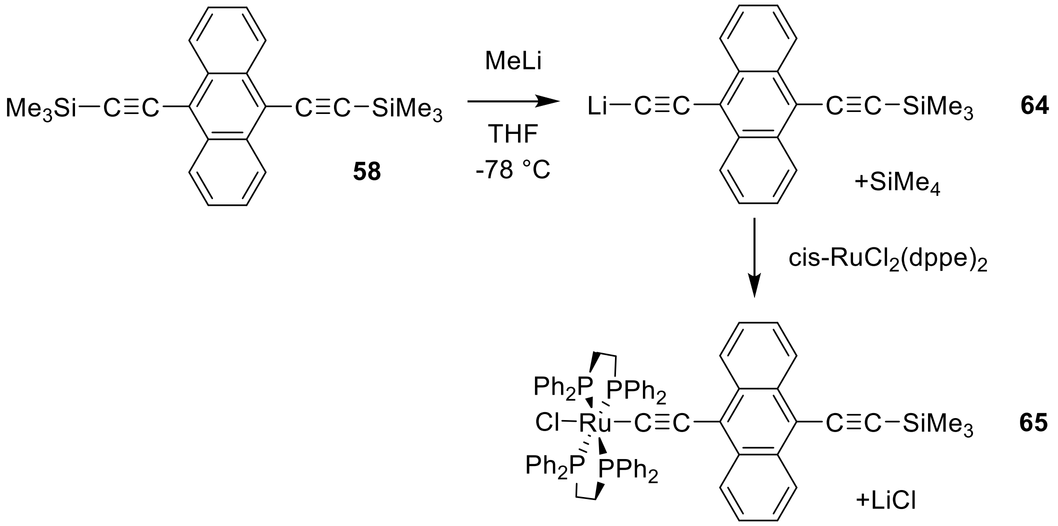

Scheme 3.17: Single pot lithiation of 4,7-[di(trimethylsilyl)ethynyl]-2,1,3-benzothiadiazole and addition of *cis*-RuCl$_2$(dppe)$_2$ forming compound 65

The ^{1}H NMR spectrum for compound **65** showed resonances for the TMS protecting group at 0.42 ppm. The splitting of the anthracene protons was evidence with the two outside protons appearing as doublets at 8.37 (red) and 7.64 (blue) ppm (**Figure 3.24**) each with a coupling constant of 8.5 Hz. The two central protons at 7.33 (green) and 6.72 ppm (black) are each seen as a doublet of doublets of doublets (ddd), some of the resonance at 6.72 ppm is hidden under the dppe resonance at 6.68 ppm however the splitting patter is clear (**Figure 3.23**). The coupling constants are the same for both ddd, with the largest splitting occurring at 8.5 Hz (the same as the doublets), the second at 6.5 Hz and the smallest coupling to the *meta* proton at 1.2 Hz. The dppe resonances occurred as 8 protons at 2.96 ppm and the aromatic protons as triplets or multiplets at 6.68 (J_{HH} = 7.6 Hz), 6.91 (J_{HH} = 7.4 Hz), 6.99 (J_{HH} = 7.6 Hz), 7.11, 7.20 (J_{HH} = 7.4 Hz) and 7.60 ppm.

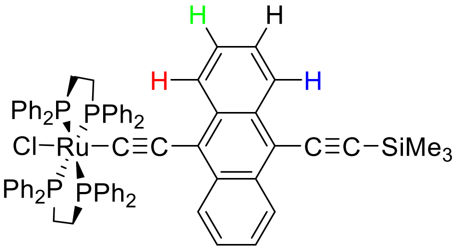

Figure 3.24: Compound 65 with the anthracene protons highlighted.

The $^{13}C\{^1H\}$ NMR spectrum for compound **65** resonances were seen at 0.50 ppm for TMS, 30.30 ppm for the dppe ethane, and the aromatic carbons at 127.27, 127.77, 129.13, 129.73, 134.56, 134.66, 136.06 and 136.42 ppm. The alpha carbon was seen as a multiplet at 148.58 ppm followed by the beta carbon at 109.23 ppm. The other alkyne carbons are at 103.72 and 105.01 ppm. The four resonances on the central benzene were seen at 116.05, 132.12, 133.42 and 127.86 ppm. On the outside benzene rings the carbons were assigned, around the ring from red to blue, from 126.33, 126.20, 123.65 and 129.43 ppm. Also, the $^{31}P\{^1H\}$ NMR resonance occurred at 45.27 which similar to the other RuCl(dppe)$_2$ acetylide complexes.

The mass spectrum showed a peak for this compound at *m/z* 1195.2863 close to the calculated *m/z* value of 1195.2844. Also, some evidence for the compound formed from the removal of TMS was obtained from the Mass Spectrum with a complex with ruthenium splitting pattern at 1123.2481 *m/z* (calculated 1123.2449) however it is impossible to know if this loss was due to the conditions of ESI(+)-MS or an impurity. However due to the lack of extra resonances in any of the NMR spectra it is unlikely to be an impurity.

Addition of electrophiles was not carried out for this compound based on the knowledge of attempted electrophile addition to compound **13**, RuCl(C≡C-C_6H_4-4-C≡CSiMe$_3$)(dppe)$_2$, which proved to be unsuccessful, likely due to steric hinderance from the two dppe ligands.

3.12 Conclusions

The synthesis of monometallic diethylylaryl groups other than benzene proved to be more difficult than anticipated, with use of the bis(trimethylsilyl)aryl only forming a monometallic complex when the aryl group is anthracene. The use of methyl lithium to selectively add lithium to one of the trimethylsilyl protecting groups, followed by *in situ* addition to the desired metal fragment, proved to be the most successful method for both naphthalene and benzothiadiazole. Careful use of a chloride abstraction agent is required for the Ru(dppe)Cp* fragment and stoichiometric MeLi makes full conversion to the desired product difficult. Some further work is required to ensure a repeatable and robust purification method for these reactions.

Synthesis of Ru(C≡C-$C_{12}H_8$-10-C≡$CSiMe_3$)(dppe)Cp* was much easier and was successful using basic 'KF' catalysis methods.[162] As this method does not work for RuCl$(dppe)_2$ fragments, RuCl(C≡C-$C_{12}H_8$-10-C≡$CSiMe_3$)$(dppe)_2$ was also synthesised through selective lithiation of TMS.

The addition of small electrophiles, H^+ and $C_7H_7^+$, to **36** and **54** occurred in a predictable manner, forming vinylidene complexes. The addition of CN^+ was not observed although it is likely to occur in a methanol solvent system. For **60** the addition of H^+ showed characteristics, such as a colour change, of vinylidene formation however the high reactivity in this experiment means that many by-products were formed that were impossible to separate.

The interesting products came from the addition of CPh_3^+. For all the Ru(dppe)Cp* monometallic acetylides, **36**, **54** and **60** the addition occurred at the 8th carbon in the chain, which is nucleophilic once a cumulene has been formed. After the addition one of two things occurred, either 1) a intramolecular cyclization between the 7th carbon and one of the phenyl rings, or 2) a radical dimerization at the 7th carbon.

Overall, the switch of aromatic group did not stabilise the cumulene intermediate as desired, but made the compounds much more reactive, leading to the difficulties experienced in synthesising the monometallic compounds and purifying the products of reaction.

Chapter 4 Electrochemistry and other analyses

More in depth analysis of some of the compounds synthesised in **Chapters 2** and **3** was carried out. These included electrochemical analysis for new acetylide compounds and solvatochromic UV-vis analysis for compounds for which a solution-based colour change was observed. These specialist techniques can provide insight into the structure and properties of molecules.

4.1 Electrochemistry

In the process of making the mono-metallic ethynyl-benzene, naphthalene and benzothiadiazole complexes, a number of intermediate protected products were synthesised (**Figure 4.1**) which have not previously been subject to electrochemical analysis. There is a possibility that cumulene type complexes may be synthesised through electrochemical oxidation which makes analysis through electrochemical means of interest, and spectroelectrochemistry can be used to monitor the formation of these types of compound.[184] Even if cumulene compounds are not formed during oxidation there is also a general interest in the redox properties of metal acetylide complexes.[184,185] Given these reasons a complete electrochemical analysis was performed using cyclic voltammetry, IR spectroelectrochemistry and UV-Vis-NIR spectroelectrochemistry.

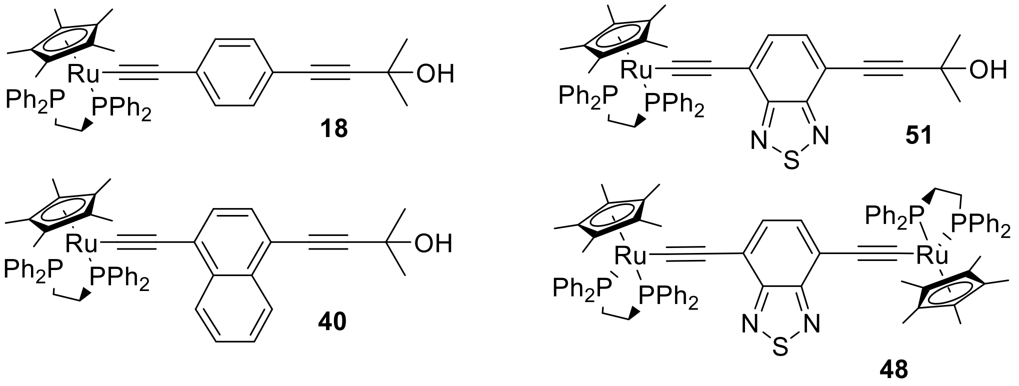

Figure 4.1: Compounds for electrochemical analysis, 18) Ru(C≡CC$_6$H$_4$-4-C≡C(CH$_3$)$_2$OH)(dppe)Cp*, 40) Ru(C≡CC$_{10}$H$_6$-4-C≡C(CH$_3$)$_2$OH)(dppe)Cp*, 51) Ru(C≡CC$_6$H$_2$(NSN)-4-C≡C(CH$_3$)$_2$OH)(dppe)Cp* and 48) {Ru(dppe)Cp*}$_2$(μ-C≡CC$_6$H$_2$(NSN)-4-C≡C). C$_6$H$_2$(NSN) = benzothiadiazole

Three monometallic compounds from the literature, which have been studied by electrochemical methods, relevant for comparison to this work are Ru(C≡C-C_6H_5)(dppe)Cp*, Ru(C≡C-$C_{10}H_9$)(dppe)Cp* and Ru(C≡C-$C_{14}H_{13}$)(dppe)Cp*[186] (**Figure 4.2**). Bimetallic compounds with diethynyl-aryl spacer groups such as Cp*(dppe)Ru-C≡C-Ar-C≡C-Ru(dppe)Cp*[169] have also been studied (**Figure 4.2**). These have similar structures to the compounds studied in this work with the same Ru(C≡CR)(dppe)Cp* moiety, and benzene, naphthalene and anthracene aromatic groups. This means that they are likely to have similar electrochemical properties and can be used to give insight to how all four molecules relate to the existing literature. These properties are described in **Sections 4.2** for cyclic voltammetry, **4.4** for UV-vis-NIR spectroelectrochemistry and **4.6** for IR spectroelectrochemistry.

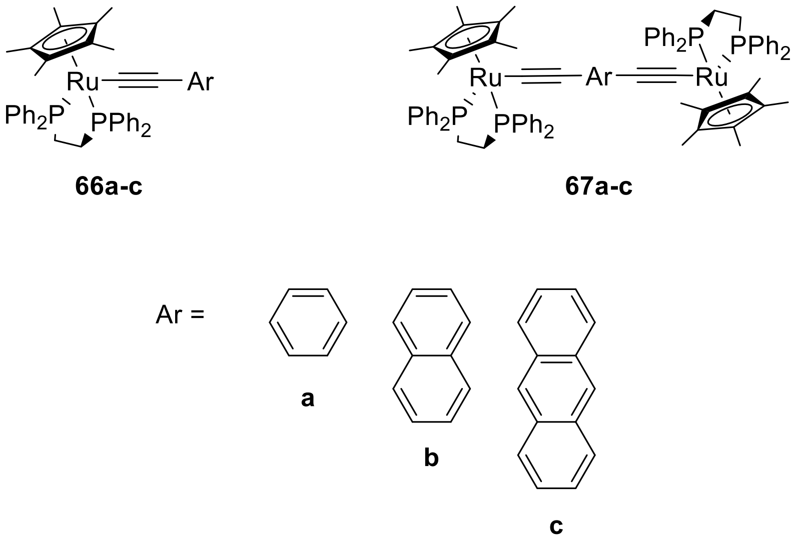

66a-c

67a-c

Figure 4.2: Literature compounds of electrochemical relevance.[169,186]

4.2 Cyclic Voltammetry

4.2.1 Introduction

Cyclic voltammetry (CV) is arguably the most common voltametric technique. In this three-electrode method, the current flowing between the working and counter electrodes is measured. To reduce solution resistance, especially in organic solvents, the analyte solution contains a significant concentration of a supporting electrolyte (e.g. 0.1 M NBu_4PF_6). Since current and potential are related, the applied potential at the working electrode is defined by a second circuit arm between the working and the reference electrodes. An ideal reference electrode is designed to offer a reliable and reproducible fixed potential in a given solvent and electrolyte. Alternatively, a more robust pseudo-reference electrode, such as a platinum wire can be employed, as is used in this work, and potential data referenced against an internal standard, such as the ferrocene / ferrocenium couple.[187]

During a CV experiment a saw-tooth potential (**Figure 4.3**) is applied to the working electrode (relative to the reference electrode) and the current flowing between the working and counter electrodes recorded.[188] As the potential at the working electrode approaches the redox potential of an analyte in solution, electron transfer from the analyte to/from the electrode causes an increase in the measured current. Current increases until the diffusion limited current is reached, which reflects the equilibrium position of migration of analyte and redox products to and from the bulk solution to the electrode interface and the electron transfer rate. The current is plotted vs potential to give the cyclic voltammogram.

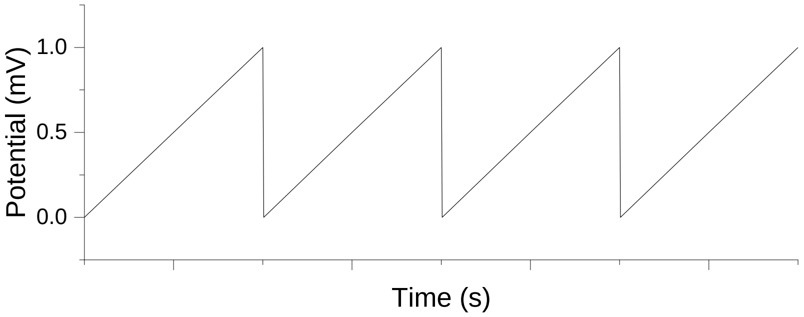

Figure 4.3: Change of potential in a saw-tooth manor during CV collection

The physical shape of the wave-forms observed in a cyclic voltammogram is dependent on the rate of electron transfer between the working electrode and the electroactive species, and the rate of diffusion of the active species to and from the electrode. When a redox event is reversible it means that the current is limited by the rate of diffusion of the active compound in solution to and from the electrode, not the rate of electron transfer. A redox event can also be irreversible meaning that the limiting rate is the rate of is electron transfer not diffusion or mass transport. A quasi-reversible redox event is one in which the rates of electron transfer and mass transport are comparable which makes a general theoretical description more complicated.[188] However, a useful characteristic of quasi-reversible systems is the improvement in apparent reversibility at *slower* scan rates, and more irreversible behaviour at faster scan rates.

The relationships governing the interplay of the measured current the rate of diffusion of a compound in solution with scan rate, and therefore its electrical reversibility, can be defined by the Randles–Ševčík equation (**Equation 4.1**).[189,190]

$$i_p = (2.69 \text{ x } 10^{-5})\, n^{\frac{3}{2}}\, A\, D^{\frac{1}{2}}\, C\, v^{\frac{1}{2}}$$

Equation 4.1: Randles–Ševčík equation

Where i_p = peak current (A), n = electron stoichiometry, A = electrode area (cm^{-1}), D = diffusion coefficient (cm^3 s^{-1}), C = concentration (mol cm^{-3}) and v = scan rate (V s^{-1}). This states that i_p increases with $v^{\frac{1}{2}}$ but is directly proportional to concentration.[189] The consequences of **Equation 4.1** can be observed experimentally by running the same CV sweep at different scan rates, if the potential vs. (scan rate)$^{1/2}$ is linear then the redox event meets one of the criteria for electrochemical reversibility.[190]

Chemical reversibility is a separate phenomenon to electron reversibility. If the oxidation and reduction peaks are at close potentials (59.5 mV[191]) and of equal intensity, then the system is also chemically reversible. If the species formed on the electrode is unstable and reacts very rapidly leaving it unavailable for the reverse sweep then the compound is chemically irreversible, this is observed by a lack of return wave. The system can also be partially chemically reversible if the intensity of the return wave is reduced.[188]

4.2.2 Results

The electrochemical responses of compounds **18**, **40**, **51** and **48** (**Figure 4.1**) were examined by cyclic voltammetry in CH_2Cl_2 solutions containing 0.1 M tetra-butylammonium hexafluorophosphate ($[NBu_4]PF_6$) as the supporting electrolyte. Potentials are quoted against ferrocene using an internal decamethylferrocene/ decamethylferrocenium reference ($[Fe(\eta^5\text{-}C_5Me_5)_2]$ / $[Fe(\eta^5\text{-}C_5Me_5)_2]^+$ = – 0.55 V[192] vs. $[Fe(\eta^5\text{-}C_5H_5)_2]$ / $[Fe(\eta^5\text{-}C_5H_5)_2]^+$) and a platinum working electrode and platinum *pseudo*-reference electrode (**Table 4.1**).

In all cases, the first oxidation process, normally associated with the $Ru(C{\equiv}CR)(dppe)Cp^*$ fragment, with contribution from the aryl group, of complexes **18**, **40**, **51** and **48** displayed peak currents that were proportional to the square-root of the scan rate. The forward and reverse peak potentials were separated by ca. 100 mV, larger than the idealised value of 59 mV[188] but in agreement with the peak-to-peak separation of the ferrocene wave under the same conditions and likely arising from uncompensated solution resistance. In addition, the forward and reverse peak currents were equal in intensity meaning these redox processes were adequately described as being reversible. A second, irreversible oxidation event was observed at higher potentials, and tentatively assigned to redox processes with more arylene character.

The oxidation potential for the reference monometallic compounds[186] **66a**, **66b** and **66c** (**Table 4.1**) all appear at similar potentials of 0.34, 0.36 and 0.29 V respectively (data reported vs saturated calomel reference electrode). This small difference of 20 mV between the benzene and naphthalene groups shows that in this case the additional conjugation of the arylene systems do not make a big difference to the ability of these compounds to lose an electron, in fact this difference is within the expected measurement error of cyclic voltammetry (ca. ±10 mV). A second oxidation event was also observed; however this was seen to be irreversible under all conditions.[186]

Table 4.1: Selected electrochemical data (V) with NBu_4BF_4 as the supporting electrolyte, 25 °C, where: $E_{1/2}(1)$ = half-wave potential of 1st oxidation, ΔE_p = difference between oxidation and reduction potential, $E(2)_{pc}$ = cathodic peak potential for irreversible oxidation, ΔE_p (1/2) = difference between 1st and 2nd cathodic peak potential. Referenced vs ferrocene/ferrocenium [$E_{1/2}(Fc/Fc^+)$ = 0 V] at a platinum working electrode.

Compound	$E_{1/2}(1)$ (V)	ΔE_p (1) (V)	$E(2)_{pc}$ (V)	$\Delta E_p(1/2)$ (V)
66a 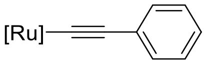 [186]	0.34[a]	0.08	1.19[a]	0.85
66b 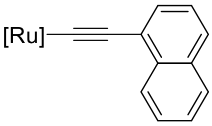 [186]	0.36[a]	0.11	1.28[a]	0.92
66c 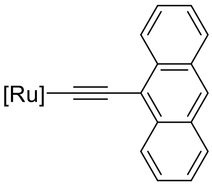 [186]	0.29[a]	0.09	1.07[a]	0.78
18 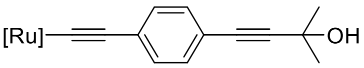	-0.16	0.11	0.81	0.91
40 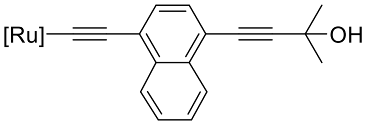	-0.19	0.09	0.64	0.78
51 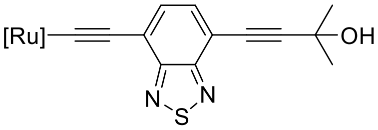	-0.14	0.12	0.73	0.87

[Ru] = Ru(dppe)Cp*. [a] = Fox *et al*,[186] vs SCE, 25 °C.

4.2.2.1 Ru(C≡CC$_6$H$_4$-4-C≡C(CH$_3$)$_2$OH)(dppe)Cp*, Compound 18

For compound **18**, with benzene as the spacer group, the half wave potential occurs at -0.16 V and is fully reversible (**Figure 4.4A**). A second oxidation process which occurs at E_p = 0.81 V, is observed in an initial scan to higher potentials (**Figure 4.4B**) but which results in passivation of the electrode surface through decomposition of the redox product.

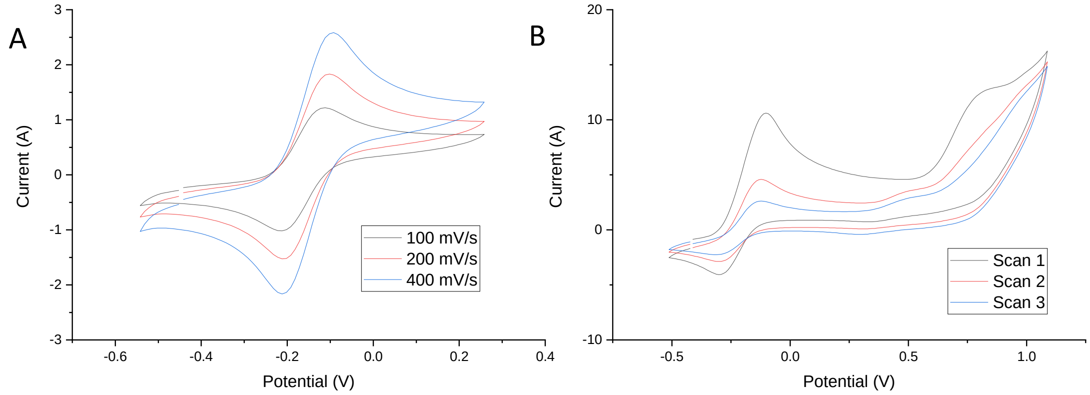

Figure 4.4: Plot of the cyclic voltammograms (CV) data for complex 18 (CH_2Cl_2, 0.1 M NBu_4PF_6, room temperature) A: at different scan rates (0.1, 0.2, 0.4, and 0.6 V s^{-1}) and B: second irreversible oxidation event. Referenced vs ferrocene/ferrocenium [$E_{1/2}$(Fc/Fc$^+$) = 0 V] at a platinum working electrode.

4.2.2.2 Ru(C≡CC$_{10}$H$_6$-4-C≡C(CH$_3$)$_2$OH)(dppe)Cp*, Compound 40

Compared to the benzene spacer group, compound **18**, compound **40** with a naphthalene spacer group, has the same half wave potential for the first redox event, -0.16 V vs -0.19 V, and is also reversible (**Figure 4.5A**). The second oxidation is also irreversible with the oxidation occurring at 0.64 V, which is 0.78 V higher than the first oxidation (**Figure 4.5B**).

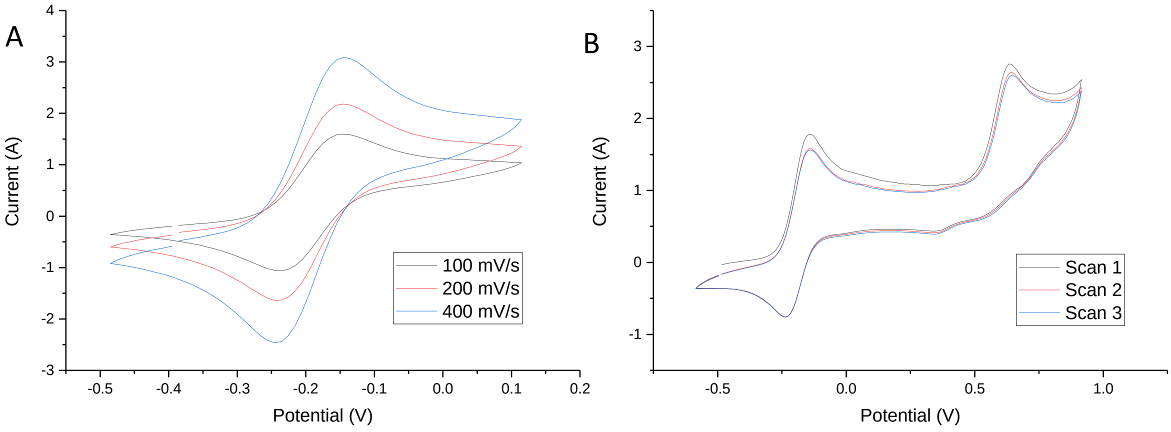

Figure 4.5: Plot of the cyclic voltammograms (CV) data for complex 40 (CH_2Cl_2, 0.1 M NBu_4PF_6, room temperature) A: at different scan rates (0.1, 0.2, 0.4, and 0.6 V s^{-1}) and B: second irreversible oxidation event. Referenced vs ferrocene/ferrocenium [$E_{1/2}(Fc/Fc^+)$ = 0 V] at a platinum working electrode.

4.2.2.3 Ru(C≡CC_6H_2(NSN)-4-C≡$C(CH_3)_2OH$)(dppe)Cp*, Compound 51

In contrast to the naphthalene compound **40**, the benzothiadiazole compound **51** requires the input of more energy in order to lose an electron, with an oxidation potential of -0.14 V (**Figure 4.6A**). Despite the electron withdrawing effects of the nitrogen and sulfur atoms of this compound is has the same oxidation potential as the naphthalene compound **40**.

The second oxidation occurred at 0.73 V, which is 0.87 V higher than the first oxidation (**Figure 4.6B**). The second oxidation is irreversible with no corresponding reduction taking place, which, along with a reduction in the intensity of the first oxidation shows that whatever compound is formed is adhering to the electrode surface as it reacts.

Also, a small third set of peaks can be seen in the second and third scans, between the two main oxidations, with a half wave potential of 0.42 V (cathodic peak = 0.47 V, anodic peak= 0.38 V). The species responsible for this redox process is unknown, although doping with additional RuCl(dppe)Cp* or free dppe does not affect this in any way, meaning that it is likely due to the oxidation of the decomposition products that are made during the second oxidation event.

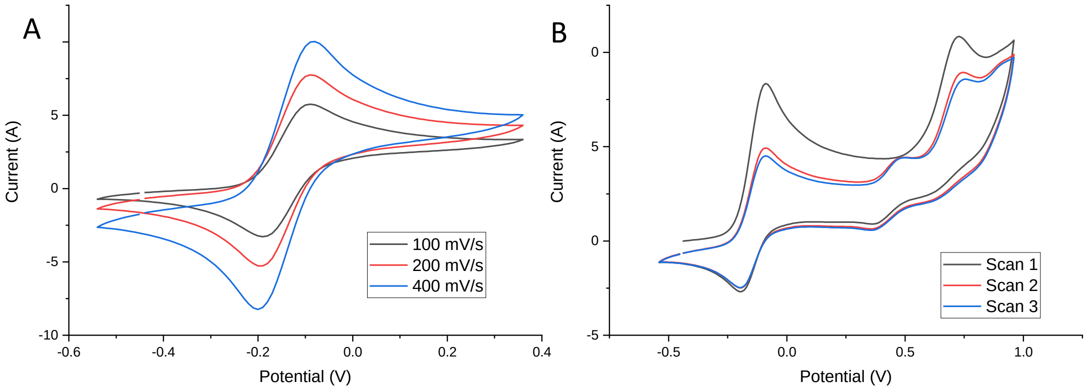

Figure 4.6: Plot of the cyclic voltammograms (CV) data for complex 51 (CH_2Cl_2, 0.1 M NBu_4PF_6, room temperature) A: at different scan rates (0.1, 0.2, 0.4, and 0.6 V s^{-1}) and B: second irreversible oxidation event. Referenced vs ferrocene/ferrocenium [$E_{1/2}(Fc/Fc^+)$ = 0 V] at a platinum working electrode.

4.2.2.4 [{Ru(dppe)Cp*}$_2$(μ-C≡CC$_6$H$_2$(NSN)-4-C≡C)], Compound 48

In contrast to the reference monometallic compounds, the corresponding bimetallic compounds **67** (**Table 4.2**) have a wide range of potentials (0.18 V) with the benzene spaced compound **67a** at 0.01 V, naphthalene, **67b**, at -0.06 V and -0.17 V (vs Ferrocene/ferrocenium) for anthracene, **67c**.[169] The oxidation of these bimetallic compounds has been shown to be significantly ligand based.

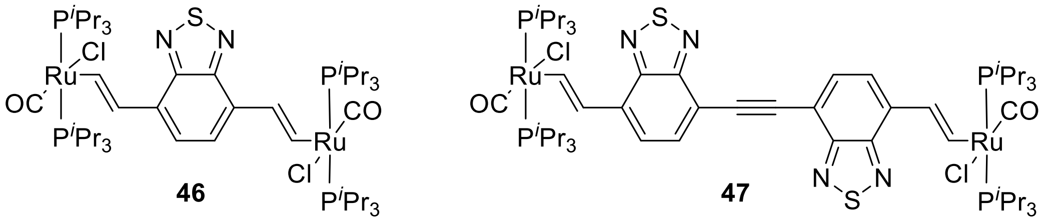

Figure 4.7: Structure of compounds 46 and 47

The only examples of redox-active bimetallic complexes featuring benzothiadiazole-based bridging ligands of which we are aware are those described by Rotthowe *et al.*[177] Two of these compounds **46**, and **47** are shown in Figure 4.7. These compounds have vinyl rather than acetylide connection to the ruthenium centre, which also has different spectator ligands, meaning that the electrochemical data are not directly comparable to Ru(dppe)Cp* acetylide complexes.

Table 4.2: Selected electrochemical data (V) with NBu_4BF_4 as the supporting electrolyte, 25 °C, where: $E_{1/2}(1)$ = half-wave potential of 1st oxidation, ΔE_p = difference between oxidation and reduction potential, $E_{1/2}(2)$ = half-wave potential of 2nd oxidation, ΔE_p (1/2) = difference between 1st and 2nd cathodic peak potential. Referenced vs ferrocene/ferrocenium [$E_{1/2}(Fc/Fc^+)$ = 0 V] at a platinum working electrode

Compound	$E_{1/2}(1)$ (V)	ΔE_p	$E_{1/2}(2)$ (V)	ΔE_p (1/2) (V)
67a 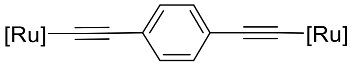 169	0.01	-	0.30	0.29
67b 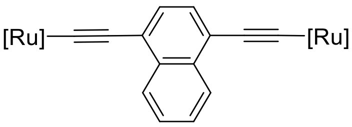 169	-0.06	-	0.24	0.29
67c 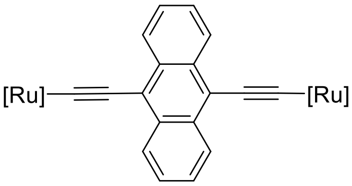 169	-0.17	-	0.13	0.30
Compound **46**[177]	-0.20	-	0.80[a]	0.28
Compound **47**[177]	0.10	0.15	0.18[a]	0.08
48 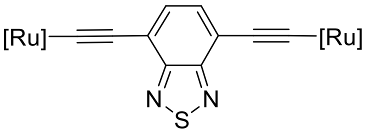	-0.13	0.08	0.63[b]	0.72

[Ru] = Ru(dppe)Cp*. [169] = Fox *et al.* [177]= Rotthowe *et al.* [a] = TBABAr^F electrolyte. [b] = cathodic peak potential for irreversible oxidation

The small increase in the redox potential for bimetallic compounds **67a** and **67b** (reported vs Fc)[193] compared to similar monometallic ones, **18** and **40** (**Table 4.1**) is due to the presence of the additional Ru(C$\equiv$C)(dppe)Cp* electron donor. As there is then higher electron density on the aromatic group it therefore has a larger influence on the accessibility of the 1+ oxidation state.

The CV (**Figure 4.8A**) of the bimetallic benzothiadiazole compound **48** ($E_{1/2}$ = -0.13 V) has a redox potential that is experimentally indistinguishable from that of the acetone protected monometallic complex **18** ($E_{1/2}$ = -0.14 V), see **Table 4.2**.

In the majority of aromatic spaced bimetallic acetylide complexes a second oxidation can be achieved in reversible fashion.[169] However, for compound **48** the second oxidation event (**Figure 4.8B**) at 0.63 V, 0.72 V higher than the first, is also irreversible and the same new oxidation event seen in **Figure 4.6B** is also observed for this compound in **Figure 4.8B** and has the same half wave potential of 0.43 V.

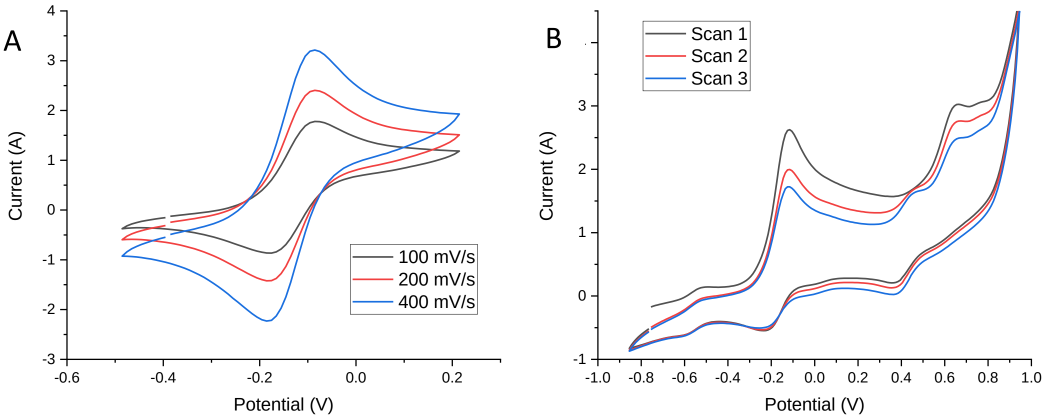

Figure 4.8: Plot of the cyclic voltammograms (CV) data for complex 48 (CH_2Cl_2, 0.1 M NBu_4PF_6, room temperature) A: at different scan rates (0.1, 0.2, 0.4, and 0.6 V s^{-1}) and B: second irreversible oxidation event. Referenced vs ferrocene/ferrocenium [$E_{1/2}(Fc/Fc^+)$ = 0 V] at a platinum working electrode.

4.3 Summary

Overall, the CV analysis of compounds **18** and **40** was consistent with the literature values for monometallic compounds with the same metal fragment and similar aromatic group. This indicated that the addition of an additional alkyne and protecting group did not affect the electrochemical properties of these compounds. However, despite there being no direct literature comparisons for the two benzothiadiazole compounds **51** and **48** the half wave potentials are in a similar range to that of the naphthalene analogues and in the expected range.

4.4 UV-vis-NIR Spectroelectrochemistry

4.4.1 Introduction

UV-vis-NIR spectroelectrochemistry (SEC) is a technique in which UV-vis-NIR spectra are collected as a function of applied potential and hence maps spectroscopic changes with changes in redox state of the analyte. SEC measurements are carried out using an optically transparent thin layer electrochemical (OTTLE) cell which houses a semi-transparent working electrode, normally as a mesh electrode,[194] in a solution cell with windows which allow for the passage of light with the desired wavelength range, while allowing electrolysis to be performed. UV-vis-NIR measurements are taken at various stages during both the forward and backwards sweeps of the CV.

As with CV the solvent used contains an excess of electrolyte that is used to reduce solution resistance as well as the use of a counter and reference electrode, which are positioned in the OTTLE cell so not to interfere with the spectroscopic window.[194] An inert environment, N_2, is used to keep the OTTLE cell free of oxygen and moisture.

Three reference monometallic compounds **66a**, **66b** and **66c**[186] (**Figure 4.2**) have been analysed through UV-vis-NIR SEC methods by others elsewhere. They each had strong absorbance bands between 30,000 cm^{-1} and 20,000 cm^{-1} (**Table 4.3**), which are red shifted for the larger aromatic groups. These bands are generally described as being due to a metal-to-ligand charge transfer band (MLCT),[195] however, density functional theory (DFT) calculations showed that the main absorbance band for the compounds with benzene and naphthalene was mixed with (d/π) to phenyl π* charge transfer characteristics rather than solely MLCT. In contrast for the anthracene-based compound the significantly lower absorbance at 20,600 cm^{-1} is an anthryl-centred π-to-π* transition (HOMO to LUMO).

Table 4.3: Summary of UV-vis-NIR spectroelectrochemical data (from 0.1 M NBu_4PF_6/CH_2Cl_2 solutions, 25 °C) for various monometallic ruthenium acetylide complexes. 0 = neutral state, +1 = oxidised state

Compound	UV/Vis 0 (cm^{-1})	UV/Vis +1 (cm^{-1})
66a 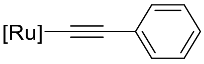 [186]	29 500	22 600, 21 100, 11 200, 8 100
66b 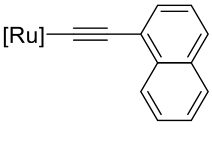 [186]	26 200	20 200, 18 600, 11 000, 7 600
66c 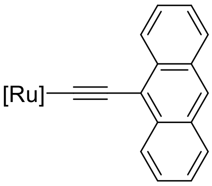 [186]	20 600	27 200, 17 900, 15 200, 10 100, 7 800
18 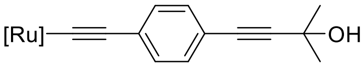	27 780	25 510, 13 180, 7 650
40 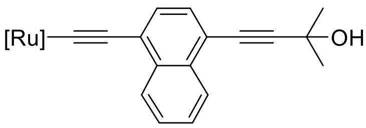	24 160	29 590, 19 760, 11 360, 7 490
51 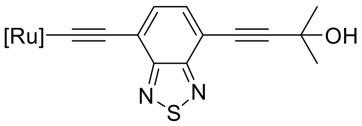	30 490, 17 420	22 370

[Ru] = Ru(dppe)Cp*. [186] = Fox *et al.*

Upon oxidation of the reference compound **66a**, with a benzene spacer group, to [**66a**]$^+$ in the SEC cell, two major new absorption bands appeared at 21,100 and 11,200 cm^{-1}, with a smaller envelope at 8100 cm^{-1}. The highest band at 21,100 cm^{-1} is attributed (through DFT calculations) to a transfer of charge from the Ru(C≡CAr)(dppe)Cp* fragment to the phenyl π ring and an electronic transition from the α-HOSO (highest occupied spin orbital) with high alkyne character to the α-LUSO with high Ru character. The next band around 11200 cm^{-1} is then due to the transition between the β-HOSO orbitals with high Ru/Cp* character to the β-LUSO orbitals with more alkyne character.[186] And finally the NIR band at low energy is due to a general [Ru(C≡CAr)(dppe)Cp*] radical cation which is attributed to formally forbidden ligand-field type transitions that are centred on the Ru^{III} centre.[195]

4.4.2 Results

Complexes **18**, **40**, **51** and **48** in 0.1 M $[NBu_4]PF_6$ CH_2Cl_2 solutions were also subjected to UV-Vis-NIR spectroelectrochemical investigations, with selected absorption maxima in **Table 4.3**. As the CV data for these compounds shows that the second oxidation is chemically irreversible, only the first redox event was studied using this technique. There UV-vis-NIR SEC data were collected by Dr Masnun Naher at UWA.

4.4.2.1 Ru(C≡CC$_6$H$_4$-4-C≡C(CH$_3$)$_2$OH)(dppe)Cp*, Compound 18

For compound **18**, which is yellow in colour, the closed-shell neutral state has one main band in the near UV region of the spectra at 27780 cm^{-1} (**Figure 4.9**) which can be attributed to the π-to-π* transition for the conjugated benzene and alkyne groups by analogy with **66a**.[186] After oxidation of compound **18** to [**18**]$^+$ two new bands were observed at 25510 cm^{-1} and 13180 cm^{-1}; this increase in the number of bands and the shift to lower wavenumbers is typical for a UV-vis SEC spectrum for this type of compound.[169,186] The band at 13180 cm^{-1} is similar to the band observed for aromatic radical cations[196,197] and indicates the appreciable ligand character to the oxidation event. The other band at 25510 cm^{-1} related to the charge transfer from the ruthenium fragment (with some acetylide π character) to the aryl π* ring.[186] It is also possible to see the near-IR (NIR) band at 7651 cm^{-1} which is due to formally forbidden dπ-to-dπ transitions.

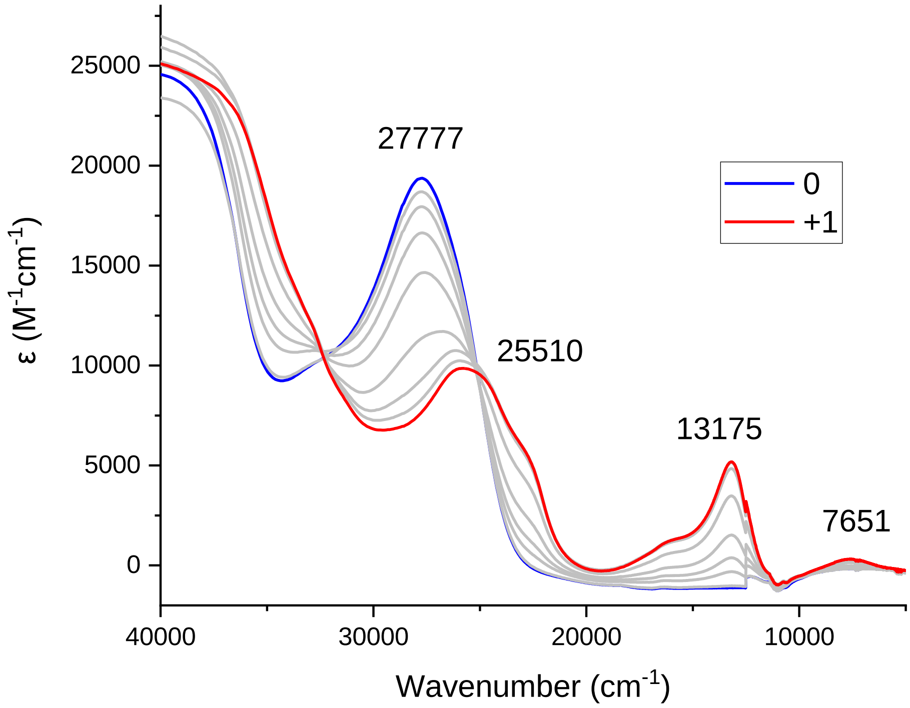

Figure 4.9: The UV-Vis-NIR spectra of compound 18 between 5000 – 40,000 cm^{-1}. Spectra were collected via spectroelectrochemical methods from a 0.1 M [NBu_4]PF_6 CH_2Cl_2 solution. 0 = neutral state, +1 = oxidised state

4.4.2.2 Ru(C≡C$C_{10}H_6$-4-C≡C(CH_3)$_2$OH)(dppe)Cp*, Compound 40

In the spectrum below (**Figure 4.10**) for compound **40** the absorption band at 24160 cm^{-1} appears in the violet region of the visible spectrum, this fits with the orange colour of the compound, as the blue region of light is absorbed. A second, small UV band can be seen at 34360 cm^{-1}. As compound **40** is oxidised to [**40**]$^+$ three additional absorption bands were seen at 29590, 19760 and 11360 cm^{-1}. The latter two show similar shifts when compared to the benzene analogue and are again likely to be due to the formation of an aromatic radical cation, with the entire spectrum red-shifted through the effects of the extended conjugation.[169] A very weak and broad NIR band can also be seen in the 1^+ spectrum at 7485 cm^{-1} arising from the dπ-to-dπ transitions that typify the formally $[Ru^{III}C{\equiv}CR]^+$ fragment.

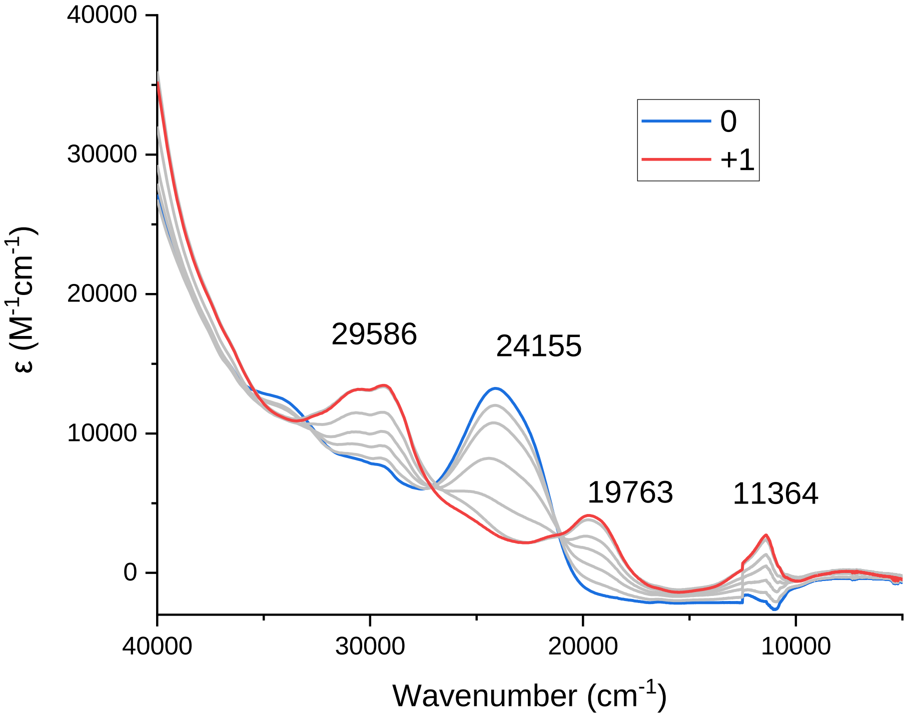

Figure 4.10: The UV-Vis-NIR spectra of compound 40 between 5000 – 40,000 cm^{-1}. Spectra were collected via spectroelectrochemical methods from a 0.1 M $[NBu_4]PF_6$ CH_2Cl_2 solution. 0 = neutral state, +1 = oxidised state

4.4.2.3 Ru(C≡CC$_6$H$_2$(NSN)-4-C≡C(CH$_3$)$_2$OH)(dppe)Cp*, Compound 51

For compound **51** (**Figure 4.11**) two absorption bands are observed. The lower energy transition at 17420 cm^{-1}, which has no analogy with the spectra recorded for the other spacer groups, falls in the visible region and means that the yellow wavelengths of light are absorbed and accounts for the blue/purple colour of compound **51**. As this visible light band, and the distinctive colour, is not observed for the dibromo-BTD organic fragment, this band can be attributed to a MLCT event. The other band which appears at 30490 cm^{-1} has more similarities to the UV absorption for benzene and naphthalene so can be attributed to the benzene/alkyne conjugated system. However, this occurs at a higher energy than for the benzene analogue, **18**, which is in opposition to the trend for shifting down in energy with an increasing number of rings, and indicates the substantial stabilisation of the ligand based occupied orbitals through the additional electron withdrawing diathiazole moiety.[169,186]

Upon oxidation to [**51**]$^+$ the intensity of the band at 30490 cm^{-1} was reduced significantly and the one at 17420 cm^{-1} collapsed completely. The new band which appeared at 22370 cm^{-1} is likely to be due to the formation of the radical cation species. The low intensity dπ-dπ bands below 10000 cm^{-1} were not observed for this compound, and possibly masked by spectral noise in this region.

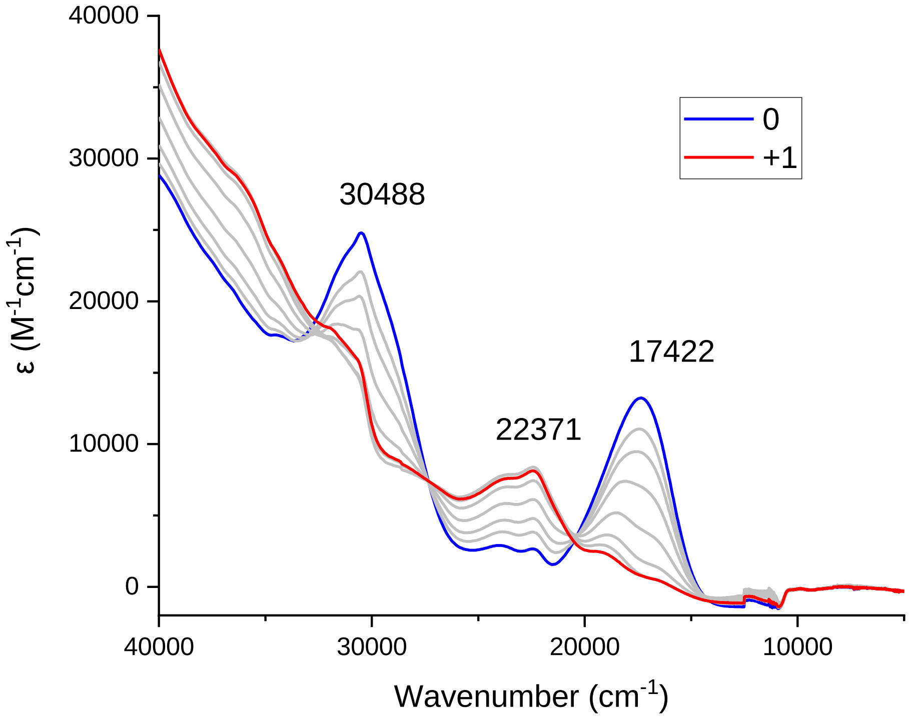

Figure 4.11: The UV-Vis-NIR spectra of compound 51 between 5000 – 40,000 cm^{-1}. Spectra were collected via spectroelectrochemical methods from a 0.1 M [NBu$_4$]PF$_6$ CH$_2$Cl$_2$ solution. 0 = neutral state, +1 = oxidised state

4.4.2.4 $[\{Ru(dppe)Cp^*\}_2(\mu\text{-}C\equiv CC_6H_2(NSN)\text{-}4\text{-}C\equiv C)]$, Compound 48

For the bimetallic compounds **67a**, **67b** and **67c**[169] the first oxidation follows similar characteristics as the monometallic compounds with the same aromatic groups,[186] and the behaviours of the benzene and naphthalene compounds were almost identical to each other. The initial UV-vis-NIR spectra for these two compounds are dominated by a single absorption band at 28000 cm^{-1} for benzene and 22000 cm^{-1} for naphthalene, which can be attributed to the diethynyl aryl π-to-π* transitions. In contrast there are two bands for anthracene at 34000 and 18000 cm^{-1}, with the lower also being attributed to the diethynyl anthracene π-to-π* transition.[169] These show the same red-shift with larger aromatic groups as seen by Fox *et al.*[186]

Table 4.4: Summary of UV-vis/NIR spectroelectrochemical data (from 0.1 M NBu_4PF_6/CH_2Cl_2 solutions, 25 °C) for various bimetallic ruthenium acetylide complexes. 0 = neutral state, +1 = oxidised state

Compound	UV/Vis 0 (cm^{-1})	UV/Vis +1 (cm^{-1})
67a 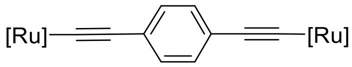 [169]	28 000	20 000, 18 000, 5 000
67b 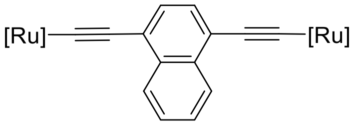 [169]	22 000	26 000, 15 000, 5 000
67c 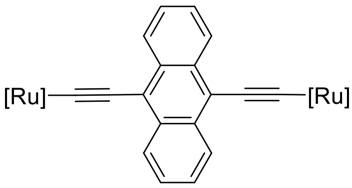 [169]	34 000, 18 000	32 000, 24 000, 12 000, 10 000, 5 000
48 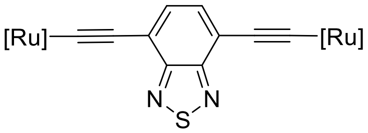 	43 670, 17 270	17 270, 11 880, 6 210

[Ru] = Ru(dppe)Cp*. [169] = Fox *et al.*

Upon oxidation to the radical cation species these features collapse, and new transitions are observed with one band with a shoulder around 19000 cm^{-1} and a single band in the NIR region around 5000 cm^{-1} for compounds **67a** and **67b**. Again, the anthracene compound, **67c**, shows slight differences with the main absorption band appearing at 11000 cm^{-1}, although it also shows the NIR band at 5000 cm^{-1}. These data suggest that for bimetallic compounds the type of aromatic group used as a spacer group impacts the redox character of the compounds.[169]

For compound **48** the absorption band which occurs at 17270 cm^{-1} (**Figure 4.12**) can likely be attributed to the MLCT processes involving the thiadiazole fragment as it is the same band that is seen in the initial UV-vis-NIR spectra for the monometallic analogue, compound **51**. The other UV band is very high at 43670 cm^{-1}, which likely arises from higher energy MLCT bands arising from lower energy d-orbitals to the ligand π* system that are shifted out of the observable spectral region in the other compounds.

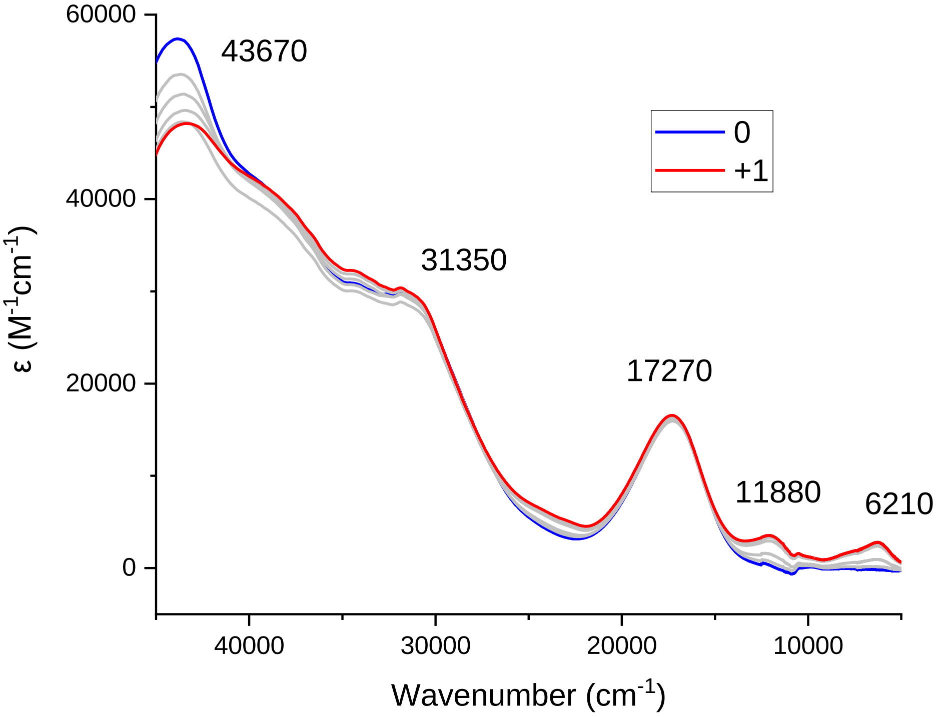

Figure 4.12: The UV-Vis-NIR spectra of compound 48 between 5000 – 45,000 cm^{-1}. Spectra were collected via spectroelectrochemical methods from a 0.1 M [NBu$_4$]PF$_6$ CH$_2$Cl$_2$ solution. 0 = neutral state, +1 = oxidised state

During the oxidation of this compound there is a reduction in the intensity of the absorption band at 43670 cm^{-1}, consistent with the MLCT assignment, and the growth of two bands at 11876 cm^{-1} (for the aromatic radical transition) and in the NIR region at 6210 cm^{-1} for the dπ-dπ transition. Interestingly the band at 17270 cm^{-1} stays constant during oxidation, this indicates that the first oxidation does not affect the part of the molecule that causes this transition. This would only work if the oxidation occurred on only one of the metal fragments and has no contribution from the rest of the molecule. This is backed up by the fact that the band at 43670 cm^{-1} does not decrease in intensity as much as similar bands do for the monometallic species, this indicates that the transition that is contributing to this band is not removed completely as one metal alkyne is expected to still be present.

4.5 Summary

The UV-vis-NIR analysis of compounds show that all three monometallic compounds contain π-to-π* transitions in the neutral state which appear between 27780 cm^{-1} and 30490 cm^{-1}. However, compounds **51** and **48** also show large MLCT bands at around 17300 cm^{-1}, as the position of this absorption band is statistically the same for both compounds and is not seen for organic dibromo-benzothiadiazole fragment, it must be caused by an interaction between the metal centre and the benzothiadiazole fragment. The bimetallic compound **48**, also has a second higher MLCT band at 43670 cm^{-1}.

Upon oxidation of all compounds a band that can be attributed to a radical cation is observed between 11360 cm^{-1} and 22370 cm^{-1}, as well as a broad band in the NIR region which can be attributed to a formally forbidden dπ-dπ transition. Metal to ligand charge transfer bands were also observed for all compounds (except compound **51**) and occurred between 17270 cm^{-1} and 29590 cm^{-1}.

The change from bands related to π-to-π* transitions to those of a radical cation or MLCT indicates that there is a loss of conjugation across the molecule which could be due to the loss of the acetylide triple bond. This can be identified through infra-red SEC.

4.6 IR Spectroelectrochemistry

4.6.1 Introduction

Infra-red spectroelectrochemistry (SEC) is very similar to UV-vis-NIR SEC but the IR spectrum is recorded during the electrochemical transformation rather than UV-vis-NIR spectrum. IR spectroscopy contains information concerning molecular structure and is especially useful for compounds which contain groups with strong IR absorbing chromophores such as CO, CN or in this case alkynes. The measurements were carried out in the same solution state OTTLE cell that was used for the UV-vis-NIR SEC (**Section 4.4.1**).

When the literature compounds, **66a**, **66b** and **66c**,[186] were analysed by IR SEC an obvious shift in the ν(C≡C) stretch was observed during oxidation. In the initial IR spectra these compounds had ν(C≡C) stretches of 2072, 2053 and 2041 cm^{-1} respectively, which are characteristic of 18 electron ruthenium acetylide complexes. Each of these stretches decreased by more than 100 cm^{-1} upon oxidation the radical cation species with ν(C≡C) stretches at 1929 (**66a**), 1916 (**66b**) and 1925 (**66c**) cm^{-1}. The comparable shifts of these spectra indicate that acetylide ligand is significantly involved in the oxidation with similar structures (tending towards cumulated valence descriptions) in all of the resulting radical cations.

Table 4.5: Summary of IR spectroelectrochemical data (from 0.1 M NBu_4PF_6/CH_2Cl_2 solutions) for various monometallic ruthenium acetylide complexes. 0 = neutral state, +1 = oxidised state

Compound	νC≡C (cm^{-1}) n = 0	νC≡C (cm^{-1}) n = 1	ΔνC≡C (cm^{-1})
66a 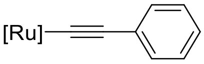 [186]	2072	1929	-143
66b 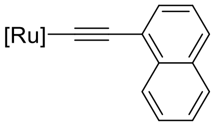 [186]	2053	1916	-137
66c 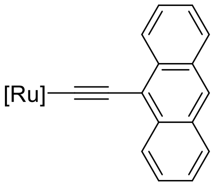 [186]	2041	1925	-116
18 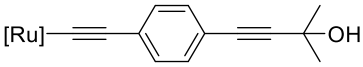	2063	1926	-137
40 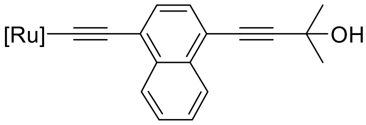	2047	1908	-139
51 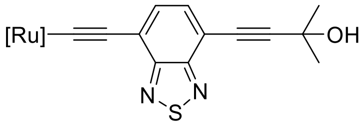	2036	1907	-129

[Ru] = Ru(dppe)Cp*. [186] = Fox *et al.*

4.6.2 Results

The first full oxidation of compounds **18**, **40**, **51** and **48** were monitored by IR spectroscopy with a range of 1000 to 10000 cm^{-1}. This wide range for the IR window into the near-IR region allows for monitoring of both the mid-IR ν(C≡C) bands and the dπ-dπ bands diagnostic of the oxidation event and allowing correlation with the UV-vis-NIR spectra discussed above. The spectroelectrochemical IR data for both the near-IR region as well as the key 1800 to 2200 cm^{-1} range, which includes the alkyne stretches, is seen (**Table 4.5**) for all four of the compounds **18**, **40**, **51** and **48**.

4.6.2.1 Ru(C≡CC$_6$H$_4$-4-C≡C(CH$_3$)$_2$OH)(dppe)Cp*, Compound 18

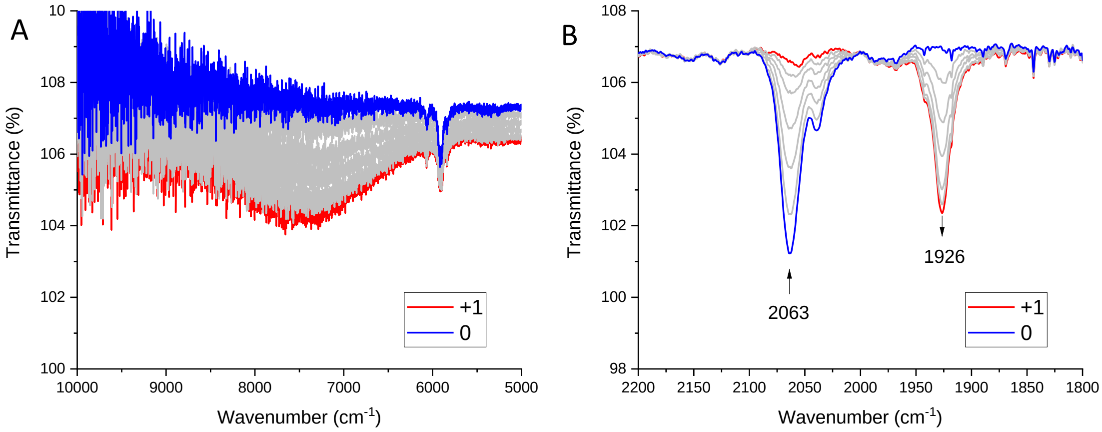

Figure 4.13: Plot of the normalised IR spectroelectrochemical results (from 0.1 M NBu$_4$PF$_6$/ CH$_2$Cl$_2$ solutions) for compound 18^{n+} (n= 0, 1). A) between 10,000 – 5000 cm^{-1} B) between 2200 – 1800 cm^{-1}. 0 = neutral state, +1 = oxidised state

In the initial IR spectrum for compound **18** an asymmetric ν(C≡C) stretch at can be observed at 2063 cm^{-1} (**Figure 4.13B**), with a small shoulder at 2039 cm^{-1} arising from the presence of multiple conformers. During oxidation the alkyne stretch shifts down to 1926 cm^{-1}, which is a relatively large shift of more than 100 cm^{-1} which means that the oxidation is likely to be primarily occurring on the ligand rather than the metal centre in a manner entirely consistent with the reference compounds.

4.6.2.2 Ru(C≡CC$_{10}$H$_6$-4-C≡C(CH$_3$)$_2$OH)(dppe)Cp*, Compound 40

For compound **40**, with a naphthalene spacer group (**Figure 4.14**) the broad dπ-to-dπ transition is also observed on oxidation. In the alkyne ν(C≡C) region of the spectra on oxidation the single symmetrical stretch for **40** at 2047 cm^{-1} is replaced by one at 1908 cm^{-1} for [**40**]$^+$, at the same rate as the appearance of the dπ-dπ band. This is a shift of 139 cm^{-1}, as this is more than 100 wavenumbers it means it is likely the oxidation is mainly on the alkyne. When compared to the literature compound **66b**, the IR SEC spectra are almost identical, each starting at about 2050 cm^{-1}, and reaching an oxidised stretch at around 1910 cm^{-1}, which was a difference of 137 or 139 cm^{-1}. This indicates that the addition of the ($C{\equiv}C(CH_3)_2OH$) group does not affect the IR SEC of these compounds.

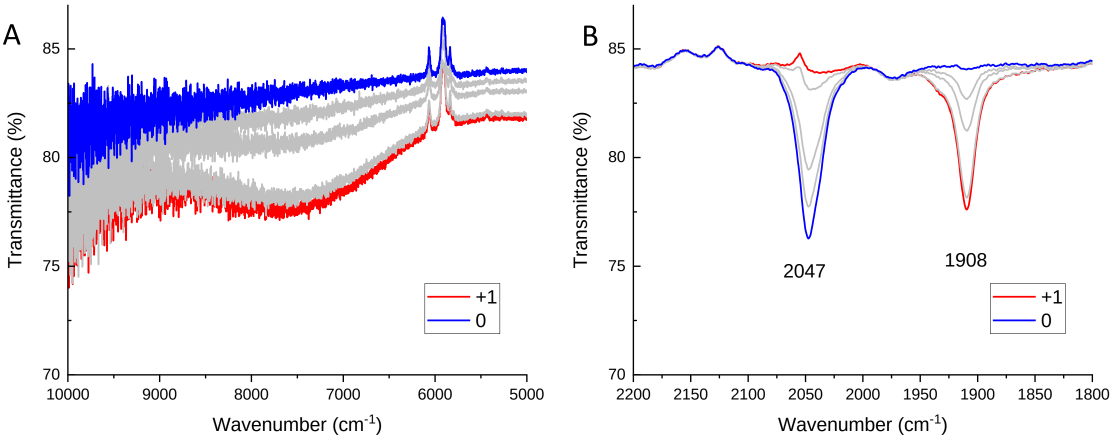

Figure 4.14: Plot of the normalised IR spectroelectrochemical results (from 0.1 M NBu_4PF_6/ CH_2Cl_2 solutions) for compound 40^{n+} (n= 0, 1). A) between 10,000 – 5000 cm^{-1} B) between 2200 – 1800 cm^{-1}. 0 = neutral state, +1 = oxidised state

The benzene **18** (**Figure 4.9 and Figure 4.13**) and naphthalene **40** (**Figure 4.10 and Figure 4.14**) spacer groups show UV and IR SEC spectra which are unsurprising for ruthenium species, and have lots of similarities to each other and to similar literature compounds[186] which further shows that the change in the spacer group from benzene to naphthalene does not make much difference to the electrochemical activity of these complexes.

4.6.2.3 Ru(C≡CC$_6$H$_2$(NSN)-4-C≡C(CH$_3$)$_2$OH)(dppe)Cp*, Compound 51

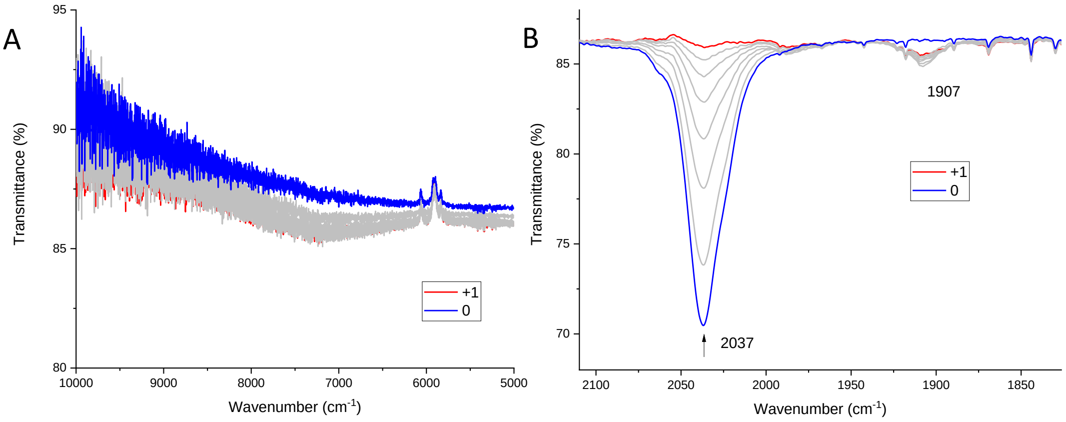

Figure 4.15: Plot of the normalised IR spectroelectrochemical results (from 0.1 M NBu$_4$PF$_6$/ CH$_2$Cl$_2$ solutions) for compound 51^{n+} (n= 0, 1). A) between 10,000 – 5000 cm^{-1} B) between 2200 – 1800 cm^{-1}. 0 = neutral state, +1 = oxidised state

The IR SEC data collected during oxidation of **51** (**Figure 4.15B**) shows the growth of a small ν(C≡C) band at 1907 cm^{-1}; however, this band does not increase in intensity at the same rate as the loss of the initial IR stretch at 2037 cm^{-1}. The ν(C≡C) band at 1907 cm^{-1} rises and then starts to decrease before the compound is fully oxidised. This phenomenon was seen by IR SEC for multiple batches however if it is due to an impurity, it was not visible in the NMR or CV characterisation. One explanation for the loss of this stretch is the reactivity of the oxidised complex, especially if a cumulene type compound is being formed as these are highly reactive (as we believe that the stretch at 1907 cm^{-1} could be attributed to). This reactivity might not be evident in the CV due to the shorter lifespan of the oxidised species during this characterisation. However, as we know this did not occur for any of the other spacer groups this indicates that the highly electron withdrawing properties of the benzothiadiazole spacer group greatly affects the reactivity of the oxidised compound. The NIR band can also be observed as a very broad band centred at 7306 cm^{-1} which not observed in the UV-vis-NIR SEC for this compound (**Figure 4.15A**).

4.6.2.4 [{Ru(dppe)Cp*}$_2$(μ-C≡CC$_6$H$_2$(NSN)-4-C≡C)], Compound 48

For the reference bimetallic compounds[169] (**Figure 4.2**) the initial IR spectra show one stretch for the benzene compound **67a**, 2068 cm^{-1}, and naphthalene compound **67b**, 2051 cm^{-1}, which come from the asymmetric stretching modes of the bridging ligands. The anthracene compound **67c** is again different with two stretches at 2045 and 2031 cm^{-1}, which is likely due to the presence of multiple conformers.[198]

Table 4.6: Summary of IR spectroelectrochemical data (from 0.1 M NBu$_4$PF$_6$/CH$_2$Cl$_2$ solutions) for various bimetallic ruthenium acetylides. 0 = neutral state, +1 = oxidised state

Spacer group	νC≡C (cm^{-1}) n = 0	νC≡C (cm^{-1}) n = 1	ΔνC≡C (cm^{-1})
67a 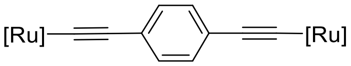 169	2068	1974	-94
67b 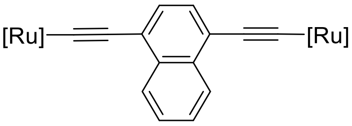 169	2051	1963	-88
67c 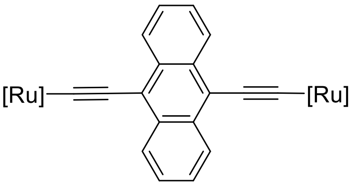 169	2045 (2031)	1954	-91
48 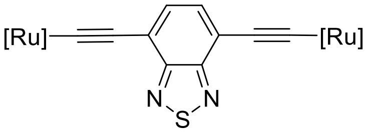 	2039	1978	-61

[Ru] = Ru(dppe)Cp*. [169] = Fox *et al.*

Upon one-electron oxidation, these band envelopes shift to lower wavenumbers due to the removal of electron density from the alkyne π-system. The complex band envelopes have been analysed in detail and shown to arise from a mixture of conformers in solution, which differ in the relative orientations of the metal fragments and plane of the bridging arylene fragment. These different orientations result in differing degrees of d-π-d orbital overlap along the molecular backbone leading in turn to conformers offering electronic character from strongly localised to strongly delocalised electronic structures.[198]

The IR SEC spectra for the bimetallic benzothiadiazole compound **48** (**Figure 4.16B**) shows the growth of a ν(C=C) band at 1978 cm^{-1} with only a modest decrease in the intensity of the ν(C≡C) band at 2039 cm^{-1} ; these changes correlate with the growth of the dπ-dπ NIR band (**Figure 4.16A**). The two-band pattern is quite characteristic of a strongly localised mixed-valence complex, such as the 1,3-substituted bimetallic benzene, $[\{Ru(dppe)Cp^*\}_2(\mu\text{-}C{\equiv}C\text{-}C_6H_4\text{-}3\text{-}C{\equiv}C)]$.[193]

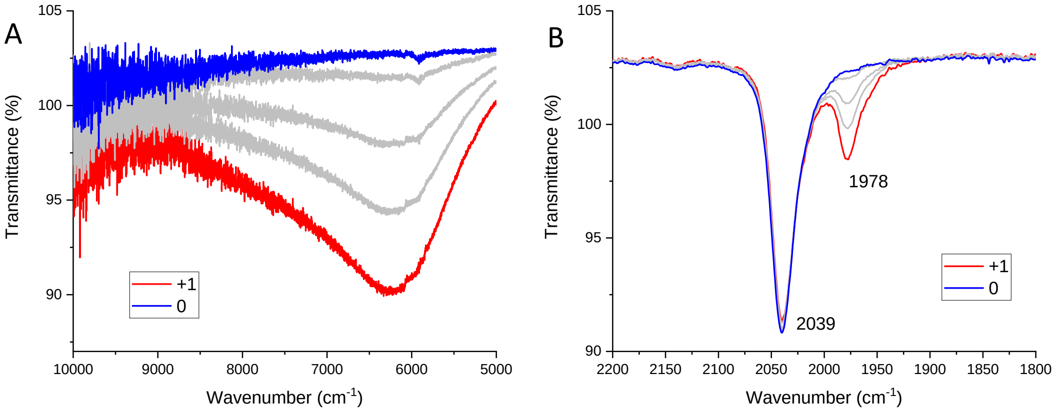

Figure 4.16: Plot of the normalised IR spectroelectrochemical results (from 0.1 M NBu_4PF_6/ CH_2Cl_2 solutions) for compound 48^{n+} (n= 0, 1). A) between 10,000 – 5000 cm^{-1} B) between 2200 – 1800 cm^{-1}. 0 = neutral state, +1 = oxidised state

By looking at both the UV-vis-NIR and IR SEC spectra for compound **48** we can see that there is little to no communication between the two metal centres when this compound is oxidised. This is because there is no change in the UV-vis-NIR band at 17 271 cm^{-1} nor the loss of the IR stretch at 2039 cm^{-1}. Meaning that at least one alkyne group is still present in the 1^+ species as well as the thiadiazole fragment being unaffected. A complete lack of communication between metal groups in bimetallic aryl bridged compounds is highly unusual, as normally complete or partial communication is observed.[169] Other compounds which have been shown to have little communication between metal centre are ruthenium carborane compounds,[199] with either $C_2B_{10}H_{11}$ (**Figure 4.17**) or $C_2B_8H_8$ carboranes as spacer groups, these also showed a persistence of a ν(C≡C) stretch at ca. 2100 cm^{-1} although no persistent UV-vis-NIR bands were observed.

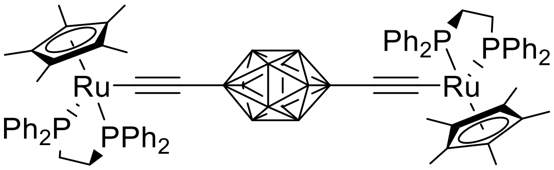

Figure 4.17: Structure of [{Ru(dppe)Cp*}$_2${μ-1,12−(C≡C)$_2$−1,12-$C_2B_{10}H_{10}$}], a compound with no metal-metal communication[199]

4.7 Summary

The benzene **18** (**Figure 4.9 and Figure 4.13**) and naphthalene **40** (**Figure 4.10 and Figure 4.14**) spacer groups show UV and IR SEC spectra which are unsurprising for ruthenium species, and have lots of similarities to each other and to similar literature compounds[186] which further shows that the change in the spacer group from benzene to naphthalene does not make much difference to the electrochemical activity of these complexes.

The use of benzothiadiazole **51**, however, formed a compound that was not stable in the SEC cell, this was shown by the loss of the vinylidene band at 1907 cm^{-1} before the compound was fully oxidised. This could also explain the lack of a clear MLCT band in the UV-vis-NIR spectrum. Compound **48** is unusual for a bimetallic compound as the IR SEC shows that there is no communication between the two metal fragments, which is rare. This is known as there is no loss of the acetylide stretch at 2039 cm^{-1} while there was also the growth of the expected stretch for the oxidised complex at 1978 cm^{-1}.

4.8 Solvatochromic compounds

Solvatochromism is the phenomenon in which the absorption maxima of a compound are affected by the nature of the solvent, which usually results in a colour change if the visible region is affected. The main reason for this effect is the change of relative energy between the ground and the excited state. Based on the chosen solvent and its interaction with the analyte, either a stabilization of predominantly the ground state or the excited occurs, which increases or decreases the energy difference, respectively.[200] The most important of these solvent effects are the polarizability or dipolarity of a solvent and its electron donating or withdrawing properties. The exact reason that solvatochromism occurs is not fully known, despite its widespread use, but is likely to be different for every system. This difference can be used to determine how a molecule is generally interacting with a solvent and therefore the nature of intermolecular interactions that may affect a compounds reactivity.

It is believed there is a change in the charge distribution across the molecule due to different solvent-solute interactions leading to a change in dipole moment, however, computational studies of solvatochromism has proven to be complicated.[201] These measurement are based on solvent properties of defined by Kamlet and Taft[202–206] from measurements of 4-nitroaniline, *N*-*N*-diethyl-4-nitroaniline, 4-nitrophenol and 4-nitrobenzene. Another set of properties was defined by Catalan[207,208] from measurements of 2-fluoro-7-nitrofluorene (FNF) and 2-(dimethylamino)-7-nitrofluorene (DMANF) (**Figure 4.18**).

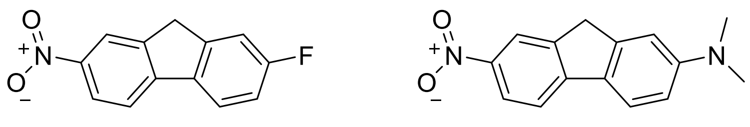

68 **69**

Figure 4.18: Structure of FNF, 68 and DMANF, 69

4.9 Ru(C≡CC$_6$H$_2$(NSN)-4-C≡C(CH$_3$)$_2$OH)(dppe)Cp*

Both benzothiadiazole complexes (**51** and **48**) exhibited a noticeable solvatochromic effect. Both complexes were blue when dissolved in DCM or methanol, and visibly purple when in hexane solution. Therefore, a comprehensive study of the solvent-dependence of the UV/Vis spectra of the monometallic benzothiadiazole **51** was carried out. Bimetallic **48** showed almost identical absorption maxima in both DCM and hexane, wherefore similar properties were assumed and thus not investigated in detail. The visible band is due to MLCT event as described in **Section 4.6.2.3**.

The absorption maxima of **51** in 30 different solvents are summarized in Table 4.7.

Table 4.7: Maximum wavelength of compound 51 in the visible region

Solvent	λ_{max} / nm	Solvent	λ_{max} / nm
Triethylamine	554	Anisole	571
Hexane	554	Methanol	572
Pentane	555	2-Propanol	573
1,4-Dioxane	557	Ethanol	573
Cyclohexane	559	*N,N*-Dimethylacetamide	573
Ethyl acetate	561	*N,N*-Dimethylformamide	575
Mesitylene	561	Hexanol	575
Toluene	561	DCM	576
Ethyleneglycol	563	Fluorobenzene	576
Dimethoxyethane	564	1-Butanol	577
Benzene	567	1,2-Dichloroethane	577
Tetrahydrofuran	567	Dimethylsulfoxide	578
Acetonitrile	569	Benzonitrile	580
Diethylether	569	Chloroform	581
Acetone	569	Nitrobenzene	587

The highest energy absorbance was recorded for triethylamine at 553 nm (18083 cm^{-1}) and the lowest for nitrobenzene at 587 nm (17036 cm^{-1}), with the difference between them being 34 nm (1047 cm^{-1}). Spectra of **51** in selected solvents are shown in **Figure 4.19** and the colour of **51** in NEt$_3$ and nitrobenzene (**Photo 4.1**). In the UV region of the spectra the most intense band appeared at around 30769 cm^{-1} (325 nm), with the lowest observable band occurring at 31153 cm^{-1} (321 nm) for pentane and the highest at 30395 cm^{-1} (329 nm) for DCM with a difference of 758 cm^{-1}.

Although for some solvents this region was not observable due to the properties of the solvents. For this reason, along with the even smaller difference in wavelength between solvents further analysis is not carried out using the absorption in the UV region.

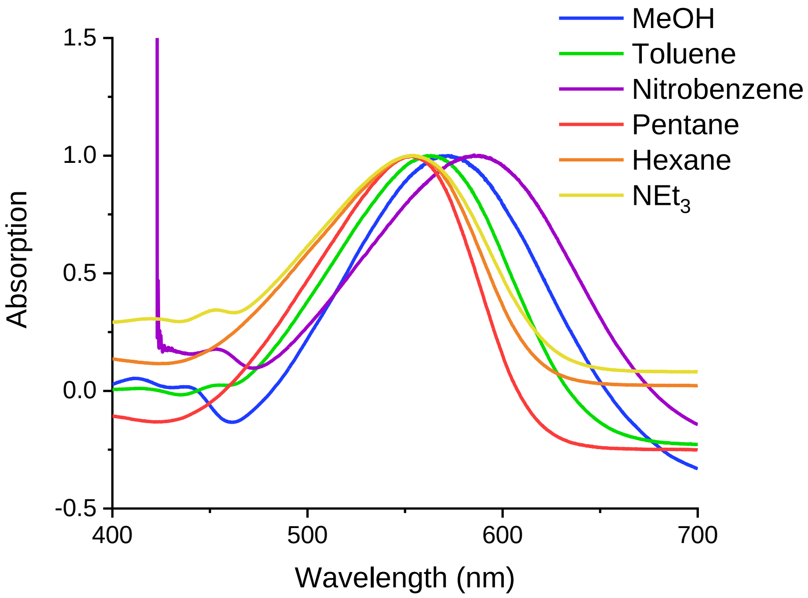

Figure 4.19: Selection of spectra showing the solvatochromic shift of compound 51, the absorbance in the visible region normalised so λ_{max} = 1

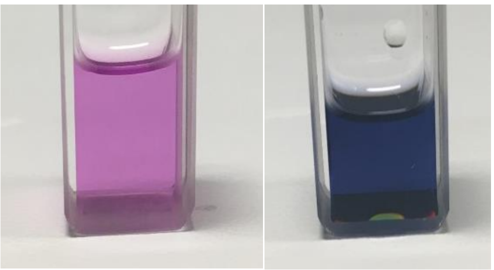

Photo 4.1: Colour of compound 51 dissolved in NEt_3, left, and Nitrobenzene, right

Based on linear regression analysis with known parameters of the used solvents, the most likely interaction effect, and hence cause of the solvatochromic effect, can be determined. The parameters established by Kamlet and Taft[202–206] are: hydrogen-bonding donor capacity (α); hydrogen-bonding acceptor capacity (β) and dipolarity/polarizability (π*). The scale of Catalan[207,208] uses four parameters, which are: acidity (SA); basicity (SB); polarizability (SP) and dipolarity (SdP). Results are summarized in **Table 4.8**.

Table 4.8: Absorption maxima of compound 51 in different solvents together with solvent parameters reported by Kamlet-Taft[202–206] and Catalan[207,208]

Solvent	ν_{max} / cm^{-1}	α	β	π*	SA	SB	SP	SdP
Chloroform	17217	0.20	0.10	0.58	0.047	0.071	0.783	0.614
Diethylether	17567	0.00	0.47	0.27	0.000	0.562	0.617	0.385
Ethylacetate	17840	0.00	0.45	0.55	0.000	0.542	0.656	0.603
Acetone	17567	0.08	0.43	0.71	0.000	0.475	0.651	0.907
Toluene	17811	0.00	0.11	0.54	0.000	0.128	0.782	0.284
Ethanol	17456	0.86	0.75	0.54	0.400	0.658	0.633	0.783
Acetonitrile	17580	0.19	0.40	0.75	0.044	0.286	0.645	0.974
DMF[b)]	17383	0.00	0.69	0.88	0.031	0.613	0.759	0.977
1,4-Dioxane	17931	0.00	0.37	0.55	0.000	0.444	0.737	0.312
Methanol	17493	0.98	0.66	0.60	0.605	0.545	0.608	0.904
1-Butanol	17347	0.84	0.84	0.47	0.341	0.809	0.674	0.655
Benzene	17645	0.00	0.10	0.59	0.000	0.124	0.793	0.270
1,2-Dichloroethane	17338	0.00	0.10	0.81	0.030	0.126	0.771	0.742
Ethyleneglycol	17772	0.90	0.52	0.92	0.717	0.534	0.777	0.910
Tetrahydrofuran	17645	0.00	0.55	0.58	0.000	0.591	0.714	0.634
Dimethyl sulfoxide	17312	0.00	0.76	1.00	0.072	0.647	0.830	1.000
2-Propanol	17465	0.76	0.84	0.48	0.283	0.830	0.633	0.808
Benzo nitrile	17248	0.00	0.37	0.90	0.047	0.281	0.851	0.852
Nitrobenzene	17028	0.00	0.39	1.01	0.056	0.240	0.891	0.873
Fluorobenzene	17361	0.00	0.07	0.62	0.000	0.113	0.761	0.511
Mesitylene	17821	0.00	0.13	0.41	0.000	0.190	0.775	0.155
Anisole	17581	0.00	0.32	0.73	0.084	0.299	0.82	0.543
1,2-Dimethoxyethane	17739	0.00	0.41	0.53	0.000	0.636	0.68	0.625
1-Hexanol	17383	0.80	0.84	0.40	0.315	0.879	0.698	0.552
DMA[c)]	17447	0.00	0.76	0.88	0.028	0.650	0.763	0.987
Dichloromethane	17365	0.13	0.10	0.82	0.040	0.178	0.761	0.769
Hexane	18033	0.00	0.00	–0.04	0.000	0.056	0.616	0.000
Cyclohexane	17907	0.00	0.00	0.00	0.000	0.073	0.683	0.000
Triethylamine	18057	0.00	0.71	0.14	0.000	0.885	0.660	0.108
Water	n.s.[a)]	1.17	0.47	1.09	1.062	0.000	0.681	0.997

α = hydrogen-bonding donor capacity; β = hydrogen-bonding acceptor capacity; π* = dipolarity/polarizability; SA = acidity; SB = basicity; SP = polarizabiliy; SdP = dipolarity; a) not soluble in the respective solvent. b) *N,N*-dimethylformamide; c) *N,N*-dimethylacetamide.

Both sets of solvent parameters are used as they contain slightly different parameters that have been calculated in different ways (**Table 4.9**), only 29 of the 30 solvents were used in this analysis because compound **51** was not soluble in water. For this the wavelengths were converted into wavenumbers, this conversion is because wavelength is not linear with energy.

Table 4.9: Results of a Multi-Factor Correlation for solvent parameters of compound 51

Kamlet-Taft		Catalán	
R	0.688	R	0.772
R^2	0.474	R^2	0.596
Adjusted R^2	0.410	Adjusted R^2	0.528
Used solvents	29	Used solvents	29
Significance F	0.000964	Significance F	0.000155
$\nu_{max,0}$ / cm^{-1}	17966 (± 100)	$\nu_{max,0}$ / cm^{-1}	18551 (± 328)
α	–146 (± 130)	SA	87 (± 206)
β	15 (± 165)	SB	73 (± 150)
π*	–643 (± 143)	SP	–925 (± 513)
		SdP	–586 (± 132)

α = hydrogen-bonding donor capacity; β = hydrogen-bonding acceptor capacity; π* = dipolarity/polarizability; SA = acidity; SB = basicity; SP = polarizability; SdP = dipolarity

Although the correlation with both scales shows relatively low R values (0.688 for Kamlet-Taft and 0.772 for Catalán) and high standard error, the π* and SP/SdP parameters, representing the dipolarity of the solvents, is clearly the dominating effect. The SdP parameter has a P-value of 0.00018 (any value less than 0.05 can be said to be statistically significant as it means that there is a good correlation in the data). The Kamlet-Taft scale also has large standard error on the parameters, although dipolarity/polarizability (π*) parameter shows good correlation. The negative signs for the SdP and π* represent a positive solvatochromism, which results in a bathochromic shift for solvents with higher dipolarity.

Using the Kamlet-Taft parameters the hydrogen bond donor properties, α, of the solvent are very slightly bathochromic towards compound **51**, because it has a negative value, however due to the very large standard error in relation to the value this is unlikely to contribute much to the overall colour change. In contrast, the analogous data from Catalán shows that the acidity of the solvent has a bathochromic effect on the colour but because the parameter number is close to zero and the standard error is bigger than that value it is not statistically significant (P-value = 0.67748).

Both the hydrogen bond acceptor properties and the basicity (β/SB) indicate a hypsochromic shift, however, these numbers are small with large standard errors and P-values (β = 0.928905 and SB = 0.632943) which indicates that this data are essentially random meaning these properties must not be contributing much to the change in colour. The numbers for the acidity and basicity work together meaning that for compound **51**, solvents that are more acidic and therefore less basic, stabilize the excited state and result in a bathocromic shift.

The main contribution to the solvatochromism in compound **51** is due to the polarizability and dipolarity of the solvent. A more polar solvent, such as nitrobenzene (SP = 0.873, π* = 1.01), therefore has a positive solvatochromic effect, making the wavelength of light absorbed higher which is observed with the highest wavelength at 587 nm, and triethyl amine with an SP of 0.660 (and π* of 0.14) and the lowest wavelength of 554 nm. The analysis reveals that the absorption properties of **51** are neither dominated by hydrogen bonds towards the imine nitrogens of the BTD, nor towards the OH group, which could have been expected.

4.10 RuCl(C≡C-9-$C_{14}H_8$-10-C≡CSiMe_3)$(dppe)_2$

Another compound for which a solvatochromic behaviour was visibly observed was RuCl(C≡C$C_{14}H_8$-10-C≡CSiMe_3)$(dppe)_2$, **65** (**Figure 4.20**). The compound was orange when dissolved in hexane and pink when dissolved in DCM. Thus, a comprehensive study of the solvent-dependence of the UV/Vis spectra of compound **65** was carried out.

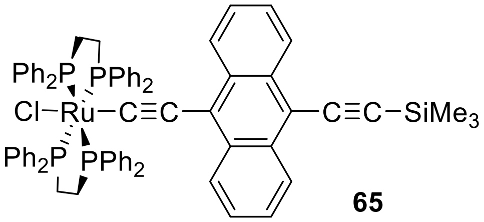

65

Figure 4.20: Structure of RuCl(C≡C$C_{14}H_8$-10-C≡CSiMe_3)$(dppe)_2$, compound 65

Table 4.10: Maximum wavelength in the visible region for compound 65 in multiple solvents

Solvent	λ_{max} / nm	Solvent	λ_{max} / nm
Methanol	484	Acetone	528
2-Propanol	486	DCM	530
Ethanol	492	Flourobenzene	530
1-Butanol	508	Tetrahydrofuran	530
Pentane	520	Benzene	532
1-Hexanol	522	1,4-Dioxane	532
Diethylether	524	Mesitylene	532
Dimethyl sulfoxide	524	Toluene	532
Hexane	524	*N,N*-Dimethylacetamide	534
Acetonitrile	526	*N,N*-Dimethylformamide	534
Cyclohexane	526	Nitrobenzene	534
Triethylamine	526	Benzo nitrile	534
Ethyl acetate	526	Anisole	534
Dimethoxyethane	528	1,2-Dichloroethane	542
Chloroform	528		

The absorption maxima in 29 different solvents (**Table 4.10**) show the lowest wavenumber for dichloroethane at 18416 cm^{-1} (543 nm) and the highest at 20661 cm^{-1} (484 nm) when dissolved in methanol. Notably five of the six solvents with the highest wavenumber are alcohols, meaning that the colour may be influenced by the presence of hydrogen bonds. The solvatochromic shift of 2245 cm^{-1} is significantly larger compared to the solvatochromic shift for compound **51** (1047 cm^{-1}, **Section 4.7**). Spectra in selected solvents are displayed in **Figure 4.21** and the colour of **65** in butanol and toluene in **Photo 4.2**. In similarity to compound **48**, absorptions in the UV region overlap with those of solvents, which makes their assignment unreliable and where therefore not analysed further.

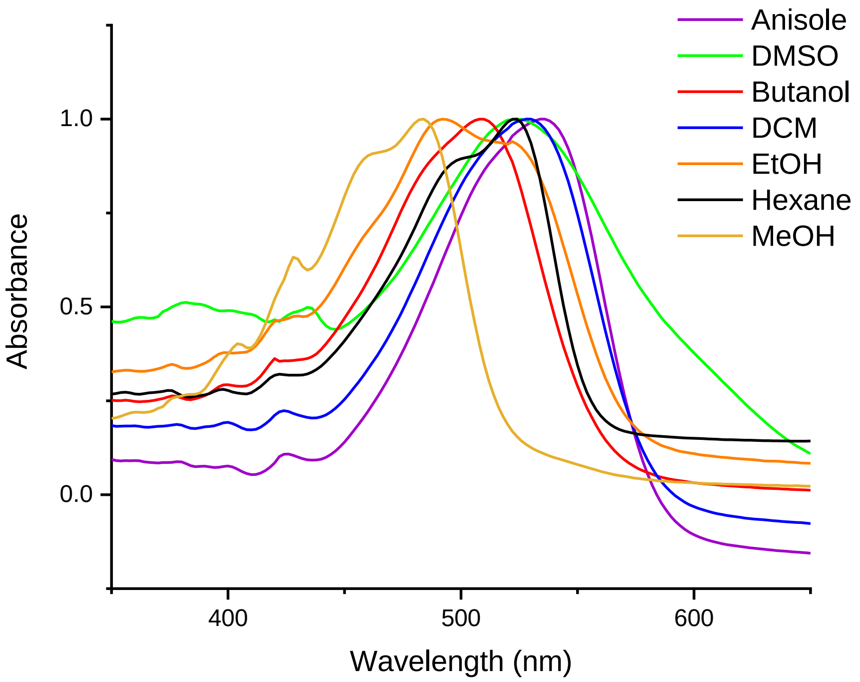

Figure 4.21: Selection of spectra showing the solvatochromic shift of RuCl($C{\equiv}CC_{14}H_8$-10-$C{\equiv}CSiMe_3$)(dppe)$_2$, the absorbance in the visible region normalised so λmax = 1

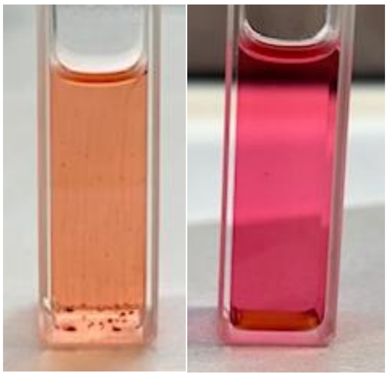

Photo 4.2: Colour of compound 65 dissolved in BuOH, left, and toluene, right

Notably, there appears to be overlapping bands in the visible region for most solvents, although some are very broad. However, in some of the solvents, e.g. ethanol and methanol, compound **65** prominently displays more than one sharp absorption maximum. Although only the most intense λ_{max} was selected for the regression analysis below, the occurrence of multiple absorption indicates a more complex interaction pattern and may cause uncertainties. The effect is not specific for OH functionalities. In other alcohols, such as hexanol, compound **65** only showed one absorption maxima (**Figure 4.21**). Three additional solvents show the same spectral profile as hexane; cyclohexane, mesitylene and triethylamine, however, there is no obvious correlation between these solvents and their properties.

A regression analysis (**Table 4.12**) was carried out using the data obtained from the UV-Vis data and two different sets of solvent property data compiled by Kamlet-Taft[202–206] and Catalan[207,208] (**Table 4.11**). Again, these data were converted from wavelengths into wavenumbers.

Table 4.11: Absorption maxima of compound 65 in different solvents together with solvent parameters reported by Kamlet-Taft[202–206] and Catalan[207,208]

Solvent	ν_{max} / cm^{-1}	α	β	π*	SA	SB	SP	SdP
Chloroform	18939	0.20	0.10	0.58	0.047	0.071	0.783	0.614
Diethylether	19084	0.00	0.47	0.27	0.000	0.562	0.617	0.385
Ethyl acetate	19011	0.00	0.45	0.55	0.000	0.542	0.656	0.603
Acetone	18939	0.08	0.43	0.71	0.000	0.475	0.651	0.907
Toluene	18797	0.00	0.11	0.54	0.000	0.128	0.782	0.284
Ethanol	20325	0.86	0.75	0.54	0.400	0.658	0.633	0.783
Acetonitrile	19011	0.19	0.40	0.75	0.044	0.286	0.645	0.974
DMF d)	18727	0.00	0.69	0.88	0.031	0.613	0.759	0.977
1,4-Dioxane	18797	0.00	0.37	0.55	0.000	0.444	0.737	0.312
Methanol	20661	0.98	0.66	0.60	0.605	0.545	0.608	0.904
1-Butanol	19685	0.84	0.84	0.47	0.341	0.809	0.674	0.655
Benzene	18797	0.00	0.10	0.59	0.000	0.124	0.793	0.270
1,2-Dichloroethane	18450 b)	0.00	0.10	0.81	0.030	0.126	0.771	0.742
Ethylene glycol	n.s. c)	0.90	0.52	0.92	0.717	0.534	0.777	0.910
Tetrahydrofuran	18868	0.00	0.55	0.58	0.000	0.591	0.714	0.634
Dimethyl sulfoxide	19084	0.00	0.76	1.00	0.072	0.647	0.83	1.000
2-Propanol	20576	0.76	0.84	0.48	0.283	0.830	0.633	0.808
Benzo nitrile	18727	0.00	0.37	0.90	0.047	0.281	0.851	0.852
Nitrobenzene	18727	0.00	0.39	1.01	0.056	0.240	0.891	0.873
Fluorobenzene	18868	0.00	0.07	0.62	0.000	0.113	0.761	0.511
Mesitylene	18797	0.00	0.13	0.41	0.000	0.190	0.775	0.155
Anisole	18727	0.00	0.32	0.73	0.084	0.299	0.82	0.543
1,2-Dimethoxyethane	18939	0.00	0.41	0.53	0.000	0.636	0.68	0.625
1-Hexanol	19157	0.80	0.84	0.40	0.315	0.879	0.698	0.552
DMA e)	18727	0.00	0.76	0.88	0.028	0.650	0.763	0.987
Dichloromethane	18868	0.13	0.10	0.82	0.040	0.178	0.761	0.769
Hexane	19084	0.00	0.00	–0.04	0.000	0.056	0.616	0.000
Cyclohexane	19011	0.00	0.00	0.00	0.000	0.073	0.683	0.000
Triethylamine	19011	0.00	0.71	0.14	0.000	0.885	0.660	0.108
Water	n.s. c)	1.17	0.47	1.09	1.062	0.000	0.681	0.997

a) α = hydrogen-bonding donor capacity; β = hydrogen-bonding acceptor capacity; π* = dipolarity/polarizability; SA = acidity; SB = basicity; SP = polarizability; SdP = dipolarity; b) not the major band but the most reasonable; c) not soluble in the respective solvent, d) *N*,*N*-dimethylformamide; e) *N,N*-dimethylacetamide.

Table 4.12: Results of a Multi-Factor Correlation for solvent parameters of compound 65

Kamlet-Taft		**Catalán**	
R	0.878	R	0.939
R^2	0.772	R^2	0.881
Adjusted R^2	0.743	Adjusted R^2	0.860
Used solvents	28	Used solvents	28
Significance F	7.23 x10^{-8}	Significance F	2.63 x10^{-10}
$\nu_{max,0}$ / cm^{-1}	18954 (± 142)	$\nu_{max,0}$ / cm^{-1}	20271 (± 465)
α	1347 (± 207)	SA	2950 (± 326)
β	176 (± 240)	SB	94 (± 174)
π*	–301 (± 212)	SP	–1944 (± 629)
		SdP	–97 (± 155)

α = hydrogen-bonding donor capacity; β = hydrogen-bonding acceptor capacity; π* = dipolarity/polarizability; SA = acidity; SB = basicity; SP = polarizability; SdP = dipolarity

For compound **65** the correlation towards the Kamlet-Taft scale, with an R value of 0.878, as well as the Catalán scale, R = 0.939, both indicate a good, valid fit. The most significant parameter for compound **65** is the acidity of the solvent.

The removal of the alcohols from the regression analysis (**Table 4.13**), as it appeared that the presence of the OH group has a large impact on the solvatochromism of compound **65**. This analysis showed a reduction in the R value for both scales, indicating a reduction in the fit of the data. However, is also showed similar numbers for the values of each of the parameters with smaller significant errors. This shows that although it appears that the presence of alcohols in the analysis could be skewing the results, the removal of them does not affect the conclusions from this analysis.

Table 4.13: Results of a Multi-Factor Correlation for solvent parameters of compound 65, without alcohols

Kamlet-Taft		Catalán	
R	0.740	R	0.689
R^2	0.548	R^2	0.474
Adjusted R^2	0.477	Adjusted R^2	0.358
Used solvents	23	Used solvents	23
Significance F	0.0161	Significance F	0.00146
$\nu_{max,0}$ / cm^{-1}	18986 (± 57)	$\nu_{max,0}$ / cm^{-1}	19961 (± 340)
α	1067 (± 407)	SA	2289 (± 1484)
β	295 (± 108)	SB	100 (± 125)
π^*	–408 (± 91)	SP	–1479 (± 463)
		SdP	–144 (± 111)

α = hydrogen-bonding donor capacity; β = hydrogen-bonding acceptor capacity; π^* = dipolarity/polarizability; SA = acidity; SB = basicity; SP = polarizability; SdP = dipolarity

The positive signs for α and SA indicate that a hypsochromic shift for solvents with a higher hydrogen bond donor capacity should occur. The correlation for this dependency is better using the Catalán scale, although both α and SA show large correlations with significantly smaller standard errors (P-value α = 9.9 x10^{-7}, SA = 4.9 x10^{-9}). For the basicity parameters, P-values of β = 0.47006 and SB = 0.5957 were calculated, showing that the respective parameters are not significant and are therefore not taken into consideration.

In contrast according to the Catalán scale the increase in polarizability of a solvent causes a positive, bathochromic shift. According to the Kalmet-Taft scale the combined polarizability and dipolarity is also bathochromic overall, although the standard error is a large percentage of the parameter value, the P-value is also high with a value of 0.16895 meaning that the significance of this statistical data is questionable.

Both the acidity (α/SA) and the polarizability (SP) have a large effect on the stability of the excited state of compound **65**. The hydrogen bond donor interaction is likely to be with the chloride ligand, due to its high electronegativity, rather than the TMS group at the other end of the compound. A red, bathochromic shift is experienced in solvents that are more polar but less acidic with an overall solvatochromic shift of 1935 cm^{-1}. The dipolarity and basicity have less effect on the colour of the compound.

4.11 Summary

Despite the structural similarities between compounds **51** and **65** the interactions with solvents that cause a solvatochromic shift are influenced mainly by different physical properties of the solvents, the polarizability and dipolarity for compound **51** and the acidity of the solvent for compound **65**. The overall solvatochromic shift is larger for compound **65**, and the removal of the alcohol parameters had no effect on the outcome, than for compound **51** as well as a more highly correlated shift.

Chapter 5 Conclusions and Future Work

1.4 Conclusions

This work has demonstrated that multiple aromatic groups can be used as spacer groups in reactions where quinoidal cumulene ligands can be invoked. Although the cumulenic intermediate has not been isolated, or even observed through spectroscopic methods, more reactions with both nucleophiles and electrophiles have been observed that are likely to occur *via* a cumulene intermediate. The presence of the cumulene has been inferred through the products of these trapping reactions that have been observed and characterised.

The use of a simple benzene as a spacer group in the vinylidene compound *trans*-[RuCl(=C=C=C_6H_4-4-C≡CH)(dppe)$_2$], **2**, showed predictable Markovnikov addition reactions with multiple nucleophiles, including halide ions, water and the non-basic nucleophile *N*-methylpyrrole (**Scheme 2.22**). The presence of acid in these reactions was required for the reaction to proceed and the formation of these products is consistent with the reaction of nucleophilic reagents with the putative quinoidal cumulene complex *trans*-[RuCl(=C=C=C_6H_4=C=CH_2)(dppe)$_2$]. However, the addition of electrophiles (CN^+, $C_7H_7^+$ and CPh_3^+) to the representative acetylide complex *trans*-[RuCl(C≡CHC_6H_4-4-C≡CH)(dppe)$_2$], **13**, did not occur in the expected manner, the exception to this was H^+ which returned the acetylide to the vinylidene form. Because the reactions of nucleophiles occur at the 7th carbon in the chain, the same as reported by Eaves *et al*.[144] it can be inferred that the intermediate in these reactions is a cumulene intermediate and increases the evidence for this.

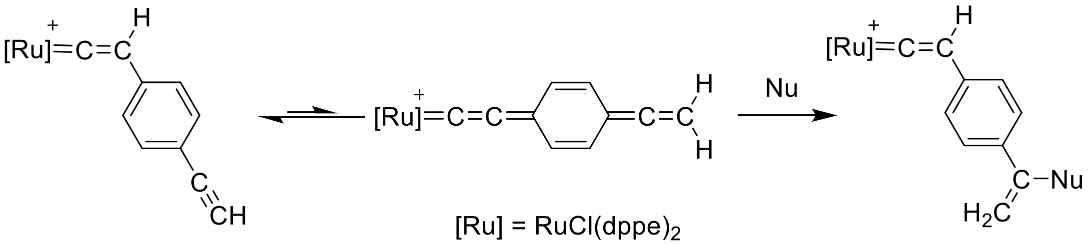

Scheme 5.1: Addition of nucleophiles to ruthenium vinylidenes through a cumulene intermediate

The use of half-sandwich metal groups with a benzene spacer group has been explored previously[152] which lead to the $[Ru(dppe)Cp^*]^+$ fragment being utilised for further electrophile addition reactions. This led to further evidence for the extended cumulene intermediate in the reaction of electrophiles (H^+, CN^+ and $C_7H_7^+$) with acetylide complexes which contained sterically bulky terminal groups, $Ru(C{\equiv}CC_6H_4\text{-}4\text{-}C{\equiv}CR)(dppe)Cp^*$ (R = $(CH_3)_2OH$ [**18**], C_6H_4-4-OMe [**25**], C_6H_4-4-CO_2Me [**26**]) (**Scheme 2.23**). However rather than stabilising the cumulene intermediate formed from the addition of CPh_3^+ at the eighth carbon in the chain (as seen for the literature terminal alkyne species)[152] and preventing the subsequent water addition, these bulky terminal groups blocked the addition completely and instead the residual acid from the synthesis of $[CPh_3][BF_4]$ meant that the proteo-vinylidene was formed. This tells us that we need smaller terminal groups or terminal groups that are easily lost during reaction in order to exploit this chemistry.

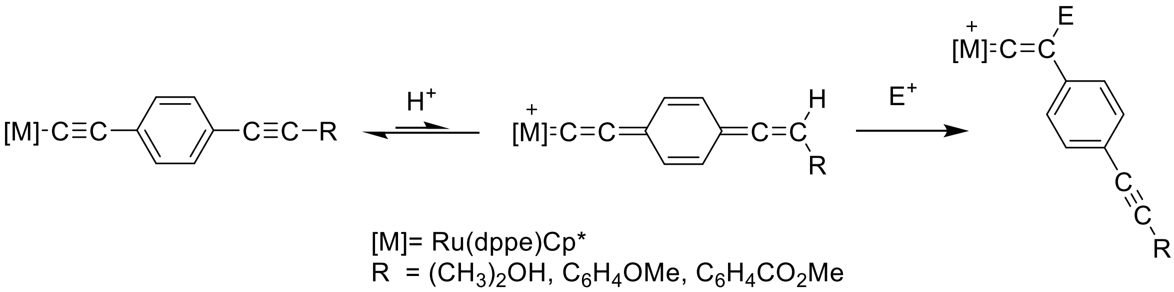

Scheme 5.2: Addition of small electrophiles to substituted terminal alkynes through a cumulene intermediate

The synthesis of monometallic diethynyl naphthalene and benzothiadiazole compounds proved to be complicated, with existing methods using TMS-diethynylaryl complexes reacting with RuCl(dppe)Cp* with KF only forming bimetallic compounds. Attempts to remove the $(CH_3)_2OH$ protecting group from Ru(C≡C-Ar-C≡C$(CH_3)_2$OH)(dppe)Cp* (Ar = $C_{10}H_6$ [**40**], C_6H_2(NSN) [**54**]) were not successful despite this being possible for the benzene analogue. The monometallic compounds Ru(C≡CAr-C≡C$SiMe_3$)(dppe)Cp* (Ar = $C_{10}H_6$ [**36**], C_6H_2(NSN) [**54**]) were eventually synthesised through selective lithiation of diethynyl(trimethyl)aryl and addition to $[Ru(dppe)Cp^*]^+$, this same technique could also be used in the synthesis of RuCl(C≡CAr-C≡C$SiMe_3$)$(dppe)_2$ (Ar = $C_{10}H_6$ [**42**], C_6H_2(NSN) [**53**], $C_{12}H_8$ [**65**]) (**Scheme 5.3**). The difficulty in the synthesis of these monometallic complexes is due to their increased solubility in polar solvents, compared to other acetylide compounds, and an increase in reactivity which accompanies the change in aromatic group and therefore aromatic stabilisation energy.

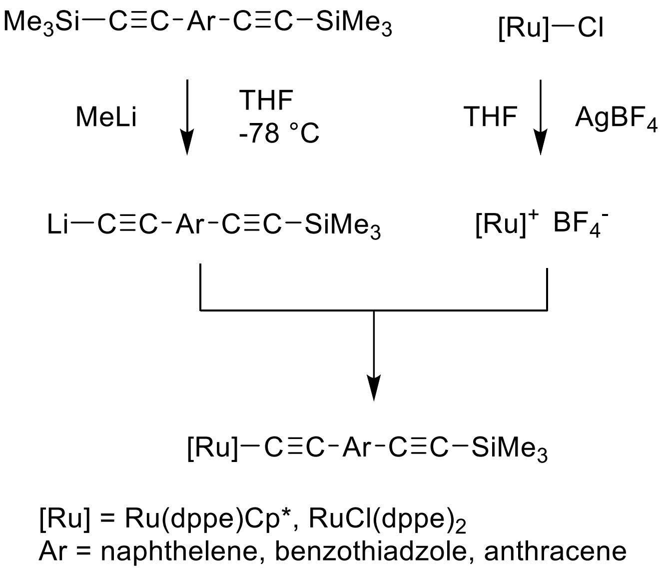

Scheme 5.3: Synthesis of monometallic ruthenium compounds through selective lithiation

By changing the spacer group from benzene to naphthalene or benzothiadiazole did not affect the reactivity of the Ru(C≡C$C_{10}H_8$-4-C≡C$SiMe_3$)(dppe)Cp*, **36**, or Ru(C≡CC_6H_2(NSN)-4-C≡C$SiMe_3$)(dppe)Cp*, **54**, with the small electrophiles H^+ and

$C_7H_7^+$ which formed the expected addition at β carbon forming vinylidenes. The reaction with CN^+ did not occur, although this is likely due to non-ideal reaction conditions being used. The addition of CPh_3^+ occurred at the terminal, eighth carbon and the presence of larger spacer group stopped the secondary addition of water as seen with benzene.[152] However, the high reactivity of the cumulene intermediate led to immediate intramolecular cyclisation between one of the phenyl groups from CPh_3 and the seventh carbon in the chain. This shows that the cumulene, or other, intermediate is highly reactive and can form interesting functional groups.

The synthesis of $Ru(C{\equiv}CC_{12}H_8\text{-}10\text{-}C{\equiv}CSiMe_3)(dppe)Cp^*$, **60**, turned out to be possible using the simple 'KF' reaction method as this acetylide proved to be completely insoluble in methanol which stopped the formation of bimetallic compounds. The addition of all electrophiles, (H^+, CN^+, $C_7H_7^+$ and CPh_3^+), to the compound with an anthracene spacer group, $Ru(C{\equiv}CH\text{-}C_{12}H_8\text{-}10\text{-}C{\equiv}CSiMe_3)(dppe)Cp^*$, **60**, showed a characteristic colour change which usually accompanies an acetylide to vinylidene transformation. However, many compounds were formed during these reactions were almost impossible to separate through traditional separation techniques. Although one compound $\{Ru(dppe)Cp^*\}_2(C{\equiv}CC_{14}H_8\text{-}10\text{-}C({=}CCPh_3))_2$, **62**, was isolated from the reaction with CPh_3^+. It is believed that the mechanism starts in a similar way to the addition of trityl to the naphthalene and benzothiadiazole analogues. However, instead of the internal cyclization of the cumulene intermediate which is seen for these compounds a radical dimerization occurs. This is probably due to steric hindrance for cyclization from the large anthracene spacer group and the presence of an excess for CPh_3^+ which is also known to act as a radical initiator.

The electrochemical and spectroelectrochemical properties of the three compounds $Ru(C{\equiv}C\text{-}Ar\text{-}C{\equiv}C(CH_3)_2OH)(dppe)Cp^*$ (Ar = C_6H_4 [**18**], $C_{10}H_6$ [**40**], $C_6H_2(NSN)$ [**54**]), were very similar to literature compounds[186] with similar structures. The spectroelectrochemical analysis of $\{Ru(dppe)Cp^*\}_2(\mu\text{-}C{\equiv}CC_6H_2(NSN)\text{-}4\text{-}C{\equiv}C)$, **48**, showed that there is no electrochemical communication between the two metal centres, which is unusual.

Overall, the switch of aromatic group did not stabilise the cumulene intermediate as desired, but made the compounds much more reactive, leading to the difficulties experienced in synthesising the monometallic compounds and purifying the products of reaction. However, these reactions provide further evidence that quinoidal cumulenes are intermediates in these reactions, as all reactivity of nucleophiles and electrophiles are in keeping with this theory. A summary of the addition of nucleophiles and electrophiles to cumulene intermediates can be seen in **Scheme 5.4**.

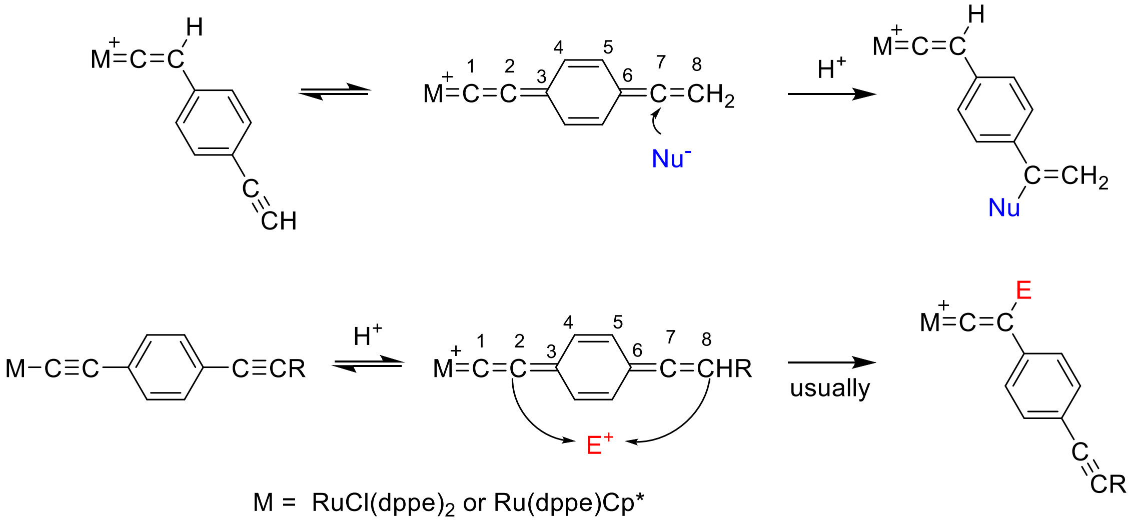

M = RuCl(dppe)$_2$ or Ru(dppe)Cp*
Ar= benzene, naphthalene, benzothiadiazole, anthracene
Nu= H_2O, N-Me pyrrole, halide
E = CPh_3, C_7H_7, CN, H
R = H, $SiMe_3$, $(CH_3)_2OH$, Ph-OMe, Ph-CO_2Me

Scheme 5.4: Summary of nucleophile and electrophile additions to cumulene intermediates

1.5 Future work

There is a lot more work to be done to prove that cumulenes are the intermediates in this reaction, through both experimental and computational studies. Both of the large terminal groups used to protect the distant alkyne had similar steric hinderance properties, switching this terminal group one which is smaller, for example an alkyl chain, could allow the reaction of CPh_3^+ to take place. It should also be possible to use other aromatic groups, including heteroaromatics, and these could be incorporated into the chain.

For the synthesis of RuCl(C≡CAr-4-C≡CSiMe$_3$)(dppe)$_2$ (Ar = $C_{10}H_6$ [**42**], C_6H_2(NSN) [**53**]) it may also be possible to use the 16 electron species [RuCl(dppe)$_2$][OTf] as the starting material in place of *cis*-RuCl$_2$(dppe)$_2$, which would form TMS-OTf as a by-product instead of TMS-Cl, along with LiCl. The low yields for these reactions may also be improved through a change in work-up procedure, as this may be where product is lost. A change of the solid phase in column chromatography from alumina to florisil (MgO_3Si) could increase the yield.

As the samples of Ru(C≡CAr-C≡CSiMe$_3$)(dppe)Cp* (Ar = $C_{10}H_6$ [**36**], C_6H_2(NSN) [**54**]) were not isolated as completely pure product: RuCl(dppe)Cp* was a frequent contaminant. Therefore, more work is required in order to purify these compounds or using a more effective halide abstractor, such as thallium salts or by using a different silver salt e.g. $AgSbF_6$.[209]

In order to understand the reactivity of compounds Ru(C≡CAr-C≡CSiMe$_3$)(dppe)Cp* (Ar = $C_{10}H_6$ [**36**], C_6H_2(NSN) [**54**]) with [CAP][BF$_4$], which show products with the desired *m/z* in the recorded mass spectra despite the ^{1}H and ^{31}P{^{1}H} NMR showing no reaction has taken place, these reactions need to be repeated in a more dilute reaction to aid with [CAP][BF$_4$] solvation, in a different solvent system such as methanol, or heating the reaction. It is believed that the CN^+ should react at the β carbon.

The electrochemical and spectroelectrochemical properties of Ru(C≡CAr-C≡CSiMe$_3$)(dppe)Cp* (Ar = $C_{10}H_6$ [**36**], C_6H_2(NSN) [**54**]) and RuCl(C≡CAr-C≡CSiMe$_3$)(dppe)$_2$ (Ar = $C_{10}H_6$ [**42**], C_6H_2(NSN) [**53**]) are currently unknown and could show interesting results, especially the benzothiadiazole compounds. The synthesis of other bimetallic acetylide benzothiadiazole compounds, using other metal fragments, for electrochemical analysis may also show no communication across the compound (**Compound 48**), especially as bimetallic vinyl benzothiadiazole compounds do show communication.[177] Although the focus on synthesis of compounds for molecular electronics has mainly focused on molecular wires,[140,210,211] 'valence-locked' compounds are of interest as they are unusual and further studies may provide insights to improve the synthesis of molecular wires, switches or as use themselves as resistors.

Chapter 6 Experimental

7.1 General Conditions

Solvents and Reagents

Commercially available reagents and solvents were purchased from Sigma-Aldrich, Alfa Aesar, Fisher Scientific, Acros Organics, VWR, Combi-Blocks or Fluorochem and used as received unless otherwise noted. Petrol refers to the fraction of petroleum ether boiling in the range 40-60 °C. Ether refers to diethylether.

Typical Conditions

Reactions requiring anhydrous conditions were carried out in oven-dried glassware under a nitrogen atmosphere. Room temperature (RT) refers to reactions where no thermostatic control was applied and was recorded as 16-23 °C. Where reaction temperature is reported as above room temperature, the temperature being measured is of the oil bath unless otherwise noted. Nitrogen gas was oxygen-free and dried immediately prior to use by passing through a column of potassium hydroxide pellets and silica.

Chromatography

Thin layer chromatography (TLC) analysis was carried out using Merck 5554 aluminium backed silica plates and visualised using UV light (254 nm). Prep-TLC plates were made in house using Silica containing Gypsum. All column chromatography was performed using Merck silica gel K60 (particle sizes 40 – 63 μm), Alumina or Florisil as stated in the text and a solvent system as stated in the text.

NMR spectroscopy

^{1}H, ^{13}C and ^{31}P NMR spectra were recorded on a Jeol ECS400 or Jeol ECX400 or Bruker AV400 spectrometer at 400, 101 and 162 MHz, respectively. Alternatively, and where specified, ^{1}H, ^{13}C and ^{31}P NMR spectra were recorded on a Bruker AV500 spectrometer at 500, 126 and 202 MHz, respectfully. Chemical shifts are reported in parts per million (ppm) and were referenced to residual undeuterated solvent (^{1}H: $CHCl_3$ – 7.26 ppm, ^{13}C: $CHCl_3$ 77.16 ppm, ^{1}H: CH_2Cl_2 – 5.32 ppm, ^{13}C: CH_2Cl_2 53.84 ppm) Coupling constants (*J*) have been quoted to the nearest 0.1 Hz. ^{1}H, ^{13}C and ^{31}P NMR chemical shifts are reported to 2 decimal places. Multiplicities are described as singlet (s), doublet (d), triplet (t), quartet (q), quintet (quin), multiplet (m), apparent (app) and broad (br.). Spectra were typically recorded at 298 K, unless otherwise specified. ^{13}C and ^{31}P spectra were obtained with ^{1}H decoupling. Spectra were processed using Bruker TopSpin 4.1.3.

Mass Spectrometry

Electrospray ionization (ESI) mass spectrometry was performed using a Bruker daltronics micrOTOF spectrometer or Waters Micromas LCT Spectrometer from chloroform or acetonitrile, with less than 5 ppm error for all HRMS.

Infrared Spectroscopy

IR spectroscopy was performed using a Bruker Alpha with an ATR attachment, or an Agilent Cary 630 FT-IR from samples in Nujol mounted between NaCl discs or ATR attachment. Absorption maxima (max) are reported in wavenumbers (cm^{-1}) to the nearest whole number and described as weak (w), medium (m), strong (s) or broad (br).

UV-Visible Spectroscopy

UV-visible spectroscopy was performed on a Jasco V-560 or Agilent Cary 60 spectrometer, with a background taken in the appropriate solvent prior to recording spectra, using a quartz cell with a path length of 1 cm. The wavelength of maximum absorption (λ_{max}) is reported in nm along with the molar absorption coefficient (ε) in mol dm^{-3} cm^{-1}.

Electrochemistry

Samples for the spectroelectrochemical study were prepared in a solution of dried DCM containing 0.1 M NBu_4PF_6 (recrystallised from ethanol) as a supporting electrolyte and sparged with N_2 prior to measurement. Spectroelectrochemical studies were conducted on Agilent Cary 5000 UV-vis-NIR and Agilent Carey 600 FTIR at room temperature in an OTTLE cell of Hartl design,[212] with an approximate path length of 150 µm and fitted with CaF_2 windows.

X-ray diffraction

Diffraction data in the University of York were collected at 110(2) K on a Bruker Smart Apex diffractometer with Mo-K_α radiation (λ = 0.71073 Å) or Cu-K_α radiation (λ = 1.54184 Å). Diffraction data in the University of Western Australia were collected at 150.00(10) K on a XtaLAB Synergy, single source at home/near, HyPix diffractometer with Cu-K_α radiation (λ = 1.54184 Å) or at 101(8) K on a Xcalibur, Ruby, Gemini ultra diffractometer with Mo-K_α radiation (λ = 0.71073 Å). In all cases the structures were solved with the ShelXT structure solution program using the Intrinsic Phasing solution method and by using Olex2 as the graphical interface. The model was refined with ShelXL using least-squares minimization.

4.12 Chapter 2 compounds

Synthesis and characterisation of bis-(dppe) benzene-spaced compounds

trans-[RuCl(=C=CHC$_6$H$_4$-4-C≡CH)(dppe)$_2$]OTf, [**2**]OTf

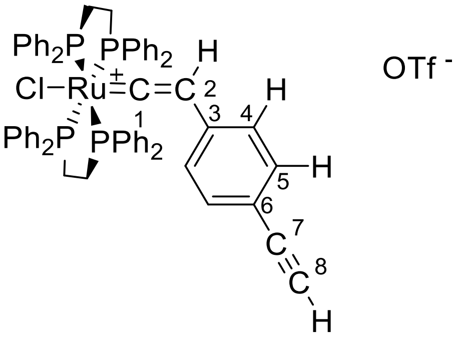

[RuCl(dppe)$_2$][OTf][147] (250 mg, 0.232 mmol) and 1,4-diethynyl benzene (58.5 mg, 0.464 mmol) were dissolved in dry DCM (15 mL) and stirred under N$_2$ at room temperature for 1 hour. The solvent was removed by vacuum, and washed with pentane (15 mL), diethylether (3 x 15 mL) and hexane (2 x 15 mL) and dried under vacuum to give a green/brown microcrystalline solid (223 mg, 0.184 mmol, 80 %).

^{1}H NMR (CD$_2$Cl$_2$, 500 MHz, 295 K) δ/ppm: 2.78 (m, dppe), 2.97 (m, dppe), 3.05 (s, 1H, H^8), 3.39 (quin, J = 2.7 Hz, 1H, H^2), 5.61 (d, J = 8.3 Hz, 2H, H^4), 6.83 (d, J = 8.3 Hz, 2H, H^5), 7.06-7.37 (m, dppe). ^{13}C{^{1}H} NMR (CD$_2$Cl$_2$, 126 MHz, 295 K) δ/ppm: 35.1 (C^8), 82.2 (C^6), 109.6 (C^2), 120.4 (C^3), 127.0 (C^5), 132.1 (C^4), 355.4 (C^1). ^{31}P{^{1}H} NMR (CD$_2$Cl$_2$, 202 MHz, 295 K) δ/ppm: 38.24 (s). ESI(+)-MS (*m/z*): Calculated for [M]$^+$ ([C$_{62}$H$_{54}$ClP$_4$Ru]$^+$) 1059.1903. Observed 1023.2179 for [M-HCl]$^+$ (Calculated 1023.2316)

trans-RuCl(C≡CHC$_6$H$_4$-4-C≡CH)(dppe)$_2$, **2a**

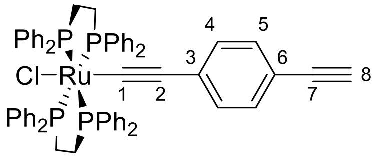

[RuCl(dppe)$_2$][OTf] (250 mg, 0.230 mmol) and 1,4-diethynyl benzene (63 mg, 0.500 mmol) were dissolved in dry MeOH (10 mL) and stirred under N$_2$ at room temperature for 1.5 hours during which time the reaction changed from red to green. NEt$_3$ (0.5 mL) was added, and a yellow precipitate was formed instantly and stirred for 1 hour. The precipitate was collected by filtration, and washed with cold MeOH, giving the product as a pale orange powder (220 mg, 0.207 mmol, 90 %).

^{1}H NMR (CDCl$_3$, 500 MHz) δ/ppm: 2.64 (m, dppe), 2.71 (m, dppe), 3.10 (s, 1H, H^8), 6.51 (d, *J* = 8.14 Hz, 2H, H^4), 6.94 (t, *J* = 7.5 Hz, dppe), 7.00 (t, *J* = 7.5 Hz, dppe), 7.18 (m, dppe), 7.22 (d, *J* = 8.14 Hz, 2H, H^5), 7.30-7.49 (m, dppe). ^{13}C{^{1}H} NMR (CDCl$_3$, 126 MHz) δ/ppm: 29.5 (C^8), 30.3 (dppe), 85.8 (C^7), 114.5 (C^2), 129.9 (C^4), 131.2 (C^3), 131.5 (C^5), 132.15 (C^6). ^{31}P{^{1}H} NMR (CDCl$_3$, 202 MHz) δ/ppm: 49.21 (s).

trans-[{RuCl(dppe)$_2$}$_2$(=C=CHC$_6$H$_4$-4-CH=C=)]$_2$(BF$_4$)$_2$, **3**

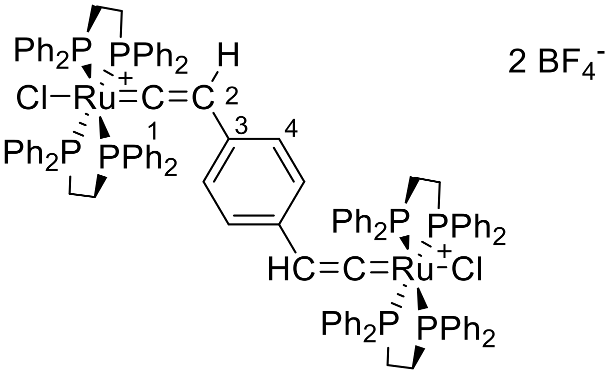

[RuCl(dppe)$_2$][OTf] (20 mg, 0.018 mmol) and 1,4-diethynyl benzene (1.17 mg, 0.009 mmol) were dissolved in dry DCM-d_2 under a nitrogen atmosphere, and NMR spectra run after 1 hour. Full conversion was observed by NMR. Crystals suitable for X-ray diffraction were grown from DCM/pentane.

^{1}H NMR (CD$_2$Cl$_2$, 400 MHz, 298 K) δ /ppm: 3.60 (s, 1H, H^1), 5.68 (d, *J* = 8.36 Hz, 2H, H^2). ^{31}P{^{1}H} NMR (CD$_2$Cl$_2$, 126 MHz, 298 K)) δ /ppm: 38.9 (s)

trans-[RuCl(=C=CHC$_6$H$_4$-4-C=OCH$_3$)(dppe)$_2$]OTf, **5**

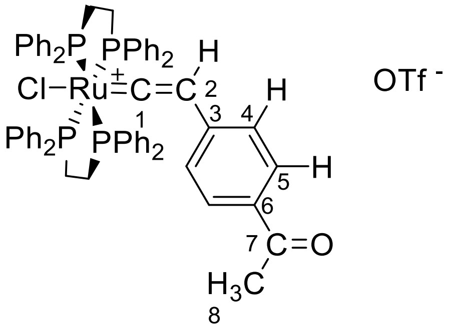

[RuCl(dppe)$_2$][OTf] (250 mg, 0.232 mmol) and 4-ethynylacetophenone (43.2 mg, 0.300 mmol) were dissolved in CH$_2$Cl$_2$ (7 mL) and stirred under N$_2$ at room temperature for 1 hour. The solvent was removed under vacuum and the red solid washed with diethylether (2 x 20 mL) and hexane (20 mL), giving a dark red powder (262 mg, 0.213 mmol, 92 %). Crystals of [**2**]OTf suitable for X-ray diffraction were grown from DCM/pentane.

^{1}H NMR (CD$_2$Cl$_2$, 500 MHz, 295 K) δ /ppm: 2.52 (s, 3H, H^8), 2.70 (br t, *J* = 7.8 Hz, 8H, dppe), 6.57 (d, *J* = 8.4 Hz, 2H, H^4), 6.93 (t, *J* = 7.6 Hz, dppe), 7.06 (t, *J* = 7.6 Hz, dppe), 7.18 (t, *J* = 7.6 Hz, dppe), 7.25 (t, *J* = 7.6 Hz, dppe), 7.30 (d, *J* = 6.6 Hz, dppe), 7.43 (d, *J* = 6.9 Hz, dppe), 7.68 (d, *J* = 8.4 Hz, 2H, H^5). ^{13}C NMR (CD$_2$Cl$_2$, 125.8 MHz, 295 K) δ /ppm: 26.5 (C^8), 33.8 (C^6), 115.5 (C^2), 127.4 (C^p), 127.6 (C^p), 128.2 (C^5), 129.2 (C^m, dppe), 129.6 (C^m, dppe), 130.2 (C^4, dppe), 134.2 (C^o, dppe), 135.0 (C^o, dppe), 136.5 (C^i, dppe), 135.7 (C^3), 197.7 (C^7). ^{31}P NMR (CD$_2$Cl$_2$, 202 MHz, 298 K) δ /ppm: 37.58 (s). ESI(+)-MS (*m/z*): Calculated for [M]$^+$ ([C$_{62}$H$_{56}$ClOP$_4$Ru]$^+$) 1077.2014. Observed 1041.2313 for [M-HCl]$^+$ (calculated 1041.2421)

trans-[RuCl(=C=CHC$_6$H$_4$-4-C(C$_4$H$_3$NCH$_3$)$_2$CH$_3$)(dppe)$_2$]OTf or BF$_4$, **7**

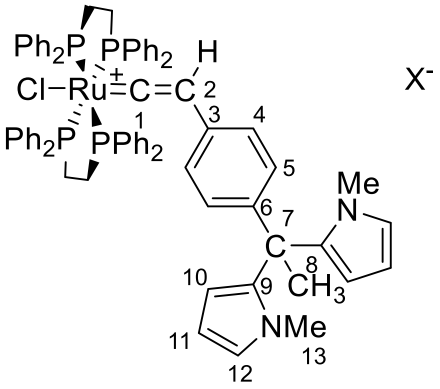

50 mg (0.041 mmol) of *trans*-[Ru(=C=CHC$_6$H$_4$-4-C≡CH)Cl(dppe)$_2$][OTf], 6 µL (0.090 mmol) of *N*-methylpyrrole and 3 µL of HBF$_4$.(OEt$_2$) were dissolved in dry DCM and stirred under nitrogen for 2 hours. A gradual darkening of the solution occurred. The solvent was removed by vacuum, washed with diethylether (x2) and hexane to yield 22.8 mg of a grey/purple solid. This product contained 43 % *N*-methylpyrrole by NMR).

^{1}H NMR (CD$_2$Cl$_2$, 500 MHz, 295 K) δ /ppm: 3.05 (m, CH$_3$, H^8), 3.30 (app quin, *J* = 1.96 Hz, H^2), 3.58 (s, N-CH$_3$, H^{13}), 3.63 (s, free *N*-methylpyrrole), 5.73 (d, *J* = 8.4 Hz, H^5), 5.80 (app. t, H^{12}), 6.19 (app. t, H^{11}), 6.20 (t, *J* = 2.05 Hz, free *N*-methylpyrrole), 6.53 (app. t, H^{10}), 6.59 (t, *J* = 2.05 Hz, free *N*-methylpyrrole), 6.76 (d, *J* = 8.4 Hz, H^4) 7.12 (m, dppe), 7.26 (m, dppe), 7.34 (m, dppe), 7.38 (m, dppe). ^{13}C{^{1}H} NMR (CD$_2$Cl$_2$, 125.8, 295 K) δ /ppm: 35.2 (C^{13}), 108.4 (C^{12}), 109.6 (C^2), 120.0 (C^{11}), 121.3 (C^{10}), 122.3 (C^3), 124.7 (C^9), 127.2 (C^5), 128.3 (C^4), 134.2 (C^9), 137.6 (C^7), 150.6 (C^6), 355.1 (C^1). ^{31}P{^{1}H} NMR (CD$_2$Cl$_2$, 126 MHz, 295 K) δ /ppm: 40.39 (s), methyl ketone product 37.73 (s). ESI-MS (*m/z*): Observed 1221.3137 for [M]$^+$, [C$_{72}$H$_{68}$ClN$_2$P$_4$Ru]$^+$, (Calculated 1221.3065).

trans-RuCl(C≡CHC$_6$H$_4$-4-C=OCH$_3$)(dppe)$_2$, **10**

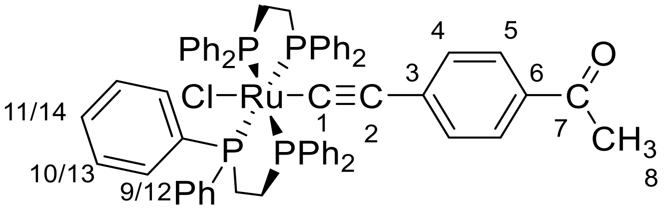

50 mg (0.041 mmol) of [RuCl(dppe)$_2$(=C=CH–C$_6$H$_4$-4-C=OCH$_3$)][OTf] was dissolved in dry DCM (15 mL) and 6 µL (0.820 mmol) of *N*-methylpyrrole and 3 µL of HBF$_4$,OEt$_2$ were added. The solution was stirred for 3 hours, with the colour changing from red, to brown, to black then blue. The solvent reduced to 10 mL by reduced pressure and 5 drops of triethylamine added, turning the solution yellow. The rest of the solvent was removed then passed through a basic alumina plug with DCM giving 37 mg (83 % yield) of a yellow microcrystalline powder. The same product can be made by passing [RuCl(dppe)$_2$(=C=CH–C$_6$H$_4$-4-C=OCH$_3$)][OTf] through a plug of basic alumina.

^{1}H NMR (CD$_2$Cl$_2$, 500 MHz, 295 K) δ /ppm: δ 2.52 (s, 3H, H^8), 2.70 (br t, J_{HH} = 7.75 Hz, 8H, dppe aliphatic H), 6.57 (d, J_{HH} = 8.38 Hz, 2H, H^4), 6.93 (t, J_{HH} = 7.58 Hz, H$^{10/13}$), 7.06 (t, J_{HH} = 7.58 Hz, H$^{10/13}$), 7.18 (t, J_{HH} = 7.58 Hz, H$^{11/14}$), 7.25 (t, J_{HH} = 7.58 Hz, H$^{11/14}$), 7.30 (d, J_{HH} = 6.59 Hz, H$^{9/12}$), 7.43 (d, J_{HH} = 6.92 Hz, H$^{9/12}$), 7.68 (d, J_{HH} = 8.38 Hz, 2H, H^5). ^{13}C{^{1}H} NMR (CD$_2$Cl$_2$, 125.8, 295 K) δ /ppm: 26.55 (C^8), 30.83 (dppe), 115.14 (C^2), 120.16 (C^1), 127.43 (C$^{11/14}$), 127.61 (C$^{11/14}$), 128.17 (C^5), 129.22 (C$^{10/13}$), 129.48 (C$^{10/13}$), 130.18 (C^4), 131.71 (C^6), 134.31 (C$^{9/12}$), 134.96 (C$^{9/12}$), 135.73 (C^3), 197.28 (C^7). ^{31}P{^{1}H} NMR (CD$_2$Cl$_2$, 126 MHz, 295 K) δ /ppm: 48.38 (s). ESI-MS (*m/z*): Calculated for [M]$^+$ ([C$_{62}$H$_{55}$ClON$_2$P$_4$Ru]) 1076.1935. Observed 1041.2251 for [C$_{62}$H$_{56}$OP$_4$Ru]$^+$ (Calculated 1041.2241)

trans-RuCl(C≡CC$_6$H$_4$-4-C(Cl)=CH$_2$)(dppe)$_2$, **11a**

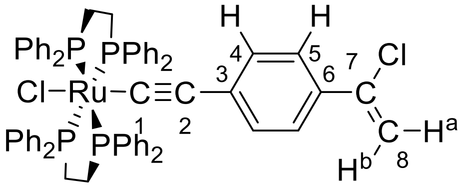

trans-[RuCl(=C=CHC$_6$H$_4$-4-C≡CH)(dppe)$_2$][OTf] (13 mg, 0.010 mmol) was dissolved with Bu$_4$NCl (3 mg, 0.011 mmol, 1.1 eq.) in DCM where an immediate colour change from brown to red was observed. The solution was left to react for 5 hours then passed through a basic alumina plug with DCM and the solvent removed. The recovered solid was dissolved in DCM-*d* for analysis.

^{1}H NMR (CD$_2$Cl$_2$, 500 MHz, 295 K) δ/ppm: 2.69 (m, dppe), 5.43 (d, *J* = 1.80 Hz, 1H, H^{8a}), 5.74 (d, *J* = 1.76 Hz, 1H, H^{8b}), 6.57 (d, *J* = 8.4 Hz, 2H, H$^{4/5}$), 6.97- 7.46 (m, dppe), 7.38 (d, *J* = 8.4 Hz, 2H, H$^{4/5}$), ^{31}P{^{1}H} NMR (CD$_2$Cl$_2$, 202 MHz, 295 K) δ/ppm: 48.63 (s). ESI(+)-MS (*m/z*): Calculated for [M]$^+$ ([C$_{62}$H$_{54}$Cl$_2$P$_4$Ru]$^+$) 1094.1597. Observed 1059.1920 for [M-Cl]$^+$ (calculated 1059.1908), Observed 1041.2253 for [C$_{62}$H$_{56}$OP$_4$Ru]$^+$ (Calculated 1041.2241)

trans-RuCl($C{\equiv}CC_6H_4$-4-C(Br)=CH_2)(dppe)$_2$, **11b**

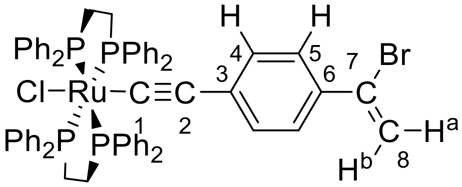

trans-[RuCl(=C=CHC_6H_4-4-C≡CH)(dppe)$_2$][OTf] (13 mg, 0.010 mmol) was dissolved with Bu_4NBr (3.5 mg, 0.011 mmol, 1.1 eq.) in DCM where an immediate colour change from brown to red was observed. The solution was left to react for 5 hours then passed through a basic alumina plug with DCM and the solvent removed. The recovered solid was dissolved in DCM-*d* for analysis. NMR showed some peaks similar to the literature values, for the chlorinated species, RuCl(C≡CHC_6H_4-4-CCl=CH_2)(dppe)$_2$, but also showed the brominated species, **11b**.

^{1}H NMR (CD_2Cl_2, 500 MHz, 295 K) δ/ppm: 7.38 (app. d, $H^{4/5}$), 6.55 (d, *J* = 8.68 Hz, $H^{4/5}$), 6.07 (d, *J* = 2.06 Hz, 1H, H^{8b}), 5.67 (d, *J* = 2.16 Hz, 1H, H^{8a}). $^{31}P\{^1H\}$ NMR (CD_2Cl_2, 202 MHz, 295 K) δ/ppm: 48.66. ESI(+)-MS (*m/z*): Calculated for $[M]^+$ ($[C_{62}H_{54}BrClP_4Ru]^+$) 1140.1167. Observed for [M-Cl] 1151.1270 (calculated 1151.1259). Observed 1059.1920 for $[C_{62}H_{54}ClP_4Ru]^+$ (calculated 1059.1908), Observed 1041.2253 for $[C_{62}H_{56}OP_4Ru]^+$ (Calculated 1041.2241)

trans-RuCl(C≡CC$_6$H$_4$-4-C(I)=CH$_2$)(dppe)$_2$, **11c**

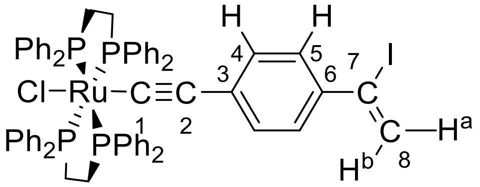

trans-[RuCl(=C=CHC$_6$H$_4$-4-C≡CH)(dppe)$_2$][OTf], **1**, (13 mg, 0.010 mmol) was dissolved with Bu$_4$NI (4 mg, 0.011 mmol, 1.1 eq.) in DCM where an immediate colour change from brown to red was observed. It was left to react for 5 hours then passed through a basic alumina plug with DCM and the solvent removed. The recovered solid was dissolved in DCM-*d* for analysis. NMR showed peaks similar to the literature values, for a chlorinated species, RuCl(C≡CHC$_6$H$_4$-4-CCl=CH$_2$)(dppe)$_2$, but also showed the iodinated species, **11c**.

^{1}H NMR (CD$_2$Cl$_2$, 500 MHz, 295 K) δ/ppm: 7.28 (d, J = 8.48 Hz, H$^{4/5}$), 6.51 (d, J = 8.41 Hz, H$^{4/5}$), 6.44 (d, J = 1.8 Hz, 1H, H$^{8a/b}$), 6.00 (d, J = 1.8 Hz, 1H, H$^{8a/b}$). ^{31}P{^{1}H} NMR (CD$_2$Cl$_2$, 202 MHz, 295 K) δ/ppm: 43.91, 48.51. ESI(+)-MS (*m/z*): Calculated for [M]$^+$ ([C$_{62}$H$_{54}$IClP$_4$Ru]$^+$) 1187.1118. Observed for [M-Cl] 1151.1270 (calculated 1151.1259). Observed 1059.1920 for [C$_{62}$H$_{54}$ClP$_4$Ru]$^+$ (calculated 1059.1908), Observed 1041.2253 for [C$_{62}$H$_{56}$OP$_4$Ru]$^+$ (Calculated 1041.2241).

Synthesis and characterisation of Ru(dppe)Cp* benzene spaced compounds

Ru(C≡CC$_6$H$_4$-4-C≡C(CH$_3$)$_2$OH)(dppe)Cp*, **18**

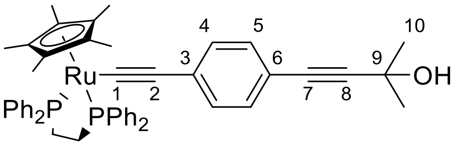

An oven-dried (120 °C, 12 hours) Schlenk flask was charged with RuCl(dppe)Cp* (200 mg, 0.300 mmol), 4-[(trimethylsilyl)ethynyl]-1-(3-hydroxyl-3-methylbutynyl)benzene (82 mg, 0.320 mmol) and KF (20 mg, 0.344 mmol), followed by dry MeOH (15 mL). The reaction was heated to reflux for 2 hours, then 0.3 mL NEt$_3$ added, further heating for 4 hours gave a small amount of yellow precipitate. The solvent was reduced under vacuum and more yellow powder precipitated from the green solution. The precipitate was collected by filtration and washed with cold MeOH, giving the product as a yellow powder (148 mg, 0.181 mmol, 60 %).

IR (nujol, cm^{-1}): 2035 (C≡C, shoulder), 2063 (C≡C), 3490 (OH). ^{1}H NMR (CDCl$_3$, 500 MHz) δ /ppm: 1.54 (s, 15H, Cp*), 1.59 (s, 6H, H^{10}), 2.06 (m, dppe), 2.65 (m, dppe), 6.64 (d, *J* = 8.3 Hz, 2H, H^4), 7.07 (d, *J* = 8.3 Hz, 2H, H^5), 7.21 (app. t, dppe), 7.28- 7.34 (m, dppe), 7.73 (t, *J* = 8.0 Hz, dppe). ^{13}C{^{1}H} NMR (CDCl$_3$, 125.8 MHz) δ /ppm: 10.16 (Cp* CH$_3$), 29.52 (dppe), 31.76 (C^{10}), 65.89 (C^9), 83.43 (C^7), 92.83 (Cp*), 93.25 (C^8), 110.74 (C^2), 115.87 (C^3), 127.35 (t, dppe), 127.59 (t, dppe), 129.00 (dppe), 129.08 (dppe), 130.07 (C^4), 131.03 (C^5), 131.55 (C^1), 133.32 (dppe), 133.76 (dppe). ^{31}P{^{1}H} NMR (CDCl$_3$ 243 MHz) δ /ppm: 80.70. ESI(+)-MS (*m/z*): Calculated for [M]$^+$ ([C$_{49}$H$_{50}$OP$_2$Ru]$^+$) 818.2380. Observed for [M+H] 819.2581 (Calculated 819.2451).

[Ru(=C=C(H)C_6H_4-4-C≡C$(CH_3)_2$OH)(dppe)Cp*]BF_4, **21**

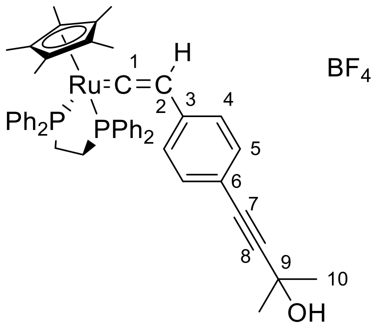

An oven-dried (120 °C, 12 hours) Schlenk flask was charged with Ru(CCC_6H_4CC$(CH_3)_2$OH)(dppe)Cp* (60 mg, 0.073 mmol), and dry CH_2Cl_2 (8 mL). 2 drops of HBF_4.OEt_2 were added, an immediate yellow to purple colour change occurred, and the reaction was stirred under nitrogen for 3 hours after which time the solvent was removed by vacuum. The resulting solid was dissolved in a minimum of CH_2Cl_2 and the product isolated by precipitation upon rapid addition of the CH_2Cl_2 solution into stirred, ice-cold ether. The precipitate was collected by filtration, giving the product as a pale purple powder (44 mg, 0.054 mmol, 74 %).

IR (nujol, cm^{-1}): 1630 (M=C=C), 1971 (C≡C), 3052 (OH). ^{1}H NMR ($CDCl_3$, 500 MHz) δ /ppm: 1.65 (s, 6H, H^{10}), 1.69 (s, 15H, Cp*), 2.54 (m, dppe), 3.05 (m, dppe), 6.02 (d, *J* = 8.3 Hz, 2H, H^4), 6.89 (d, *J* = 8.3 Hz, 2H, H^5), 7.10 (app. t, dppe), 7.38 (app. t, dppe), 7.44-7.49 (m, dppe), 7.56 (m, dppe). $^{13}C\{^1H\}$ NMR ($CDCl_3$, 125.8 MHz) δ /ppm: 10.41 (Cp* CH_3), 28.04 (dppe), 31.68 (C^{10}), 63.49 (C^9), 99.72 (C^8), 103.76 (Cp*), 105.08 (C^2), 125.60 (C^4), 129.10 (dppe), 129.47 (dppe), 131.75 (C^5), 131.91 (dppe), 132.09 (dppe), 133.09 (dppe), 133.24 (dppe). $^{31}P\{^1H\}$ NMR ($CDCl_3$ 243 MHz) δ /ppm: 71.90. ESI(+)-MS (*m/z*): Calculated for $[M]^+$ ($[C_{49}H_{51}P_2RuO]^+$) 819.2453. Observed for $[M]^+$ 819.2526.

[Ru(=C=C(CN)C_6H_4-4-C≡C$(CH_3)_2$OH)(dppe)Cp*]BF_4, **22**

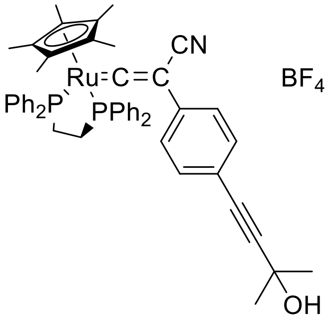

An oven-dried (120 °C, 12 hours) Schlenk flask was charged with Ru($CCC_6H_4CC(CH_3)_2OH$)(dppe)Cp* (60 mg, 0.073 mmol), and [CAP]BF_4 (19 mg, 0.080 mmol) followed by dry CH_2Cl_2 (8 mL). The orange solution immediately turned red and was stirred under nitrogen for 3 hours after which time the solvent was removed by vacuum. The resulting solid was dissolved in a minimum of CH_2Cl_2 and the product isolated by precipitation upon rapid addition of the CH_2Cl_2 solution into stirred, ice-cold ether. The precipitate was collected by filtration, giving the product as a pale-yellow powder (53 mg, 0.063 mmol, 86 %).

IR (nujol, cm^{-1}): 1643 (M=C=C), 1964 (C≡C), 2197 (C≡N), 3493 (OH). ^1H NMR ($CDCl_3$, 500 MHz) δ /ppm: 1.61 (s, 6H, H^{10}), 1.69 (s, 15H, Cp*), 2.87 (m, dppe), 3.06 (m, dppe), 6.41 (d, *J* = 8.3 Hz, 2H, H^4), 6.95 (d, *J* = 8.3 Hz, 2H, H^5), 7.09 (app, t, dppe), 7.38 (m, dppe), 7.50 (t, *J* = 7.7 Hz, dppe), 7.59 (app. t, dppe). $^{13}C\{^1H\}$ NMR ($CDCl_3$, 125.8 MHz) δ /ppm: 10.26 (Cp* CH_3), 28.96 (dppe), 29.33 (dppe), 31.63 (C^{10}), 40.12, 65.76 (C^9), 81.40 (C^7), 95.05 (C^8), 105.73 (Cp*), 106.55 (C^2), 108.25 (CN), 122.30 (C^3), 123.45 (C^6), 125.74 (C^4), 129.34 (t, dppe), 129.55 (t, dppe), 132.18 (C^5), 132.37 (dppe), 132.57 (t, dppe), 132.67 (dppe), 133.16 (t, dppe), 343.58 (app t, C^1). $^{31}P\{^1H\}$ NMR ($CDCl_3$ 243 MHz) δ /ppm: 70.49. ESI(+)-MS (*m/z*): Calculated for $[M]^+$ ($[C_{50}H_{50}P_2RuNO]^+$) 844.2411. Observed for [M] 844.2451

[Ru(=C=C(C_7H_7)C_6H_4-4-C≡C($(CH_3)_2$OH)(dppe)Cp*]BF_4, **23**

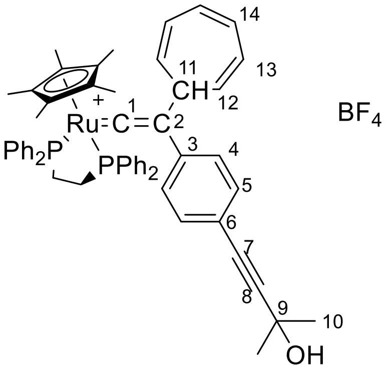

An oven-dried (120 °C, 12 hours) Schlenk flask was charged with Ru($CCC_6H_4CC(CH_3)_2OH$)(dppe)Cp* (60 mg, 0.073 mmol), and [C_7H_7]BF_4 (11 mg, 0.090 mmol) followed by dry CH_2Cl_2 (8 mL). The orange solution was stirred under nitrogen for 4 hours after which time the solvent was removed by vacuum. The resulting solid was dissolved in a minimum of CH_2Cl_2 and the product isolated by precipitation upon rapid addition of the CH_2Cl_2 solution into stirred, ice-cold ether. The precipitate was collected by filtration, giving the product as a pale-yellow powder (48 mg, 0.052 mmol, 71 %).

IR (nujol, cm^{-1}): 1649 (M=C=C), 1962 (C≡C), 3490 (OH). ^{1}H NMR ($CDCl_3$, 500 MHz) δ /ppm: 1.60 (s, 1H, H^{11}), 1.63 (s, 6H, H^{10}), 1.68 (s, 15H, Cp*), 2.80 (m, dppe), 3.10 (m, dppe), 4.98 (dd, *J* = 5.4 Hz, *J* = 9.1 Hz, 2H, H^{12}), 5.96 (d, *J* = 9.1 Hz, 2H, H^{13}), 6.28 (t, *J* = 2.9 Hz, 1H, H^{14}), 6.76 (d, *J* = 8.1 Hz, 2H, H^{4}), 6.91 (m, dppe), 6.95 (d, *J* = 8.1 Hz, 2H, H^{5}), 7.14-7.23 (m, dppe), 7.34 (m, dppe), 7.47 (m, dppe), 7.55 (m, dppe). $^{13}C\{^{1}H\}$ NMR ($CDCl_3$, 125.8 MHz) δ /ppm: 10.43 (Cp* CH_3), 28.58 (dppe), 31.68 (C^{10}), 33.74 (C^{11}), 65.78 (C^{9}), 81.69 (C^{7}), 94.69 (C^{8}), 103.38 (Cp*), 122.04 (C^{2}), 124.10 (C^{12}), 124.81 (C^{13}), 127.10 (C^{6}), 127.59 (C^{3}), 128.72 (t, dppe), 129.03 (t, dppe), 129.91 (C^{4}), 130.88 (C^{14}), 131.22 (C^{5}), 131.69 (s, dppe), 131.74 (s, dppe), 132.25 (t, dppe), 133.12 (t, dppe). $^{31}P\{^{1}H\}$ NMR ($CDCl_3$ 243 MHz) δ /ppm: 74.45. ESI(+)-MS (*m/z*): Calculated for $[M]^+$ ($[C_{56}H_{57}P_2RuO]^+$) 909.2923. Observed for $[M]^+$ 909.3024.

Ru(C≡CC$_6$H$_4$-4-C≡CC$_6$H$_4$-4-OMe)(dppe)Cp*, **25**

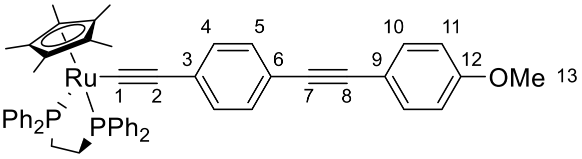

An oven-dried (120 °C, 12 hours) Schlenk flask was charged with RuCl(dppe)Cp* (535 mg, 0.798 mmol), $(CH_3)_3SiCCC_6H_4CCC_6H_4OCH_3$ (255 mg, 0.838 mmol) and KF (55 mg, 0.800 mmol), followed by dry MeOH (25 mL). The reaction was heated to reflux for 5 hours during which time a yellow precipitate formed. The precipitate was collected by filtration and washed with cold MeOH, giving the product as a yellow powder (605 mg, 0.699 mmol, 88 %).

^{1}H NMR (CDCl$_3$, 500 MHz) δ /ppm: 1.56 (s, 15H, Cp*), 2.06 (m, dppe), 2.67 (m, dppe), 3.82 (s, 3H, H^{13}), 6.69 (d, J= 8.3 Hz, 2H, C$^{4/5}$), 6.85 (d, J= 8.8 Hz, 2H, C$^{10/11}$), 7.17 (d, J= 8.3 Hz, 2H, C$^{4/5}$), 7.22 (t, J= 7.8 Hz, 4H, dppe), 7.31 (m, dppe), 7.42 (d, J= 8.8 Hz, 2H, C$^{10/11}$) , 7.75 (t, J= 7.9 Hz, 4H, dppe). ^{31}P{^{1}H} NMR (CDCl$_3$ 243 MHz) δ /ppm: 80.70
These data match those previously reported.[165]

Ru(C≡CC$_6$H$_4$-4-C≡CC$_6$H$_4$-4-CO$_2$Me)(dppe)Cp*, **26**

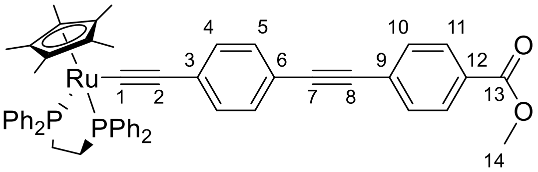

An oven-dried (120 °C, 12 hours) Schlenk flask was charged with RuCl(dppe)Cp* (990 mg, 1.300 mmol), (CH$_3$)$_3$SiCCC$_6$H$_4$CCC$_6$H$_4$CO$_2$CH$_3$ (490 mg, 1.474 mmol) and KF (55 mg, 0.800 mmol), followed by dry MeOH (25 mL). The reaction was heated to reflux for 5 hours during which time a yellow precipitate formed. The precipitate was collected by filtration and washed with cold MeOH, giving the product as a yellow powder (986 mg, 1.103 mmol, 85 %).

^{1}H NMR (CDCl$_3$, 500 MHz) δ /ppm: 1.56 (s, 15H, Cp*), 2.06 (m, dppe), 2.67 (m, dppe), 3.92 (s, 3H, H^{14}), 6.70 (d, J_{HH} = 8.3 Hz, 2H, C$^{4/5}$), 7.19 (d, J_{HH} = 8.3 Hz, 2H, C$^{4/5}$), 7.23 (m, dppe), 7.31 (m, dppe), 7.53 (d, J_{HH} = 8.5 Hz, 2H, C$^{10/11}$), 7.74 (t, J_{HH} = 8.1 Hz, 4H, dppe), 7.98 (d, J_{HH} = 8.5 Hz, 2H, C$^{10/11}$). ^{31}P{^{1}H} NMR (CDCl$_3$ 243 MHz) δ /ppm: 80.66.
These data match those previously reported.[165]

Ru(C≡CC$_6$H$_4$-4-Br)(dppe)Cp*, **27**

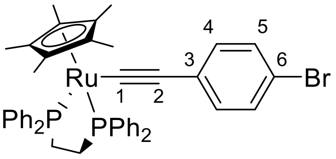

An oven-dried (120 °C, 12 hours) Schlenk flask was charged with RuCl(dppe)Cp* (500 mg, 0.745 mmol), $(CH_3)_3SiCCC_6H_4Br$ (250 mg, 0.990 mmol) and KF (30 mg, 0.516 mmol), followed by dry MeOH (20 mL) and NEt_3 (1 mL). The reaction was heated to reflux for 17 hours during which time a yellow precipitate formed. The precipitate was collected by filtration and washed with cold MeOH, giving the product as a yellow powder (478 mg, 0.587 mmol, 79 %). Crystals suitable for X-ray diffraction were grown from DCM/hexane.

IR (nujol, cm^{-1}):2061 (C≡C). ^{1}H NMR ($CDCl_3$, 500 MHz) δ /ppm: 1.55 (s, 15H, Cp*), 2.05 (m, dppe), 2.64 (m, dppe), 6.57 (d, J_{HH} = 8.5 Hz, 2H, C^4), 7.10 (d, J_{HH} = 8.5 Hz, 2H, C^5), 7.21 (t, J_{HH} = 8.2 Hz, 4H, dppe), 7.31 (m, 12H, dppe), 7.74 (t, J_{HH} = 8.2 Hz, 4H, dppe) ^{13}C{^{1}H} NMR ($CDCl_3$, 125.8 MHz) δ /ppm: 10.16 (Cp* CH_3), 29.33-29.70 (dppe), 92.76 (Cp*), 109.02 (C^2), 115.64 (C^1), 127.34 (t, dppe), 127.59 (t, dppe), 129.00 (s, dppe), 129.07 (s, dppe), 130.24 (C^6), 130.56 (C^5), 131.80 (C^4), 132.57 (C^3), 133.31 (t, dppe), 133.78 (t, dppe). ^{31}P{^{1}H} NMR ($CDCl_3$ 243 MHz) δ /ppm: 80.78. ESI(+)-MS (*m/z*): Calculated for [M]$^+$ ([$C_{44}H_{43}P_2RuBr$]$^+$) 814.1061. Observed for [M]$^+$ 814.1038.

[Ru(=C=C(H)C_6H_4-4-C≡CC_6H_4-4-OMe)(dppe)Cp*]BF_4, **29**

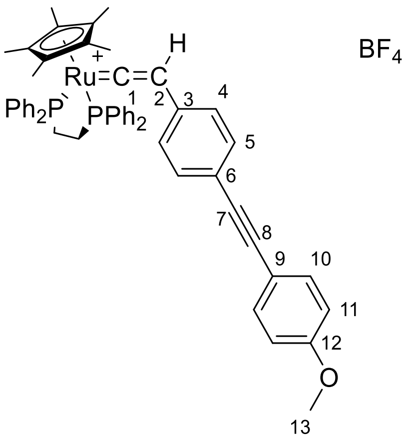

An oven-dried (120 °C, 12 hours) Schlenk flask was charged with Ru($CCC_6H_4CCC_6H_4OCH_3$)(dppe)Cp* (100 mg, 0.115 mmol), and dry CH_2Cl_2 (10 mL). 2 drops of $HBF_4.OEt_2$ were added, an immediate yellow to brown colour change occurred, and the reaction was stirred under nitrogen for 3 hours after which time the solvent was removed by vacuum. The resulting solid was dissolved in a minimum of CH_2Cl_2 and the product isolated by precipitation upon rapid addition of the CH_2Cl_2 solution into stirred, ice-cold ether. The precipitate was collected by filtration, giving the product as a pale yellow/brown powder (83 mg, 0.086 mmol, 75 %).

IR (nujol, cm^{-1}): 1630 (M=C=C), 1966 (C≡C). ^1H NMR ($CDCl_3$, 500 MHz) δ /ppm: 1.70 (s, 15H, Cp*), 2.53 (m, dppe), 3.06 (m, dppe), 3.83 (s, 3H, H^{13}, OMe), 4.39 (app. t, 1H, H^2), 6.04 (d, J_{HH} = 8.30 Hz, 2H, H^4), 6.88 (d, J_{HH} = 8.87 Hz, 2H, H^{10}), 6.96 (d, J_{HH} = 8.30 Hz, 2H, H^5), 7.10 (app. t, dppe), 7.38- 7.50 (m, dppe), 7.42 (d, J_{HH} = 8.87 Hz, H^{11}), 7.55 (app t, dppe). $^{13}C\{^1H\}$ NMR ($CDCl_3$, 125.8 MHz) δ /ppm: 10.40 (Cp* CH_3), 27.92 (dppe), 55.48 (C^{13}), 88.08 (C^7), 89.81 (C^8), 103.76 (Cp*), 114.18 (C^{10}), 115.39 (C^2), 121.16 (C^3), 125.65 (C^4), 126.92 (C^6), 129.13 (t, dppe), 129.41 (t, dppe), 131.58 (C^5), 131.86 (dppe), 132.12 (t, dppe), 132.21 (C^9), 133.03 (dppe), 133.15 (C^{11}), 159.79 (C^{12}), 353.83 (C^1). $^{31}P\{^1H\}$ NMR ($CDCl_3$ 243 MHz) δ /ppm: 71.97. ESI(+)-MS (*m/z*): Calculated for $[M]^+$ ($[C_{53}H_{51}P_2RuO]^+$) 867.2453. Observed for $[M]^+$ 867.2287

[Ru(=C=C(H)C_6H_4-4-C≡CC_6H_4-4-CO_2Me)(dppe)Cp*]BF_4, **30**

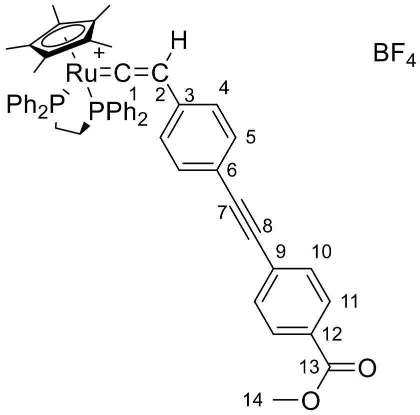

An oven-dried (120 °C, 12 hours) Schlenk flask was charged with Ru(CCC_6H_4CC$C_6H_4$$CO_2CH_3$)(dppe)Cp* (100 mg, 0.112 mmol), and dry CH_2Cl_2 (10 mL). 2 drops of HBF_4.OEt_2 were added, an immediate yellow to orange colour change occurred, and the reaction was stirred under nitrogen for 3.5 hours after which time the solvent was removed by vacuum. The resulting solid was dissolved in a minimum of CH_2Cl_2 and the product isolated by precipitation upon rapid addition of the CH_2Cl_2 solution into stirred, ice-cold ether. The precipitate was collected by filtration, giving the product as a pale yellow/beige powder (81 mg, 0.081 mmol, 72 %).

IR (nujol, cm^{-1}): 1623 (M=C=C), 1718 (C=O), 1964 (C≡C). ^{1}H NMR ($CDCl_3$, 500 MHz) δ /ppm: 1.70 (s, 15H, Cp*), 2.53 (m, dppe), 3.05 (m, dppe), 3.93 (s, 3H, H^{14}, CO_2Me), 4.39 (app. t, 1H, H^2), 6.07 (d, J_{HH} = 8.3 Hz, 2H, H^4), 6.98 (d, J_{HH} = 8.3 Hz, 2H, H^5), 7.10 (m, dppe), 7.39 (m, dppe), 7.48 (m, dppe), 7.54 (d, J_{HH} = 8.4 Hz, H^{10}), 7.57 (m, dppe), 8.01 (d, J_{HH} = 8.4 Hz, 2H, H^{11}). $^{13}C\{^1H\}$ NMR ($CDCl_3$, 125.8 MHz) δ /ppm: 10.41 (Cp* CH_3), 28.75 (dppe), 52.40 (C^{14}), 89.07 (C^8), 92.49 (C^7), 103.82 (Cp*), 115.35 (C^2), 120.07 (C^6), 125.67 (C^4), 128.09 (C^3), 128.19 (C^{12}), 129.13 (t, dppe), 129.68 (C^{11}), 129.40 (m, dppe), 129.56 (C^9), 131.57 (C^5), 131.90 (C^{10}), 132.14 - 132.45 (m, dppe), 133.04 (t, dppe), 166.71 (C^{13}), 343.58 (C^1) . $^{31}P\{^1H\}$ NMR ($CDCl_3$ 243 MHz) δ /ppm: 71.80. ESI(+)-MS (*m/z*): Calculated for $[M]^+$ ($[C_{54}H_{51}P_2RuO_2]^+$) 895.2402. Observed for $[M]^+$ 895.2219. Observed for [M+OH_2] 913.2295 (Calculated: 913.2508)

[Ru(=C=C(H)C_6H_4-4-C(=O)CH_2-C_6H_4-4-CO_2Me)(dppe)Cp*]BF_4, **31**

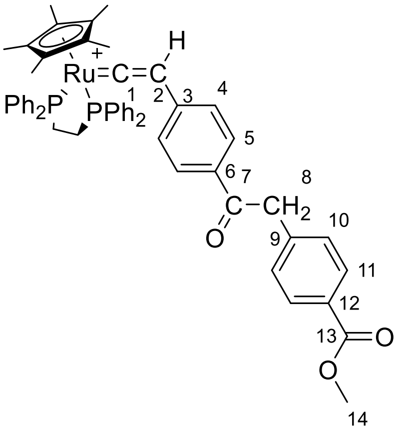

An oven-dried (120 °C, 12 hours) Schlenk flask was charged with Ru($CCC_6H_4CCC_6H_4CO_2CH_3$)(dppe)Cp* (50 mg, 0.056 mmol) and dry CH_2Cl_2 (10 mL). 2 drops of $HBF_4.OEt_2$ were added, an immediate yellow to brown colour change occurred, and the reaction was stirred under nitrogen for 3 days after which time the solvent was removed by vacuum. The resulting solid was dissolved in a minimum of CH_2Cl_2 and the product isolated by precipitation upon rapid addition of the CH_2Cl_2 solution into stirred, ice-cold ether. The precipitate was collected by filtration, giving the product as a pale yellow/brown powder (42 mg, 0.042 mmol, 75 %)

IR (nujol, cm^{-1}): 1625 (M=C=C), 1718, 1966 (C≡C). ^1H NMR ($CDCl_3$, 500 MHz) δ /ppm: 1.71 (s, 15H, Cp*), 2.17 (s, 1.5H, H^8 or acetone) 2.55 (m, dppe), 3.07 (m, dppe), 3.93 (s, 3H, H^{14}, CO_2Me), 6.07 (d, J_{HH} = 8.3 Hz, 2H, H^4), 6.99 (d, J_{HH} = 8.3 Hz, 2H, H^5), 7.12 (t, J_{HH} = 9.17 Hz, dppe), 7.39-7.50 (m, dppe), 7.55 (app. d, H^{10}), 7.56 (m, dppe), 8.02 (d, J_{HH} = 8.4 Hz, 2H, H^{11}). $^{31}P\{^1H\}$ NMR ($CDCl_3$ 243 MHz) δ /ppm: 71.80

[Ru(=C=C(CN)C_6H_4-4-C≡CC_6H_4-4-OMe)(dppe)Cp*]BF_4, **32**

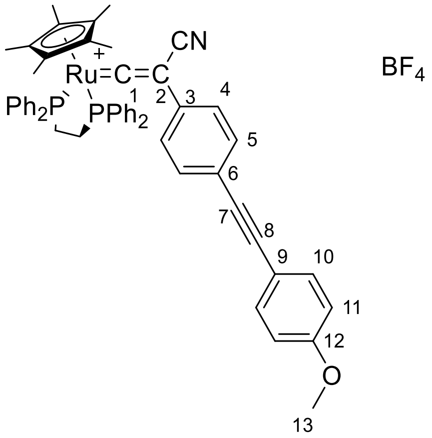

An oven-dried (120 °C, 12 hours) Schlenk flask was charged with Ru(CCC_6H_4CC$C_6H_4OCH_3$)(dppe)Cp* (100 mg, 0.115 mmol), and [CAP]BF_4 (45 mg, 0.149 mmol) followed by dry CH_2Cl_2 (10 mL). The reaction was stirred under nitrogen for 4.5 hours after which time the solvent was removed by vacuum. The resulting solid was dissolved in a minimum of CH_2Cl_2 and the product isolated by precipitation upon rapid addition of the CH_2Cl_2 solution into stirred, ice-cold ether. The precipitate was collected by filtration, giving the product as a pale pink powder (102 mg, 0.104 mmol, 90 %).

IR (nujol, cm^{-1}): 1650 (M=C=C), 1966 (C≡C), 2198 (C≡N). ^1H NMR ($CDCl_3$, 500 MHz) δ /ppm: 1.70 (s, 15H, Cp*), 2.53 (m, dppe), 3.06 (m, dppe), 3.83 (s, 3H, H^{13}, OMe), 6.04 (d, J_{HH} = 8.4 Hz, 2H, H^5), 6.88 (d, J_{HH} = 8.9 Hz, 2H, H^{11}), 6.96 (d, J = 8.4 Hz, 2H, H^4), 7.10 (app. t, dppe), 7.38- 7.50 (m, dppe), 7.42 (d, J_{HH} = 8.90 Hz, H^{10}), 7.55 (app t, dppe). $^{13}C\{^1H\}$ NMR ($CDCl_3$, 125.8 MHz) δ /ppm: 10.23 (Cp* CH_3), 27.92 (dppe), 55.48 (C^{13}), 87.08 (C^7), 89.81 (C^8), 103.76 (Cp*), 114.18 (C^{11}), 115.39 (C^2), 115.40 (C^6), 122.87 (CN), 125.65 (C^5), 126.92 (C^3), 129.13 (t, dppe), 129.41 (t, dppe), 131.58 (C^4), 131.86 (dppe), 132.12 (t, dppe), 132.31 (C^9), 133.03 (dppe), 133.15 (C^{10}), 159.79 (C^{13}), 343.76 (C^1). $^{31}P\{^1H\}$ NMR ($CDCl_3$ 243 MHz) δ /ppm: 70.70. ESI(+)-MS (*m/z*): Calculated for $[M]^+$ ($[C_{54}H_{50}P_2RuNO]^+$) 892.2406. Observed for $[M]^+$ 892.2150

[Ru(=C=C(CN)C$_6$H$_4$-4-C≡CC$_6$H$_4$-4-CO$_2$Me)(dppe)Cp*]BF$_4$, **33**

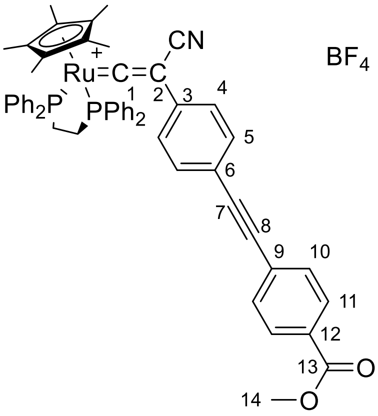

An oven-dried (120 °C, 12 hours) Schlenk flask was charged with Ru(CCC$_6$H$_4$CCC$_6$H$_4$CO$_2$CH$_3$)(dppe)Cp* (100 mg, 0.112 mmol), and [CAP]BF$_4$ (45 mg, 0.149 mmol) followed by dry CH$_2$Cl$_2$ (10 mL). The reaction was stirred under nitrogen for 2.5 hours after which time the solvent was removed by vacuum. The resulting solid was dissolved in a minimum of CH$_2$Cl$_2$ and the product isolated by precipitation upon rapid addition of the CH$_2$Cl$_2$ solution into stirred, ice-cold ether. The precipitate was collected by filtration, giving the product as a pale pink powder (105 mg, 0.104 mmol, 93 %).

IR (nujol, cm^{-1}): 1649 (M=C=C), 1717 (C=O), 1965 (C≡C), 2199 (C≡N). ^{1}H NMR (CDCl$_3$, 500 MHz) δ /ppm: 1.70 (s, 15H, Cp*), 2.83 (m, dppe), 3.05 (m, dppe), 3.92 (s, 3H, H^{14}, CO$_2$Me), 6.47 (d, J_{HH} = 8.4 Hz, 2H, H^4), 7.07 (d, J_{HH} = 8.4 Hz, 2H, H^5), 7.09 (m, dppe), 7.40 (m, dppe), 7.51 (t, J_{HH} = 7.6 Hz, dppe), 7.57 (d, J_{HH} = 8.5 Hz, H^{10}), 7.60 (m, dppe), 8.02 (d, J_{HH} = 8.5 Hz, 2H, H^{11}). ^{13}C{^{1}H} NMR (CDCl$_3$, 125.8 MHz) δ /ppm: 10.25 (Cp* CH$_3$), 29.00 (dppe), 52.42 (C^{14}), 89.83 (C^8), 91.65 (C^7), 105.82 (Cp*), 106.56 (C^2), 116.51 (C^3), 122.07 (CN), 124.08 (C^6), 125.84 (C^4), 127.72 (C^{12}), 129.35 (t, dppe), 129.56 (t, dppe), 129.69 (C^{11}), 129.83 (C^9), 132.24 (dppe), 132.40 (dppe), 132.56 (t, dppe), 131.71 (C^{10}), 132.24 (C^5), 133.13 (dppe), 166.65 (C^{13}), 343.20 (app t, C^1). ^{31}P{^{1}H} NMR (CDCl$_3$ 243 MHz) δ /ppm: 70.55. ESI(+)-MS (*m/z*): Calculated for [M]$^+$ ([C$_{55}$H$_{50}$P$_2$RuNO$_2$]$^+$) 920.2355. Observed for [M] 920.2140

[Ru(=C=C(C_7H_7)C_6H_4-4-C≡CC_6H_4-4-OMe)(dppe)Cp*]BF_4, **34**

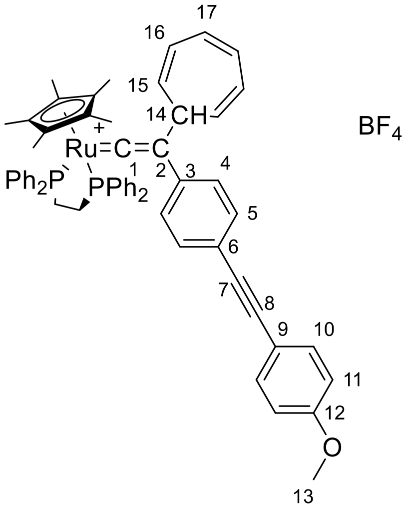

An oven-dried (120 °C, 12 hours) Schlenk flask was charged with Ru(CCC_6H_4CC$C_6H_4OCH_3$)(dppe)Cp* (100 mg, 0.115 mmol), and [C_7H_7]BF_4 (17.7 mg, 0.150 mmol) followed by dry CH_2Cl_2 (10 mL). The reaction was stirred under nitrogen for 3 hours after which time the solvent was removed by vacuum. The resulting solid was dissolved in a minimum of CH_2Cl_2 and the product isolated by precipitation upon rapid addition of the CH_2Cl_2 solution into stirred, ice-cold ether. The precipitate was collected by filtration, giving the product as a pale pink powder (84 mg, 0.081 mmol, 70 %). Crystal suitable for X-ray crystallography grown from DCM/hexane.

IR (nujol, cm^{-1}): 1648 (M=C=C), 1959 (C≡C). ^1H NMR ($CDCl_3$, 500 MHz) δ /ppm: 1.64 (t, *J* = 5.34 Hz, 2H, H^{14}), 1.68 (s, 15H, Cp*), 2.80 (m, dppe), 3.09 (m, dppe), 3.85 (s, 3H, H^{13}, OMe), 5.02 (dd, J_{HH} = 5.37 Hz, *J* = 9.2 Hz 2H, H^{15}), 5.98 (d, J_{HH} = 9.2 Hz, 2H, H^{16}), 6.29 (t, J_{HH} = 3.0 Hz, 1H, H^{17}), 6.89 (d, J_{HH} = 8.9 Hz, 2H, H^{11}), 6.78 (d, J_{HH} = 8.4 Hz, 2H, H^4), 6.91 (m, dppe), 7.03 (t, J_{HH} = 8.4 Hz, 2H, H^5), 7.20 (m, dppe), 7.35 (t, J_{HH} = 7.3 Hz, dppe), 7.47 (d, J_{HH} = 8.9 Hz, H^{10}), 7.53 (m, dppe). $^{13}C\{^1H\}$ NMR ($CDCl_3$, 125.8 MHz) δ /ppm: 10.41 (Cp* CH_3), 28.75 (dppe), 33.75 (C^{14}), 53.56 (C^{13}), 87.75 (C^7), 90.32 (C^8), 99.69 (C^2), 103.41 (Cp*), 114.19 (C^{11}), 115.32 (C^9), 124.12 (C^{15}), 124.82 (C^3), 126.71 (C^6), 124.82 (C^{16}), 128.70 (t, dppe), 129.02 (t, dppe), 129.94 (C^4), 130.89 (C^{17}), 131.27 (C^5), 131.86 (dppe), 132.23 (t, dppe), 133.09 (dppe), 133.26 (C^{10}), 159.88 (C^{13}). $^{31}P\{^1H\}$

NMR ($CDCl_3$ 243 MHz) δ /ppm: 74.48. ESI(+)-MS (*m/z*): Calculated for $[M]^+$ ($[C_{60}H_{57}P_2RuO]^+$) 957.2923. Observed for $[M-C_7H_7+H]^+$ 867.2480 (Calculated: 867.2453)

[Ru(=C=C(C_7H_7)C_6H_4-4-C≡CC_6H_4-4-CO_2Me)(dppe)Cp*]BF_4, **35**

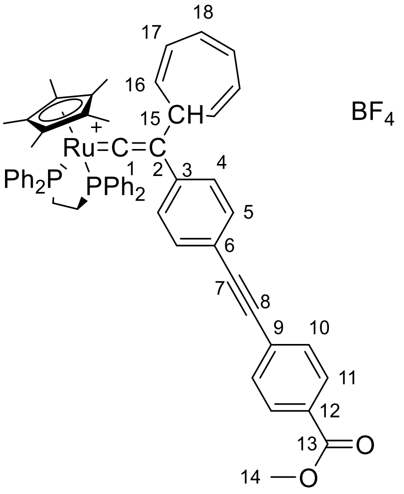

An oven-dried (120 °C, 12 hours) Schlenk flask was charged with Ru($CCC_6H_4CCC_6H_4CO_2CH_3$)(dppe)Cp* (100 mg, 0.112 mmol), and [C_7H_7]BF_4 (17.7 mg, 0.150 mmol) followed by dry CH_2Cl_2 (10 mL). The reaction was stirred under nitrogen for 3 hours after which time the solvent was removed by vacuum. The resulting solid was dissolved in a minimum of CH_2Cl_2 and the product isolated by precipitation upon rapid addition of the CH_2Cl_2 solution into stirred, ice-cold ether. The precipitate was collected by filtration, giving the product as a pale pink powder (84 mg, 0.082 mmol, 73 %).

IR (nujol, cm^{-1}): 1653 (M=C=C), 1719 (C=O), 1967 (C≡C). ^1H NMR ($CDCl_3$, 500 MHz) δ /ppm: 1.64 (t, J_{HH} = 5.67 Hz, 1H, H^{15}), 1.69 (s, 15H, Cp*), 2.80 (m, dppe), 3.12 (m, dppe), 3.85 (s, 3H, H^{13}, CO_2Me), 5.02 (dd, J_{HH} = 5.4 Hz, J_{HH} = 9.1 Hz, 2H, H^{16}), 5.98 (d, J_{HH} = 9.1 Hz, 2H, H^{17}), 6.24 (t, J_{HH} = 2.9 Hz, 1H, H^{18}), 6.82 (d, J_{HH} = 8.4 Hz, 2H, H^4), 6.91 (m, dppe), 7.07 (d, J_{HH} = 8.4 Hz, 2H, H^5), 7.19 (t, J_{HH} = 7.9 Hz, dppe), 7.35 (m, dppe), 7.59 (d, J_{HH} = 8.7 Hz, H^{10}), 7.47 (t, J_{HH} = 7.5 Hz, dppe), 7.54 (m, dppe), 8.03 (d, J_{HH} = 8.4 Hz, 2H, H^{11}). $^{13}C\{^1H\}$ NMR ($CDCl_3$, 125.8 MHz) δ /ppm: 10.42 (Cp* CH_3), 28.75 (dppe), 33.75 (C^{15}), 52.40 (C^{14}), 89.43 (C^8), 92.07 (C^7), 99.71 (C^2), 103.46 (Cp*), 121.78 (C^3), 124.20 (C^{16}), 124.91 (C^{17}), 127.62 (C^6), 128.05 (C^{12}), 128.70 (t, dppe), 129.04 (t, dppe), 129.72 (C^{11}), 129.99 (C^4), 130.90 (C^{18}), 131.71 (C^{10}), 131.92 (C^5), 132.99 (t, dppe), 133.12 (t, dppe), 166.70 (C^{13}). $^{31}P\{^1H\}$ NMR ($CDCl_3$ 243 MHz) δ /ppm: 74.41. ESI(+)-MS (*m/z*): Calculated for $[M]^+$ ($[C_{61}H_{57}P_2RuO_2]^+$) 985.2872. Observed for $[M\text{-}C_7H_7\text{+}H]^+$ 895.2221 (Calculated: 895.2402)

4.13 Chapter 3 compounds

Synthesis and characterisation of naphthalene spaced compounds

$(SiMe_3)C{\equiv}CC_{10}H_6\text{-}4\text{-}C{\equiv}C(SiMe_3)$

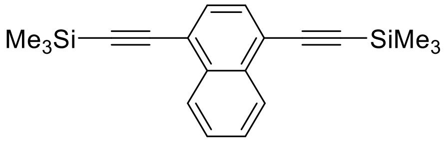

To an oven and flame dried Schlenk flask was added 2 g (7 mmol) of 1,4-dibromonaphthalene, 49 mg (0.070 mmol, 1 mol %) of $PdCl_2(PPh_3)_2$ and 13.3 mg (0.070 mmol, 1 mol %) of CuI. To this was added 50 mL of dry Et_2NH followed by 2.08 mL (14.7 mmol) of TMSA. The resulting yellow suspension was heated to 55 °C under nitrogen for 52 hours, and then at 75 °C for 5 hours. The salts were removed from the solution by filtration and washed with hexane (2 x 20 mL with sonication) and the solvent removed from the combined washings under vacuum. The solids were passed through a short silica column with DCM and the first orange fraction collected. The solvent was then removed leaving a grainy orange powder (2.29 g) that was then recrystallised from hot methanol to give 1.50 g (4.70 mmol, 67 %) of orange crystalline 1,4-bis(trimethylsilyl)ethynyl naphthalene.

^1H NMR ($CDCl_3$, 500 MHz) δ /ppm: 0.39 (s, TMS), 7.65 (dd, J_{HH} = 6.3 Hz, J_{HH} = 3.3 Hz), 7.68 (s), 8.41 (dd, J_{HH} = 6.3 Hz, J_{HH} = 3.3 Hz). $^{13}C\{^1H\}$ NMR ($CDCl_3$, 125.8 MHz) δ /ppm: 0.22 (s, TMS), 101.34 (s, alkyne), 102.74 (s, alkyne), 121.49 (s), 126.51 (s), 127.21 (s), 129.94 (s), 133.03 (s).

Br-$C_{10}H_6$-4-C≡C($SiMe_3$), **38**

Procedure modified from Ganesh *et al.*[171]

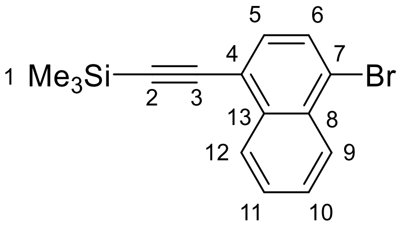

To an oven and flame dried Schlenk flask was added 500 mg (1.50 mmol) of 1-bromo,4-iodonaphthalene, 14 mg (0.020 mmol) of $PdCl_2(PPh_3)_2$ and 4 mg (0.020 mmol) of CuI. To this was added 8 mL of dry THF and 2 mL of dry Et_2NH followed by 0.17 mL (1.65 mmol) of TMSA. The resulting yellow solution was stirred at room temperature under nitrogen for 3 hours. The reaction was quenched with ether, filtered through a silica plug and the solvent removed under vacuum. This was purified by column chromatography with hexane and ether 3%, the first colourless fraction was collected, and the solvent was then removed leaving a pale-yellow oil (390 mg, 1.29 mmol, 86 %)

^1H NMR ($CDCl_3$, 500 MHz) δ /ppm: 0.34 (s, 9H, H^1), 7.53 (d, *J* = 7.7 Hz, 1H, H^{12}), 7.62 (m, 2H, $H^{10/11}$), 7.73 (d, *J* = 7.7 Hz, 1H, H^9), 8.24 (m, 1H, H^5), 8.35 (m, 1H, H^6). $^{13}C\{^1H\}$ NMR ($CDCl_3$, 125.8 MHz) δ /ppm: 0.17 (TMS CH_3), 100.87 (C^2), 102.39 (C^3), 121.06 (C^6), 124.01 (C^4), 126.94 (C^5), 127.65 (C^6), 127.75 ($C^{10/11}$), 127.93 ($C^{10/11}$), 129.46 (C^9), 130.92 (C^{12}), 131.84 (C^{13}), 134.55 (C^8). ESI(+)-MS (*m/z*): Calculated for $[M]^+$ ($[C_{15}H_{15}BrSi]^+$) 302.0129. Observed for [M] 302.0119

$(SiMe_3)C{\equiv}C\text{-}C_{10}H_6\text{-}4\text{-}C{\equiv}C(CH_3)_2OH$, **39**

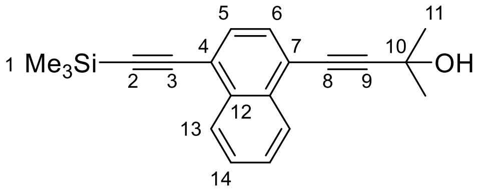

To an oven and flame dried Schlenk flask was added 1 g (3.29 mmol) of 1-bromo, 4(trimethylsilyl)ethynylnaphthalene, 28 mg (0.04 mmol) of $PdCl_2(PPh_3)_2$ and 8 mg (0.04 mmol) of CuI. To this was added 5 mL of dry THF and 10 mL of dry Et_2NH followed by 0.32 mL (3.33 mmol) of 2-methyl-3-butyn-2-ol. The yellow solution turned orange then brown quickly and was heated to reflux under nitrogen for 20 hours. The reaction was quenched with ether, filtered through a silica plug and the solvent removed under vacuum. The orange oil was purified by column chromatography with hexane and ether 2%, the second orange fraction was collected, and the solvent was then removed leaving a yellow/orange solid (940 mg, 3.07 mmol, 93 %)

IR (ATR, cm^{-1}): 2145 (C≡C), 3345 (br, OH). ^1H NMR ($CDCl_3$, 500 MHz) δ /ppm: 0.33 (s, 9H, H^1), 1.74 (s, 6H, H^{11}), 7.60 (m, 4H), 8.27 (m, 1H, H^6), 8.34 (m, 1H, H^5). $^{13}C\{^1H\}$ NMR ($CDCl_3$, 125.8 MHz) δ /ppm: 0.15 (TMS CH_3, C^1), 31.70 (CH_3, C^{11}), 66.01 (C^{10}), 80.19 (C^8), 100.87 (C^9), 101.36 (C^2), 102.85 (C^3), 121.27 (quat-C), 121.46 (C-H), 126.47 (C-H), 126.79 (C^5), 127.32 (C-H), 127.37 (C-H), 129.78 (C-H), 130.12 (C-H), 133.04 (quat-C), 133.22 (quat-C).

$Ru(C\equiv CC_{10}H_6$-4-$C\equiv C(CH_3)_2OH)(dppe)Cp^*$, **40**

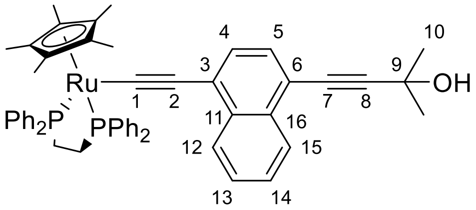

To an oven and flame dried Schlenk flask was added 201 mg (0.300 mmol) of RuCl(dppe)Cp*, 100 mg (0.326 mmol) of 4-[(trimethylsilyl)ethynyl]-1-(3-hydroxyl-3-methylbutynyl)naphthalene, 25 mg (0.430 mmol) of potassium fluoride and 12 mL of dry methanol. The reaction was stirred under nitrogen at reflux for 4 hours during which time an orange powder was formed. The suspension was filtered and washed with cold methanol leaving a yellow solution and 237 mg (0.268 mmol, 89 %) of orange microcrystalline powder.

IR (ATR, cm^{-1}): 2047 (C≡C), 3284 (OH). ^{1}H NMR ($CDCl_3$, 500 MHz) δ /ppm: 1.62 (s, 15H, Cp*), 1.71 (s, 6H, H^{10}), 2.14 (m, dppe), 2.75 (m, dppe), 6.66 (d, *J* = 7.6 Hz, 1H, H^4), 7.02 (m, 1H, H^{14}), 7.04 (m, dppe), 7.21- 7.37 (m, dppe), 7.33 (m, 1H, H^5), 7.38 (m, 1H, H^{12}), 7.71 (d, *J* = 8.3 Hz, 1H, H^{15}), 7.76 (t, *J* = 8.4 Hz, dppe), 8.11 (d, *J* = 8.3 Hz, 1H, H^{13}). ^{13}C{^{1}H} NMR ($CDCl_3$, 125.8 MHz) δ /ppm: 10.27 (Cp* CH_3), 29.54 (dppe), 31.94 (C^{10}), 66.13 (C^9), 81.75 (C^7), 93.04 (Cp*), 97.88 (C^8), 109.84 (C^2), 113.39 (C^2), 124.91 (C^{14}), 125.56 (C^{13}), 125.99 (C^5), 127.17 (C^4), 127.60 (t, dppe), 128.40 (C^{15}), 128.95 (C^{12}), 129.12 (dppe), 130.08 (m, C^1), 130.46 (C^6), 133.31 (t, dppe), 133.49 (C^{16}), 133.79 (t, dppe), 133.97 (C^{11}). ^{31}P{^{1}H} NMR ($CDCl_3$ 243 MHz) δ /ppm: 80.94. ESI(+)-MS (*m/z*): Calculated for $[M]^+$ ($[C_{53}H_{52}OP_2Ru]^+$) 868.2537. Observed for [M+H] 869.2791 (Calculated 869.2610).

$RuCl(C{\equiv}CC_{10}H_6\text{-}4\text{-}C{\equiv}CSiMe_3)(dppe)_2$, **42**

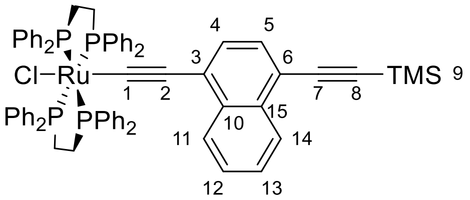

A 1.6 M commercial solution of MeLi in Et_2O (1.09 mmol) was added dropwise to a cooled solution (−78 °C) of 1,4-diethynyl(trimethylsilyl)naphthalene (350 mg, 1.09 mmol) in 20 mL of THF. The solution was stirred for 1 hour at −78 °C and then 2 hours at room temperature (r.t.). This solution was then added to a suspension of *cis*-$(dppe)_2RuCl_2$ (1.06 g, 1.09 mmol) in 20 mL of THF with an immediate yellow to brown colour change and was stirred overnight at r.t. The reaction was filtered, and the solvent was removed *in vacuo*. The crude product was dissolved in DCM and purified via column chromatography (Florisil) with diethylether with the second, purple fraction collected. This yielded a orange powder which purified by column (Al_2O_3) using hexane to elute an impurity followed by DCM to elute product. The solvent was removed by vacuum giving an orange solid (40 mg, 0.034 mmol, 3 %).

^1H NMR (CD_2Cl_2, 500 MHz, 295 °C) δ /ppm: 0.35 (s, 9H, H^9), 2.76 (dppe), 2.86 (dppe), 6.61 (d, *J* = 7.6 Hz, 1H, H^4), 6.87 (t, *J* = 7.1 Hz, dppe), 6.90* (1H, H^{13}), 7.00 (t, *J* = 7.1 Hz, dppe), 7.10 (t, *J* = 7.1 Hz dppe), 7.20 (m, dppe), 7.36 (m, 1H, H^{14}), 7.38 (m, 1H, H^{11}), 7.42 (d, *J* = 7.5 Hz, 1H, H^5), 7.62 (br s, dppe), 8.17 (d, *J* = 8.4 Hz, 1H, H^{12}). $^{13}C\{^1H\}$ NMR (CD_2Cl_2, 125.8 MHz, 295 °C) δ /ppm: 2.40 (TMS, C^9), 30.10 (dppe), 30.75 (dppe), 98.94 (C^8), 104.86 (C^7), 114.16 (C^3), 115.15 (C^2), 125.28 (C^{13}), 125.82 (C^{12}), 126.36 (C^{11}), 127.75 (C^4), 127.30 (s, dppe), 127.75 (s, dppe), 128.28 (C^{14}), 129.27 (C^{15}), 129.77 (C^{10}), 129.15 (s, dppe), 129.60 (s, dppe), 130.89 (C^5), 133.90 (C^6), 134.62 (s, dppe), 134.83 (s, dppe), 136.14 (m, dppe), 136.73 (m, dppe), 138.72 (m, C^1). $^{31}P\{^1H\}$ NMR (CD_2Cl_2, 243 MHz, 295 °C) δ /ppm: 48.05. ESI(+)-MS (*m/z*): Calculated for $[M]^+$ ($[C_{69}H_{63}ClP_4RuSi]^+$) 1180.2382. Observed for [M-Cl] 1145.2680 (Calculated 1145.2687).

* Completely obscured by the triplet at 6.87 assigned to dppe and identified by COSY, HSQC and HMBC correlations.

Ru(C≡CC$_{10}$H$_6$-4-C≡CSiMe$_3$)(dppe)Cp*, **36**

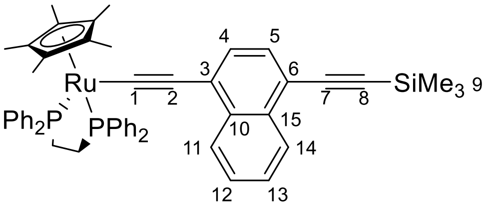

A 1.6 M commercial solution of MeLi in Et$_2$O (2.96 mmol) was added dropwise to a cooled solution (−78 °C) of 1,4-diethynyl(trimethylsilyl)naphthalene (950 mg, 2.96 mmol) in 7 mL of THF. The solution was stirred for 1 hour at −78 °C and then 2 hours at room temperature (r.t.). Meanwhile RuCl(dppe)Cp* (1.8 g, 1.34 mol) was stirred with AgBF$_4$ (270 mg, 1.35 mol) in 10 mL of THF, which had turned from a red solution to a green suspension and while stirring for 15 minutes at room temperature. The addition of the alkyne to the metal caused an immediate colour change to an orange/brown solution and was stirred for 30 mins. The solvent was removed *in vacuo* and the crude product was dissolved in DCM and purified via column chromatography (Florisil) using hexane to remove the free alkyne and Et$_2$O for the orange product. Solvent was removed *in vacuo* yielding an orange powder (884 mg, 1.00 mmol, 34 %). Contains RuCl(dppe)Cp* impurity, 40%.

^{1}H NMR (CD$_2$Cl$_2$, 500 MHz, 295 °C) δ /ppm: 0.30 (s, 9H, H^9), 1.41 (s, 15H, Cp*), 2.12 (dppe), 2.60 (dppe), 6.64 (d, *J* = 7.4 Hz, 1H, H^{11}), 7.05 (m, H^4), 7.18 (t, *J* = 8.3 Hz, dppe), 7.30 (app. t, dppe), 7.32 (d, *J* = 7.4 Hz, H^{12}), 7.36 (app. d, H^{13}), 7.39 (app. t, dppe), 7.66 (app, t, dppe), 7.69 (m, H^5), 7.76 (t, *J* = 8.3 Hz, dppe), 8.11 (d, *J* = 8.3 Hz, 1H, H^{14}). ^{13}C{^{1}H} NMR (CD$_2$Cl$_2$, 125.8 MHz, 295 °C) δ /ppm: 1.30 (TMS, C^9), 9.90 (CH$_3$ Cp*), 28.66 (dppe), 29.75 (dppe), 89.44 (Cp*), 93.30 (C^8), 108.91 (C^7), 110.24 (C^2), 113.76 (C^3), 125.23 (C^4), 125.86 (C^{14}), 126.39 (C^{13}), 127.38 (C^{11}), 127.76 (s, dppe), 127.97 (s, dppe), 128.30 (C^{12}), 128.50 (C^5), 129.148 (s, dppe), 133.42 (C^{15}), 133.56 (s, dppe), 133.83 (C^{10}), 134.09 (s, dppe), 134.31 (s, dppe), 135.24 (C^6), 135.64 (m, dppe), 137.46 (m, C^1), 139.23 (m, dppe). ^{31}P{^{1}H} NMR (CD$_2$Cl$_2$, 243 MHz, 295 °C) δ /ppm: 80.85, 75.19 (RuCl(dppe)Cp*). ESI(+)-MS (*m/z*): Calculated for [M]$^+$ ([C$_{53}$H$_{55}$P$_2$RuSi]$^+$) 883.2586. Observed for [M] 883.2646.

[Ru(=C=C(H)$C_{10}H_6$-4-C≡$CSiMe_3$)(dppe)Cp*]BF_4, **43**

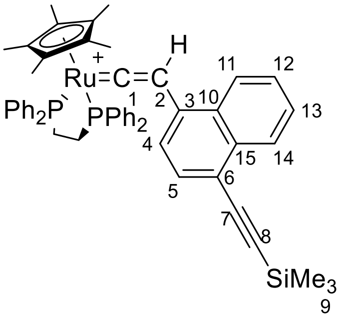

To 7.5 mg (0.0085 mmol) of Ru(4-ethynyl-7-(trimethylsilyl)-2,1,3-benzothiadiazole)(dppe)Cp* dissolved in DCM-*d* was added $HBF_4.OEt_2$ (1 drop) where an immediate colour change from orange to yellow was observed. NMR spectra were then recorded after 1 hour at which time full conversion had been achieved.

^{1}H NMR (CD_2Cl_2, 500 MHz, 295 °C) δ /ppm: 0.33 (s, H^9), 1.61 (t, *J* = 1.7 Hz, H^2), 1.71 (s, Cp*), 2.21 (dppe), 3.02 (dppe), 6.19 (d, *J* = 7.6 Hz, H^4), 6.34 (d, *J* = 7.7 Hz, H^{11}), 7.02 (d, *J* = 7.6 Hz, H^5), 7.12 (app. t, dppe), 7.20 (app. d, H^{12}), 7.55 (app. d, H^{13}), 7.40 (app, t, dppe), 7.49 (app. t, dppe), 7.57 (app. t, dppe), 8.26 (d, *J* = 8.9 Hz, 1H, H^{14}). $^{13}C\{^1H\}$ NMR (CD_2Cl_2, 125.8 MHz, 295 °C) δ /ppm: 0.12 (TMS, C^9), 10.46 (CH_3 Cp*), 27.82 (dppe), 30.02 (dppe), 100.33 (C^8), 104.15 (Cp*), 107.1 (C^7), 111.53 (C^2), 120.94 (C^3), 124.50 (C^6), 125.00 (C^{12}), 126.37 (C^4), 126.75 (C^{11}), 127.10 (C^{14}), 128.89 (s, dppe), 129.34 (s, dppe), 130.00 (s, dppe), 131.18 (C^5), 131.73 (s, dppe), 131.88 (C^{15}), 132.06 (s, dppe), 132,67 (s, dppe), 132.55 (s, dppe), 132.83 (s, dppe), 133.19 (C^{10}), 133.29 (s, dppe), 134.12 (C^{13}). $^{31}P\{^1H\}$ NMR (CD_2Cl_2, 243 MHz, 295 °C) δ /ppm: 72.33

[Ru(=C=C(C_7H_7)$C_{10}H_6$-4-C≡CSiMe$_3$)(dppe)Cp*]BF$_4$, **44**

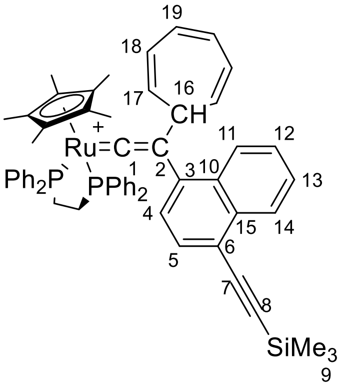

To 7.5 mg (0.0085 mmol) of Ru(4-ethynyl-7-(trimethylsilyl)-2,1,3-benzothiadiazole)(dppe)Cp* dissolved in DCM-*d* was added [C_7H_7]BF$_4$ (1.5 mg, 0.0085 mmol) where an immediate colour change from orange to yellow was observed. NMR spectra were then recorded after 1 hour at which time full conversion had been achieved.

^{1}H NMR (CD_2Cl_2, 500 MHz, 295 °C) δ /ppm: 0.38 (s, H^9), 1.72 (s, Cp*), 1.78 (s, H^{16}), 2.39 (dppe), 2.79 (dppe), 6.16 (d, J_{HH} = 7.5 Hz, H^4), 6.25 (app. dd, H^{17}), 6.37 (t, J_{HH} = 3.0 Hz, H^{18}), 6.70 (t, J_{HH} = 3.0 Hz, H^{19}), 6.97 (d, J_{HH} = 7.5 Hz, H^5), 7.05 (app. d, H^{11}), 7.15 (d, dppe), 7.25 (app. d, H^{12}), 7.30 (app. t, dppe), 7.35 (app, t, dppe), 7.44 (t, J_{HH} = 7.0 Hz, dppe), 7.50 (app. d, H^{13}), 7.65 (app. t, dppe), 7.97 (d, J_{HH} = 7.0 Hz, 1H, H^{14}). ^{13}C{^{1}H} NMR (CD_2Cl_2, 125.8 MHz, 295 °C) δ /ppm: 0.20 (TMS, C^9), 10.69 (CH_3 Cp*), 30.08 (dppe), 35.23 (C^{16}), 100.37 (C^8), 103.20 (C^7), 104.11 (Cp*), 124.40 (C^3), 125.28 (C^2), 125.89 (C^4), 126.00 (C^{17}), 127.08 (C^{14}), 127.84 (s, dppe), 128.07 (s, dppe), 128.90 (C^{13}), 129.54 (s, dppe), 130.00 (C^{11}), 131.20 (C^{18}), 131.89 (C^{19}), 132.27 (C^5), 133.37 (s, dppe), 134.77 (C^{12}). ^{31}P{^{1}H} NMR (CD_2Cl_2, 243 MHz, 295 °C) δ /ppm: 71.67.

[Ru(=C=C(H)$C_{10}H_6$-indene-3-(Ph)$_2$)(dppe)Cp*]BF_4, **45**

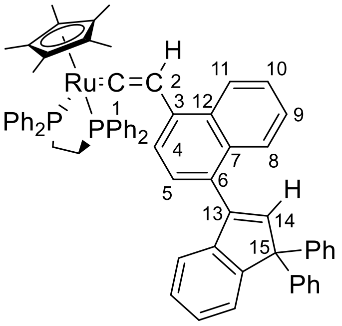

To 7.5 mg (0.0085 mmol) of Ru(4-ethynyl-7-(trimethylsilyl)-2,1,3-benzothiadiazole)(dppe)Cp* dissolved in DCM-*d* was added [CPh_3]BF_4 (3 mg, 0.0085 mmol) where an immediate colour change from orange to green/brown was observed. NMR spectra were then recorded after 1 hour at which time full conversion had been achieved.

^{1}H NMR (CD_2Cl_2, 500 MHz, 295 °C) δ /ppm: 1.76 (s, Cp*), 2.49 (dppe), 3.15 (dppe), 5.03 (app. t, H^2), 5.56 (s, H^{14}), 6.17 (d , J_{HH} = 7.5 Hz, H^4), 6.41 (t, J_{HH} = 7.4 Hz, H^9), 6.96 (app. d, H^{11}), 6.98 (d, J_{HH} = 7.5 Hz, H^5), 7.12 (d, J_{HH} = 7.2 Hz, Ph), 7.21 (t, J_{HH} = 7.4 Hz, Ph/dppe), 7.28 (m, H^{10}), 7.29 (app. t, Ph), 7.34 (m, Ph/dppe), 7.40 (app. t, Ph/dppe), 7.52 (m, Ph/dppe), 7.91 (d, J_{HH} = 7.8 Hz, H^8). ^{13}C{^{1}H} NMR (CD_2Cl_2, 125.8 MHz, 295 °C) δ /ppm: 10.36 (CH_3 Cp*), 29.65 (dppe), 57.21 (C^{14}), 104.12 (Cp*), 107.65 (C^2), 118.83 (C^3), 126.68 (C^4 and C^9), 128.26 (s, Ph/dppe), 128.53 (C^{10}), 128.67 (s, Ph/dppe), 129.02 (t, Ph/dppe), 129.17 (C^8), 129.34 (C^6), 129.52 (C^{11}), 129.72 (C^{13}), 131.82 (m, Ph/dppe), 132.08 (s, Ph/dppe), 132.26 (C^5), 132.76 (s, Ph/dppe), 133.19 (s, Ph/dppe), 134.37 (t, Ph/dppe), 135.14 (C^{12}), 135.52 (C^7), 144.37 (C^{15}), 352.0 (C^1). ^{31}P{^{1}H} NMR (CD_2Cl_2, 243 MHz, 295 °C) δ /ppm: 72.36.

Synthesis and characterisation of benzothiadiazole spaced compounds

$(SiMe_3)C{\equiv}CC_6H_2(NSN)$-4-$C{\equiv}C(SiMe_3)$[176,213]

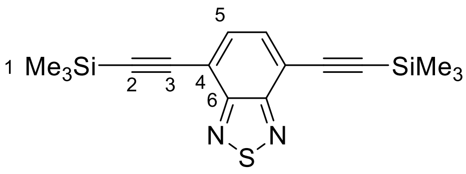

To an oven and flame dried Schlenk flask was added 500 mg (1.70 mmol) of 4,5-dibromo-2,1,3-benzothiadiazole, 6.27 mg (0.009 mmol, 0.5 mol %) of $PdCl_2(PPh_3)_2$, 6.27 mg (0.033 mmol, 5 mol %) of CuI and 22 mg of PPh_3. To this was added 10 mL of dry NEt_3 followed by 0.5 mL (4.5 mmol) of TMSA. The resulting yellow suspension was heated to reflux under nitrogen for 16 hours. The solvent was removed under vacuum. It was purified by column chromatography (diethylether) under nitrogen and the first yellow spot collected. The solvent was then removed by vacuum yielding 488 mg (1.49 mmol, 88 %) of yellow/orange microcrystalline 4,5-[di(trimethylsilyl)ethynyl]-2,1,3-benzothiadiazole. Stored at 0 °C.

^1H NMR ($CDCl_3$, 500 MHz) δ /ppm: 0.07 (TMS, 18H), 7.29 (C-H, 2H). $^{13}C\{^1H\}$ NMR ($CDCl_3$, 125.8 MHz) δ /ppm: 0.01 (TMS), 100.11 (C^2), 103.76 (C^3), 117.39 (C^4), 133.27 (C^5), 154.34 (C^6).

Characterisation matches literature.[176,213]

{Ru(dppe)Cp*}$_2$(C≡CC$_6$H$_2$(NSN)-4-C≡C), **48**

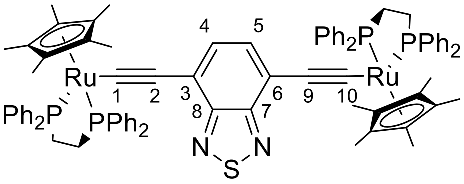

To an oven and flame dried Schlenk flask was added 100 mg (0.149 mmol) of RuCl(dppe)Cp*, 52 mg (0.16 mmol) of 4,5-di(trimethylsilylethynyl)-2,1,3-benzothiadiazole, 12 mg (0.16 mmol) of potassium fluoride, 1 mL of NEt$_3$ and 15 mL of dry methanol. The reaction was stirred under nitrogen at reflux for 2 hours during which the solution changed from orange to dark blue and a dark blue/black powder was formed. The suspension was filtered and washed with methanol leaving a purple solution and 34 mg (0.0234 mmol, 31 %) of dark blue powder.

IR (nujol, cm^{-1}): 2062 (C≡C). ^{1}H NMR (CDCl$_3$, 500 MHz) δ /ppm: 1.60 (s, 30H, Cp*), 1.62 (s shoulder, Cp*), 2.17 (m, dppe), 2.95 (m, dppe), 6.76 (d, J_{HH} = 7.7 Hz, 1H, H^4), 7.01 (app t, dppe), 7.20 (t, J = 7.9 Hz, dppe), 7.28 (app t, dppe), 7.34 (app t, dppe), 7.46 (d, J_{HH} = 7.7 Hz, 1H, H^5), 7.58 (app t, dppe), 7.79 (m, dppe). ^{13}C{^{1}H} NMR (CDCl$_3$, 125.8 MHz) δ /ppm: 10.05 (Cp* CH$_3$), 10.22 (Cp* CH$_3$), 29.51 (dppe), 29.70 (dppe), 29.88 (dppe), 93.50 (Cp*), 93.67 (Cp*), 99.65 (C$^{2/9}$), 104.98 (C$^{2/9}$), 124.23 (C$^{6/3}$), 127.31 (t, dppe), 127.62 (t, dppe), 127.90 (C^4), 128.97 (dppe), 129.16 (dppe), 132.54 (m, C$^{1/10}$), 132.81 (m, C$^{1/10}$), 132.80 (C^5), 133.34 (t, dppe), 133.74 (t, dppe), 153.53 (C^7), 156.38 (C^8). ^{31}P{^{1}H} NMR (CDCl$_3$ 243 MHz) δ /ppm: 80.64. ESI(+)-MS (*m/z*): Calculated for [M]$^+$ ([C$_{82}$H$_{80}$N$_2$P$_4$P$_4$Ru$_2$S]$^+$) 1452.3080. Observed for [M] 1452.3467

$(SiMe_3)C{\equiv}CC_6H_2(NSN)\text{-}4\text{-}C{\equiv}C(CH_3)_2OH$[177], **50**

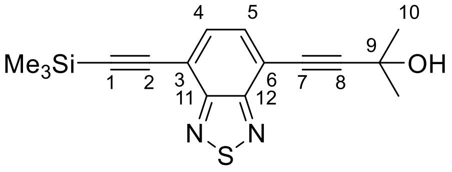

To an oven and flame dried Schlenk flask was added 1 g (3.4 mmol) of 4,5-dibromo-2,1,3-benzothiadiazole, 70 mg (0.10 mmol, 0.5 mol %) of $PdCl_2(PPh_3)_2$ and 19 mg (0.10 mmol, 5 mol %) of CuI. To this was added 30 mL of dry NEt_3 and was heated to reflux. Then 0.1 mL (1.00 mmol) of 2-methyl-2-butyn-2-ol was added to the hot yellow solution and heating resumed for 50 mins. The solvent was removed under vacuum. It was purified by column chromatography, hexane/diethylether (7:3), the second spot was collected and dried. The resulting solid was dissolved in acetone giving a yellow solution and remaining pink/white starting material filtered off. 260 mg (0.88 mmol) of white/pink starting material was recovered, and 570 mg of yellow powder was collected. Product 80% pure by NMR, remaining compound is unreacted 4,5-dibromo-2,1,3-benzothiadiazole. Impure product used in further reactions.

To an oven and flame dried Schlenk flask was added 750 mg (2.52 mmol if pure, but here ~1.91 mmol) of impure 4,5-dibromo-2,1,3-benzothiadiazole, 50 mg (0.071 mmol, 0.5 mol %) of $PdCl_2(PPh_3)_2$ and 14 mg (0.074 mmol, 5 mol %) of CuI. To this was added 30 mL of dry NEt_3 and 3 mL of dry THF followed by 0.55 mL (4.00 mmol) of TMSA was added and heated to reflux for 32 hours. The solvent was removed under vacuum. It was purified by column chromatography, hexane: diethylether (7:3), the second spot was collected and dried. The resulting solid was dissolved in acetone giving a yellow solution and remaining pink/white starting material filtered off. 260 mg (0.608 mmol) of bis-TMSA-benzothiadiazole was recovered, and 400 mg (1.27 mmol, 67 %) of yellow powder was collected.

IR (nujol, cm^{-1}): 2148 (C≡C), 2158 (C≡C), 3468 (OH). ^1H NMR ($CDCl_3$, 500 MHz) δ /ppm: 0.33 (s, 9H, TMS), 1.69 (s, 6H, H^{10}), 7.64 (d, J_{HH} = 7.35 Hz, 1H, H^4), 7.70 (d, J_{HH} = 7.35

Hz, 1H, H^5). $^{13}C\{^1H\}$ NMR ($CDCl_3$, 100.6 MHz) δ /ppm: 0.01 (s, C^{TMS}), 31.46 (C^{10}), 65.95 (C^9), 78.11 (C^7), 100.05 (C^2), 102.17 (C^8), 103.62 (C^1), 117.09 (s, C^3), 117.19 (C^6), 132.58 (C^5), 133.30 (C^4), 154.36 ($C^{11/12}$).

Ru(C≡CC$_6$H$_2$(NSN)-4-C≡C(CH$_3$)$_2$OH)(dppe)Cp*, **51**

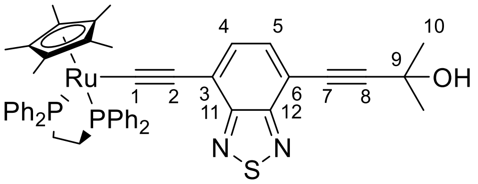

To an oven and flame dried Schlenk flask was added 300 mg (0.447 mmol) of RuCl(dppe)Cp*, 180 mg (0.570 mmol) of 4-[(trimethylsilyl)ethynyl]-5-(3-hydroxyl-3-methylbutynyl)-2,1,3-benzothiadiazole, 33 mg (0.520 mmol) of potassium fluoride and 10 mL of dry methanol. The reaction was stirred under nitrogen at reflux for 4 hours during which the solution changed from orange to blue and a dark blue/black powder was formed. The suspension was chilled to 0 °C before being filtered and washed with a minimum of ice-cold methanol leaving a purple solution and 301 mg (0.337 mmol, 75 %) of dark blue/black powder.

IR (ATR, cm^{-1}): 1964 (C≡C), 2035 (C≡C), 3374 (OH). ^{1}H NMR (CDCl$_3$, 400 MHz) δ /ppm: 1.61 (s, 15H, Cp*), 1.69 (s, 6H, H^{10}), 2.17 (m, dppe), 2.41 (s, 1H, OH), 2.98 (m, dppe), 6.87 (d, J_{HH} = 7.5 Hz, 1H, H^4), 7.18 (m, dppe), 7.31 (app. t, dppe), 7.34 (m, dppe), 7.40 (d, J_{HH} = 7.5 Hz, 1H, H^5), 7.78 (t, J_{HH} = 7.8 Hz, dppe). ^{13}C{^{1}H} NMR (CDCl$_3$, 100.6 MHz) δ /ppm: 10.24 (Cp* CH$_3$), 29.47 (dppe), 31.75 (C^{10}), 66.04 (C^9), 79.77 (C^7), 93.63 (Cp*), 98.35 (C^8), 107.91 (C^2), 112.24 (C^3), 125.15 (C^6), 127.29 (t, dppe), 127.16 (C^4), 127.62 (t, dppe), 128.97 (dppe), 128.97 (dppe), 129.18 (dppe), 133.37 (t, dppe), 133.69 (t, dppe), 134.25 (C^5), 138.5 (m, C^1), 155.26 (C^{12}), 156.37 (C^{11}). ^{31}P{^{1}H} NMR (CDCl$_3$, 162 MHz) δ /ppm: 80.69. ESI(+)-MS (*m/z*): Calculated for [M]$^+$ ([C$_{49}$H$_{48}$N$_2$OP$_2$RuS]$^+$) 876.2001. Observed for [M+H] 877.2115 (Calculated 8177.2079).

$RuCl(C{\equiv}CC_6H_2(NSN)\text{-}4\text{-}C{\equiv}CSiMe_3)(dppe)_2$, **53**

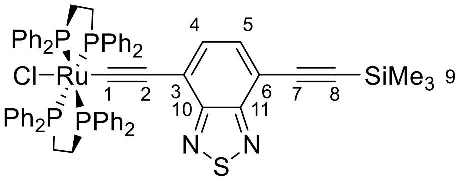

A 1.6 M commercial solution of MeLi in Et_2O (1.2 mmol) was added dropwise to a cooled solution (−78 °C) of 4,5-[di(trimethylsilyl)ethynyl]-2,1,3-benzothiadiazole (500 mg, 1.52 mmol) in 20 mL of THF. The solution was stirred for 1 hour at −78 °C with a yellow to red colour change and then 2 hours at room temperature (r.t.) after which it was light brown. This solution was then added to a suspension of *cis*-$(dppe)_2RuCl_2$ (755 mg, 0.780 mmol) in 20 mL of THF and was stirred overnight at r.t over which time the solution turned dark purple. The reaction was filtered, and the solvent was removed *in vacuo*. The crude product was washed with pentane then dissolved in THF and purified via column chromatography (Al_2O_3) using hexane to elute an impurity followed by DCM to elute product. This yielded a purple powder (40 mg, 0.067 mmol, 8 %).

^1H NMR (CD_2Cl_2, 500 MHz, 295 °C) δ /ppm: 0.33 (s, 9H, H^9), 2.76 (dppe), 3.06 (dppe), 5.88 (d, *J* = 7.5 Hz, 1H, H^4), 6.68 (t, *J* = 7.6 Hz, dppe), 7.01 (t, *J* = 7.4 Hz, dppe), 7.09 (t, *J* = 7.1 Hz dppe), 7.12 (m, dppe), 7.12 (m, dppe), 7.27 (t, *J* = 7.4 Hz, dppe), 7.40 (d, *J* = 7.5 Hz, 1H, H^5), 7.57 (m, dppe).$^{13}C\{^1H\}$ NMR (CD_2Cl_2, 125.8 MHz, 295 °C) δ /ppm: 0.30 (TMS, C^9), 30.90 (dppe), 99.55 (C^8), 102.64 (C^7), 108.92 (C^2), 115.61 (C^1), 124.41 (C^3), 127.39 (s, dppe), 127.40 (s, dppe), 129.73 (C^4), 128.86 (s, dppe), 129.63 (s, dppe), 134.59 (C^5), 134.79 (C^6), 134.02 (s, dppe), 135.10 (s, dppe), 136.25 (m, dppe), 136.50 (m, dppe), 155.51 (C^{11}), 156.60 (C^{10}). $^{31}P\{^1H\}$ NMR (CD_2Cl_2, 243 MHz, 295 °C) δ /ppm: 47.83. ESI(+)-MS (*m/z*): Calculated for $[M]^+$ ($[C_{69}H_{63}ClP_4RuSi]^+$) 1188.1951. Observed for [M-Cl] 1153.2221 (Calculated 1153.2157).

Ru(C≡C-C_6H_2(NCN)-4-C≡CSiMe$_3$)(dppe)Cp*, **54**

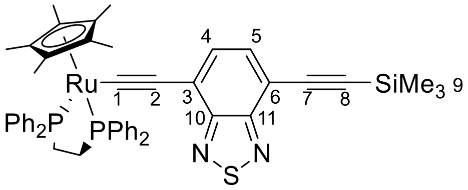

A 1.6 M commercial solution of MeLi in Et_2O (0.383 mmol) was added dropwise to a cooled solution (−78 °C) of 4,5-[di(trimethylsilyl)ethynyl]-2,1,3-benzothiadiazole (126 mg, 0.383 mmol) in 7 mL of THF. The solution was stirred for 1 hour at −78 °C and then 2 hours at room temperature (r.t.). Meanwhile RuCl(dppe)Cp* (228 mg, 0.415 mmol) with $AgBF_4$ (88 mg, 0.452 mmol) in 7 mL of THF, which had turned from a red solution to a green suspension and was stirred for 15 minutes at room temperature. The addition of the alkyne to the metal caused an immediate colour change to a green solution and was stirred for 30 mins. The solvent was removed *in vacuo* and the crude product was dissolved in DCM and purified via column chromatography (Florisil) using Et_2O, the first brown fraction was discarded, and the second purple fraction collected. This yielded a blue/black powder (74 mg, 0.083 mmol, 24 %). Contains RuCl(dppe)Cp* impurity.

IR (ATR, cm^{-1}): 1970 (C≡C), 2037 (M-C≡C). ^{1}H NMR (CD_2Cl_2, 500 MHz, 295 °C) δ /ppm: 0.33 (s, 9H, H^9), 1.41 (s, Cp*), 2.11 (dppe), 2.60 (dppe), 6.91 (d, *J* = 7.5 Hz, 1H, H^4), 7.19 (t, *J* = 8.2 Hz, dppe), 7.32 (t, *J* = 8.2 Hz, dppe), 7.36 (app. t, dppe), 7.39 (m, dppe), 7.44 (d, *J* = 7.5 Hz, 1H, H^5), 7.53 (app. t, dppe), 7.59 (app. t, dppe), 7.67 (m, dppe) ^{13}C{^{1}H} NMR (CD_2Cl_2, 125.8 MHz, 295 °C) δ /ppm: 0.25 (TMS, C^9), 28.67 (dppe), 30.04 (dppe), 100.45 (C^8), 103.71 (C^7), 113.71 (C^3), 117.54 (C^2), 125.59 (C^6), 127.56 (C^4), 127.76 (s, dppe), 127.98 (s, dppe), 129.47 (s, dppe), 132.52 (t, dppe), 133.52 (t, dppe), 134.31 (s, dppe), 134.99 (C^5), 135.66 (m, dppe), 154.67 (C^{10}), 155.58 (C^{11}). ^{31}P{^{1}H} NMR (CD_2Cl_2, 243 MHz, 295 °C) δ /ppm: 80.56, 75.19 (RuCl(dppe)Cp*). ESI(+)-MS (*m/z*): Calculated for [M]$^+$ ([$C_{49}H_{51}N_2P_2RuSSi$]$^+$) 891.2055. Observed for [M] 891.2093

[Ru(=C=C(H)C_6H_2(NSN)-C≡C$SiMe_3$)(dppe)Cp*]BF_4, **55**

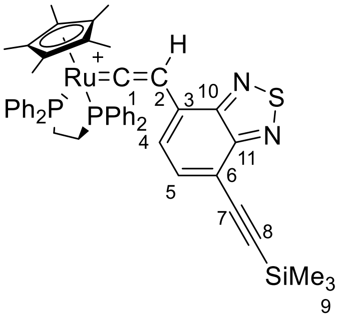

To 7 mg (0.0085 mmol) of Ru(4-ethynyl-7-(trimethylsilyl)-2,1,3-benzothiadiazole)(dppe)Cp* dissolved in DCM-*d* was added $HBF_4.OEt_2$ (1 drop) where an immediate colour change from purple to orange was observed. NMR spectra were then recorded after 1 hour at which time full conversion had been achieved.

^1H NMR (CD_2Cl_2, 500 MHz, 295 °C) δ /ppm: 0.32 (s, 9H, H^9), 1.65 (s, Cp*), 1.72 (app. t, C^2), 2.21 (dppe), 3.20 (dppe), 5.90 (d, *J* = 7.4 Hz, 1H, H^4), 6.82 (m, dppe), 7.06 (d, *J* = 7.4 Hz, 1H, H^5), 7.41 (m, dppe), 7.51 (m, dppe), 7.60 (m, dppe).$^{13}C\{^1H\}$ NMR (CD_2Cl_2, 125.8 MHz, 295 °C) δ /ppm: 0.12 (TMS, C^9), 28.25 (dppe), 30.49 (dppe), 15.42 (CH_3, Cp*), 100.41 (C^7), 103.74 (C^2), 104.15 (Cp*), 104.46 (C^8), 117.57 (C^3), 123.88 (C^6), 124.82 (C^4), 128.89 (s, dppe), 129.14 (s, dppe), 129.68 (s, dppe), 130.00 (s, dppe), 132.83 (m, dppe), 133.29 (s, dppe), 133.52 (s, dppe), 134.24 (C^5), 152.91 (C^{10}), 154.75 (C^{11}). $^{31}P\{^1H\}$ NMR (CD_2Cl_2, 243 MHz, 295 °C) δ /ppm: 71.92. ESI(+)-MS (*m/z*): Calculated for $[M]^+$ ($[C_{49}H_{51}N_2P_2RuSSi]^+$) 891.2055. Observed for [M] 891.2099

[Ru(=C=C(C_7H_7)C_6H_2(NSN)-C≡CSiMe$_3$)(dppe)Cp*]BF$_4$, **56**

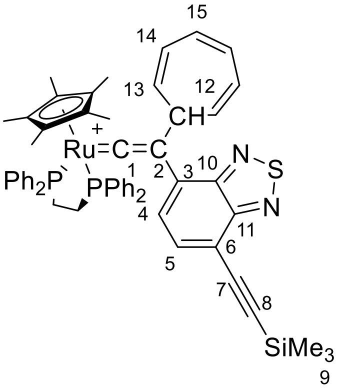

To 7 mg (0.0085 mmol) of Ru(4-ethynyl-7-(trimethylsilyl)-2,1,3-benzothiadiazole)(dppe)Cp* dissolved in DCM-*d* was added [C_7H_7]BF$_4$ (1 mg, 0.0085 mmol) where an immediate colour change from purple to orange was observed. NMR spectra were then recorded after 1 hour at which time full conversion had been achieved.

^{1}H NMR (CD_2Cl_2, 500 MHz, 295 °C) δ /ppm: 0.32 (s, 9H, H^9), 1.50 (s, 1H, H^{12}), 1.71 (Cp*), 2.53 (dppe), 3.04 (dppe), 5.90 (d, J_{HH} = 7.4 Hz, 1H, H^4), 6.18 (dt, J_{HH} = 8.9 Hz, J_{HH} = 3.1 Hz, H^{13}), 6.34 (t, J_{HH} = 3.1 Hz, H^{14}), 6.59 (t, J_{HH} = 3.1 Hz, H^{15}), 7.03 (br. S, dppe), 7.06 (d, J_{HH} = 7.4 Hz, H^5), 7.25 (app. t, dppe), 7.34-7.47 (t, dppe), 7.60 (app. t, dppe). ^{13}C{^{1}H} NMR (CD_2Cl_2, 125.8 MHz, 295 °C) δ /ppm: 4.50 (TMS, C^9), 10.50 (CH$_3$ Cp*), 26.15 (dppe), 30.43 (dppe), 33.64 (C^{12}), 100.44 (C^7), 103.72 (C^2), 104.17 (Cp*), 104.49 (C^8), 117.72 (C^3), 123.68 (C^6), 124.89 (C^4), 130.61 (C^{13}), 131.24 (C^{14}), 132.49 (C^5), 127.74 (s, dppe), 128.37 (s, dppe), 128.97 (s, dppe), 129.56 (s, dppe), 133.26 (app. t, dppe), 133.51 (s, dppe), 133.78 (s, dppe), 154.66 (C^{11}), 155.76 (C^{10}). ^{31}P{^{1}H} NMR (CD_2Cl_2, 243 MHz, 295 °C) δ /ppm: 71.93. ESI(+)-MS (*m/z*): Calculated for [M]$^+$ ([$C_{56}H_{57}N_2P_2RuSSi$]$^+$) 981.2620. Observed for [M] 981.2525

[Ru(=C=C(H)C_6H_2(NSN)-indene-3-$(Ph)_2$)(dppe)Cp*]BF_4, **57**

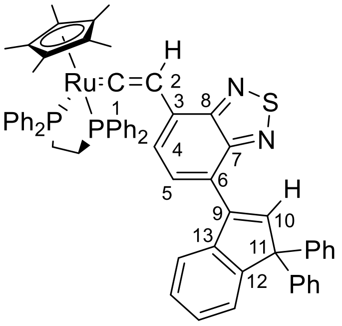

To 7 mg (0.0085 mmol) of Ru(4-ethynyl-7-(trimethylsilyl)-2,1,3-benzothiadiazole)(dppe)Cp* dissolved in DCM-*d* was added $[CPh_3]BF_4$ (3 mg, 0.0085 mmol) where an immediate colour change from purple to brown was observed. NMR spectra were then recorded after 1 hour at which time full conversion had been achieved. Single crystals suitable for X-ray crystallography, were grown by slow diffusion of pentane into a CD_2Cl_2 solution.

^1H NMR (CD_2Cl_2, 500 MHz, 295 °C) δ /ppm: 1.72 (Cp*), 2.50 (dppe), 3.16 (dppe), 5.30 (t, J_{HP} = 1.7 Hz, 1H, H^2), 5.55 (s, 1H, H^{10}), 5.90 (d, J_{HH} = 7.4 Hz, 1H, H^4), 7.07 (d, J_{HH} = 7.4 Hz, 1H, H^5), 7.12 (app. dt, Ph), 7.22 (app. dt, Ph), 7.29 (m, Ph), 7.38 – 7.60 (m, dppe). $^{13}C\{^1H\}$ NMR (CD_2Cl_2, 125.8 MHz, 295 °C) δ /ppm: 10.36 (CH_3 Cp*), 26.16 (dppe), 29.85 (dppe), 57.20 (C^{10}), 104.48 (Cp*), 107.66 (C^2), 117.62 (C^3), 123.16 (C^6), 125.24 (C^4), 126.67 (s, Ph/dppe), 127.58 (s, Ph/dppe), 128.21 (app. t, Ph/dppe), 128.67 (s, Ph/dppe), 129.02 (m, Ph/dppe), 129.40 (C^9), 129.72 (s, Ph), 129.99 (s, Ph/dppe), 131.78 (m, Ph/dppe), 131.99 (s, Ph/dppe), 132.27 (s, Ph/dppe), 132.54 (m, Ph/dppe), 133.32 (s, Ph/dppe), 135.51 (s, Ph/dppe), 133.95 (C^5), 134.37 (s, Ph/dppe), 144.37 (C^{11}), 151.48 (C^8), 154.67 (C^7), 352.7 (C^1). $^{31}P\{^1H\}$ NMR (CD_2Cl_2, 243 MHz, 295 °C) δ /ppm: 71.92.

Synthesis and characterisation of anthracene spaced compounds

Ru(C≡CC$_{14}$H$_8$-10-C≡CSiMe$_3$)Cp(PPh$_3$)$_2$, **59**

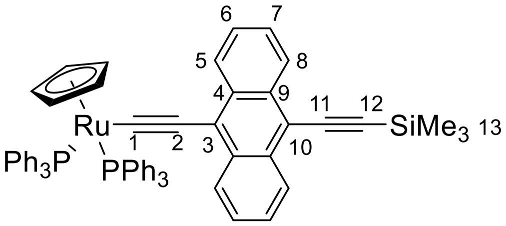

To an oven and flame dried Schlenk flask was added 100 mg (0.137 mmol) of RuCl(PPh$_3$)$_2$Cp, 59 mg (0.160 mmol) of 9,10-diethynyl(trimethylsilyl)anthracene, 10 mg (0.160 mmol) of potassium fluoride and 10 mL of dry methanol. The reaction was stirred under nitrogen at reflux for 6 hours during which the solution changed from orange to purple and a dark purple powder was formed. The suspension was filtered leaving a purple solution and 66 mg (0.067 mmol, 49 %) of dark purple powder.

IR (ATR, cm^{-1}): 2031 (C≡C), 2116 (C≡C). ^{1}H NMR (CDCl$_3$ 500 MHz) δ /ppm: 0.69 (s, TMS), 4.44 (s, Cp), 7.04 – 7.69 (m, dppe) 7.16 (anthracene), 7.44 (anthracene), 8.41 (d, J_{HH} = 8.6 Hz, anthracene), 8.59 (d, J_{HH} = 8.6 Hz, anthracene) . ^{13}C{^{1}H} NMR (CDCl$_3$ 100.6 MHz) δ /ppm: ^{31}P{^{1}H} NMR (CDCl$_3$ 243 MHz) δ /ppm: ESI(+)-MS (*m/z*): Calculated for [M]$^+$ ([C$_{62}$H$_{52}$P$_2$RuSi]$^+$) 988.2357. Observed for [M] 988.2433

Ru(C≡C$C_{14}H_8$-10-C≡C$SiMe_3$)(dppe)Cp*, **60**

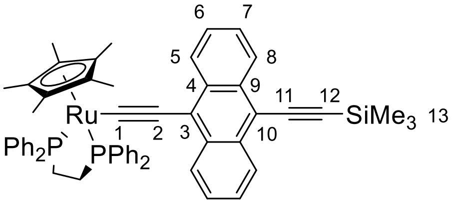

To an oven and flame dried Schlenk flask was added 1 g (1.49 mmol) of RuCl(dppe)Cp*, 1.10 g (2.95 mmol) of 9,10-diethynyl(trimethylsilyl)anthracene, 100 mg (1.60 mmol) of potassium fluoride, 2 mL of NEt_3 and 50 mL of dry methanol. The reaction was stirred under nitrogen at reflux for 6 hours during which the solution changed from orange to purple and a dark purple powder was formed. The suspension was filtered leaving a purple solution and 1.05 g (1.13 mmol, 76 %) of dark purple powder.

IR (ATR, cm^{-1}): 2016 (C≡C), 2119 (C≡C). ^1H NMR ($CDCl_3$ 500 MHz) δ /ppm: 0.38 (s, 9H, $SiMe_3$), 1.67 (s, 15H, Cp*), 6.87 (t, J_{HH} = 7.1 Hz, 2H, $H^{6/7}$), 7.10 – 7.37 (m, dppe), 7.35 (app. t, 2H, $H^{6/7}$), 7.69 (t, dppe), 7.83 (d, J_{HH} = 8.6 Hz, 2H, $H^{5/8}$), 8.39 (d, J_{HH} = 8.6 Hz, 2H, $H^{5/8}$). $^{13}C\{^1H\}$ NMR ($CDCl_3$ 100.6 MHz) δ /ppm: 0.63 ($SiMe_3$, C^{13}), 10.47 (Cp*), 29.6 (dppe), 93.49 (Cp*), 103.84 (C^{12}), 109.20 ($C^{2/11}$), 110.91 ($C^{2/11}$), 123.51 ($C^{6/7}$), 126.15 ($C^{6/7}$), 126.41 ($C^{5/8}$), 127.65 (m, dppe), 128.38 ($C^{3/10}$), 129.12 ($C^{5/8}$), 129.24 (t, dppe), 129.40 (t, dppe), 131.86 ($C^{3/10}$), 133.35 ($C^{4/9}$), 133.46 (t, dppe), 133.55 ($C^{4/9}$) 133.76 (t, dppe), 136.79 (dppe), 136.79 (dppe). $^{31}P\{^1H\}$ NMR ($CDCl_3$ 243 MHz) δ /ppm: 81.13. ESI(+)-MS (*m/z*): Calculated for $[M]^+$ ($[C_{57}H_{56}P_2RuSi]^+$) 932.2670. Observed for [M] 932.2755

Ru(C≡CC$_{14}$H$_8$-10-C≡CH)(dppe)Cp*, **61**

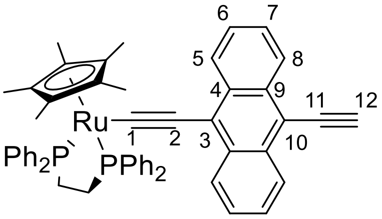

To an oven and flame dried Schlenk flask was added 10 mL of dry THF, 3 ml of MeOH and 100 mg (0.107 mmol) of Ru(C≡CC$_{14}$H$_8$-10-C≡CSiMe$_3$)Cp*(dppe). To this was added 0.75 mL (0.15 mg) of TBAF in THF. The reaction was stirred under nitrogen for 15 hours and the solvent removed by vacuum. The deep purple crude mixture was washed with hexane and methanol. This gave 38 mg (0.044 mmol, 41% yield) of purple powder.

IR (ATR, cm^{-1}): 3298 ν(≡CH), 3051, 2897, 2016. ESI(+)-MS (*m/z*): Calculated for [M]$^+$ ([C$_{60}$H$_{53}$P$_2$Ru]$^+$) 1082.1494. Observed for [M]$^+$ 1088.2131

{Ru(dppe)Cp*}$_2$(C≡CC$_{14}$H$_8$-10-C(=CCPh$_3$)), **62**

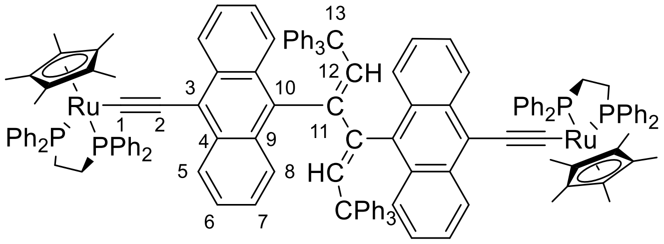

To an oven dried Schlenk flask was added 50 mg (0.053 mmol) of Ru(C≡CC$_{14}$H$_8$-10-C≡CSiMe$_3$)(dppe)Cp*, 4 mL CH$_2$Cl$_2$ and 19 mg (0.058 mmol) of [CPh$_3$][BF$_4$]. The purple solution immediately turned green and was stirred under nitrogen for 18 hours after which time the solvent was removed by vacuum. The resulting solid was dissolved in a minimum of CH$_2$Cl$_2$ and the product isolated by precipitation upon rapid addition of the CH$_2$Cl$_2$ solution into stirred, ice-cold ether. The dark green precipitate was collected by filtration (30 mg) and dissolved in dry MeOH in oven dried Schlenk flask. 3 drops of DBU were added and an immediate green to purple colour change occurred. The solution was stirred for 16 hours, and the red precipitate collected by filtration. Purified by prep-TLC (7:3 hexane: acetone with NEt$_3$). The red band close to the baseline was collected was a red powder (2 mg, 0.009 mmol, 34%). Crystals suitable for x-ray crystallography were grown from DCM/Hexane.

^{1}H NMR (CDCl$_3$, 500 MHz) δ /ppm: 1.71 (s, 30H, Cp*), 2.21 (m, 4H, dppe), 3.00 (m, 4H, dppe), 6.42 (m, H^{12}), 6.45 (m, CPh$_3$), 6.61 (t, J_{HH} = 4.9 Hz, H$^{6/7}$), 7.01 (t, dppe), 7.12 (t, dppe), 7.21 (m, H$^{6/7}$), 7.31 (app. t, dppe), 7.36 (app. t, dppe), 7.74 (m, H$^{5/8}$), 7.79 (m, dppe), 8.17 (m, H$^{5/8}$). ^{13}C{^{1}H} NMR (CDCl$_3$, 100.6 MHz) δ /ppm: 10.49 (Cp*, CH$_3$), 29.85 (dppe), 58.79 (C^{13}), 93.19 (Cp*), 98.21 (C^2), 124.02 (C$^{6/7}$), 125.08 (C$^{6/7}$), 126.17 (CPh$_3$), 127.11 (C$^{5/8}$), 127.58 (dppe), 129.02 (dppe/CPh$_3$), 129.19 (dppe/CPh$_3$), 129.67 (dppe/CPh$_3$), 133.47 (dppe), 134.02 (dppe), 141.34 (C$^{11/12}$), 146.04 (C$^{11/12}$). ^{31}P{^{1}H} NMR (CDCl$_3$, 243 MHz) δ /ppm: 81.69. ESI(+)-MS (*m/z*): Calculated for [M]$^+$ ([C$_{146}$H$_{125}$P$_4$Ru$_2$]$^+$) 2205.6813. Observed for [M]$^+$ 2205.6689. Observed for [M]$^{2+}$ 1103.8357 (Calculated: 1103.8387)

RuCl(C≡CC$_{14}$H$_8$-10-C≡CSiMe$_3$)(dppe)$_2$, **65**

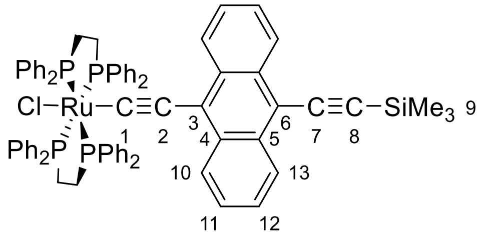

A 1.6 M commercial solution of MeLi in Et$_2$O (1.6 mmol) was added dropwise to a cooled solution (−78 °C) of 9,10-diethynyl(trimethylsilyl)anthracene (648 mg, 1.7 mmol) in 20 mL of THF. The solution was stirred for 1 hour at −78 °C and then 2 hours at room temperature (r.t.). This solution was then added to a suspension of *cis*-(dppe)$_2$RuCl$_2$ (750 mg, 0.760 mmol) in 30 mL of THF with an immediate yellow to red colour change and was stirred overnight at r.t. After filtration the solvent was removed *in vacuo*. The crude product was washed with pentane, dissolved in a mixture of THF–CH$_2$Cl$_2$ (50/50), and purified via column chromatography (Al$_2$O$_3$, Et$_2$O) giving a black crude product (429 mg, 0.373 mmol, 49 %) followed by further purification with an alumina plug (hexane/CH$_2$Cl$_2$ to remove yellow impurity) giving a pure bright red powder (130 mg, 0.105 mmol, 14 %)

^{1}H NMR (CD$_2$Cl$_2$, 500 MHz, 295 °C) δ /ppm: 0.42 (s, 9H, TMS), 2.96 (m, 8H, dppe), 6.68 (t, J_{HH} = 7.6 Hz, dppe), 6.72 (ddd, J_{1HH} = 8.5 Hz, J_{2HH} = 6.5 Hz, J_{3HH} = 1.2 Hz, H^{12}), 6.91 (t, J_{HH} = 7.4 Hz, dppe), 6.99 (t, J_{HH} = 7.6 Hz, dppe), 7.11 (m, dppe), 7.20 (t, J_{HH} = 7.4 Hz, dppe), 7.33 (ddd, J_{1HH} = 8.5 Hz, J_{2HH} = 6.5 Hz, J_{3HH} = 1.2 Hz, H^{11}), 7.60 (m, dppe), 7.64 (d, J_{HH} = 8.5 Hz, H^{13}), 8.37 (d, J_{HH} = 8.5 Hz, H^{10}). ^{13}C{^{1}H} NMR (CD$_2$Cl$_2$, 100.6 MHz, 295 °C) δ /ppm: 0.50 (TMS), 30.30 (app. t, dppe), 103.72 (C^8), 105.01 (C^7), 109.23 (C^2), 116.05 (C^3), 123.65 (C^{12}), 126.20 (C^{11}), 126.33 (C^{10}), 127.27 (dppe), 127.77 (dppe), 127.86 (C^6), 129.13 (dppe), 129.43 (C^{13}), 129.73 (dppe), 132.12 (C^4), 133.42 (C^5), 134.56 (dppe), 134.66 (dppe), 136.06 (m, dppe), 136.42 (m, dppe), 148.58 (m, C^1). ^{31}P{^{1}H} NMR (CD$_2$Cl$_2$, 243 MHz, 295 °C) δ /ppm: 45.27. ESI(+)-MS (*m/z*): Calculated for [M]$^+$ ([C$_{73}$H$_{65}$P$_4$RuSi]$^+$) 1195.2844. Observed for [M]$^+$ 1195.2863.

Appendix

trans-$[\{RuCl(dppe)_2\}_2(=C=CHC_6H_4\text{-}4\text{-}CH=C=)]2BF_4$, **3**

Identification code	jml1725
Empirical formula	$C_{124}H_{118}Cl_{18}F_6O_6P_8Ru_2S_2$
Formula weight	2970.30
Temperature/K	110.05(10)
Crystal system	triclinic
Space group	P-1
a/Å	12.8960(4)
b/Å	14.2571(4)
c/Å	18.4419(4)
α/°	75.142(2)
β/°	80.921(2)
γ/°	79.771(2)
Volume/Å^3	3202.71(16)
Z	1
ρ_{calc}g/cm^3	1.540
μ/mm^{-1}	7.129
F(000)	1510.0
Crystal size/mm^3	0.23 × 0.139 × 0.081
Radiation	CuKα (λ = 1.54184)
2Θ range for data collection/°	7.194 to 134.156
Index ranges	$-15 \le h \le 15$, $-17 \le k \le 14$, $-22 \le l \le 22$
Reflections collected	45529
Independent reflections	11424 [R_{int} = 0.0406, R_{sigma} = 0.0323]
Data/restraints/parameters	11424/16/795
Goodness-of-fit on F^2	1.048
Final R indexes [I>=2σ (I)]	R_1 = 0.0479, wR_2 = 0.1301
Final R indexes [all data]	R_1 = 0.0549, wR_2 = 0.1367
Largest diff. peak/hole / e Å^{-3}	1.68/-2.09

Data collected, solved and refined by Adrian C Whitwood

trans-$RuCl(C\equiv CHC_6H_4\text{-}4\text{-}C{=}OCH_3)(dppe)_2$, **5**

Identification code	jml1728
Empirical formula	$C_{65}H_{60}Cl_5F_3O_4P_4RuS$
Formula weight	1395.75
Temperature/K	110.05(10)
Crystal system	triclinic
Space group	P-1
a/Å	12.32464(18)
b/Å	22.8008(3)
c/Å	23.3344(4)
α/°	77.5819(12)
β/°	75.2580(13)
γ/°	85.0411(11)
Volume/Å^3	6189.55(16)
Z	4
ρ_{calc}g/cm^3	1.498
μ/mm^{-1}	0.663
F(000)	2855.0
Crystal size/mm^3	0.24 × 0.22 × 0.125
Radiation	MoKα (λ = 0.71073)
2Θ range for data collection/°	6.568 to 60.066
Index ranges	$-17 \leq h \leq 17$, $-31 \leq k \leq 32$, $-32 \leq l \leq 32$
Reflections collected	145427
Independent reflections	36151 [R_{int} = 0.0323, R_{sigma} = 0.0273]
Data/restraints/parameters	36151/25/1549
Goodness-of-fit on F^2	1.109
Final R indexes [I>=2σ (I)]	R_1 = 0.0438, wR_2 = 0.1057
Final R indexes [all data]	R_1 = 0.0529, wR_2 = 0.1122
Largest diff. peak/hole / e Å^{-3}	1.38/-2.65

Data collected, solved and refined by Adrian C Whitwood

Ru(C≡CC_6H_4-4-Br)(dppe)Cp*, **27**

Identification code	RRS-B59
Empirical formula	$C_{44}H_{43}BrP_2Ru$
Formula weight	814.70
Temperature/K	101(8)
Crystal system	triclinic
Space group	P-1
a/Å	12.0077(2)
b/Å	12.2169(3)
c/Å	15.3801(3)
α/°	74.468(2)
β/°	71.585(2)
γ/°	61.146(2)
Volume/Å^3	1856.78(8)
Z	2
ρ_{calc}g/cm^3	1.457
μ/mm^{-1}	1.615
Crystal size/mm^3	0.43 × 0.24 × 0.05
Radiation	MoKα (λ = 0.71073)
2Θ range for data collection/°	3.312 to 28.183
Reflections collected	70781
Independent reflections	8488 [R_{int} = 0.0713, R_{sigma} = ?]
Data/restraints/parameters	8488/0/438
Goodness-of-fit on F^2	1.051
Final R indexes [I>=2σ (I)]	R_1 = 0.0429, wR_2 = 0.0867
Final R indexes [all data]	R_1 = 0.0639, wR_2 = 0.0977
Largest diff. peak/hole / e Å^{-3}	1.275/-0.749

Data collected, solved and refined by Stephen Moggach

[Ru(=C=C(C_7H_7)C_6H_4-4-C≡CC_6H_4-4-OMe)(dppe)Cp*]BF_4, **34**

Identification code	RRS-B9
Empirical formula	$C_{61}H_{59}BCl_2F_4OP_2Ru$
Formula weight	1128.80
Temperature/K	119.95(10)
Crystal system	triclinic
Space group	P-1
a/Å	11.7723(5)
b/Å	13.4034(5)
c/Å	17.5805(7)
α/°	78.078(3)
β/°	79.775(3)
γ/°	79.802(3)
Volume/Å^3	2642.53(19)
Z	2
ρ_{calc} g/cm^3	1.419
μ/mm^{-1}	0.515
F(000)	1164
Crystal size/mm^3	0.3 × 0.15 × 0.02
Radiation	MoKα (λ = 0.71073)
2Θ range for data collection/°	3.293 to 24.998
Index ranges	-13 ≤ h ≤ 13, -15 ≤ k ≤ 15, -20 ≤ l ≤ 17
Reflections collected	19102
Independent reflections	9233 [R_{int} = 0.0439, R_{sigma} = ?]
Data/restraints/parameters	9233/0/654
Goodness-of-fit on F^2	1.024
Final R indexes [I>=2σ (I)]	R_1 = 0.0461, wR_2 = 0.0843
Final R indexes [all data]	R_1 = 0.0691, wR_2 = 0.0908
Largest diff. peak/hole / e Å^{-3}	0.723/-0.707

Data collected, solved and refined by Marcus Korb

[Ru(=C=C(H)C_6H_2(NSN)-indene-3-(Ph)$_2$)(dppe)Cp*]BF_4, **57**

Identification code	jml21011_twin1_hklf4
Empirical formula	$C_{66}H_{59}BCl_2F_4N_2P_2RuS$
Formula weight	1232.93
Temperature/K	110.05(10)
Crystal system	orthorhombic
Space group	$Pna2_1$
a/Å	30.783(2)
b/Å	9.3989(5)
c/Å	20.3788(15)
α/°	90
β/°	90
γ/°	90
Volume/Å^3	5896.1(7)
Z	4
ρ_{calc}g/cm^3	1.389
μ/mm^{-1}	4.278
F(000)	2536.0
Crystal size/mm^3	0.12 × 0.106 × 0.038
Radiation	Cu Kα (λ = 1.54184)
2Θ range for data collection/°	7.198 to 135.034
Index ranges	$-36 \le h \le 36$, $-9 \le k \le 11$, $-24 \le l \le 23$
Reflections collected	9296
Independent reflections	9296 [R_{int} = ?, R_{sigma} = 0.0490]
Data/restraints/parameters	9296/141/772
Goodness-of-fit on F^2	1.180
Final R indexes [I>=2σ (I)]	R_1 = 0.0662, wR_2 = 0.1492
Final R indexes [all data]	R_1 = 0.0780, wR_2 = 0.1530
Largest diff. peak/hole / e Å^{-3}	1.44/-1.54
Flack parameter	0.003(9)

Data collected, solved and refined by Adrian C Whitwood

$\{Ru(dppe)Cp^*\}_2(C{\equiv}CC_{14}H_8\text{-}10\text{-}C(=CCPh_3))_2$, **62**

Identification code	Rrsa94
Empirical formula	$C_{146}H_{126}P_4Ru_2$
Formula weight	2206.48
Temperature/K	150.00(10)
Crystal system	triclinic
Space group	P-1
a/Å	13.4443(8)
b/Å	16.4903(11)
c/Å	17.1986(6)
α/°	98.119(4)
β/°	111.678(5)
γ/°	113.152(6)
Volume/Å^3	3069.3(3)
Z	1
ρ_{calc}g/cm^3	1.194
μ/mm^{-1}	2.858
Crystal size/mm^3	0.14 × 0.08 × 0.06
Radiation	Cu Kα (λ = 1.54184)
2Θ range for data collection/°	2.935 to 76.571
Reflections collected	53023
Independent reflections	12199 [R_{int} = 0.1289, R_{sigma} = ?]
Data/restraints/parameters	12199/3/690
Goodness-of-fit on F^2	1.083
Final R indexes [I>=2σ (I)]	R_1 = 0.2734, wR_2 = 0.1029
Final R indexes [all data]	R_1 = 0.2976, wR_2 = 0.1234
Largest diff. peak/hole / e Å^{-3}	1.38/-2.65

Data collected, solved and refined by Stephen Moggach

Abbreviations

±	Plus-or-minus
°	Degrees
°C	Degrees Celsius
2D	2 Dimensional
Å	Angstroms
app.	Apparent
Ar	Aryl
ATR	Attenuated Total Reflectance
br.	broad
BTD	Benzothiadiazole
ca.	about
CAP	1-cyano-4-dimethylaminopyridinium
cm^{-1}	Wavenumber
CO	Carbon Monoxide
COSY	Correlation Spectroscopy
Cp	Cyclopentadienyl
Cp*	Pentamethylcyclopentadienyl
CV	Cyclic Voltammetry
d	Doublet
DBU	1,8-Diazabicyclo[5.4.0]undec-7-ene
DCM	Dichloromethane
dd	Doublet of Doublets
DFT	Density Functional Theory
dppe	1,2-Bis(diphenylphosphino)ethane
dppm	Bis(diphenylphosphino)methane
E	Electrophile
$E_{1/2}$	half-wave potential
E_{pa}	Anodic peak potential
E_{pc}	Cathodic peak potential

equiv.	Equivalents
ESI	Electrospray Ionisation
Et	Ethyl
Fc	Ferrocene
FT-IR	Fourier Transform Infra-Red
g	Grams
HMBC	Heteronuclear Multiple Bond Correlation
HOMO	Highest Occupied Molecular Orbital
HSQC	Heteronuclear Single Quantum Coherence
Hz	Hertz
^{i}Pr	iso-Propyl
K	Kelvin
kJ	Kilojoules
L	Ligand
LUMO	Lowest Unoccupied Molecular Orbital
M	Metal
m	Multiplet
m (prefix)	Milli
m/z	Mass/Charge
Me	Methyl
mg	Milligrams
MHz	Megahertz
min	Minutes
MLCT	Metal to Ligand Charge Transfer
mol	Moles
MS	Mass Spectroscopy
NHC	N-Heterocyclic Carbenes
NIR	Near Infra-Red
nm	nanometres
NMR	Nuclear Magnetic Resonance
Nu	Nucleophile

OTf	Triflouromethylsulfoate
Ph	Phenyl
ppm	Parts per million
q	Quartet
R	Organic Group (generic)
r.t.	Room Temperature
s	Singlet
SEC	Spectroelectrochemistry
sex.	Sextet
t	Triplet
THF	Tetrahydrofuran
TLC	Thin Layer Chromatography
TMS	Trimethylsilyl
TMSA	Trimethylsilylacetylene
UV	Ultraviolet
V	Voltage
vis	Visible
vs.	versus
W	Weak
X	Generic Group
ΔE_p	Difference between potentials
λ	wavelength

References

1 E. H. Falcao and F. Wudl, *J. Chem. Technol. Biotechnol.*, 2007, **82**, 524–531.

2 B. Pan, J. Xiao, J. Li, P. Liu, C. Wang and G. Yang, *Sci. Adv.*, 2015, **1**, e1500857.

3 M. J. Allen, V. C. Tung and R. B. Kaner, *Chem. Rev.*, 2010, **110**, 132–145.

4 K. E. Geckeler and S. Samal, *Polym. Int.*, 1999, **48**, 743–757.

5 P. M. Ajayan, *Chem. Rev.*, 1999, **99**, 1787–1800.

6 V. N. Popov, *Mater. Sci. Eng. R Rep.*, 2004, 43, 61–102.

7 C. N. R. Rao, R. Seshadri, A. Govindaraj and R. Sen, *Mater. Sci. Eng. R Rep.*, 1995, **15**, 209–262.

8 P. Liu, H. Cui and G. W. Yang, *Cryst. Growth Des.*, 2008, **8**, 581–586.

9 C. Frondel and U. B. Marvin, *Nature*, 1967, **214**, 587–589.

10 P. Németh, L. A. J. Garvie, T. Aoki, N. Dubrovinskaia, L. Dubrovinsky and P. R. Buseck, *Nat. Commun.*, 2014, **5**, 5447.

11 K. S. Novoselov, A. K. Geim, S. V Morozov, D. Jiang, Y. Zhang, S. V Dubonos, I. V Grigorieva and A. A. Firsov, *Science (80-.).*, 2004, **306**, 666–669.

12 The Nobel Prize in Chemistry, https://www.nobelprize.org/nobel_prizes/chemistry/laureates/2005/, (accessed 30 June 2018).

13 Andel, Eight Allotropes of Carbon, https://commons.wikimedia.org/wiki/File:Eight_Allotropes_of_Carbon.svg, (accessed 12 October 2020).

14 M. T. Weller, T. Overton, J. Rourke and F. A. Armstrong, *Inorganic chemistry*, Oxford University Press, 6th edn., 2016.

15 J. M. Plc, *Johnson Matthey Technol. Rev.*, 2017, 48.

16 S. Cotton, *Chemistry of Precious Metals*, Springer-Verlag New York, LLC., 1997.

17 P. B. Arockiam, C. Bruneau and P. H. Dixneuf, *Chem. Rev.*, 2012, **112**, 5879–5918.

18 M. J. Clarke, *Coord. Chem. Rev.*, 2002, **232**, 69–93.

19 C. S. Allardyce and P. J. Dyson, *Platin. Met. Rev.*, 2001, **45**, 62.

20 J. M. R. Narayanam and C. R. J. Stephenson, *Chem. Soc. Rev.*, 2011, **40**, 102–113.

21 C. Michel and P. Gallezot, *ACS Catal.*, 2015, **5**, 4130–4132.

22 T. Weskamp, W. C. Schattenmann, M. Spiegler and W. A. Herrmann, *Angew. Chem.,*

Int. Ed., 1998, **37**, 2490–2493.

23 J. Le Paih, C. V.-L. Bray, S. Dérien and P. H. Dixneuf, *J. Am. Chem. Soc.*, 2010, **132**, 7391–7397.

24 W. Markownikoff, *Ann. der Chemie und Pharm.*, 1870, **153**, 228–259.

25 P. Hughes, *J. Chem. Educ.*, 2006, **83**, 1152.

26 M. Tokunaga and Y. Wakatsuki, *Angew. Chem., Int. Ed.*, 1998, **37**, 2867–2869.

27 M. Beller, J. Seayad, A. Tillack and H. Jiao, *Angew. Chem., Int. Ed.*, 2004, **43**, 3368–3398.

28 C. Bruneau and P. H. Dixneuf, *Angew. Chem., Int. Ed.*, 2006, **45**, 2176–2203.

29 A. Labonne, T. Kribber and L. Hintermann, *Org. Lett.*, 2006, **8**, 5853–5856.

30 B. Breit, U. Gellrich, T. Li, J. M. Lynam, L. M. Milner, N. E. Pridmore, J. M. Slattery and A. C. Whitwood, *Dalt. Trans.*, 2014, **43**, 11277–11285.

31 A. L. K. Shi Shun and R. R. Tykwinski, *Angew. Chem., Int. Ed.*, 2006, **45**, 1034–1057.

32 W. A. Chalifoux and R. R. Tykwinski, *Nat. Chem.*, 2010, **2**, 967–971.

33 F. Diederich, P. J. Stang and R. R. Tykwinski, *Acetylene Chemistry: chemistry, biology and material science*, Wiley-VCH, 2005.

34 S. Rigaut, J. Perruchon, L. Le Pichon, D. Touchard and Pierre H. Dixneuf, *J. Organomet. Chem.*, 2003, **670**, 37–44.

35 M. I. Bruce, *Chem. Rev.*, 1998, **98**, 2797–2858.

36 M. Hermann, *Ann. der Chemie und Pharm.*, 1855, **95**, 211–225.

37 D. Bourissou, O. Guerret, F. P. Gabbaï and G. Bertrand, *Chem. Rev.*, 2000, **100**, 39–91.

38 E. O. Fischer and A. Maasböl, *Angew. Chem., Int. Ed.*, 1964, **3**, 580–581.

39 R. R. Schrock, *J. Am. Chem. Soc.* , 1974, **96**, 6796–6797.

40 S. T. Nguyen, L. K. Johnson, R. H. Grubbs and J. W. Ziller, *J. Am. Chem. Soc.*, 1992, **114**, 3974–3975.

41 G. C. Bazan, J. H. Oskam, H.-N. Cho, L. Y. Park and R. R. Schrock, *J. Am. Chem. Soc.* , 1991, **113**, 6899–6907.

42 J.-L. Hérisson and Y. Chauvin, *Die Makromol. Chemie*, 1971, **141**, 161–176.

43 C. M. Crudden and D. P. Allen, *Coord. Chem. Rev.*, 2004, **248**, 2247–2273.

44 J. Huang, E. D. Stevens, S. P. Nolan and J. L. Petersen, *J. Am. Chem. Soc.* , 1999, **121**, 2674–2678.

45 M. Scholl, T. M. Trnka, J. P. Morgan and R. H. Grubbs, *Tetrahedron Lett.*, 1999, **40**,

2247–2250.

46 F. E. Hahn and M. C. Jahnke, *Angew. Chem., Int. Ed.*, 2008, **47**, 3122–3172.

47 A. Igau, H. Grutzmacher, A. Baceiredo and G. Bertrand, *J. Am. Chem. Soc.*, 1988, **110**, 6463–6466.

48 A. J. Arduengo, R. L. Harlow and M. Kline, *J. Am. Chem. Soc.*, 1991, **113**, 361–363.

49 M. C. Jahnke and F. E. Hahn, in *N-heterocyclic Carbenes*, 2010, pp. 1–41.

50 M. N. Hopkinson, C. Richter, M. Schedler and F. Glorius, *Nature*, 2014, 510, 485–496.

51 C. Bruneau and P. Dixneuf, Eds., *Metal Vinylidenes and Allenylidenes in Catalysis*, Wiley-VCH, Weinheim, Germany, 2008.

52 M. I. Bruce, *Chem. Rev*, 1991, **91**, 197–257.

53 K. H. Dötz, *Angew. Chem., Int. Ed.*, 1984, **23**, 587–608.

54 O. S. Mills and A. D. Redhouse, *Chem. Commun.*, 1966, 444.

55 R. B. King and M. S. Saran, *J. Chem. Soc., Chem. Commun.*, 1972, 1053.

56 J. M. Lynam, *Chem. - Eur. J.*, 2010, 8238–8247.

57 C. Bruneau and P. H. Dixneuf, *Acc. Chem. Res*, 1999, **32**, 311–323.

58 H. Katayama and F. Ozawa, *Coord. Chem. Rev.*, 2004, **248**, 1703–1715.

59 R. B. King, *Coord. Chem. Rev.*, 2004, **248**, 1533–1541.

60 R. Mahé, P. H. Dixneuf and S. Lécolier, *Tetrahedron Lett.*, 1986, **27**, 6333–6336.

61 P. Thaddeus, M. C. McCarthy, M. J. Travers, C. A. Gottlieb and W. Chen, *Faraday Discuss.*, 1998, **109**, 121–135.

62 J. Cernicharo, C. A. Gottlieb, M. Guelin, T. C. Killian, P. Thaddeus and J. M. Vrtilek, *Astrophys. J.*, 1991, **368**, L43–L45.

63 L. Shi, P. Rohringer, K. Suenaga, Y. Niimi, J. Kotakoski, J. C. Meyer, H. Peterlik, M. Wanko, S. Cahangirov, A. Rubio, Z. J. Lapin, L. Novotny, P. Ayala and T. Pichler, *Nat. Mater.*, 2016, **15**, 634–639.

64 C. S. Casari and A. Milani, *MRS Commun.*, 2018, **8**, 207–219.

65 K. Brand, *Berichte der Dtsch. Chem. Gesellschaft (A B Ser.*, 1921, **54**, 1987–2006.

66 R. Kuhn and K. Wallenfels, *Berichte der Dtsch. Chem. Gesellschaft (A B Ser.*, 1938, **71**, 783–790.

67 P. H. Dixneuf, A. Romero and A. Vegas, *Angew. Chem., Int. Ed.*, 1990, **29**, 215–216.

68 A. Wolinska, D. Touchard, P. H. Dixneuf and A. Romero, *J. Organomet. Chem.*, 1991,

420, 217–226.

69 J. R. Lomprey and J. P. Selegue, *Organometallics*, 1993, 616–617.

70 M. I. Bruce, P. Hinterding, E. R. T. Tiekink, B. W. Skelton and A. H. White, *J. Organomet. Chem.*, 1993, **450**, 209–218.

71 K. Venkatesan, F. J. Fernández, O. Blacque, T. Fox, M. Alfonso, H. W. Schmalle and H. Berke, *Chem. Commun.*, 2003, 2006–2008.

72 M. Franz, J. A. Januszewski, D. Wendinger, C. Neiss, L. D. Movsisyan, F. Hampel, H. L. Anderson, A. Görling and R. R. Tykwinski, *Angew. Chem., Int. Ed.*, 2015, **54**, 6645–6649.

73 A. Hoffmann-Röder and N. Krause, *Angew. Chem., Int. Ed.*, 2004, **43**, 1196–1216.

74 S. G. Eaves, UWA/ Durham, 2015.

75 J. A. Januszewski and R. R. Tykwinski, *Chem. Soc. Rev.*, 2014, **43**, 3184–3203.

76 Z. Wang, X. Ke, Z. Zhu, F. Zhang, M. Ruan and J. Yang, *Phys. Rev. B*, 2000, **61**, 2472.

77 L. Ravagnan, F. Siviero, C. Lenardi, P. Piseri, E. Barborini, P. Milani, C. S. Casari, A. L. Bassi and C. E. Bottani, *Phys. Rev. Lett*, 2002, **89**, 285506.

78 L. Ravagnan, P. Piseri, M. Bruzzi, S. Miglio, G. Bongiorno, A. Baserga, C. S. Casari, A. L. Bassi, C. Lenardi, Y. Yamaguchi, T. Wakabayashi, C. E. Bottani and P. Milani, *Phys. Rev. Lett*, 2007, **98**, 216103.

79 M. Franz, J. A. Januszewski, F. Hampel and R. R. Tykwinski, *Eur. J. Org. Chem.*, 2019, 3503–3512.

80 A. J. Apponi, M. C. McCarthy, C. A. Gottlieb and P. Thaddeus, *Astrophys. J.*, 2000, **530**, 357–361.

81 D. Wendinger and R. R. Tykwinski, *Acc. Chem. Res*, 2017, **50**, 1468–1479.

82 D. Touchard, P. Haquette, A. Daridor, L. Toupet and P. H. Dixneuf, *J. Am. Chem. Soc.* , 1994, **116**, 11157–11158.

83 S. Rigaut, J. Perruchon, S. Guesmi, C. Fave, D. Touchard and P. H. Dixneuf, *Eur. J. Inorg. Chem.*, 2005, 447–460.

84 J. P. Selegue, *Coord. Chem. Rev.*, 2004, **248**, 1543–1563.

85 V. Guillaume, P. Thominot, F. Coat, A. Mari and C. Lapinte, *J. Organomet. Chem.*, 1998, **565**, 75–80.

86 F. Coat, P. Thominot and C. Lapinte, *J. Organomet. Chem.*, 2001, **629**, 39–43.

87 F. Coat, M. Guillemot, F. Paul and C. Lapinte, *J. Organomet. Chem.*, 1999, **578**, 76–84.

88 M. I. Bruce, P. Hinterding, P. J. Low, B. W. Skelton and A. H. White, *Chem. Commun.*, 1996, 1009–1010.

89 M. I. Bruce, P. Hinterding, P. J. Low, B. W. Skelton and A. H. White, *Dalt. Trans.*, 1998, **0**, 467–474.

90 R. F. Winter and F. M. Hornung, *Organometallics*, 1997, **16**, 4248–4250.

91 R. F. Winter and F. M. Hornung, *Organometallics*, 1999, **18**, 4005–4014.

92 K. Ilg and H. Werner, *Angew. Chem., Int. Ed.*, 2000, **39**, 1632–1634.

93 K. Venkatesan, O. Blacque, T. Fox, M. Alfonso, H. W. Schmalle and H. Berke, *Organometallics*, 2004, **23**, 4661–4671.

94 A. Romero, D. Peron and P. H. Dixneuf, *J. Chem. Soc., Chem. Commun.*, 1990, 1410–1412.

95 G. Roth and H. Fischer, *Organometallics*, 1996, **15**, 5766–5768.

96 M. Dede, M. Drexler and H. Fischer, *Organometallics*, 2007, **26**, 4294–4299.

97 K. Thirumoorthy, M. Viji, A. P. Pandey, T. G. Netke, B. Sekar, G. Yadav, S. Deshpande and V. S. Thimmakondu, *Chem. Phys.*, 2019, **527**, 110496.

98 A. Marrone, C. Coletti and N. Re, *Organometallics*, 2004, **23**, 4952–4963.

99 A. J. Apponi, M. C. McCarthy, C. A. Gottlieb and P. Thaddeus, *Astrophys. J.*, 2000, **530**, 357–361.

100 D. Touchard, S. Guesmi, M. Bouchaib, P. Haquette, A. Daridor and P. H. Dixneuf, *Organometallics*, 1996, **15**, 2579–2581.

101 N. Re, A. Sgamellotti and C. Floriani, *Organometallics*, 2000, **19**, 1115–1122.

102 A. Marrone and N. Re, *Organometallics*, 2002, **21**, 3526–3571.

103 N. Auger, D. Touchard, S. Rigaut, J.-F. Halet and J.-Y. Saillard, *Organometallics*, 2003, **22**, 1638–1644.

104 C. Coletti, A. Marrone and N. Re, *Acc. Chem. Res*, 2012, **45**, 139–149.

105 H. Fischer and N. Szesni, *Coord. Chem. Rev.*, 2004, **248**, 1659–1677.

106 M. H. Garner, R. Hoffmann, S. Rettrup and G. C. Solomon, *ACS Cent. Sci.*, 2018, **4**, 688–700.

107 B. Bildstein, M. Schweiger, H. Kopacka and K. Wurst, *J. Organomet. Chem.*, 1998, **553**, 73–81.

108 B. Bildstein, M. Schweiger, H. Kopacka, K.-H. Ongania and K. Wurst, *Organometallics*,

1998, **17**, 2414–2424.

109 B. Bildstein, *Coord. Chem. Rev.*, 2000, **206**–**207**, 369–394.

110 G. Roth and H. Fischer, *Organometallics*, 1996, **15**, 1139–1145.

111 G. Roth, H. Fischer, T. Meyer-Friedrichsen, J. Heck, S. Houbrechts and A. Persoons, *Organometallics*, 1998, **17**, 1511–1516.

112 B. E. Woodworth, P. S. White and Templeton. J. L., *J. Am. Chem. Soc.*, 1997, **119**, 828–829.

113 I. Kovacik, M. Laubender and H. Werner, *Organometallics*, 1997, **16**, 5607–5609.

114 R. W. Lass, P. Steinert, J. Wolf and H. Werner, *Chem. - Eur. J.*, 1996, **2**, 19–23.

115 K. Ilg and H. Werner, *Chem. - Eur. J.*, 2002, **8**, 2812.

116 S. Szafert, P. Haquette, S. B. Falloon and J. A. Gladysz, *J. Organomet. Chem.*, 2000, **604**, 52–58.

117 T. Bartik, W. Weng, J. A. Ramsden, S. Szafert, S. B. Falloon, A. M. Arif and J. A. Gladysz, *J. Am. Chem. Soc.* , 1998, **120**, 11071–11081.

118 H. P. Xia, W. S. Ng, J. S. Ye, X.-Y. Li, W. T. Wong, Z. Lin, C. Yang and G. Jia, *Organometallics*, 1999, **18**, 4552–4557.

119 J. Li, J. Zhao, G. Ma, R. McDonald and R. G. Cavell, *J. Organomet. Chem.*, 2019, **895**, 7–14.

120 M. I. Bruce, *Coord. Chem. Rev.*, 2004, **248**, 1603–1625.

121 M. H. Garner, W. Bro-Jørgensen, P. D. Pedersen and G. C. Solomon, *J. Phys. Chem. C*, 2018, **122**, 26777–26789.

122 I. Kinoshita, M. Kijima and H. Shirakawa, *Macromol. Rapid Commun.*, 2000, **21**, 1205–1208.

123 A. D. Allen and T. T. Tidwell, *Chem. Rev.*, 2013, **113**, 7287–7342.

124 S. Liu, Y. Lei, X. Qi and Y. Lan, *J. Phys. Chem. A*, 2014, **118**, 2638–2645.

125 H. Ulrich, *Cumulenes in click reactions*, Wiley, 2009.

126 Y. Kuwatani, G. Yamamoto, M. Oda, M. Iyoda, K. Yoshiyuki, Y. Gaku, O. Masaji and I. Masahiko, *Bull. Chem. Soc. Jpn.*, 2005, **78**, 2188–2208.

127 L. T. Scott and G. J. Decicco, *J. Org. Chem*, 1980, **45**, 4055–4056.

128 V. Parasuk, J. Almlöf and M. W. Feyereisen, *J. Am. Chem. Soc.* , 1991, **113**, 1049–1050.

129 G. V. Baryshnikov, R. R. Valiev, A. V. Kuklin, D. Sundholm and H. Ågren, *J. Phys. Chem.*

Lett., 2019, **10**, 6701–6705.

130 K. Kaiser, L. M. Scriven, F. Schulz, P. Gawel, L. Gross and H. L. Anderson, *Science (80-.).*, 2019, **365**, 1299–1301.

131 F. Diederich, *Nature*, 1994, **369**, 199–207.

132 E. A. Rohlfing, D. M. Cox and A. Kaldor, *J. Chem. Phys.*, 1984, **81**, 3322–3330.

133 SciFinder, https://scifinder.cas.org/scifinder/view/scifinder/scifinderExplore.jsf.

134 J. Chandrasekhar, E. D. Jemmis and P. von Ragué Schleyer, *Tetrahedron Lett.*, 1979, **20**, 3707–3710.

135 N. D. Charistos and A. Muñ Oz-Castro, *Phys. Chem. Chem. Phys*, 2020, **22**, 9240.

136 R. Jasti, J. Bhattacharjee, J. B. Neaton and C. R. Bertozzi, *J. Am. Chem. Soc.*, 2008, 130, 17646–17647.

137 E. J. Leonhardt and R. Jasti, *Nat. Rev. Chem.*, 2019, 3, 672–686.

138 Y. Xu and M. von Delius, *Angew. Chem., Int. Ed.*, 2020, 59, 559–573.

139 G. Povie, Y. Segawa, T. Nishihara, Y. Miyauchi and K. Itami, *Science (80-.).*, 2017, **356**, 172–175.

140 S. Wolfgang, H. Kopacka, K. Wurst, C. Salzmann, K.-H. Ongania, F. Fabrizi de Biani, P. Zanello and B. Bildstein, *Organometallics*, 2004, **23**, 1024–1041.

141 I. Alkorta and J. Elguero, *Struct. Chem.*, 2005, **16**, 77–79.

142 B. M. Trost and A. McClory, *Chem. - Asian J.*, 2008, **3**, 164–194.

143 A. D. Scaccabarozzi, A. Milani, S. Peggiani, S. Pecorario, B. Sun, R. R. Tykwinski, M. Caironi and C. S. Casari, *J. Phys. Chem. Lett.*, 2020, **11**, 1970–1974.

144 S. G. Eaves, S. J. Hart, A. C. Whitwood, D. S. Yufit, P. J. Low and J. M. Lynam, *Chem. Commun.*, 2015, **51**, 9362–5.

145 S. Roué and C. Lapinte, *J. Organomet. Chem.*, 2005, **690**, 594–604.

146 C. G. Bangcuyo, U. Evans, M. L. Myrick and U. H. F. Bunz, *Macromolecules*, 2001, **34**, 7592–7594.

147 M. A. Fox, J. E. Harris, S. Heider, V. Pérez-Gregorio, M. E. Zakrzewska, J. D. Farmer, D. S. Yufit, J. A. K. Howard and P. J. Low, *J. Organomet. Chem.*, 2009, **694**, 2350–2358.

148 B. Chin, A. J. Lough, R. H. Morris, C. T. Schweitzer and C. D'Agostino, *Inorg. Chem.*, 1994, **33**, 6278–6288.

149 R. F. Winter and S. Záliš, *Coord. Chem. Rev.*, 2004, **248**, 1565–1583.

150 M. Juribašić, L. Bellotto, P. Traldi and L. Tušek-Božić, *J. Am. Soc. Mass Spectrom. 2011 2210*, 2011, **22**, 1815–1825.

151 S. Guesmi, D. Touchard and P. H. Dixneuf, *Chem. Commun.*, 1996, 2773.

152 M. R. Hall, R. R. Steen, M. Korb, A. N. Sobolev, S. A. Moggach, J. M. Lynam and P. J. Low, *Chem. - Eur. J.*, 2020, **26**, 7226–7234.

153 S. J. Ergas, K. Kinney, M. E. Fuller and K. M. Scow, *Biotechnol. Bioeng.*, 1994, **44**, 1048–1054.

154 Y. Tanimoto, H. Kobayashi, S. Nagakura and Y. Saito, *Acta Crystallogr. B*, 1973, **29**, 1822–1826.

155 C.-Y. Wong, C. M. Che, M. C. W. Chan, K.-H. Leung, D. L. Phillips and N. Zhu, *J. Am. Chem. Soc.*, 2004, **126**, 2501–2514.

156 E. Bustelo, M. Jimenez-Tenorio, K. Mereiter, M. C. Puerta and P. Valerga, *Organometallics*, 2002, **21**, 1903–1911.

157 D. Touchard, P. Haquette, N. Pirio, L. Toupet and P. H. Dixneuf, *Organometallics*, 1993, **12**, 3132–3139.

158 D. Touchard, P. Haquette, S. Guesmi, L. Le Pichon, A. Daridor, L. Toupet and P. H. Dixneuf, *Organometallics*, 1997, **16**, 3640–3648.

159 M. R. Hall, S. A. Moggach and P. J. Low, *Chem. - Asian J.*, 2021, asia.202100850.

160 M. R. Hall, University of Western Australia, 2018.

161 H. Kukula, S. Veit and A. Godt, *Eur. J. Org. Chem.*, 1999, 277–286.

162 M. I. Bruce, B. C. Hall, B. D. Kelly, P. J. Low, B. W. Skelton and A. H. White, *J. Chem. Soc., Dalt. Trans.*, 1999, **21**, 3719–3728.

163 M. Iyoda, K. Nishioka, M. Nose, S. Tanaka and M. Oda, *Chem. Lett.*, 1984, **13**, 131–134.

164 H. Dauben, Jr., L. Honnen and K. Harmon, *J. Org. Chem.*, 1960, **25**, 1442–1445.

165 W. M. Khairul, M. A. Fox, P. A. Schauer, D. Albesa-Jové, D. S. Yufit, J. A. K. Howard and P. J. Low, *Inorg. Chim. Acta.*, 2011, **374**, 461–471.

166 T. Ren, *Chem. Rev.*, 2008, **108**, 4185–4207.

167 A. G. Orpen, L. Brammer, F. H. Allen, O. Kennard, D. G. Watson and R. Taylor, *Struct. Correl.*, 1994, 752–858.

168 A. Burrows, J. Holman, A. Parsons, G. Pilling and G. Price, .

169 M. A. Fox, B. Le Guennic, R. L. Roberts, D. A. Brue, D. S. Yufit, J. A. K. Howard, G. Manca,

J.-F. Halet, F. Hartl and P. J. Low, *J. Am. Chem. Soc.*, 2011, **133**, 18433–18446.

170 S. K. Hurst and T. Ren, *J. Organomet. Chem.*, 2002, **660**, 1–5.

171 V. Ganesh, M. Odachowski and V. K. Aggarwal, *Angew. Chem., Int. Ed.*, 2017, **56**, 9752–9756.

172 A. C. Benniston, S. Mitchell, S. A. Rostron and S. Yang, *Tetrahedron Lett.*, 2004, **45**, 7883–7885.

173 J. B. G. Gluyas, N. J. Brown, J. D. Farmer and P. J. Low, *Aust. J. Chem.*, 2017, **70**, 113.

174 S. Li, X. Yang, L. Zhang, J. An, B. Cai and X. Wang, *RSC Adv.*, 2020, **10**, 9203–9209.

175 E. Bundgaard and F. C. Krebs, *Macromolecules*, 2006, **39**, 2823–2831.

176 Y. Dong, B. Koken, X. Ma, L. Wang, Y. Cheng and C. Zhu, *Inorg. Chem. Commun.*, 2011, **14**, 1719–1722.

177 N. Rotthowe, J. Zwicker and R. F. Winter, *Organometallics*, 2019, **38**, 2782–2799.

178 D. Xia, X.-Y. Wang, X. Guo, M. Baumgarten, M. Li and K. Müllen, *Cryst. Growth Des.*, 2016, **16**, 7124–7129.

179 J. Kaleta, P. I. Dron, K. Zhao, Y. Shen, I. Císařová, C. T. Rogers and J. Michl, *J. Org. Chem.*, 2015, **80**, 6173–6192.

180 M. I. Bruce, B. C. Hall, P. J. Low, B. W. Skelton and A. H. White, *J. Organomet. Chem.*, 1999, **592**, 74–83.

181 T. De Vijlder, D. Valkenborg, F. Lemière, E. P. Romijn, K. Laukens and F. Cuyckens, *Mass Spectrom. Rev.*, 2018, **37**, 607.

182 K. Venkatesan, O. Blacque, T. Fox, M. Alfonso, H. W. Schmalle, S. Kheradmandan and H. Berke, *Organometallics*, 2005, **24**, 920–932.

183 C. J. Beddows, A. D. Burrows, N. G. Connelly, M. Green, J. M. Lynam and T. J. Paget, *Organometallics*, 2001, **20**, 231–233.

184 P. J. Low and S. Bock, *Electrochim. Acta*, 2013, **110**, 681–692.

185 M. C. B. Colbert, J. Lewis, N. J. Long, P. R. Raithby, M. Younus, A. J. P. White, D. J. Williams, N. N. Payne, L. Yellowlees, D. Beljonne, N. Chawdhury and R. H. Friend, *Organometallics*, 1998, **17**, 3034–3043.

186 M. A. Fox, R. L. Roberts, W. M. Khairul, F. Hartl and P. J. Low, *J. Organomet. Chem.*, 2007, **692**, 3277–3290.

187 N. G. Connelly and W. E. Geiger, *Chem. Rev.*, 1996, **96**, 877–910.

188 D. Astruc, *Electron transfer and radical processes in transition-metal chemistry*, VCH, 1995.

189 P. T. Kissinger and W. R. Heineman, *J. Chem. Educ.*, 1983, **60**, 702–706.

190 J. J. Van Benschoten, J. Y. Lewis, W. R. Heineman, D. A. Roston and P. T. Kissinger, *J. Chem. Educ.*, 1983, **60**, 772–776.

191 N. Elgrishi, K. J. Rountree, B. D. McCarthy, E. S. Rountree, T. T. Eisenhart and J. L. Dempsey, *J. Chem. Educ.*, 2018, **95**, 197–206.

192 J. B. G. Gluyas, A. J. Boden, S. G. Eaves, H. Yu and P. J. Low, *Dalt. Trans.*, 2014, **43**, 6291–6294.

193 M. A. Fox, J. D. Farmer, R. L. Roberts, M. G. Humphrey and P. J. Low, *Organometallics*, 2009, **28**, 5266–5269.

194 W. Kaim and A. Klein, *Spectroelectrochemistry*, Royal Society of Chemistry, 2008.

195 F. Paul, B. G. Ellis, M. I. Bruce, L. Toupet, T. Roisnel, K. Costuas, J.-F. Halet and C. Lapinte, *Organometallics*, 2005, **25**, 649–665.

196 A. Liu, M. C. Sauer, D. M. Loffredo and A. D. Trifunac, *J. Photochem. Photobiol*, 1992, **67**, 197–208.

197 C. Lambert, S. Amthor and J. Schelter, *J. Phys. Chem. A*, 2004, **108**, 6474–6486.

198 S. Marqués-González, M. Parthey, D. S. Yufit, J. A. K. Howard, M. Kaupp and P. J. Low, *Organometallics*, 2014, **33**, 4947–4963.

199 M. A. Fox, R. L. Roberts, T. E. Baines, B. Le Guennic, J.-F. Halet, F. Hartl, D. S. Yufit, D. Albesa-Jové, J. A. K. Howard and P. J. Low, *J. Am. Chem. Soc.*, 2008, **130**, 3566–3578.

200 M. Korb, S. M. B. H. Ghazvini, S. A. Moggach, J.-F. Meunier, A. Bousseksou and P. J. Low, *Inorg. Chem.*, 2021, **60**, 4986–4995.

201 A. Marini, A. Muñoz-Losa, A. Biancardi and B. Mennucci, *J. Phys. Chem. B*, 2010, **114**, 17128–17135.

202 M. J. Kamlet and R. W. Taft, *J. Am. Chem. Soc.*, 1976, **98**, 377–383.

203 R. W. Taft and M. J. Kamlet, *J. Am. Chem. Soc.*, 1976, **98**, 2886–2894.

204 M. J. Kamlet, J. L. M. Abboud and R. W. Taft, *J. Am. Chem. Soc.*, 1977, **99**, 6027–6038.

205 M. J. Kamlet, T. N. Hall, J. Boykin and R. W. Taft, *J. Org. Chem.*, 1979, **44**, 2599–2604.

206 M. J. Kamlet, J. L. M. Abboud, M. H. Abraham and R. W. Taft, *J. Org. Chem.*, 1983, **48**, 2877–2887.

207 J. Catalán, V. López, P. Pérez, R. Martin-Villamil and J.-G. Rodríguez, *Liebigs Ann.*, 1995, 241–252.

208 J. Catalán, *J. Phys. Chem. B*, 2009, **113**, 5951–5960.

209 A. S. Tsai, M. E. Tauchert, R. G. Bergman and J. A. Ellman, *J. Am. Chem. Soc.*, 2011, **133**, 1248–1250.

210 W. M. Khairul, L. Porrès, D. Albesa-Jové, M. S. Senn, M. Jones, D. P. Lydon, J. A. K. Howard, A. Beeby, T. B. Marder and P. J. Low, *J. Clust. Sci.*, 2006, **17**, 65–85.

211 A. Milani, V. Barbieri, A. Facibeni, V. Russo, A. Li Bassi, A. Lucotti, M. Tommasini, M. D. Tzirakis, F. Diederich and C. S. Casari, *Sci. Rep.*, 2019, **9**, 1648.

212 M. Krejčik, M. Daněk and F. Hartl, *J. Electroanal. Chem. Interf. Electrochem.*, 1991, **317**, 179–187.

213 B. A. DaSilveira Neto, A. S. Lopes, G. Ebeling, R. S. Gonçalves, V. E. U. Costa, F. H. Quina and J. Dupont, *Tetrahedron*, 2005, **61**, 10975–10982.